Nuclear Space Application Program

The Martian Surface Reactor: An Advanced Nuclear Power Station for Manned Extraterrestrial Exploration

A. Bushman, D.M. Carpenter, T.S. Ellis, S.P. Gallagher, M.D. Hershcovitch, M.C. Hine, E.D. Johnson, S.C. Kane, M.R. Presley, A.H. Roach, S. Shaikh, M.P. Short, M.A. Stawicki

MIT-NSA-TR-003

December 2004

Abstract

As part of the 22.033/22.33 Nuclear Systems Design project, this group designed a 100 kW_e Martian/Lunar surface reactor system to work for 5 EFPY in support of extraterrestrial human exploration efforts. The reactor design was optimized over the following criteria: small mass and size, controllability, launchability/accident safety, and high reliability. The Martian Surface Reactor was comprised of four main systems: the core, power conversion system, radiator and shielding.

The core produces 1.2 MW_{th} and operates in a fast spectrum. Li heat pipes cool the core and couple to the power conversion system. The heat pipes compliment the chosen pin-type fuel geometry arranged in a tri-cusp configuration. The reactor fuel is UN ($33.1^{w}/_{o}$ enriched), the cladding and structural materials in core are Re, and a Hf vessel encases the core. The reflector is Zr_3Si_2, chosen for its high albedo. Control is achieved by rotating drums, using a TaB_2 shutter material. Under a wide range of postulated accident scenarios, this core remains sub-critical and poses minimal environmental hazards.

The power conversion system consists of three parts: a power conversion unit, a transmission system and a heat exchanger. The power conversion unit is a series of cesium thermionic cells, each one wrapped around a core heat pipe. The thermionic emitter is Re at 1800 K, and the collector is molybdenum at 950 K. These units, operating at 10^{+}% efficiency, produce 125 kW_e DC and transmit 100 kW_e AC. The power transmission system includes 25 separate DC-to-AC converters, transformers to step up the transmission voltage, and 25 km of 22 gauge copper wire for actual electricity transmission. The remaining 900 kW_{th} then gets transmitted to the heat pipes of the radiator via an annular heat pipe heat exchanger that fits over the thermionics. This power conversion system was designed with much redundancy and high safety margins; the highest percent power loss due to a single point failure is 4%.

The radiator is a series of potassium heat pipes with carbon-carbon fins attached. For each core heat pipe there is one radiator heat pipe. The series of heat pipe/fin combinations form a conical shell around the reactor. There is only a 10 degree temperature drop between the heat exchanger and radiator surface, making the radiating temperature 940 K. In the radiator, the maximum cooling loss due to a single point failure is less than 1%.

The shielding system is a bi-layer shadow shield that covers an 80º arc of the core. The inner layer of the shield is a boron carbide neutron shield; the outer layer is a tungsten gamma shield. The tungsten shield is coated with SiC to prevent oxidation in the Martian atmosphere. At a distance of 11 meters from the reactor, on the shielded side, the radiation dose falls to an acceptable 2 mrem/hr; on the unshielded side, an exclusion zone extends to 14 m from the core. The shield is movable to protect crew no matter the initial orientation of the core.

When combined together, the four systems comprise the MSR. The system is roughly conical, 4.8 m in diameter and 3 m tall. The total mass of the reactor is 6.5 MT.

Acknowledgements

The design team would like to acknowledge our advisor Professor Andrew Kadak for creating such an exciting project for us to work on and coordinating our efforts with the Department of Aeronautics and Astronautics to provide context and meaning to our work. We would also like to extend our thanks to him for giving us feedback at every major milestone of the project.

Peter Yarsky, the Teaching Assistant for this class, was an invaluable guide and resource to the design team. He tirelessly answered our questions, provided us extra material to consider, edited our chapters, prepared us for our final presentation and generally supported us every step of the way. The design team would like to sincerely thank Mr. Yarsky for going above and beyond his role as a TA; in addition to his technical expertise, his enthusiasm for this project sustained ours.

We would like to extend our deepest gratitude to Joseph Palaia, a graduate student in the Nuclear Science and Engineering Department. In addition to helping us locate information relevant to Martian operation, he spent countless hours with our group creating CAD drawings of the MSR system.

The design team would like to thank the Nuclear Science and Engineering Department of MIT for supporting our project, and the faculty for answering our endless stream of questions. Graduate student Marc Berte supplied valuable feedback on our initial design. We would like to extend a special thanks to Professors Linn Hobbs, Michael Golay, Elias Gyftopoulos, and Neil Todreas for taking the time to come to a preliminary presentation and critiquing our work.

Additionally, we would like to express our appreciation to Dr. Larry Foulke of Bechtel Bettis, Dr. Paul Baldasaro of Knolls Atomic Power Laboratory, and Dr. Ady Hershcovitch of Brookhaven National Laboratory, for attending our final presentation and providing insightful commentary and critique of the MSR design.

Finally, the design team would like to acknowledge Professor Jeffrey Hoffman of the Department of Aeronautics and Astronautics at MIT for being a resource for information specific to space and extraterrestrial exploration.

Table of Contents

List of Figures

List of Tables

1 Introduction

Since the era of space exploration began in 1957 it has captivated the human imagination. Having reached the Moon, the next frontier is Mars. Recently, NASA has undergone great effort to redirect their focus to the human exploration of this planet. However, to justify committing the resources necessary to put humans on Mars, the capabilities must exist for these explorers to spend months on the surface, to conduct meaningful scientific studies and to use Martian resources to survive. All of these applications require power. Only nuclear fission power is capable of providing energy in sufficient quantities for long enough periods to support this exploration.

At MIT, students in the Nuclear Science and Engineering Department are required to participate in a Nuclear Systems Design project (22.033/22.33). Traditionally this 12-week project has challenged students to explore new applications of nuclear technology. For the fall 2004 term, this class focused on the design of a nuclear power system to support Martian surface exploration. The mission of the project was to design a fission reactor that could generate 100kW of electric power for five effective full power years (EFPY). Realizing that any technology used for human exploration of Mars might first be tested on the Moon, this system had to be capable of operating in both of these environments. This report details the design of the Martian Surface Reactor (MSR), the culmination of the design project.

Work on the MSR began with generation of specific goals and criteria to evaluate options. A formal decision methodology was developed and applied for all major design choices. As options were selected a process of iteration, integration and optimization ensured the highest possible performance characteristics of the overall system. Work focused around four primary subsystems: the reactor core, the power conversion system, the radiator and the shielding.

The core of the MSR produces 1.2 MW_{th} and operates in the fast spectrum, using uranium nitride fuel pins in a tricusp arrangement with lithium heat pipes for cooling. This configuration exhibits excellent thermal conductivity and allows the heat pipes to

remove thermal energy from the core at 1800 K while still maintaining large thermal margins to protect against damage during transients. External control drums provide control for the core with a tantalum di-boride (TaB_2) shutter material placed inside a tri-zirconium di-silicide (Zr_3Si_2) reflector. A hafnium (Hf) vessel offers structural support around the core, inside of the reflector and control drums, and absorbs thermal neutrons helping to reduce reactivity under certain launch accident scenarios.

After removing thermal energy from the core, the power conversion system converts this energy into electricity, and provides for transmission capability. A series of out-of-core cesium thermionics surround each of the lithium heat pipes to accomplish thermal to electric conversion. After generation of electrical power in the thermionics, inverters convert DC to AC and transformers step up voltage before transmission. Thermal power not converted by the thermionics to electricity is removed by annular potassium heat pipes that cover each thermionic and couple to the radiator.

The MSR radiator is composed of potassium heat pipes that run from the reactor power conversion unit (PCU) and curve into a conical shell above the reactor. A thin fin extends from each heat pipe to form a conical radiating surface around the reactor. The panels and heat pipes are constructed of a Carbon-Carbon composite, which provides good thermal conductivity and emissivity with very low density. The exposed surfaces of all Carbon-Carbon composites are coated with silicon carbide (SiC) to prevent oxidation.

To protect humans from ionizing radiation from the core, the MSR employs a bi-layer shielding design comprising a boron carbide (B_4C) layer placed against the reactor reflector and a tungsten (W) layer placed against the B_4C. The B_4C is responsible for stopping neutrons, while the tungsten attenuates gamma rays. These layers are in the shape of a semi-cylindrical shell, covering eighty degrees of arc around the reactor. At a distance of 11 meters from the outer tungsten surface, the dose falls to 2 mrem/hr, an acceptable level for human exposure.

The design of the MSR focused primarily on issues of size, mass and safety. The design team selected technologies in order to minimize the overall mass of the system while at

the same time ensuring that there was still high redundancy, minimum potential for single point failure and minimal hazard posed to humans during launch and operation. The most limiting factor of this design effort was the gap in current knowledge applicable to extraterrestrial surface reactor design. These areas were dedicated to future work. A reliable and safe 100 kW_e nuclear power source for Mars will greatly enhance Martian exploration efforts, and the MSR concept provides a first step toward such a system.

2 Decision Methodology

2.1 Introduction

To being to design a reactor to provide surface power for Martian exploration, it is important to lay out goals for the system and a path to reach those goals. To this end, the design team created a formal decision methodology to facilitate optimization of the total reactor design. This chapter describes the decision methodology and the goals of the MSR in detail.

2.2 Need for a Decision Methodology

The first step of designing the MSR was to decide what the most important design criteria were beyond the three mandated criteria of: 100 kWe, 5 EFPY and works both on the Moon and Mars. Further analysis resulted in a number of significant, and sometimes contradictory, objectives which the MSR needed to fulfill. Excessive complexity in design requirements often leads to difficulties in picking an option that best satisfies all the goals. The design team employed the following decision methodology to ensure that no technology was unduly overlooked, thus yielding the best result for each decision.

The design team was broken into four sections: Core, PCU, Radiator and Shielding, with each section in charge of the final design of their reactor component. Given this organization, it could have been very easy for each group to optimize their system independently of the entire team, thus leading to a non-optimal overall design. As an example, in general, a power conversion unit (PCU) operates most efficiently when there is a large drop between the inlet and outlet temperatures. However, a radiator, connected to the outlet of the PCU, operates most efficiently at higher temperatures; the core, providing the inlet temperature, works best at lower temperatures. In order to optimize the PCU in light of the overall design, the PCU team must chose an appropriate option that balances the needs of the Core, PCU and Radiator groups. The formal decision methodology encourages this type of systems thinking by functioning as a mechanism to

capture the tradeoffs between systems while still addressing all the design goals outlined below.

It is important to note that, while the formal decision methodology does aid in pinpointing trouble spots in respect to integration and optimization between different parts of the MSR, it does not capture the full extent of intergroup interaction. In addition to including these integration and optimization issues in the decision methodology, the design team also underwent much discussion and many iterations of compromise to design the best MSR possible.

2.3 Decision Methodology Explained

The formal decision methodology is composed of two tests: a litmus test and an extent-to-which (ETW) test. The litmus test is a set of must-be-met criteria that allows the team to reject, without any further consideration, any technology that does fulfill these goals. The ETW is a more resolving test that allows the design team to distinguish between viable candidates. The test consists of a list of weighted goals; the options are then ranked according to how relatively well they fulfill each goal, and the option with the highest total ranking is considered the best option.

Example of Decision Methodology Applied

Assume that one is trying to pick footwear for around the house from a list of five options: designer high-heeled shoes, socks, fuzzy slippers, hiking boots and sneakers. By applying a litmus test, with the criteria of comfort, one will down select the footwear options to socks, fuzzy slippers and sneakers, and then use the ETW to make an optimal selection. See Table 2.3-1 below for an illustration of the ETW test.

Table 2.3-1: Extent-to-Which Test Demonstration for Determination of Best Household Footwear

	Socks	**Fuzzy Slippers**	**Sneakers**
Warm	3	2	1
Easy to Put On	2	3	1
Durable	1	2	3
Total	***6***	***7***	***5***

In this ETW test for proper household footwear, the equally rated goals are warmth, ease of application and durability; the options are socks, fuzzy slippers and sneakers. The best option, with the highest ranking, is clearly the fuzzy slippers.

Goal Determination

To begin, the entire design team generated a series of general goals appropriate for all groups. It is important to note that the team understands that no one set of criteria can completely encompass all necessary goals for each group; this is why we chose a set of universal criteria to be further defined by each group independently, based on the technology being decided upon. After eliminating redundancies, the following nine goals remained:

1.) Works on the Moon and Mars
2.) Provides 100 kWe
3.) Works for 5 EFPY
4.) Obeys Environmental Regulations – NASA's Planetary Protection Policy
5.) Launchable/Accident Safe – Launchable is restricted by landing capabilities, assuming a lander vehicle of cylindrical shape 5 m in diameter and 5 m tall, which can hold up to 10 MT. Accident safety refers primarily to mitigation of hazards upon launch accident scenarios.
6.) High Reliability/Limited Maintenance
7.) Small Mass and Size (Cost)
8.) Controllable – Components assist in developing a completely autonomous control scheme.
9.) Uses Proven Technology

The reader will notice that in the above list, the criterion "safe" is missing. This is not an oversight, as the design team believes that safety is a top priority for the MSR; however, we found it more useful to break down safety into three explicit categories of launchability/accident safety, reliability and controllability, rather than having one vague "safety" criterion.

The first three goals – works on the Moon and Mars, provides 100 kWe and works for five EFPY – are part of the design team's charter, and must be satisfied. The fourth goal, obeys the Planetary Protection Policy, is a constraint imposed by NASA. Thus, the design team moved the first four goals to the litmus test category and proceeded to rank and weight the remaining goals.

Using a ranking system based in the Analytic Hierarchy Process (AHP) [1], each member of the design team independently ranked each of the nine criteria (A) relative to the other remaining criteria (B) based on the following scale:

Table 2.3-2: AHP-based Criteria Ranking System

Scale	Relative Ranking
1	A is much less important than B
3	A is moderately less important than B
5	A is equally important to B
7	A is moderately more important than B
9	A is much more important than B

Applying the above ranking system and normalizing the results, the design team calculated weighting factors for the five remaining criteria. Table 2.3-3 below displays the results of the first iteration of the ETW goal ranking.

Table 2.3-3: Preliminary ETW Test Goal Ranking

	Weighting Factor
Small Mass and Size	1.99
Controllable	1.68
Launchable/Accident Safe	1.66
High Reliability/Limited Maintenance	1.48
Uses Proven Technology	1

After reviewing the results, the design team decided to group "uses proven technology" with "high reliability" for simplicity, as NASA's Technology Readiness Levels (TRLs) are not readily available for most options considered.

Left with four remaining ETW criteria with which to judge the MSR options, once again the design team ranked the goals to produce the revised weighted ETW seen below:

Table 2.3-4: Final ETW Test Goal Ranking

	Weighting Factor
Small Mass and Size	1.35
Controllable	1.14
Launchable/Accident Safe	1.13
High Reliability/Limited Maintenance	1

2.4 Decision Methodology Applied

There are five steps to applying the decision methodology described above. Figure 2.4-1 below illustrates this process via a flow chart. First, the decision maker researches and documents all possible options, no matter how unproven or impractical the option maybe. This ensures that every option, regardless of personal bias, receives fair consideration in the design process. This also ensures that analysis of each option is documented in case of criticism. The second step is application of the litmus test. Any option that fails, without remedy, any of the litmus tests is automatically discarded.

The third step is to define the goals of the ETW test as they apply to the system under investigation. For example, if one were using the ETW to determine PCU type, one would want to define "high reliability" as a system that requires no moving parts, has no single point failures and is radiation resistant. These break downs should include relationships with other systems. For example, low inlet temperature should be included in the subset of "high reliability," because a low core operating temperature puts less thermal stress on the core and PCU, making the overall system more reliable. On the same note, for "small mass and size," high outlet temperature should appear because a high outlet temperature reduces the mass of the entire system by reducing the size of the radiator. After defining the ETW test goals, the ETW test is applied and the highest-ranking option identified.

The fifth and last step occurs only after the ETW test is applied and a best option identified. Once this happens, the design team must then examine the highest scoring option, with particular attention to categories of the ETW that received low markings for this system. If these low markings can demonstrably be mitigated, or are deemed acceptable shortcomings, then the highest-ranking option becomes the design of choice. Else, the design team must rule out that option and take the next highest-ranking option for scrutiny. Thus, through this five-step process, the design team can choose the option that best satisfies all the goals enumerated in the decision methodology, ensuring a quality over-all design.

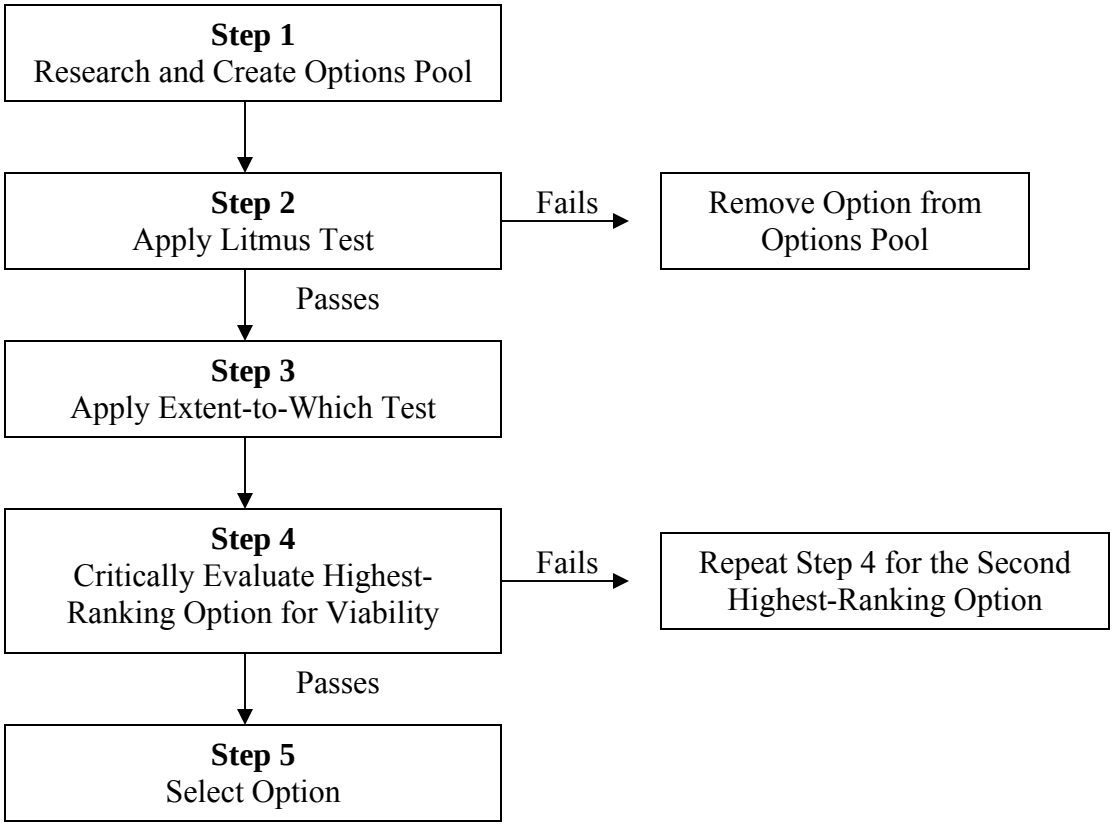

Figure 2.4-1: Decision Methodology Flow Chart

2.5 Conclusion

The litmus test and ETW test comprise the formal decision methodology employed in all major decisions for this reactor system. This methodology ensures proper weighting of all goals, impartial analysis of all options, and consistency in decision-making. While this methodology provides much-needed guidance to the decision-making process, decision makers need to be cognizant of the shortcomings of this system; it does not necessarily capture all the important aspects for every decision. For example, in choosing proper power transmission cables, the only difference according to the decision criteria between OO gauge and OOOO gauge copper wire is mass; but in reality, OO gauge has more electrical losses than OOOO gauge copper wire, and may not be as well suited for transmission purposes over long distances despite the mass savings. Thus, the decision maker may use this tool as an aid in the decision-making process, but he cannot entirely

rely upon this tool without being conscious of what trade-offs are implicit in this methodology.

3 Core Design

3.1 Introduction

The central component of the MSR is the core, as it provides the thermal energy for the system. The core group designed a safe, robust and highly reliable reactor core to provide full power, of 1.2 MW_{th}, for five years on either the Moon or Mars. This chapter presents the design process of the MSR core from choosing the neutron energy spectrum all the way through accident analyses.

In order to meet the ultimate goals of the project, the design group set two core specific goals for the design. The first goal is to attain core temperatures around 1800 K, in order to keep the system mass as low as possible. Section 4.4.1 further describes the motivation for this goal. The second goal is to create a core that uses only external core control (ex-core), as it increases reliability and reduces sudden reactivity addition/subtraction events.

The design team chose a high operating temperature after some initial iteration on the design. High temperatures reduce radiator size and allow power conversion group to choose a solid-state power conversion system. Specifically, thermionics are the power conversion system and an operating temperature of 1800 K would best fulfill fuel temperature limits and the temperatures required by thermionics.

Ex-core control allows operation without the threat of a sudden reactivity insertion event. Intrinsic core control requires elaborate mechanisms to move in and out of the core. The ex-core does not have these problems. See Section 3.6 for further explanation.

3.2 Spectrum

3.2.1 Options

The first step in designing the core was selecting the neutron energy spectrum. Three possible choices exist: thermal, epithermal and fast. A thermal spectrum is one where primarily moderated, thermalized neutrons at about 0.025 eV induce fission in a system

at about 300 K. At the high temperature selected for the MSR system, thermal neutrons have energy about 0.15 eV. An epithermal spectrum consists of slightly moderated neutrons that are absorbed in fission resonances between about 1–100 keV. A fast spectrum is mostly comprised of un-moderated neutrons with energy around 0.5 MeV, which are the primary source of fission [2].

Each of these spectra had inherent advantages and disadvantages; no one spectrum was obviously superior. All of the options are capable of providing a core capable of running for five EFPYs, generating sufficient thermal energy to produce 100 kWe and operating in a safe, environmentally friendly manner on both the Lunar and Martian surfaces. Accordingly, the team applied the formal decision methodology as described in Chapter 2 to rank the three options based on the established project goals in Section 2.3. The selected spectrum for the core was that which ranked highest in this procedure.

3.2.2 Decision Methodology

The neutron energy spectrum will drive the rest of the core design, so it is critical, at this juncture, that we choose the best possible spectrum. The decision methodology used spectrum specific design criteria developed for each of the project goals to evaluate each of the choices. As seen in Table 3.2-1 below, the numerical rankings of these design criteria indicate a fast spectrum is the best choice.

Table 3.2-1: Spectrum Choice Decision [2][3][4][5]

		Spectrum		
		Thermal	Epithermal	Fast
Criterion	***Small Mass and Size (Cost) - 1.35***			
	Small Heavy Metal Mass	3	2	1
	Small Moderator Mass	3	2	1
	Small Reflector Mass	1	2	3
	Small Dimensions	1	2	3
	Controllable – 1.14			
	Flat Keff	2	1	3
	Ex-Core Control	1	2	3
	Slow Transients	3	2	1
	Launchable/Accident Safe - 1.13			
	No Criticality Accident	3	2	1
	Fits in Rocket	1	2	3
	High Reliability and Limited Maintenance - 1			
	Few Moving Parts	1	2	3
	Little Radiation Damage	3	2	1
Performance Index		***26.12***	***25.02***	***27.3***

3.2.3 Spectrum Comparison by Design Criteria

From the decision methodology, we not only see that the fast spectrum is the best choice, but it also indicates what the shortcomings of this system might be. The sections below will address the reason for the rankings as well as provide a discussion of the shortcomings of a fast spectrum.

Small Mass and Size

The spectrum, in part, determines the mass of the core as it affects the required heavy metal mass. For a small core with a 5-year life, a thermal spectrum minimizes the required heavy metal mass. As the spectrum softens to lower energies, the fission cross section increases, thus less enrichment is required [3]. For this reason, fast reactors need high-enriched fuel to operate. Breeding in the fuel can also reduce the amount of heavy

metal required because the initial enrichment does not have to provide reactivity over the lifetime of operation.

Different spectra require different amounts of reflecting and moderating material. Again, the chosen spectrum should minimize the mass of these peripheral systems. A fast spectrum requires no moderating material and so will best minimize these requirements. Epithermal and thermal systems require neutrons to slow, thus requiring the addition of bulky moderators [4]. Moderating material also limits the temperature of the system since these materials typically have melting temperatures that would not withstand the high operating temperature requirement chosen.

The spectrum should facilitate the construction of a small core. This implies high power density and enrichment. Again, a fast spectrum is best suited for this requirement as it allows the highest power density of the three choices [3]. As stated above, a fast spectrum core allows a smaller volume core because temperature considerations in the moderator are not a concern.

Controllable

Spectrum should assist in achieving a flat k_{eff} over the life of the core without complicated movement of control assemblies. Over life, fissile isotope concentrations gradually decrease and the criticality, k, of the core drops. Continuously converting fertile isotopes to fissile isotopes, breeding, minimizes this effect [3]. As it is possible to obtain a higher conversion ratio in a fast spectrum than in either of the other two spectra, it will be easiest to meet this goal with a fast spectrum.

For simplicity in geometry and reliability in operation, the spectrum should assist in achieving external core control. In cases where the unreflected core has a large leakage fraction, the neutron worth contribution from the reflector is necessarily larger. As the large migration length of fast neutrons typically increases neutron leakage in these types of cores, it is possible to manipulate a large fraction of the core reactivity through manipulation of the neutron reflector.

The spectrum should maximize reactor period and insure relatively slow transients to allow time to respond to abnormal events. The most common type of transient to consider is a power transient where power levels change over time from an initial value to a final value. If the power transient is slow, more time is available to use control systems to control the process and avoid inadvertent supercriticality. Transients are slowest in thermal reactors and increase in speed as the spectrum becomes more energetic [3]. As spectrum energy increases, neutrons spend less time thermalizing and the time between reactions decreases therefore, transients proceed faster.

Launchable/Accident Safe

The chosen spectrum should reduce the risk of criticality accidents during launch. As a worst-case scenario, removal of the reflector and ex-core control devices, and water or wet sand ingress in the case of a crash. A thermal spectrum core is easiest to design to meet these needs as the system normally operates with moderated neutrons. In a fast or epithermal spectrum core, the moderation of the neutrons by water increases reactivity beyond normal operation conditions because the fission cross sections decrease with increasing neutron energy. In fact, this issue becomes more significant as the average operating energy of the neutrons increases.

The spectrum should lend itself to a compact system design that will easily fit inside existing rockets. As with the concerns of small mass and size, a fast spectrum is best suited to provide a compact design.

High Reliability and Limited Maintenance

Minimizing moving parts in the core is especially important for reliability in that astronauts will have no access to the actual core for maintenance due to human radiation dose limits. A fast reactor is optimal for this requirement due to its high leakage characteristics. As mentioned above, high leakage eliminates the need for in core moving parts and simplifies control geometries. As the spectrum slows, leakage decreases and more moving parts are required in the core to control the system.

To reduce radiation damage to reactor materials and minimize shielding, the chosen spectrum should be soft and have a small flux. A soft spectrum is characteristic of a

thermal reactor. As the spectrum hardens, neutrons become more damaging and components degrade faster.

3.2.4 Discussion

As shown in Table 3.2-1, the fast spectrum scored higher than the other choices, therefore the design team chose a fast spectrum for the MSR. Before moving on however, it is necessary to note that while the fast spectrum scored highest overall, it ranked poorly in the three areas related to safety. In the area of criticality safety during launch accident, a fast reactor is the most difficult to keep sub-critical. Section 3.8 addresses launch accident safety, and demonstrates that the MSR will remain subcritical in a worst-case scenario, therefore eliminating this concern. In the area of transient speed, materials and configurations chosen allow large safety margins in melting temperature, thermal expansion and pressure swelling to permit control systems time to respond to transients before components might fail. Finally, to address radiation damage, resilience to radiation embrittlement and dimensional changes became a requisite for material choices in the MSR. With these design measures in place, it was easy to mitigate the three poor rankings of the fast spectrum, thus allowing the fast spectrum to remain the spectrum of choice for the MSR.

3.3 Coolant System

This section intends to investigate all viable coolant system options, compare them using the decision methodology described in Chapter 2 and provide an in-depth description of the coolant system that best fits the needs of MSR.

3.3.1 Options

A wide variety of coolant system designs exist, however after examining a number of existing cooling options the design group determined the most feasible options were the designs considered for the Jupiter Icy Moons Orbiter mission. The next section contains a short description of the three coolant systems considered, gas-cooled, liquid metal-cooled and heat pipe-cooled, along with any noteworthy design attributes.

Direct Gas-cooled System

The direct gas-cooled system utilizes a gas coolant, often a He/Xe mixture or CO_2, which flows through the core directly to a gas turbine generator to produce electricity. This relatively simple system has an extensive testing knowledgebase because of previous development of the SP-100 and SNAP-10A programs. The design also utilizes existing industrial manufacturing infrastructure to fabricate the robust superalloy materials required for core construction. However, because of the low thermal conductivity of the gaseous phase, these systems have to operate at relatively high pressures (~200 psia) and low temperatures (~1000 K) [6] in order to attain the proper thermal transfer properties.

High pressures are undesirable for extraterrestrial reactor systems because the low-pressure atmospheres of the Moon and Mars create a high-pressure gradient, which greatly exacerbates the problem of leakage. In addition, given the stress of launch and the abundance of meteorites that bombard the Martian and Lunar surfaces, a break in the coolant pipes can create a rapid loss of coolant accident (LOCA). This single-point failure accident scenario is highly undesirable from a mission-planning point of view. In addition, low operating temperatures mean an increased mass for both the power conversion system and radiator since the primary mode of heat rejection in space is radiation to the ambient environment. This mass increase of the power conversion unit and radiator system has the potential to make this design too massive for cost effective implementation (See Sections 4.4.2 and 5.3).

Liquid Metal-Cooled System

The liquid metal-cooled system pumps liquid metal through flow channels in the core to the power conversion unit, which extracts the heat. This system is quite flexible concerning the power conversion interface and, at least for previous designs, has tended to be less massive than the other coolant system options [6].

Options available for the working fluid were sodium-potassium eutectic, sodium, lithium, silver and lead. Out of these options, only Li, Ag and Pb have appropriate thermal transfer properties for temperatures above the mission mandated operating temperature of 1800 K. Lithium characteristics, which are very similar to the extensively documented

fluidic characteristics of Na/NaK eutectic, are by far the most proven out of the three remaining options. Both silver and lead have a higher operating temperature range when compared to lithium, but due to the lack of testing experience and dissimilarity of the chemical characteristics, the comparative performance of silver and lead are unknown. Silver and lead also have a significantly higher density than lithium, resulting in a much heavier system. Ultimately, the design group chose lithium as the working fluid because of the design temperature and mass requirements.

Unfortunately, there is little development concerning the major thermal hydraulic components, such as turbines and pumps. The liquid-metal systems also require supplementary testing for start-up procedures because the working fluid needs to thaw completely before cooling can properly occur. Finally, just as the gas-cooled system, the liquid metal design is also susceptible to single point failures although not to as an appreciable extent as the gas-cooled system since loosing the entire inventory would necessitate a break at the lowest point of the coolant loop.

Heat Pipe-Cooled System

Heat pipes utilize the phase change of a liquid metal coolant to transmit heat isothermally from the hot section of the heat pipe to the cold section of the heat pipe via capillary action. The in-core section of the heat pipe is the hot section, or the evaporator end; the power conversion unit removes heat from the cold section, or the condenser end. See Section 3.3.4 for a full discussion on how heat pipes work. These heat pipes provide the efficiency of two-phase liquid-metal heat transfer in a passively simple and well-characterized volume [7].

As discussed in the previous section on liquid metal-cooled systems, lithium will be the working fluid because of its thermal transfer properties and low density. This design choice will undoubtedly limit the option space for the wick structure as well as for the containment pipe structure.

Historically, heat pipe systems have been limited to lower heat flux applications due to the five main limiting factors of heat pipe operation. Section 3.3.4 discusses these limiting factors further. However, this system remains an option because preliminary

calculations assure us that heat pipes, if designed appropriately, can work at the heat flux level produced by this reactor. Furthermore, the Marshall Space Flight Center demonstrated a lithium heat pipe system to work well beyond the mission timeframe requirement of 5 years [6]; however, further system characterization will be necessary before integration can occur.

3.3.2 Option Comparison by Design Criteria

Small Mass and Size

On the average, the liquid metal cooled system tends to be the lowest mass of the three designs, but existing work has shown the other two designs to be competitive. The actual mass of the system varies on a design-by-design basis, making the mass differential between the three systems negligible. Volume considerations, however, show the gas-cooled systems to be the largest and liquid metal-cooled systems to be the smallest. This is primarily due to density and geometry differences between the three systems.

Controllable

The heat pipe-cooled system has the best thermal transient response because it has the inherent capacity to absorb heat up to its heat flux limit. The liquid metal cooled system has the second best thermal transient rating because the heat produced will be deposited in the liquid metal. The gas-cooled system received the lowest rating because the heat capacity of the gas coolant results in the deposition of the heat in the fuel.

Both the gas-cooled and liquid metal systems were not able to accommodate the increased thermal load associated with a major increase in normal reactivity due to control malfunction. For example, a stuck slider or drum at beginning of life or a slider or drum failed in the “in” position would cause an increase normal reactivity. For the gas-cooled system in particular, the spectral safety is difficult because of the large core void fraction. It requires the use of BeO for the reflector, which will increase the core mass. The heat pipe design is not susceptible to these problems.

Launchable/Accident Safe

With appropriate engineering standards, the heat pipe coolant system mitigates the possibility of an accidental supercriticality after a core compaction or splashdown

scenario. See Section 3.8 for more information on why this is. Launching a reactor into space requires the reactor to be in its most reactive state when launched so that any possible deformation would reduce the reactivity of the core. A heat pipe system requires the core arrangement to be in its most reactive state whereas the gas-cooled and the liquid metal-cooled systems do not require this configuration. The gas-cooled system is less desirable because it is easier to evacuate the coolant inventory.

High Reliability and Limited Maintenance

One of the issues regarding reliability is material degradation from irradiation. In the gas-cooled design, the fuel pin is subject to a wide temperature range so the Nb1Zr may have some ductility issues near the core inlet. Ensuring the cold leg temperature is not too low mitigates this concern. In addition, gas-cooled systems have higher fuel and clad temperatures. Due to the extensive operating history of the liquid metal cooled design, this concern is of negligible importance especially because the heat removal properties of liquid metal are much greater than gas. Similarly, for the heat pipe cooled system materials issues are not a problem due to the ability of stainless steel and Li to withstand more stressful environments.

Another issue facing reliability is the tolerance of the coolant to impurities. According to experimental experience, Li loops typically require the lowest level of impurities (parts per million range) in order to function properly. Na and NaK loops can usually tolerate impurities up to the parts per thousand range and gas-cooled designs can tolerate even higher levels. Heat pipe systems avoid contamination by fuel particles and cladding particles since the coolant is contained in the pipe, thus the design group expects the heat pipe system to have a smaller level of impurities compared to the liquid metal system over the lifetime of the system. Gas-cooled systems typically use inert gases therefore the erosion of materials over life is not a concern.

Susceptibility to single point failures is a crucial point for reliability. A single point failure is a small rupture in an arbitrary point in the design that causes a critical component of the MSR to fail, resulting in mission failure. Both the direct gas-cooled system and the liquid metal cooled system designs suffer from this design flaw, whereas

the heat pipe coolant system does not. Because each heat pipe channel is a self-contained unit, the system accommodates the failure of a heat pipe by having the surrounding units evenly share the heat load of the failed unit, thus avoiding mission failure.

Lifetime

Given no failures, the direct gas-cooled system design would fulfill the 5-year lifetime requirement, especially because the gas would not interact with the materials in the core. Na/NaK liquid metal-cooled reactors represent a mature and well-studied technology. Lithium cooled reactors, which is the liquid metal working fluid appropriate for the MSR given a target 1800 K operating temperature, have not been as extensively tested as the Na/NaK eutectic has; however, much of the intelligence about Na/NaK systems is expected to be applicable to the Li system due to similar chemical characteristics and design methods. The heat pipe cooled system has limited data on the lifetime failure rate where corrosion and mass transfer are the principle life-limiting issues. However, the design can most likely satisfy the operating length requirements of our mission since the longest documented demonstration with no failure was 5.2 years at 1391 K [6].

3.3.3 Decision Methodology

The design group used the decision methodology to choose the optimal cooling system.Table 3.3-1 displays the application of the decision methodology to the cooling system options. Several of the comparisons between designs were difficult to ascertain due to the heavy dependence upon design-specific parameters. Table 3.3-1 presents a generalized conclusion drawn from prior work.

Table 3.3-1: Coolant System Decision Matrix

	Coolant Type		
	Gas	Liquid Metal	Heat Pipe
Small Mass and Size (Cost) - 1.35			
Small Mass/Low Cost	2	3	2
Small Dimensions	1	3	2
Controllable - 1.14			
Thermal Transient Response	1	3	3
Launchable/Accident Safe - 1.13			
Core Compaction Considerations	1	1	3
High Reliability and Limited Maintenance - 1.0			
Material Degradation	1	3	3
Coolant Impurity Tolerance	3	1	2
Single Point Failure	1	1	3
Lifetime	3	2	1
Performance Index	***14.32***	***19.65***	***21.21***

With a small core releasing 1.2 megawatts of thermal energy during normal operation (up to 1.5 megawatts during transients), a reliable cooling system must be employed in order to get energy out of the core and into the power conversion system. Using a liquid or gaseous coolant loop presents certain failure modes not acceptable for a reactor on the Moon or on Mars, where maintenance is not an option. Natural circulation is not an option due to the limited gravity on both bodies. Therefore, for gas and liquid-metal systems, a redundant system of pumps would be required, increasing the mass of the system. A fluid coolant pumped through the core runs the risk of single point failure loss of coolant accident (LOCA). In addition, a coolant pump malfunction contributes to the system failure rate by creating the possibility for a loss of flow accident (LOFA). Both of these accidents would lead to a total meltdown of the core and failure of the mission.

As shown in the above decision methodology table, heat pipes currently present the best coolant option available. The high level of redundancy, due to the many independent heat pipe assemblies in the core, mitigates the risk of a LOCA or LOFA. The redundancy also provides a method of removing heat from the surrounding area if one heat pipe fails.

Since the heat pipe design achieved the highest performance index of the options investigated, the design group selected heat pipes as the coolant system for the MSR. A more in-depth characterization of the heat pipe coolant system follows in the next section.

3.3.4 Design Characteristics

Heat pipes are robust, reliable, compatible with the core materials and resistant to neutron damage. In addition, heat pipes are the best choice in terms of compatibility with the power conversion system. This section will describe how heat pipes work, what limitations exist and what the design specifications are for the MSR heat pipe system.

Explanation of Heat Pipe Technology

The heat pipe, first invented at Los Alamos Laboratory by G. M. Grover in 1963, is a device that uses evaporation and condensation to transport the latent heat of vaporization of a liquid isothermally across a distance [10]. Figure 3.3-1 shows a cross section of a simple heat pipe.

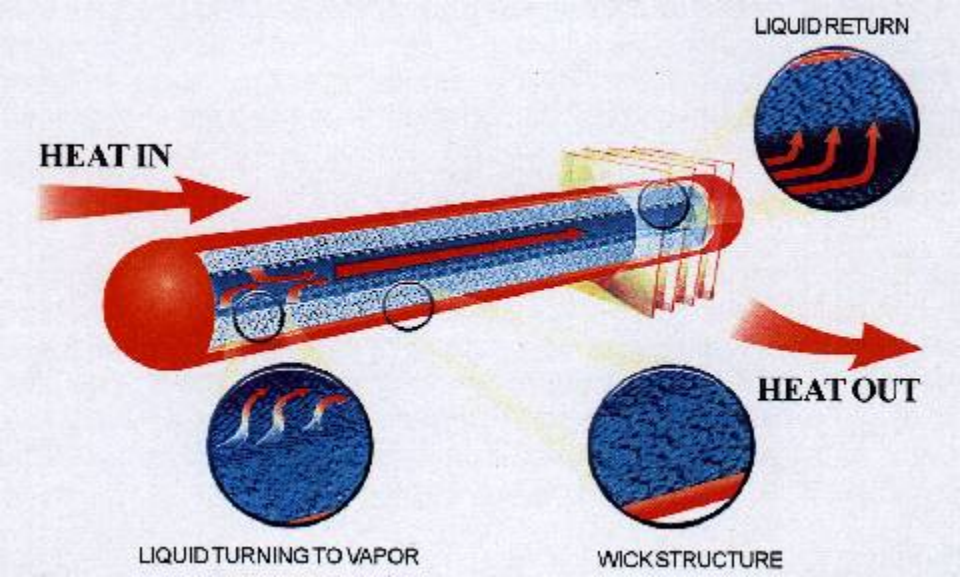

Figure 3.3-1: Cross Section of a Simple Heat Pipe [11]

A wick structure coats the inside of the heat pipe. This wick can consist of any combination of a porous metallic fiber network, grooves along the inner surface of the pipe, or arteries designed to increase the surface area along the inside of the pipe. The wick uses capillary action to ensure direct thermal contact between the working fluid and the inner wall of the pipe. This ensures a constant high heat flux into the pipe.

Heat enters the evaporator section, the left end of the pipe in Figure 3.3-1, and heats the liquid inside. Upon absorbing this heat, the working fluid boils, absorbing its latent heat of vaporization. The gaseous working fluid then travels up the vapor cavity, or the inside of the pipe not occupied by the wick. This vapor travels very quickly to the condenser section, seen in the right end of the pipe in Figure 3.3-1. Upon contact with the cold wall of the condenser section, the vapor releases its latent heat into the wall of the pipe and returns to its liquid state. Capillary forces then return the liquid to the evaporator section, where the cycle repeats itself.

Since the phase change process transfers the heat, the temperature change across the pipe is minimal during normal operation. This isothermal transfer of heat allows for very low dissipation in the device. The heat pipe therefore quickly and efficiently transfers thermal energy from one location to another.

In order for the heat pipe to work correctly it must continuously bring liquid from the condenser region to the evaporator region. If it fails to do so, the wick will dry out in the evaporator region and the heat pipe will effectively become a thermal insulator. For the heat pipe to bring liquid into the evaporator region continuously, the maximum capillary pumping head, the pressure increase due to capillary action, must be greater than the sum of the pressure drops along the heat pipe, as described by equation (3.3-1). For a full description of all variables that follow, please see Appendix I.

$$\Delta P_l + \Delta P_v + \Delta P_g \leq \Delta P_{c_{\max}} \tag{3.3-1}$$

where ΔP_l is the pressure drop required to return the liquid from the condenser to the evaporator, ΔP_v is the pressure drop in the vapor's flow through the heat pipe, and ΔP_g is the gravitational pressure loss, which may be positive or negative depending on the heat pipe orientation [8]. Equation (3.3-2) gives the maximum capillary pressure, ΔP_{Cmax}.

$$\Delta P_{c_{\max}} = 2\frac{\sigma_l}{r_e} \tag{3.3-2}$$

where σ_l is the surface tension of the liquid and r_e is the effective radius of the wick, or half the distance between the strands of the wick [8]. The pressure difference in the liquid phase (ΔP_l) is dependent on both the working fluid and the wick structure,

$$\Delta P_l = \frac{\mu_l l_{eff} m}{\rho_l K A_w} \tag{3.3-3}$$

where μ_l is the viscosity of the liquid, l_{eff} is the effective length of the heat pipe defined in equation (3.3-4), m is the mass flow rate, ρ_l is the density of the liquid, K is the wick permeability and A_w is the cross sectional area of the wick [8].

$$l_{eff} = l_{adiabatic} + \frac{1}{2} l_{evaporator} + \frac{1}{2} l_{condenser} \tag{3.3-4}$$

For a longitudinal groove wick, or a pipe with grooves along the length of the pipe, equation (3.3-5) gives the pressure loss in the liquid.

$$\Delta P_l = 8 \frac{\mu_l Q l}{\pi r_e^4 N \rho_l L} \tag{3.3-5}$$

The pressure loss in the vapor as it flows from the evaporator to the condenser is given by

$$\Delta P_v = 8 \frac{\mu_v l_{eff} m}{\pi r_v^4 \rho_v} \tag{3.3-6}$$

where r_v is the radius of the vapor channel [8]. Finally, equation (3.3-7) gives the pressure loss due to gravity.

$$\Delta P_g = \rho_l g l \sin(\varphi) \tag{3.3-7}$$

where g is the acceleration due to gravity, l is the length of the heat pipe and φ is the inclination of the heat pipe. φ is positive when the condenser is lower than the evaporator [8].

Heat Pipe Design Constraints

There are five main physical factors limiting the heat flux in heat pipes: the viscous limit, the sonic velocity limit, the entrainment limit, the boiling limit, and the capillary limit.

Viscous Limit

At lower temperatures, the liquid in the heat pipe is quite viscous. Normally only a problem during startup, the viscosity of the liquid can limit the speed at which the liquid can return to the condenser, and therefore limit the axial heat flux the heat pipe can endure. Equation (3.3-8) gives the maximum axial heat flux.

$$q_{viscous} = \frac{1}{16} \frac{r_v^2 L \rho_v P_v}{\mu_v l_{eff}} \tag{3.3-8}$$

where L is the latent heat of vaporization and P_v is the pressure of the vapor [12].

Sonic Limit

If the heat pipe is operating at too high a temperature with too narrow a vapor channel the speed of the vapor in the channel may approach the speed of sound, causing a condition known as choking in the vapor. At this point, the vapor's motion is impeded by its own shock waves. Equation (3.3-9) gives the maximum heat flux due to the sonic limit.

$$q_{sonic} = 0.474L\sqrt{\rho_v P_v} \tag{3.3-9}$$

Entrainment Limit

An interesting phenomenon occurs at the boundary of the vapor and the liquid in the heat pipe that is not obvious. As the liquid flows from the condenser to the evaporator through the wick and the vapor flows from the evaporator to the condenser through the vapor channel, the two drag across each other. This creates a shear force, impeding the flow of the liquid down the heat pipe. Equation (3.3-10) gives the maximum heat flux due to entrainment.

$$q_{entrainment} = \sqrt{2}\sqrt{\frac{\pi\rho_v L^2\sigma_l}{z}} \tag{3.3-10}$$

where z is a dimension characterizing the vapor-liquid surface. Normally, the wick spacing dictates the entrainment limit.

Boiling Limit

For very high radial heat fluxes, boiling can occur faster than the bubbles can reach the liquid/vapor interface. In this case, the bubbles may coalesce causing film boiling. This means the liquid is no longer in thermal contact with the wall of the heat pipe, stopping heat transfer. This is normally not a limiting factor except for very high temperatures relative to the melting point of the working fluid. The design group designed the MSR such that the heat pipes never approach the boiling limit.

Capillary Limit

As mentioned before, equation (3.3-1) must be satisfied in order for the heat pipe to bring liquid down to the evaporator fast enough. This limits the mass flow rate of the heat pipe and therefore the maximum amount of heat it can carry. The maximum heat transport the pipe can take is given by $Q_{max} = mL$, which can be written in calculable terms in equation (3.3-11).

$$Q_{\max} = \frac{\rho_l \sigma_l LKA_w \left(2\frac{1}{r_e} - \frac{\rho_l gl \sin(\varphi)}{\sigma_l} \right)}{\mu_l l} \qquad (3.3\text{-}11)$$

It should be noted that φ is considered negative when the condenser is above the evaporator. In the final MSR design, the heat pipes protrude downwards out of the reactor. This causes the term due to gravity to become negative, meaning that gravity impedes the liquid in returning to the evaporator. The effect is negligible compared to the flow rate inside the heat pipes, especially due to the low gravity on the Moon and Mars. It should also be noted that the r_e term on the bottom of the fraction means that using a mesh wick with smaller spacing between mesh fibers will greatly increase the heat one can send through a heat pipe.

During normal operation, the capillary limit is the main limiting factor restricting the heat flow through the heat pipe. Following in Table 3.3-2 is a short summary of the relative magnitudes of the terms in the equation as they relate to our design.

Table 3.3-2: Expected Values in the Capillary Limit Equation

Terms	Expected Values
ρ, σ, L and μ	Determined by the properties of the working fluid
K	$\sim 10^{-10}$
r_e	0.01mm - 0.1mm
g	Moon: 1.62 m/s^2 ; Mars: 3.69 m/s^2
A_w	Determined by the wick structure

As will be shown below this will give a maximum heat transport per pipe approximately 1-30kW per pipe.

In addition to the five physical limitations on the heat pipes, there are also three reactor-design specific limitations. The three basic components of the heat pipe are the working fluid, the wick structure and the wall of the pipe. The parameters involved in choosing these include the heat output of the reactor, the temperature of the reactor, the geometry of the reactor and the power conversion system employed.

Working Fluid

Since the main limit of the heat pipe is the capillary limit, choosing the fluid's properties is quite important. First, the working fluid must have a temperature range compatible

with that of the core. Next, it should have a high latent heat of vaporization, since the phase change stores the heat. Of course, the fluid should be compatible with the wick materials and the wall of the pipe to prevent corrosion. The fluid should also be compatible with the materials in the reactor should a pipe rupture for some reason. Higher vapor densities and surface tensions increase the heat flux, as does lowering the liquid and vapor viscosities to enhance flow.

Wick Material and Design

The purpose of the wick is to provide as much capillary pressure as possible [8]. The wick should be thick enough to contain all the liquid, but thin enough to prevent film boiling and let bubbles escape. In order to achieve the highest capillary pressure possible, one should increase both the permeability and wick area, while decreasing the spacing between the mesh fibers. Using a finer mesh accomplishes this balance.

Many different types of wicks are available, each with its own advantages and disadvantages, depending on the situation. Figure 3.3-2 shows diagrams of different types of wicks.

Figure 3.3-2: Mesh Wicked, Grooved, and Arterial Wicked Heat Pipes

Pipe Wall

The pipe wall should be thick enough to withstand the pressures on either side of the wall and strong enough to withstand mechanical stresses. A high thermal conductivity will also increase the radial flux, since the inner workings of the heat pipe are far more thermally conductive than even pure metals.

Design Choices and Specifications

Due to the design team's decision to create a high temperature system, the only viable working fluids at 1800 K are lithium, silver and lead. The choice is straightforward, since

lithium is an order of magnitude less dense than both lead and silver. Therefore, because of the design temperature and mass requirements, lithium is the working fluid for the MSR heat pipe system.

This choice defines many key parameters used in calculating the limits in heat flux. Table 3.3-3 summarizes the heat flux limits considering a lithium working fluid.

Table 3.3-3: Properties of Lithium at 1800 K [6]

P	3.190 bar
L	18670 J/kg
σ	0.212 N/m
ρ_v	0.2839 kg/m^3
ρ_l	380.9
μ_v	0.0000159 Ns/m^2
μ_l	0.0001432
K	73.00 W/mK

Reactor geometry defines the other parameters. The reactor is a cylinder with radius of 24 cm and height of 42 cm. This defines the evaporator length as 42 cm in order to maximize the surface area in the reactor, reducing the radial heat flux on each heat pipe. This also defines the number of heat pipes in the reactor to be 127, at a radius of 1 cm, since the reactor needs a heat pipe volume fraction of 25% in order to provide enough space for the fuel pins and structural materials.

These parameters determine much of the capillary limit defined by equation (3.3-11). The next choice is in the wick structure.

A simple wick is chosen, using twenty layers of 400-mesh Nb-1%Zr wire with a wire diameter of 0.025 mm. This gives a pore radius (r_e) of 0.015 mm, the Blake-Kosney relation, equation (3.3-12), calculates its permeability:

$$K = 0.015015 \frac{d_w^2 (1-\varepsilon)^3}{\varepsilon^2} \qquad (3.3\text{-}12)$$

The permeability for this wick is $0.302*10^{-10}$, using a wire volume fraction, ε, of about 30%. A 0.5 mm gap will also be present between the wall and the wick to allow for more liquid lithium. The cross sectional area of the wick is given by $2\pi\ r_{pipe}\ t_{mesh}$ or about 0.628 cm^2.

For simplicity's sake, the design group chose the length of the heat pipe to be one meter and the radius to be one centimeter. This gives an l/d ratio of 50, which should keep it structurally sound. A wall thickness of 2 mm should be sufficient to withstand mechanical damage. Recent studies done by El-Genk and Tournier with nearly identical parameters confirm this assumption [13]. The wall will also be made out of Nb-1%Zr to ensure wick-wall compatibility.

The principle limiting factor of heat pipe heat flux is determined from the five main limiting factors described above: the capillary limit, sonic limit, viscous limit, entrainment limit and the boiling limit . Using the parameters given in equation (3.3-11), the heat flux due to the capillary limit was determined to be about 27.5 kW per heat pipe. Similar studies using lithium heat pipes in space reactors have yielded very close results to this calculated value [13].

Using a pressure of 3.19 bar in the sonic limit of equation (3.3-9) gives a maximum heat transfer of 819 kW per heat pipe. This is clearly not a limiting factor unless the tube is at a very low pressure, which would occur immediately following startup. Equation (3.3-8) determined the viscous limit to have a heat transport limit of 32 MW per heat pipe, which is well above the capillary limit. Entrainment could potentially become a concern for this design if the wick is not properly designed. Equation (3.3-10) determined the entrainment limit to be $11.48*z^{-½}$ kW per pipe for this design. Since z relates to the wire spacing, the design group will design the wick so that entrainment does not become an issue. Other literature has shown the entrainment limit for similarly designed heat pipes to be in the 20-40 kW range [6].

The maximum radial heat flux for a single Nb-1%Zr heat pipe is cited at 115 W/cm^2 for a vapor at 1800K [8]. Since each heat pipe has a surface area of 251 cm^2 inside the core, this allows for a boiling limit heat flux of 30.16 kW per heat pipe, which is also greater than the capillary limit. Thus, the capillary limit is the primary limiting factor in the heat flux calculation, with a maximum axial heat transfer of 27.5 kW per heat pipe.

Analysis of Possible Failure Modes and Design Margins

The core geometry specifies a 25% volume fraction of heat pipes using a tricusp fuel pin arrangement consisting of a fuel pin surrounded by heat pipes. With this arrangement, six adjacent heat pipes surround each heat pipe, see Figure 3.3-3. Given the geometry of the core, 127 heat pipes can comfortably fit inside. This gives an average heat transport of only 9.4 kW in each pipe, well below the limit calculated. However, the design group must consider reactor hot spots, and each heat pipe should be able to compensate should an adjacent heat pipe fail.

Given a 1.2 MW_{th} reactor system of 127 heat pipes, and an aggregate peaking factor of no more than 1.25, each heat pipe must be able to safely transport out 7/6 of its normal heat capacity should one fail. Let us assume the heat pipe at the reactor hot spot fails, leaving the adjacent six to remove its heat. These heat pipes would see a reactor giving out 1,200,000*1.25*(7/6) = 1,750,000 W. This means the heat pipes adjacent to the failed heat pipe must remove 13.78 kW of heat, which is still well below its design limitations. This also means that, should a transient occur during failure of the hot spot heat pipe, the minimum operating margin of each heat pipe is 48%. Even if the reactor power level doubles, the heat pipes will still be able to remove the heat.

Coupling to the Power Conversion System

The thermionic devices selected as the PCU can handle a heat flux up to 83 W/cm^2. Given that the condenser section is approximately 40 cm long, this allows for the transfer of 2.086 MW of energy through the thermionic system. Given an efficiency of 10-18% this would produce between 100 kW and 187 kW of electrical energy for a 1 MW_{th} core. This would require covering only 20 cm of each heat pipe with thermionic emitters, since each heat pipe only transfers 10 kW_e in a 1 MW_{th} system. Therefore, thermionic cells have more than enough heat pipe surface area available to produce the goal of 100 kW_e. The thermionics will be kept as far from the core as possible to avoid excessive damage from neutrons traveling up the vapor core of the heat pipe. The higher the thermionics are from the core, the less damage they will receive, as fewer neutrons will penetrate the holes in the 10 cm axial shield and reach the thermionics.

3.3.5 Summary

One hundred and twenty seven meter-long lithium heat pipes, with an outer radius of 1 cm, cool the core. The heat pipe arrangement is shown in Figure 3.3-3.

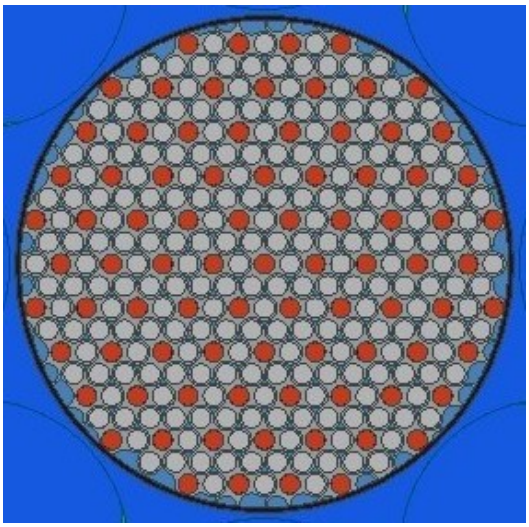

Figure 3.3-3: Heat Pipe and Fuel Pin Arrangement, Heat Pipes are Red.

A 2 mm Mo-1%Zr outer wall, with a mesh made out of similar material, forms the structure of each heat pipe. There is also a 0.5 mm annulus to allow for greater liquid flow along the wall of the heat pipe.

The capillary limit of 27.5 kW per pipe is the limiting factor during steady state operation. This would allow continuous operation to take place, with large operating margins, even in the case of a heat pipe failing at the hot spot of the core.

The heat pipes have a 42 cm evaporator section in the core and a 20 cm adiabatic section outside the core. The condenser section is only 20 cm long since each heat pipe only transfers 10 kW, resulting in enough surface area for the thermionics to work at their full potential. If the system is scaled-up for Mars to 2 MW_{th}, this would require a condenser length of 40 cm to produce 200 kW_e.

3.4 Fuel Design

Fuel encompasses many components of the reactor design, and so the design team addressed the fuel design issue in pieces: the fuel form and the fuel configuration. The

fuel form is the molecular and isotopic composition of the fuel. The fuel configuration is the physical arrangement of the fuel.

3.4.1 Fuel Form

The fuel selection for a Lunar or Martian reactor is not unlike terrestrial fuel design. There are several general parameters necessary for any operating environment; however, additional considerations require attention when designing fuel for extraterrestrial use. Lack of refueling ability and minimal maintenance requirements in space limits acceptable tolerances in fuel swelling and physical failure, thus constraining available choices. A fast neutron spectrum further limits fuel possibilities. Basic physical arguments constrained by the design goals laid out in Chapter 2 narrow down the vast array of possible nuclear fuels to three options, further evaluated in this section using the decision methodology.

This section will compare design parameters such as chemical compatibility, chemical and physical stability, fuel swelling, fissile material density, radiation effects and heat transfer characteristics of possible fuel choices. Transcending the physical parameters described above are overall reactor design considerations directly related to the fuel selection, such as desired burnup and reactivity changes due to poisons and fertile isotopes.

Isotopic Considerations

At the top of the decision-making hierarchy sits the selection and relative concentration balance of fissile and fertile isotopes in the fuel. The design group considered many fissile isotopes, including the common ^{235}U, ^{233}U and ^{239}Pu, as well as more exotic ^{242m}Am, ^{245}Cm and ^{237}Np. Fissile isotope choice depends on several parameters; chief among them are the relative fission cross sections in the fast neutron energy regime. Figure 3.4-1 shows fission cross sections as a function of energy for the six isotopes in the fast region.

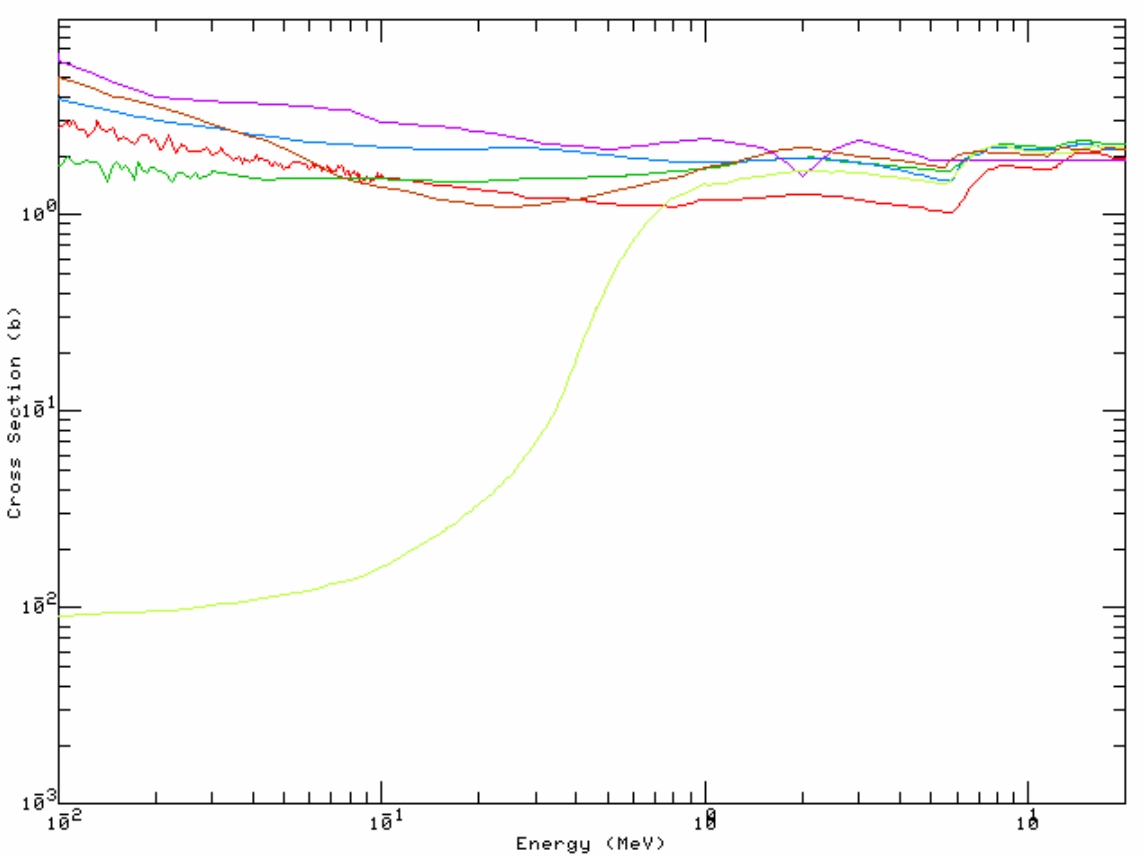

Figure 3.4-1: Fast Fission Cross Sections for Isotopes Considered (Red: 235U, Blue: 233U, Green: 239Pu, Purple: 242mAm, Light Green: 237Np, Brown: 245Cm) [15]

While fission cross sections are slightly higher, and consequently the critical mass is comparatively smaller, for ^{245}Cm, the relative scarcity of the isotope is restrictive. Also, there is very little literature about the chemical and physical properties of ^{245}Cm in a high radiation environment. ^{237}Np is also an alternative to the more common uranium and plutonium fuels in the fast region; however, the fission cross section is inferior, as shown in Figure 3.4-1.

The design team considered the use of ^{233}U for a fast-spectrum ^{232}Th/^{233}U breeder reactor. The Indian government has shown this concept is feasible for terrestrial applications; however, the fuel is highly radioactive, even in pre-fabrication, due to buildup of ^{232}U [16]. Furthermore, common breeder reactors require fuel batching, an impossible procedure for space applications.

The nuclear space application community has considered ^{242m}Am in recent years as a possible fuel for space applications. The isotope has an extremely small critical mass and irradiating ^{240}Pu can produce ^{242m}Am on a small scale. However, enrichment beyond 8.5 percent is cost prohibitive. Similar to curium and neptunium, there is relatively little literature on the chemical and physical properties of americium compounds exposed to reactor conditions. Due to the reasons stated above, the design team further investigated ^{235}U and ^{239}Pu.

The relative merits of choosing ^{235}U or ^{239}Pu are highly debatable. Two considerations appear to give the advantage to the use of uranium over plutonium. First, plutonium is particularly hazardous to human health because of its high radiotoxicity. Second, detailed chemical characteristics and physical properties data are available for a multitude of uranium-based fuels. Third, the plutonium fuel would have to come from weapons or reactor grade Pu. Weapons grade Pu is economically prohibitive and poses a proliferation risk, while reactor grade Pu is quite radioactive. As a minor design goal, the space reactor should rely on commercial "off-the-shelf" technology (COTS) and uranium best fits that requirement. Safety and potential R&D costs, as well as unknown trans-uranic properties have eased the choice of ^{235}U as fuel for the space reactor.

Having chosen ^{235}U as the fissile isotope, there are several types of fuel compounds that warrant consideration. Compounds with known properties in high radiation conditions include uranium metal, UZrH, U_3Mo, SiC-C-UO_2, UC, UCZrC, UO_2, UN, U^{15}N, UN (with W, W-Re and Mo), UCZrN, US and various arrangements of coated particles. Stated design goals, such as the desired fast spectrum, COTS technology and minimal maintenance, lead to the elimination of some of these compounds right away.

The low uranium density will cause Si-C-UO_2 and UN cermets to be undesirable choices because the core size will become relatively large. Furthermore, their moderating characteristics will cause a spectrum shift towards epithermal. Well-documented inconsistencies in fuel fabrication eliminate UO_2/Re, W and Mo fuels [17]. The goal of minimizing moving parts outcasts the possibility of using coated particle fuels in a pebble bed reactor setting. The high temperature requirement of 1800K further eliminates UZrH

and U_3Mo because these fuels melt below 1000K [17]. Attractive chemical and neutronic properties make US a possible fuel, however, a low uranium density of 9.58 gm/cm^3 leaves it as an unattractive alternative [18].

Thus, there are three major fuel types left to compare for the reactor fuel: UN, UC and UO_2. Below are the relative advantages and disadvantages of these fuel types. It is important to note that in terms of operation in space, fuel failure is equivalent to mission failure.

To begin the comparisons, Figure 3.4-2 below shows a melting point versus density graph for the remaining options. High density complies with one of the reactor core goals and high melting point allows for safer core operation, so it is desirable to have points in the upper-right of the chart. Uranium metal is included for reference. Only a slight advantage goes to UN.

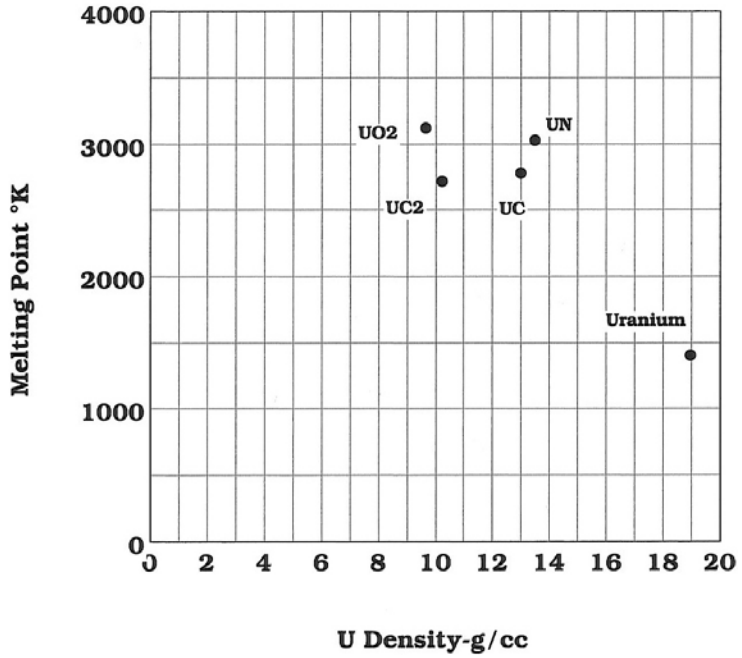

Figure 3.4-2: Uranium Density versus Melting Point Temperature [17]

Thermal Properties

Fuel should have good heat transfer characteristics; specifically, a high thermal conductivity to allow a flat temperature distribution in the fuel. By analyzing the thermal conductivity versus temperature graph shown in Figure 3.4-3, further comparisons are

possible. UN again has a slight advantage but UC follows closely. UO_2 clearly is not on par with the other compounds in this category.

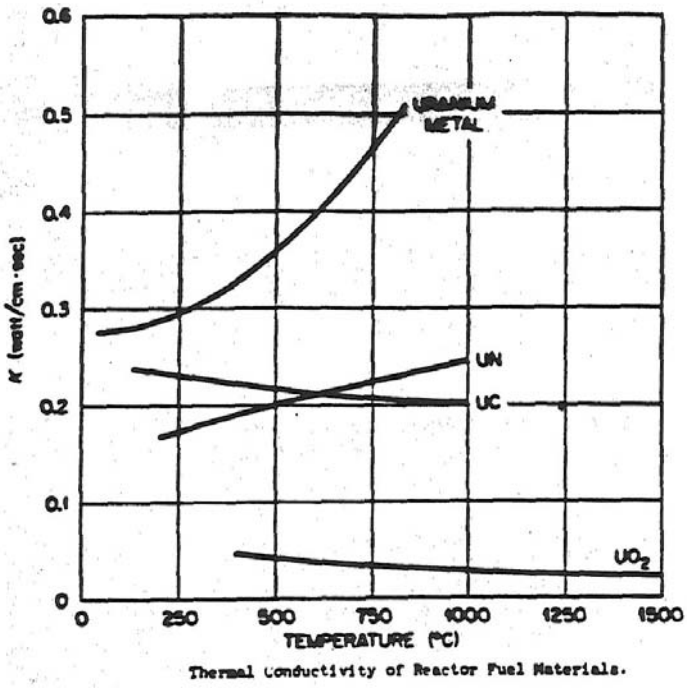

Figure 3.4-3: Thermal Conductivity of Fuel Candidates versus Temperature [17]

The design group examined the temperature profile in various fuel pellets to understand the temperature distribution in the pellets better. For the case of a power density of 200 W/cm^2 and a 1.3 cm fuel pin outside diameter, Figure 3.4-4 displays the temperature profile in UC, UN, and UO_2. The similarity between UN and UC is nearly perfect and, as expected, UO_2 has a sharply peaked centerline profile.

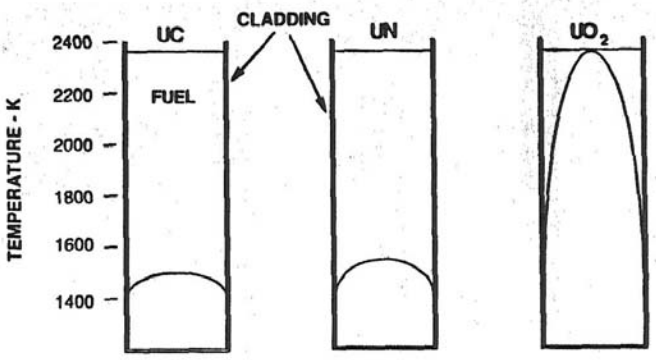

Figure 3.4-4: Temperature Profiles for UC, UN, and UO_2 [17]

Fission Product Interactions

Aside from thermo-physical properties of the fuel, it is necessary to consider the effects of fission product build up. Physical and dimensional instabilities from fission gas generation limit reactor fuel lifetime. One of the major problems with fuel burnup is the buildup of fission products in the pellets. This buildup occurs as uranium splits and creates gaseous fission fragments, causing swelling. The addition of solid fission fragments can also cause expansion. Figure 3.4-5 shows the pellet swelling versus temperature for candidate fuels in the early stages of operation. For this parameter, UC appears superior to UO_2 and UN fuels. Although not depicted, it is notable that swelling is linear with burnup.

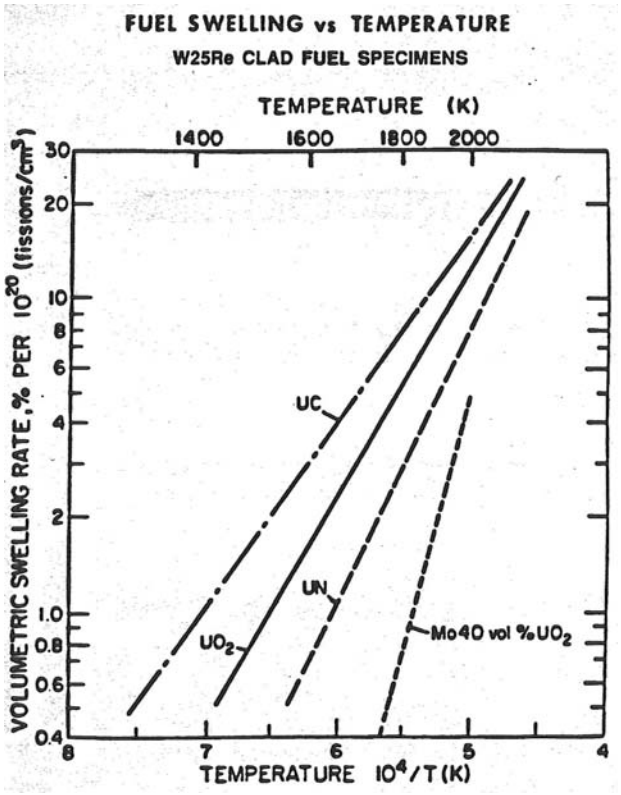

Figure 3.4-5: Volumetric Swelling Rate versus Temperature [17]

Further complicating the problem, gaseous fragments that escape the pellets can increase pressure within the cladding, a problem generally solved by engineering open spacers on the ends of the fuel pins [20]. One other defense often employed is to leave a gap between the pellet and cladding, sometimes filled with helium. Another method is to cusp

the fuel pellets in the manner shown in Figure 3.4-6. As the fuel burns, the pellets can expand into the air gap and reform the cusps.

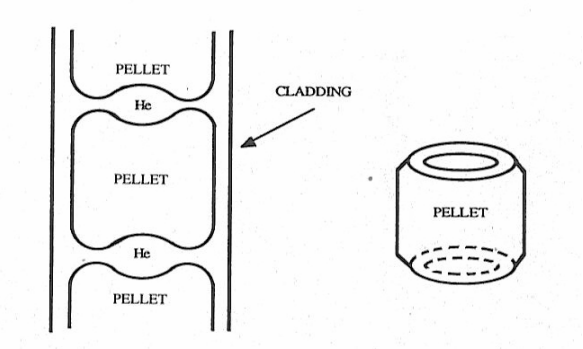

Figure 3.4-6: Drawing of Cusped Fuel Pellets [20]

Cusps do not solve the problem entirely as fuel pellets can still fail, which we assumed to be undesirable. Therefore, the compound chosen should allow the migration of fission products, especially gasses, to relieve some of the pellet's internal pressure. Figure 3.4-7 displays the vapor pressure, which can cause the pellet to burst, as a function of temperature for various compounds. The UC fuels exhibit superiority over other compounds. UO_2 exhibits the second lowest pressure, while UN has the highest. A notable property of UC is that, with burnup, the porosity of the compound will shift from open to closed, disallowing gaseous fission product escape and causing further swelling, which the design team assumed would lead to fuel pellet failure. [17]

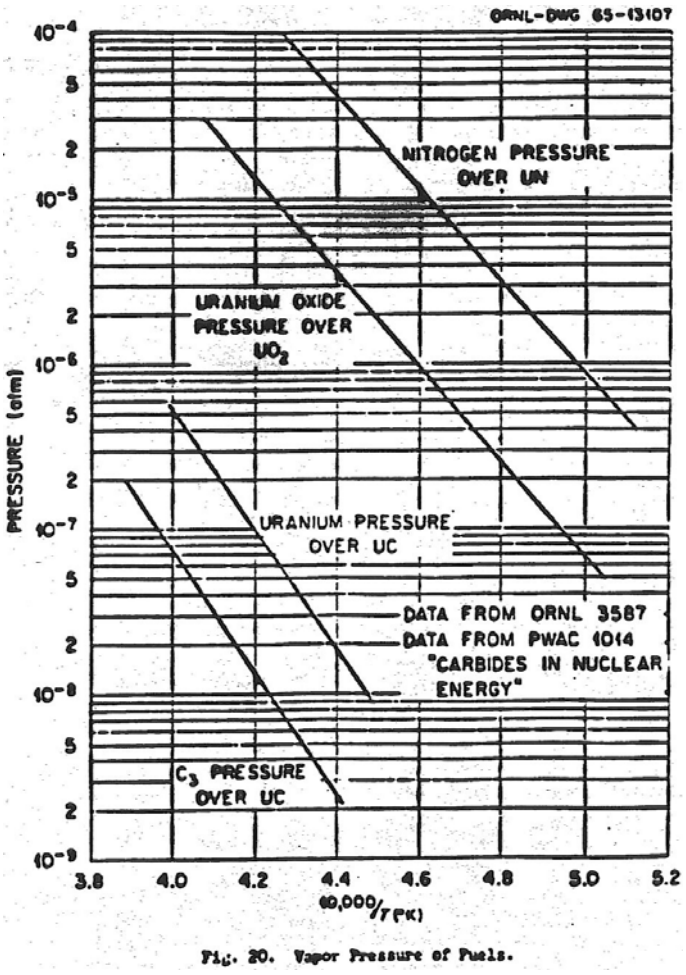

Fig. 20. Vapor Pressure of Fuels.

Figure 3.4-7: Vapor Pressure of Candidate Fuels versus Temperature [17]

Spectrum Considerations

The neutron spectrum shifts due to the fissile material and moderating characteristics of the fuel. One measure of merit for various fuels is the average neutron energy of the spectrum. For UO_2, the average energy is 281 keV; for UC, it is 312 keV; and for UN, it is 348 keV [18]. Of all well-known ceramics, UN has the hardest spectrum [18]. Given the choice of a fast spectrum, UN therefore gains an advantage over the other two options.

Chemical Interactions

Various chemical reactions constrain the design of the core. Almost all ceramic fuels will react with CO_2, leaving them at a disadvantage to metallic fuels; however, the low melting points exclude the use of all metallic fuels. An argument against the use of

ceramic fuels is CO_2 ingress on the Martian surface, however, should CO_2 ingress occur, other components of the reactor would have failed before the ingress reached the fuel. The possibility of ingress highlights the need to quarantine the reactor system from the Martian atmosphere, a sealant problem commonly faced in terrestrial applications and easily overcome. The important conclusion to use ceramic fuels places a restriction on the use of CO_2 coolants.

Additionally, UC cannot be placed in contact with potential cladding materials such as Rhenium, Molybdenum or Niobium because there will be corrosive reactions; UN will also react unfavorably with Niobium.

Fertile Fuel Form

To extend the lifetime of the MSR to at least five years, the design team chooses to incorporate fertile material in the design to flatten the reactivity versus burnup curve via breeding. At the beginning of life, the core will have no excess reactivity due to the fertile isotopes. As burnup takes place, fertile isotopes will breed fissile isotopes, causing a gradual addition of reactivity into the system. This slow addition will counteract the downward reactivity slope of a purely fissile system, especially near the end of core life. The combination of poison burnup towards the beginning of life and breeding buildup towards the end of life will stabilize the neutron economy, keeping the reactivity curve as straight as possible.

Three fertile isotopes were identified for their breeding potential: ^{232}Th (for ^{233}U), ^{238}U (for ^{239}Pu) and ^{240}Pu (for ^{242m}Am). For the three fertile isotopes, Figure 3.4-8 below depicts absorption cross section plots as a function of energy. Given the fissile fuel selection of uranium, in the reactor, ^{238}U will be abundant in company with ^{235}U, thereby eliminating the need of further addition of ^{238}U. The relative unavailability of high purity ^{240}Pu is a drawback as well as its high spontaneous fission rate, which leads to neutron radiation hazards. The design group scrutinized ^{232}Th in much more detail because ^{232}Th is extremely abundant in the earth's crust.

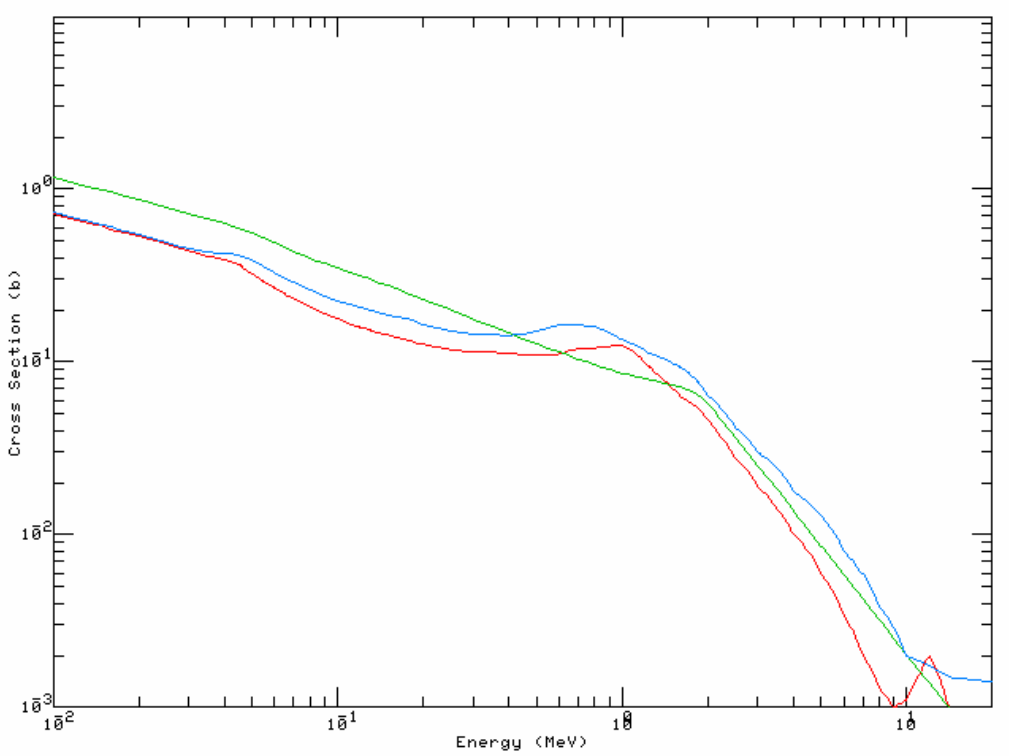

Figure 3.4-8: Fast Absorption Cross Sections for the Isotopes Considered (Red: 238U, Blue: 232Th, Green: 238Pu) [15]

^{232}Th has well-known chemical and physical properties in the form of ThO_2, but the neutronic performance of ^{232}Th is worse than ^{238}U. The average number of neutrons produced per fission, ν, is higher in a fast spectrum for a ^{238}U system than a ^{232}Th system. Therefore, the design group decided the reactor will utilize the breeding of ^{238}U, already in the fuel, as a way to add reactivity to the core as burnup increases.

Decision Methodology

Summarized below are the relative physical advantages of the four major compounds under consideration. For uranium carbide, advantages include a low vaporization rate, a high uranium density and a high thermal conductivity. Its disadvantages are a high swelling rate, reactions with rhenium, molybdenum and niobium and the porosity shift. Uranium dioxide has several advantages including high chemical stability, fuel swelling saturation, and almost no reaction with rhenium or molybdenum. Its disadvantages are low thermal conductivity, low fuel density and high vaporization rate. Uranium nitride has the advantage of the highest uranium density (of refractory materials), a hard spectrum, a high thermal conductivity, and will not react with almost all cladding and

matrix materials. Its disadvantages include the high N_2 overpressure and reaction with niobium.

The design group used the decision methodology to make the final decision of the fuel form, taking these benefits and drawbacks into consideration. An additional design criterion, fuel specific properties, was added to the design methodology to address important fuel characteristics that did not fit into the other design criteria. As a result, the design group chose uranium nitride as the MSR fuel form. Table 3.4-1 below presents the decision matrix.

Table 3.4-1: Fuel Type Decision Methodology Matrix

		Fuel Type		
		UN	UC	UO2
Criterion	***Small Mass and Size (Cost) - 1.35 (High Uranium Density)***			
	Small Fuel Mass	3	2	1
	Small Reflector / Moderator Mass	2	2	2
	Small Dimensions	3	2	1
	Fuel Specific Properties - 1.25			
	Spectrum Hardness	3	2	1
	Thermal Conductivity	3	2	1
	Fuel Swelling	3	1	2
	Overpressure	2	1	3
	Reactions with Cladding	2	1	3
	Launchable/Accident Safe - 1.13			
	No Criticality Accident	2	2	2
	Fits in Rocket	2	2	2
	Controllable - 1.14			
	Flat Keff	2	2	2
	Ex-Core Control	2	2	2
	Slow Transients	3	1	2
	High Reliability and Limited Maintenance - 1.00			
	Few Moving Parts	2	2	2
	Little Radiation Damage	2	2	2
Performance Index		*41.05*	*29.82*	*29.51*

Design Optimization

Criticality and neutron economy over life depends on the chosen ^{235}U enrichment. The enrichment of the ^{235}U in the reactor directly depends on the desired burnup, with consideration given to maintaining a flat reactivity during the lifetime of the core. Enrichment levels available to the space program will add an additional constraint. Section 3.7.1 presents a discussion of uranium enrichment.

In addition to ^{235}U enrichment, the enrichment of nitrogen in the isotope ^{15}N will be required for a substantial improvement in neutronics. This will lower the self-absorption of the fuel because capture reactions are less likely for ^{15}N than ^{14}N, as shown in Figure 3.4-9. The cost of nitrogen enrichment is not restrictive at around $100/g [21].

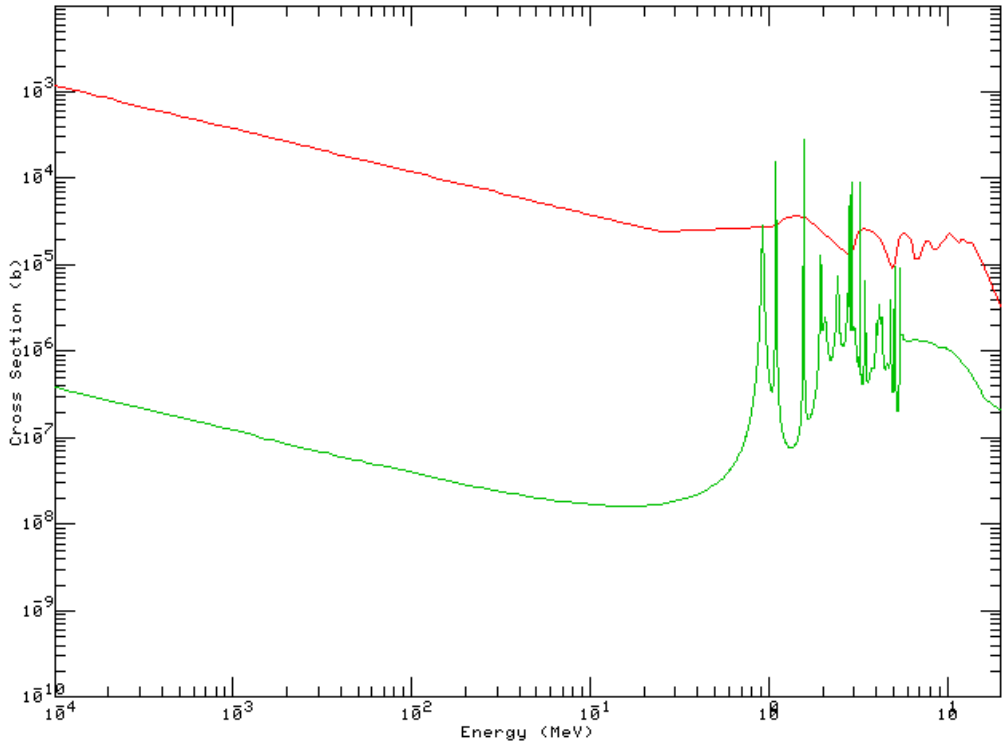

Figure 3.4-9: Radiative Capture Cross Sections for ^{14}N (red) and ^{15}N (green) [22]

Summary

The choice of fuel for the MSR is uranium in the form of uranium nitride with ^{238}U as the fertile breeding material. Subsequent relevant sections discuss the variable combination of atom percentages and enrichments as well as pellet locations in the lattice. The

combination of $U^{15}N/^{238}U$ fuel meets the goals of the surface reactor by having an extremely low rate of corrosion, high melting temperature and high density. Most importantly, a relatively flat reactivity curve creates an easily controlled reactor.

3.4.2 Fuel Element Configuration

The design group split the fuel element design into two parts: the configuration and the cladding. The configuration refers to the physical arrangement of fuel pellets while the cladding is the material that surrounds the fuel pellets in its smallest arrangement. Presented in this section is the fuel element configuration design and then the cladding design follows in Section 3.4.3. The design group compared pin, plate and block fuel elements using the design criteria identified in Chapter 2. Cladding design followed a similar approach when comparing the various possible materials.

Within the project's four main design criteria, it was necessary to identify sub-criteria specifically applicable to fuel elements. In regards to small mass and size, the fuel elements should use fuel efficiently, have a large surface area for effective heat transfer, and must be compatible with heat pipes. For launchable/accident safe concerns, the fuel elements must have the ability to withstand launch forces and should not be susceptible to single point failures. Here a single point failure is a rupture in the fuel cladding which would release all fission products. Controllable refers to the decision to use ex-core control to reduce moving parts. The fuel elements must allow for ex-core control. Lastly, high structural stability fulfills the high reliability/limited maintenance design criterion.

Options

The design group considered three types of fuel elements: pins, plates, and blocks. The most obvious differences between these options are the surface area available for heat transfer and fuel mass needed for criticality. Surface area is a large component of determining power density in the core, the larger the surface area the greater the power density can be because heat removal is more efficient. For this criterion, blocks are superior to plates, which are superior to pins [23]. For fuel mass, block elements require less mass to reach criticality than plates, while pins require the most.

Block elements, however, have lower leakage and less parasitic neutron absorption in cladding and structural materials. In addition, the available literature has not demonstrated ex-core control can be used with block fuel elements. Therefore, while block elements are attractive from a mass and surface area perspective, this option is extremely unattractive as it might prevent ex-core control.

In the area of structural stability and integrity during launch, pin elements far exceed plates and blocks [24]. Blocks and plates have inferior support structures due to axial joints as well as radial joints. Pins, though they may rattle during launch, have the support structure to prevent the fuel assemblies from falling apart. In terms of stability due to fuel swelling and fission product gases, pins are also more robust than block fuel elements because the cladding absorbs the expansion stress instead of the heat pipes.

Lastly, the fuel elements must be compatible with heat pipes. Heat pipes operate most effectively in a cylindrical shape and are easiest to construct in this form. A cylindrical heat pipe contains internal pressure with smaller pipe thicknesses than rectangular or square heat pipes, which in turn decreases mass and increases reliability. In addition, the scientific community has a greater understanding of the thermal hydraulic characteristics of cylindrical heat pipes. The Marshall Space Flight Center has already tested the tricusp fuel pin/heat pipe configuration. Other fuel elements would require extensive testing and possibly new technology [24].

Regardless of fuel element configuration, a filler material between the heat pipes and the fuel elements is necessary to improve heat transfer from the fuel elements to the heat pipes. In general, adding this material does not degrade the heat transfer significantly but adds mass to the system. Ideally, the fuel element and corresponding configuration should minimize the amount of filler material needed to reduce system mass. The block system would be ideal because the heat pipes could simply penetrate into the blocks, however, heat pipes do not support high power densities. A tight lattice pin arrangement would require a smaller amount of filler material than plates.

Decision Methodology

The design group employed the decision methodology to determine the best fuel element configuration. Table 3.4-2 below shows the decision matrix. Outranking the other two options, fuel pins best fulfill the design criteria.

Table 3.4-2: Fuel Element Decision Matrix

		Element Type		
		Pin	Plate	Block
Criterion	***Small Mass and Size (Cost) – 1.35***			
	Small Fuel Mass	1	2	3
	Large Surface Area	1	2	3
	Compatibility with Heat pipes	3	1	1
	Launchable/Accident Safe – 1.13			
	Integrity During Launch	3	2	1
	Single Point Failure	3	2	1
	Controllable – 1.14			
	Ex-Core Control	3	3	1
	High Reliability and Limited Maintenance – 1.00			
	Structural Stability	3	1	1
Performance Index		*19.95*	*15.69*	*13.85*

Discussion

Fuel pins are an excellent choice for the MSR fuel element. The knowledge base with fuel pins is more extensive than the other fuel element configurations. Pins are also optimal for use with heat pipes. All current designs with heat pipes use a tricusp pin configuration. Figure 3.4-10 depicts the tricusp configuration. The tricusp surrounds a heat pipe with fuel pins. In the MSR design, there are three fuel pins to every heat pipe, and other tricusps interface such that all heat pipes share the thermal load evenly.

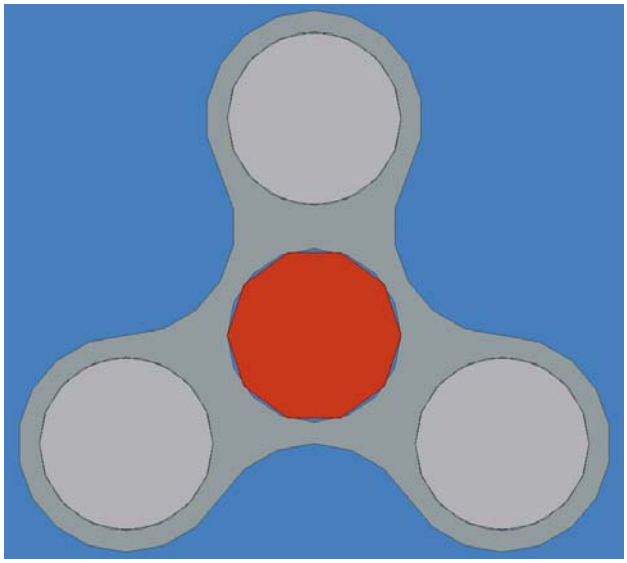

Figure 3.4-10: Tricusp Configuration with Three Fuel Pins (light grey) and One Heat Pipe (red)

The design of the fuel pins, regarding size and uranium enrichment, address areas where fuel pins scored lowest in the decision matrix. For example, decreasing the size of the fuel pins increases the percent surface area. The reactivity of each pin is consequently smaller, but higher enrichment solves this problem. Small radius and higher enrichment will mitigate the larger fuel mass required for pins when compared to plates and blocks.

Lastly, the ease of manufacture and experience with fuel pins keeps the development time for the MSR small. The existing knowledge base with terrestrial fuel pins is invaluable in the fuel element design.

3.4.3 Fuel Element Cladding

The choice of cladding material is constrained by several parameters. Generally, the cladding for a fast reactor should have low neutron absorption and low neutron moderation. Given the fuel selection and operating temperature of 1800 K, the cladding must be physically inert with UN and have a high melting temperature. It must not corrode over a wide range of temperatures and must not succumb to radiation embrittlement. Additionally, high tensile strength is desirable for accident scenarios. Finally, the cladding should have high thermal conductivity, despite its generally thin width, because it is the heat conduction interface between fuel and coolant.

Keeping with conventional fuel design, there will be an air gap between the fuel and cladding material to allow for fuel swelling and space for gaseous fission fragments to escape. The design characteristics section at the end of this section further discusses cladding and gap thicknesses.

Options

The design team investigated several options for cladding materials, including conventional PWR and BWR materials such as zirconium metal, Zircalloy-2, Zircalloy-4, Incaloy, Stainless Steel-304 (SS-304) and Stainless Steel-310 (SS-310). Other options more suited for fast reactors were considered as well, including tungsten metal, various tungsten alloys, niobium metal, Nb-1Zr, molybdenum metal, V-20Ti, rhenium metal, Re-Mo alloys, and titanium metal.

Early reactor designs of the 1970's often employed Stainless Steel (SS) cladding, SS-304 and SS-310, but zirconium-based cladding replaced SS cladding in advanced reactor designs. Following suit, the surface reactor will not use stainless steel cladding because the absorption cross sections are on the order of barns for unmoderated fission spectrum neutrons. [25]

As reactor design advanced, so did cladding material research, which led the nuclear industry to adopt zirconium metal, Zircaloy-2 and Zircaloy-4. Most reactors still use variations of zirconium alloys today because of several desirable properties. One important property of zirconium alloys is high thermal conductivity. Zircaloy-2 and Zircaloy-4 have a thermal conductivity between 21.2 - 32.6 W/mK in the temperature range of 100 – 1500 K [26]. There are drawbacks, however, to the use of zirconium alloys in space. For example, Zircaloy-2 and Zircaloy-4 have a low density of 6.55 g/cm^3 [27].

Although other reactors have used Incaloy cladding, the MSR will not use this type of cladding. Despite the relatively competitive thermal conductivity of 25.5 W/mK, the neutron absorption cross section is high in a fast spectrum and the melting temperature is 1755 K, which is too low [28]. Chemical reactivity prohibits the use of niobium-based

alloys as cladding for uranium nitride fuel. Loss of ductility and appearance of grain boundary fractures at high temperatures also prohibits the use of V-20Ti despite its previous use in terrestrial fast reactors [29].

Molybdenum metal, while not subject to hydrogen embrittlement, was unsuitable because of diminished strength at high temperatures [30] [31]. Even though molybdenum has a high melting point, it is not useful for industrial applications above 1470 K because of lowered tensile strength [32]. Furthermore, common molten metals such as iron, aluminum and tin will readily damage molybdenum metal at temperatures above 1270 K [31].

The design group also investigated titanium metal since it has high thermal conductivity and is mostly corrosion resistant. Titanium has a high melting point of 1941 K, which is attractive, but the large neutron absorption cross section, on the order of barns, is a major concern. For convenient comparison, Table 3.4-3 presents the physical properties for all cladding materials seriously considered.

Table 3.4-3: Cladding Properties of Materials Under Consideration [25] [26] [27] [28] [29] [30] [31] [32]

	Tensile Strength (GPa)	Melting Point (K)	Thermal Conductivity (W/m*K)	Density (g/cm^3)	Chemical Reactions	Absorption cross section (barns)
Rhenium Metal	454	3459	71	21.2	Extremely inert	0.2
Re-Mo (4/9 Re)	365	2723	36.8	13.55	Oxidizes at >1300 K in air	0.4
Molybdenum Metal	~970	2890	148	10.22	Reacts with molten metal at high temperature	0.2
Tungsten Metal	430	3640	166	19.3	Oxidizes when metal is red hot	0.06
Niobium Metal	~310	2770	52	8.55	Reacts with UN	0.3
Zircaloy -2, Zircaloy-4	296	2123	23	6.553	Mostly inert	7.8
SS-304	200	1672	21.4	7.9	Inert	~4.3
SS-310	200	1773	14.2	8	Inert	~4.3
Incaloy	160	1755	25.5	7.25	Mostly inert	~5.6
Zirconium Metal	68	2128	23	6.5	Inert	7.934
Titanium Metal	116	1941	22	4.5	Mostly inert	2.243

The above analysis and tabulated comparison effectively reduces the options to two: rhenium metal and tungsten metal. As can be seen in the table above, the two metals have very similar properties. Tungsten gains a slight advantage for its higher thermal conductivity; however, this metric of comparison carries less weight than for other materials in the core because the cladding will be relatively thin, leaving the potential for a lower thermal gradient. Both rhenium and tungsten have high densities and high melting points. Rhenium metal has an extremely good corrosion resistance as well as a lack of chemical impurity poisoning [33]. Tungsten has a slight reactivity with sodium, which could potentially be a problem if sodium was the coolant [31]. Tungsten also gains an advantage over rhenium for its slightly lower absorption cross section as seen below in Figure 3.4-11.

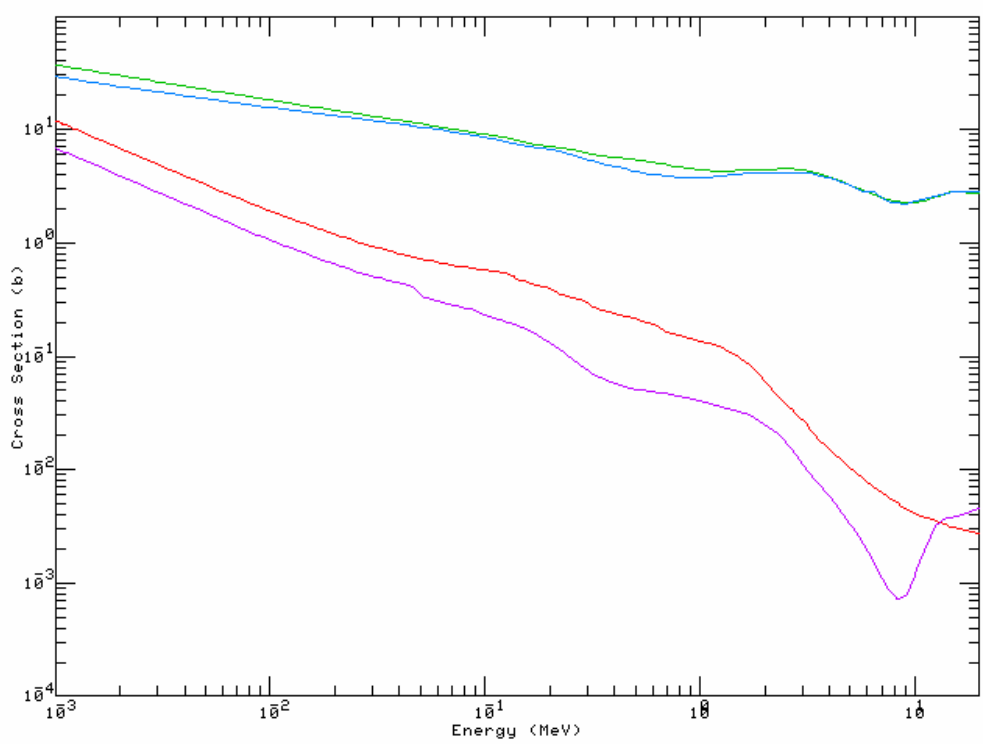

Figure 3.4-11: Comparison of Absorption and Scatter Cross-Sections for Rhenium and Tungsten Metals. (Green: Re scatter, Blue: W scatter, Red: Re absorption, Purple: W absorption) [15]

There exists almost no difference between rhenium and tungsten neutron spectral hardness because the scattering cross sections are very similar. However, rhenium has a higher absorption cross-section for average neutron energy by a factor of about 3 to 4. As it stands, tungsten has a significant advantage over rhenium in terms of neutronics. This disadvantage for rhenium is not restrictive, however, because adding extra reactivity to the core would compensate for the higher absorption.

The two metals have a similar response to mechanical stress, as can be seen in the Figure 3.4-12 below. In general, rhenium has a slight advantage in this category. Over an extended period, the higher strength of rhenium metal may add an element of safety, as there will be lower possibility of rupture.

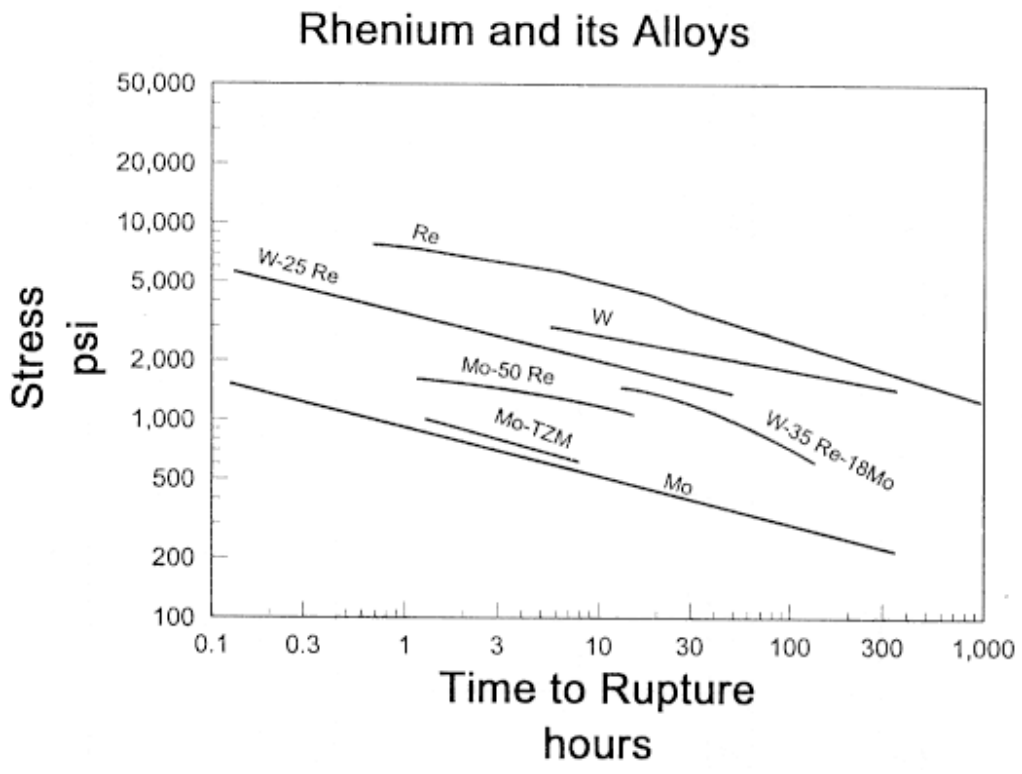

Figure 3.4-12: Stress vs. Rupture Curves for various Compounds and Metals [34]

Decision Methodology

Comparison of these two options, with such closely related properties, compelled the use of the decision methodology. Again, a design criterion for material specific properties was added because these properties are vital but do not fall under the established criteria.

Table 3.4-4 below shows the cladding decision matrix.

Table 3.4-4: Fuel Cladding Decision Matrix

		Cladding Material	
		Rhenium Metal	Tungsten Metal
Criterion	***Small Mass and Size (Cost) - 1.35***		
	Small Cladding Mass	2	1
	Small Reflector / Moderator Mass	1	2
	Small Dimensions	2	1
	Cladding Specific Properties - 1.25		
	Radiation Embrittlement	2	1
	Spectrum Hardness	2	2
	Thermal Conductivity	1	2
	Reactions with Surrounding Materials	2	2
	Launchable/Accident Safe - 1.13		
	No Criticality Accident	2	2
	Fits in Rocket	2	2
	Controllable - 1.14		
	Flat Keff	2	2
	Ex-Core Control	2	2
	Slow Transients	2	2
	High Reliability and Limited Maintenance - 1.00		
	Few Moving Parts	2	2
	Performance Index	*23.86*	*23.76*

Because the two cladding options have scored so close in the decision methodology, a more detailed scrutiny of rhenium and tungsten was undertaken. There are two further ways to delineate the relative merits of choosing one option over the other: the long-term, high-temperature effects of radiation damage on microstructure and the ability to manufacture the cladding.

Radiation Damage

One problem with using tungsten as a cladding, which could prove to be an eliminating factor, is a severe embrittlement effect. Well-documented low temperature embrittlement is not a concern considering the operating temperatures in the core. On the other hand, recrystallization embrittlement and high temperature radiation embrittlement are major

problems for tungsten cladding [35][36]. The long lifetime design criterion prohibits the use of a cladding material that cannot maintain integrity over life.

Alloying tungsten with other, less embrittlement-prone, materials at first appeared to be a solution to the embrittlement problem. Further investigation of this idea quickly reveals why tungsten is generally avoided in high temperature, high radiation environments. J.R. Stevens studied the problem in detail and concluded that aging embrittlement occurred in alloys with tungsten concentrations of more than eight atom percent [37]. Further closing the alloyed tungsten possibility, materials exhibiting ageing effects are much more susceptible to hydrogen embrittlement [37]. Rhenium is not subject to hydrogen embrittlement, even at high temperatures [31].

Manufacture of Rhenium

Because tungsten is a common structural material in many industrial applications, it is safe to conclude that there are no significant manufacturing problems associated with machining tungsten cladding. A closer look is required, however, for the rare-earth metal rhenium.

Despite the many attractive properties of rhenium metal, in the past there has been a general tendency to turn away from its use as a cladding material because it is notoriously difficult to manufacture. Rhenium is not machinable by conventional methods such as turning and milling. Instead, it can be ground and shaped using an electronic discharge machine (EDM), but the process is slow and uneconomic, especially for terrestrial power companies [31][34][37].

Development of technologies for space applications demands pushing the limits of technology to make available more advanced and cutting-edge materials. Fortunately, this is exactly what has happened for rhenium. Driven by an emerging market for rhenium rocket nozzles and thrusters, advances in manufacturing technology have made rhenium a viable option in recent years. A more advanced (and likely more economic) way of manufacturing rhenium is to shape the cladding in a hot isostatic press by using a molybdenum mandrel [38]. Then, rhenium is sintered at 80% of its melting temperature

in either a hydrogen atmosphere or a vacuum vessel for several hours [39]. The use of a hot isostatic press can achieve 99.4% theoretical density [39]. Although more difficult to machine than conventional cladding materials, considering recent advances, the manufacture of rhenium metal is not restrictive. Figure 3.4-13 is an example of the capabilities of manufacturing rhenium using the isostatic press.

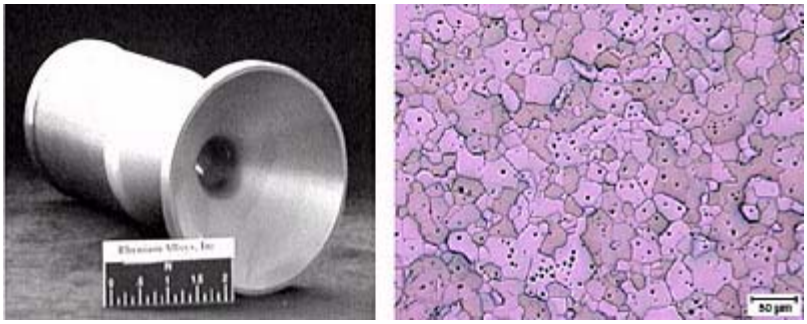

Figure 3.4-13: Rhenium Thruster and Microstructure after Hot Isostatic Pressing [39]

Mined rhenium is often in the form of rhenium-molybdenum (Re-Mo), which has several attractive properties, such as its high density, 13.55 g/cm^3, and high thermal conductivity, 36.8 W/mK [25]. The choice of Re-Mo cladding would be much better than most other options considered, but still less optimal than pure rhenium metal. Re-Mo is a viable alternative if extreme cost cuts became an issue since removing the molybdenum is not necessary.

Discussion

The design group selected rhenium metal as the cladding material for the MSR. With a density of 21.02 g/cm^3 and a melting point of 3459 K, rhenium is second only to tungsten in melting temperature and to osmium in density as compared to all other known metals. In accident scenarios, rhenium has the advantage of its ability to maintain ductility even after recrystallization [34]. Tungsten metal is unacceptable to use as a cladding material due to concerns about safety and reliability from high-temperature radiation embrittlement, despite its close competition with rhenium metal.

Chief among its desirable properties, rhenium metal has an extreme resistance to chemical reactions, especially resistance to oxidation at high temperatures. It also has the added accident scenario value of being highly shock resistant compared to other options

[34]. As seen in Figure 3.4-11, the average fast spectrum cross section is in the sub-barn range, including a large resonance dip near 10 MeV.

3.4.4 Fuel Design Characteristics

Terrestrial fuel pins are the basis for the MSR fuel pins. Twelve fuel pellets, each a height of 3.5 cm, make up the fuel mass in each pin. Modeling of the core determined a total active fuel height of 42 cm; see Section 3.7.1 for further information. The fuel pellets are cusped, as shown in Figure 3.4-6, to allow for the release of fission products. Figure 3.4-14 below shows a cut-away view of the fuel pins. The figure also shows a 10 cm axial reflector at each end of the pin. Adding the reflectors improve neutronics; Section 3.5.3 discusses this further.

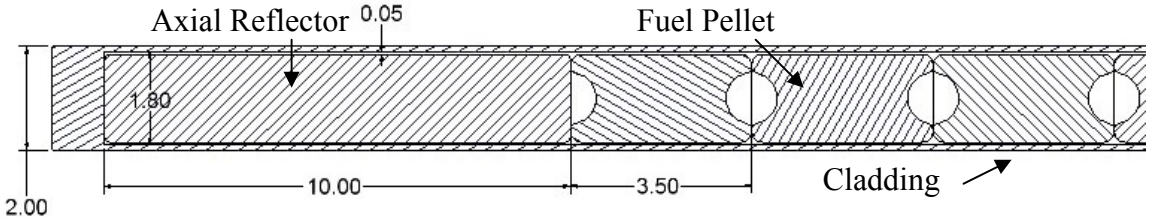

Figure 3.4-14: Cross Section View of Fuel Pin, all dimensions in cm

The design group assumed a cladding thickness of 1 mm. Given that typical PWRs and BWRs use cladding thicknesses between 0.6 mm and 0.9 mm [20], and withstand greater pressure gradients than expected for the MSR, this assumption is reasonable. Time constraints precluded an optimization of cladding thickness, thus delegating this task to future work.

Calculation of the thermal dilation of the fuel pellets established a lower limit for the gap between the fuel pellet and cladding. Equation (3.4-1) determines the increase in radius [40] [41] [42].

$$\Delta R = R \cdot \left(-1.5 \times 10^{-4} + 7.5 \times 10^{-6} * T + 1.25 \times 10^{-9} * T^2\right) \qquad (3.4\text{-}1)$$

where R is the fuel pellet radius and T is the temperature in Kelvin.

For a pellet radius of 0.85 cm at a temperature of 1880 K, ΔR is 0.0156 cm. To allow extra room for swelling due to fission products, a gap thickness of 0.05 cm is very

conservative. Given the best tricusp configuration has fuel pins the same size as the heat pipes, see Section 3.3.4, the fuel pellets are therefore a radius of 0.85 cm.

Table 3.4-5 presents a summary of the fuel pin composition and characteristics. Section 3.7.4 presents further analysis of the fuel pins and tricusp material regarding the temperature profile.

Table 3.4-5: Summary of Fuel Pin Composition and Characteristics

Fuel Pellet Composition	$(^{235}U+^{238}U)^{15}N$
Cladding Metal	Re
Fuel Pellet Radius	0.85 cm
Gap Thickness	0.05 cm
Cladding Thickness	0.1 cm
Total Fuel Pin Radius	1 cm
Fuel Pellet Height	3 cm
# Pellets per pin	12
Total Active Fuel Height	42 cm

3.5 Reflector

A review of the literature revealed that the number of possible reflector materials for use in a fast reactor is quite large. Accordingly, the design group developed a set of criteria to cull the possibilities. While the decision methodology goals do not directly apply to reflector selections, they did dictate three relevant criteria to best reflect the overall project goals.

1.) Density – Low density for any reflecting material is critical. A primary design goal of the MSR is small mass and size. An optimal reflector is therefore one that is light and compact.
2.) Albedo – Albedo is the fraction of neutrons incident on the reflector that reflect back into the core. A high albedo reflector is important to the reactor as it reduces neutron leakage, thereby improving neutron economy and helping to maintain criticality over life while reducing the size of the core.
3.) Melting Temperature – Perhaps the most obvious of the three criteria, the reflector material must not melt at the operating temperature of the core. We place an upper bound on the normal core operating temperature of 1800 K and for accident and transient purposes place a lower limit on the melting point of the reflector material at 2000 K.

3.5.1 Options

The majority of available information on fast reactor reflectors is not for the development of space reactors, but rather for terrestrial reactors. Therefore, the existing literature

focused primarily on albedo, burnup potential and negative reactivity feedback, with very little attention given to mass and size. For this reason, in addition to looking at reflectors from terrestrial reactors, the design team also included the reflector options used in previous space reactor design. In order to proceed, the design group identified the most promising terrestrial and space options and then evaluated these options relative to the three specific design goals mentioned above. Table 3.5-1 below summarizes the seven options identified for comparison.

Table 3.5-1: Reflector Options [3] [45] [46]

Material	Density (g/cc)	T Melt (K)	Albedo (%)
Ba_2Pb	4.91	1201	85.9
BeO	3.01	2781	93.5
$MoSi_2$	6.24	2303	75.3
PbS	7.6	1391	85.6
Ti_5Si_3	5.21	3223	82.1
Zr_3Si_2	5.88	2580	85.3
ZrS_2	3.82	1753	93.0

The albedo figures in Table 3.5-1 bear some explanation. All of these values are from MCNP calculations for 60 cm of reflector material in a characteristic fast spectrum reactor with uranium fuel. The albedo is the ratio of the outgoing to return current. While these are not the exact characteristics of the MSR, Yu [45] tabulates the values presented in Table 3.5-1 and the albedo will scale monotonically for varying geometry. The literature values are then appropriate to draw comparisons among the seven materials.

Based on the design criteria, Ba_2Pb, ZrS_2 and PbS can be eliminated, as their melting point is below the 2000 K minimum. Low comparative albedo eliminates $MoSi_2$ and Ti_5Si_2 from consideration. The two remaining options, BeO and Zr_3Si_2, appear closely related from the perspective of the three stated criteria. Therefore, the design group used a diffusion theory model to determine the reflector material from these two options.

3.5.2 Modeling

The first step in modeling the reflector was to develop a diffusion model to evaluate the moderating characteristics of the two material options. In this step, the model only considers radial reflection. As BeO is a relatively low Z material compared to Zr_3Si_2, it has a much larger moderating capabilities, which corresponds to a largely thermal neutron return current into the core. As a result, the core power will be shifted dramatically to the core periphery. The purpose of the diffusion model was to determine if these excess fissions would result in prohibitively high radial power peaking factors. Figure 3.5-1 illustrates schematically the behavior of the two materials. The intermediate layer in the drawing captures returned thermal neutrons. The more moderating BeO results in a much larger radial power peaking factor. Calculations indicate this factor is 8.7 times larger that in the Zr_3Si_2, thus eliminating BeO as a possible reflector material.

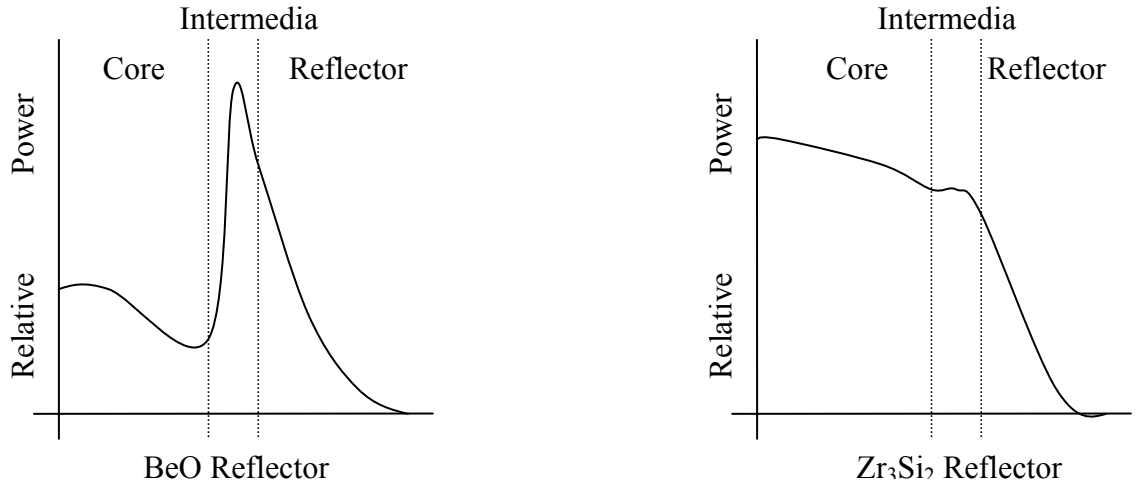

Figure 3.5-1: Relative Power Density for Reflector Material Options

The design group then placed the one remaining reflector material, Zr_3Si_2, in the MCNP core model to confirm the diffusion predictions and define a specific geometry.

3.5.3 Design Characteristics

Radial Reflector

In a fast neutron spectrum, the neutron flux in the reflector decreases exponentially. Accordingly, after a certain thickness of reflector material, adding another small increment to reflector thickness does not result in an appreciable increase in albedo. To keep the mass of the system small, the reflector thickness was limited to that thickness

where adding an addition centimeter of material increased albedo by less than one-half of one percent (0.5%). This criterion serves as a simple method of approximating the Pareto point of the system. The diffusion model for the MSR core found that, for the radial reflector, this thickness was 20 cm with a resulting reflector albedo of 83%. The geometry of this reflector is cylindrical, with the MSR core placed in the center. The mass of this configuration is approximately 1086 kg.

Axial Reflector

Ten centimeters of reflective material at the two ends of each of the fuel pins serve as the axial reflector. Adding this material results in a mass addition of about 143 kg. While this geometry significantly reduces the total fraction of reflected area compared to a slab geometry, such a configuration best balances the needs of core reflection and heat transfer out of the heat pipes. Figure 3.5-2 shows a sketch of the combined reflector geometry.

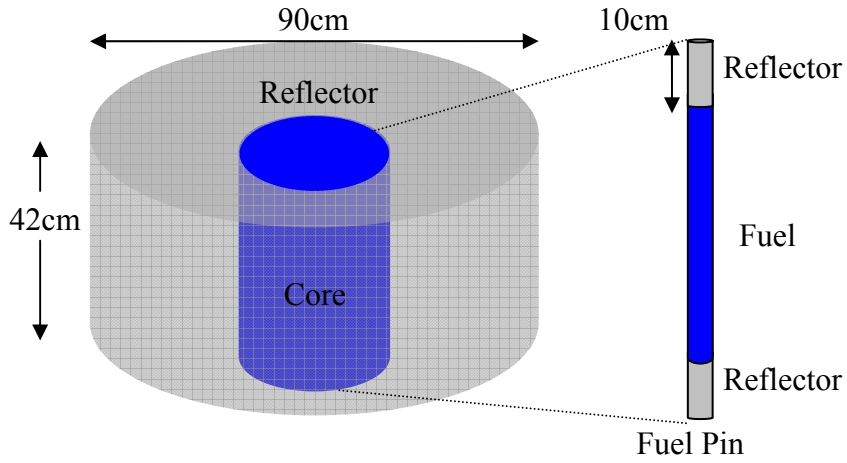

Figure 3.5-2: Reflector Geometry without Control Drums

3.6 Control Mechanisms

The process of controlling the reactor involved addressing two tasks. The first task requires a control mechanism to manage startup and shutdown operations as well as respond to transient conditions. This requires only periodic intervention of the mechanism, not continuous operation over life. The second task requires a mechanism to keep the power level, and therefore the reactivity profile, of the reactor constant. This

task requires continuous operation and fine variable worth. While it is not possible to separate these tasks in designing a control system, recognizing the need for two disparate control functions informed the design process.

External control mechanisms, which are mechanisms that are not physically part of the fuel pins, meet the needs of the first task. Control rods are an example of an external control mechanism. Intrinsic control mechanisms, which are mainly poisons, best meet the requirement of the second task. The following sections evaluate these two control mechanisms separately.

3.6.1 Extrinsic Control Mechanisms

In order to determine the best extrinsic mechanism for startup/shutdown and transient control, the four design criteria of the decision methodology had to be further defined. The first criterion required that the control mechanisms have small mass and not significantly increase the size of the core or reflector. The second criterion is controllable, which is the very purpose of this system. The third criterion spoke to launchability. To prevent the possibility of criticality during launch, the selected mechanism had to have sufficient worth to keep core reactivity well below critical levels. The final criterion dealt with high reliability. To satisfy this, the control system requires redundancy, a robust design and no in-core moving parts.

With these criteria, evaluation began on three general categories of extrinsic control mechanisms: control rods, movable reflectors and poison control drums [4].

Options

Control rods are rod or paddle-shaped devices made of a neutron absorbing material that slide into and out of the core. Insertion of control rods increases neutron absorption and decreases core reactivity. Control rods did not meet the design criterion of this system because the design group wanted to limit moving parts in the core and possible inadvertent criticality accidents. In addition, any rod system would require the displacement of rods out of the core over a distance of about half a meter. This would

have expanded the apparent dimensions of the core and resulted in heavier and more complicated core geometry.

The moving reflector option entails moving reflector material axially over the core to increase or decrease reactivity in different zones. While this option does not require moving parts inside the core, it does require the movement of more than a metric ton of reflector material, a complicated mechanical process. In addition, requiring a moving reflector prohibits its use as a core containment vessel, thereby requiring the addition of another heavy structural component. Thus the moving reflector option was also eliminated.

Poison control drums are cylinders placed inside cutouts in the reflector as shown in Figure 3.6-1. These cylinders are composed of mostly reflector material by volume, but contain a neutron absorbing shutter material along a portion of the drum surface. Drums control reactivity by rotating the coated side towards and away from the core as necessary. This option satisfies the requirement of high reliability; no moving parts exist inside the core, many drums are present for high redundancy and no translational motion is required. When all drums are facing the core, the negative reactivity worth is large. The core can therefore be placed in an extremely low reactivity state guaranteeing launch safety. This system also adds only a small amount of mass to the system, as the drums are mostly reflector material that is required regardless of the control mechanism.

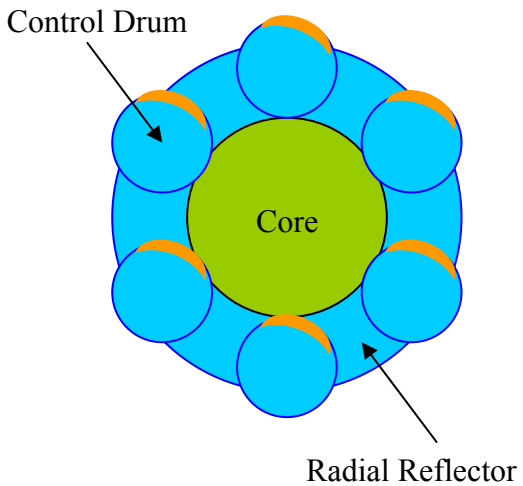

Figure 3.6-1: Poison Control Drum Concept Sketch, Top View.

Control drums are able to address both of the control tasks needed for the reactor. The ability to move the shutter material to very different proximities from the core provides the capability to induce large reactivity changes and thus control startup and shut down as well as compensate for reactivity transients. In addition, small movements of the drums can help maintain a constant reactivity profile over life.

In maintaining a flat reactivity profile over life, drums, while useful, are not optimal. Maintaining constant reactivity over life requires balancing the burnup of fuel with worth of the control mechanism. As burnup is a continuous process, the control drums would ideally require continuous adjustment; this is not practical. In addition, the drums, being nearest the outside of the core, will have less of an effect on fuel elements in the inside of the core and so will not moderate the reactivity uniformly. Accordingly intrinsic control mechanisms merited investigation to supplement drums.

3.6.2 Drum Design Characteristics

Material

The control drums are composed of two materials. Each drum will mostly consist of reflector material, which is Zr_3Si_2 for this system. A thin shutter material occupies a portion of the face of the drum. This material absorbs neutrons and provides reactor control. A shutter material must have a high absorption cross section for fast and epithermal neutrons that migrate into the reflector region. The literature offers may possible options, but two, ^{10}B and ^{181}Ta, appear to be best suited to this reactor. ^{10}B has a relatively high absorption cross section for neutrons at all energies and ^{181}Ta has large fast and epithermal resonances as shown in Figure 3.6-2. To obtain the benefits of both materials, the reactor used $^{181}Ta^{10}B_2$ for the shutter material. Other materials evaluated include cadmium, xenon and hafnium, but their absorption properties were inferior to the TaB_2 combination.

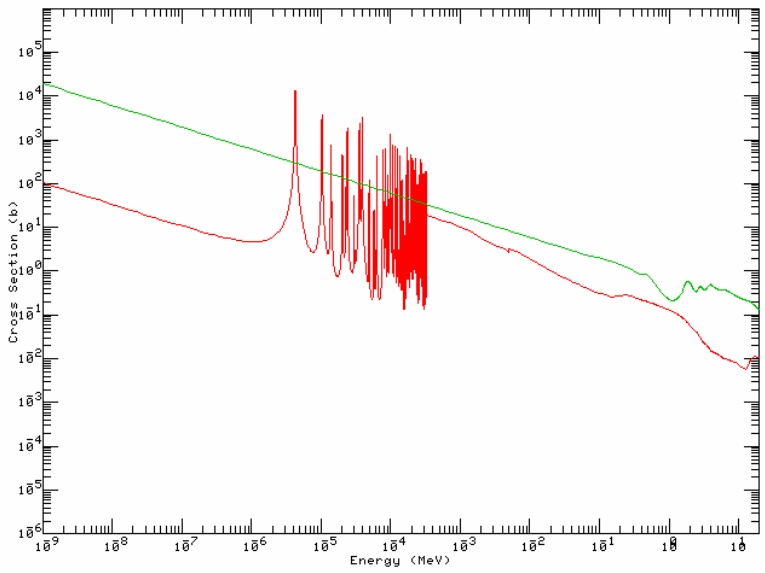

Figure 3.6-2: Neutron Absorption Cross Sections for B-10 (green) and Ta-181 (red) [47]

Design and Geometry

Based on the MCNP model of the reactor, as shown in Section 3.7.1, the team decided to place eight control drums in the reflector, as in Figure 3.6-3. This number emerged after much iteration to address launch accident concerns described in Section 3.8. As shown in Figure 3.6-4, each drum has a diameter of 30 cm and has its inner face located 0.5 cm from the core. A 120º arc on the surface of each drum contains 1.5 cm thick shutter material. The remaining volume of the drum is reflector material [48] [49]. This geometry will add 182 kg to the mass of the reflector since the density of TaB_2, at 12.38 g/cc [48], is greater than that of the reflector material.

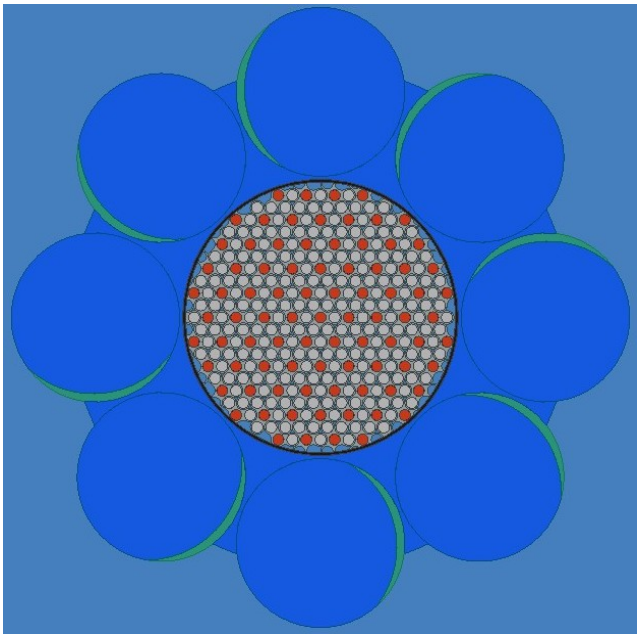

Figure 3.6-3: Control Drum Configuration

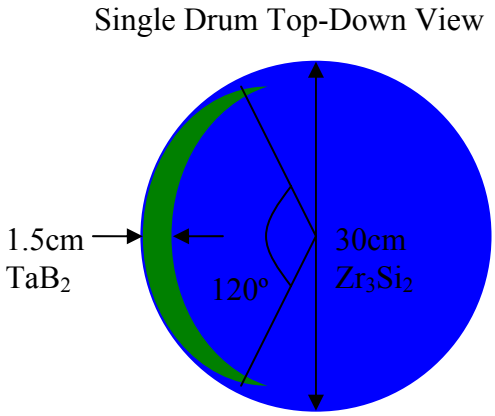

Figure 3.6-4: Sketch of Control Drum Geometry

Manufacture of the shutter material must allow high porosity to permit the accumulation of helium from neutron capture in the boron. This increased porosity prevents swelling in the absorber but will not contain the helium. There appears to be no functional or environmental need to contain this gas but further investigation is advisable.

Analysis

A study of the control worth, again using the MCNP model, indicated that with all drums rotated in toward the core, the beginning of life (BOL) k_{eff} would be 0.976 and with the drums in their minimum worth position, the k_{eff} would be 1.027. It is instructive to note that the minimum worth criterion need not occur when the drums are such that the poison

is 180º from the core. Worth is a function of both the poison distance from the core and the angular fraction of the core occluded. The poison is furthest away after a 180º rotation but the occluded angle is smallest after a 90º rotation. The worth as a function of drum rotation is a complicated expression. To avoid this complicated analysis, the MCNP model used the apparent poison density seen by the core in concentric cylinders to approximate different angles of rotation. This approximation is perfectly appropriate for determining the maximum swing in reactivity.

This model indicated that the eight drums had sufficient worth to operate the core. Given that the BOL β of the system is approximately 0.0064 [50], each drum conferred a negativity reactivity swing of about $1.00 such that only five drums are needed to suppress the BOL reactivity in the core. The core can then shutdown safely even if three drums fail. A failure would be an event such as one that causes a drum to stick in the minimum worth position or rotate uncontrollably. This redundancy is critical and implies that a full third of the control system can fail completely and the core will still be safe.

Repeating the same procedure for end-of-life (EOL), each drum conferrers a negative reactivity swing of $1.08 and, because the total reactivity has dropped somewhat, only four drums are needed to keep the system subcritical. Redundancy improves over the life of the core.

Control Drum Worth

The change in k_{eff} between the drums in and drums out position, Δk_{eff}, determines the worth of each control drum. Equation (3.6-1) shows the control drum worth in terms of Δk_{eff} and β_{eff}.

$$\text{Worth} = \frac{\Delta k_{eff}}{n\beta_{eff}} \qquad (3.6\text{-}1)$$

Here, worth is in dollars and n is the number of drums. Table 3.6-1 shows the MSR control drum worth at the beginning and end of life according to the MCNP model and Equation (3.6-1).

Table 3.6-1: Control drum worth at beginning and end of life

	Δk_{eff}	Worth
BOL	0.0519	$1.00
EOL	0.0552	$1.08

Discussion

For the MSR, the control drum method of control is ideal. The eight-drum design offers redundancy and simple control without moving parts. Control drums avoid reactivity insertion accidents such as control rod ejections. In fact, with the only accident which could occur, a drum stuck with the poison shutter facing outward, the other seven drums still control the MSR. The failed drum does not add reactivity to the system more quickly then it can be removed by the other drums.

In terms of mass, the control drums add 367 kg of reflector material. The poison shutter material adds 181 kg. Therefore, the reflector and control drums together weigh 1,777 kg.

3.6.3 Intrinsic Control Mechanisms

Poisons are neutron-absorbing materials mixed with the reactor fuel for power shaping purposes. While poisons increase the mass of the core, the additional mass is small, as the substance would only compose a small fraction of the fuel. Poisons require no moving parts, are completely reliable by nature and are ideal for maintaining a uniform reactivity profile over life.

As the reactor operates, some of the neutrons are absorbed in the poison and are not available to cause fission. When this happens, the poison transforms to another nonpoisonous isotope or element and the total poison concentration decreases. Over life then, the poison concentration drops and more neutrons are available to cause fission. This effect balances the loss of fissile isotopes and stabilizes core reactivity. Poisons were therefore the logical supplement to poison drums for the control system.

Options

The design group considered several isotopes as possible poisons, including ^{157}Gd, ^{151}Eu, ^{181}Ta, ^{10}B, ^{Nat}Hf, ^{Nat}Cd, ^{Nat}Xe, ^{157}Dy and ^{Nat}Er. To limit the amount of extra mass introduced into the core, a poison with a high absorption cross-section was ideal.

Rarity and unknown compound properties in high radiation environments prevented selection of ^{157}Dy and ^{Nat}Hf. Europium, usually used for thermal reactors because of its low energy resonance, was not useful here. The physical state of Xenon, a gas, ruled it out as part of the solid poison scheme. This left five options, ^{10}B, ^{157}Gd, ^{Nat}Er, ^{181}Ta and ^{Nat}Cd as possible poisons. All four have surprisingly similar cross sections in the fast region so other physical parameters restricted the options. Table 3.6-2 displays these properties.

Table 3.6-2: Physical Properties of Possible Poisons [52] [53]

	Density (g/cm^3)	**Melting point (K)**	**Thermal Conductivity (J/m*sec*K)**
Ta metal	16.60	3269	57.5
TaN	13.70	3300	N/A
Ta_2O_5	8.20	1800	N/A
Gd metal	7.89	1584	10.5
^{10}B	2.46	2349	27
Gd_2O_3	7.10	2330	N/A
Er_2O_3	8.64	2355	N/A
Er metal	9.05	1795	14.5
Cd metal	8.65	594.1	96.9

Erbium oxide, Er_2O_3, has a high melting point of 2355 K and a density of 8.64 g/cm^3, but Erbium is only to two parts in five, making the added poison mass per molecule low. More importantly, Er_2O_3 is hygroscopic. Hygroscopic materials readily absorb moisture and CO_2 [53]. Gd_2O_3 has a similar melting point at 2330 K, but is less dense at 7.1 g/cm^3, and therefore less desirable. Cadmium metal has a low melting point of less than 600 K, but alloying cadmium with silver and other metals increase the melting point. Alloying cadmium metals is not an option for space reactors due to the associated increase in size and mass.

Of the remaining options, tantalum metal, became the poison for this system. The high melting point of 3269 K and high density of 16.6 g/cm^3 are far superior to other poison compounds and metals. In addition, the thermal conductivity is better than all but cadmium metal and far superior to ^{10}B. Contributing greatly to the choice of tantalum metal is its relative chemical inertness and low cost of around $120/g [54].

3.7 System Characteristics

The MSR is a fast spectrum reactor with uranium nitride fuel, an intrinsic tantalum poison, Zr_3Si_2 reflector, and Zr_3Si_2/TaB_2 control drums. Lithium heat pipes cool the system and are arranged in a tricusp configuration with the fuel rods. Figure 3.7-1 shows a cross sectional view of the reactor system.

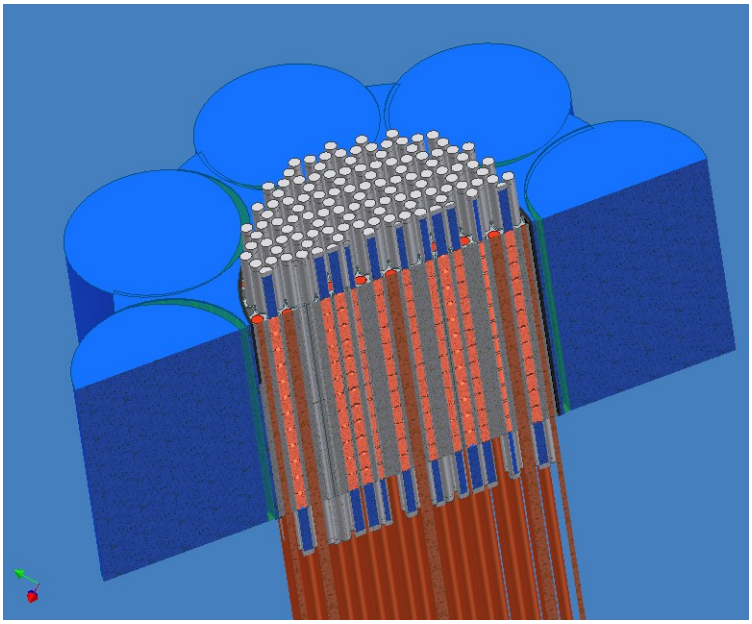

Figure 3.7-1: Cross Sectional View of Core, Reflector, and Control Drums

After choosing the components of the system, the physical and neutronic characteristics were determined. The reactor must operate as specified. Diffusion theory and Monte Carlo simulation determined these properties. Several simplifying assumptions were made that demanded the use of computer simulation for accuracy.

3.7.1 MCNP modeling

The methodology employed for core design is composed of two steps. First, the design group estimated core dimensions and enrichments by analytic calculations. Next, we

coupled the estimate with known core characteristics, such as volume fractions, and used them to obtain a numerical solution. The code employed for the second step was the Los Alamos developed Monte Carlo N-Particle Transport Code, MCNP5.

Analytic Approximations

The aim of the analytic calculations was to produce a core radius. In order to accomplish this task, we needed to establish several parameters. First, an approximation of cross sections in a fast spectrum was required. Having obtained these from cross section charts in the ENDF library, we immediately got a diffusion coefficient, D, using Equation (3.7-1)

$$D = \frac{1}{3\left(\Sigma_a + \left(1 - \frac{2}{3A}\right)\Sigma_s\right)} \approx \frac{1}{3\Sigma_s} \qquad (3.7\text{-}1)$$

where Σ_a is the macroscopic absorption cross section, A is the atomic mass of the isotope in question, and Σ_s is the macroscopic scattering cross section. The approximation is justified for a fast spectrum, especially when recognizing the result as a rough guess at radius. Migration area, M^2, follows from the diffusion coefficient:

$$M^2 = \frac{D}{\Sigma_a} \qquad (3.7\text{-}2)$$

It is then necessary to presume a reasonable k_∞ at beginning of life, where k_∞ is the infinite homogenous approximation multiplication factor. A k_{eff}, where k_{eff} is the effective multiplication factor, of around 1.03 at beginning of life can then be targeted and using

$$k_{eff} = k_\infty P_{NL} \qquad (3.7\text{-}3)$$

where P_{NL} is the probability of non-leakage given by equation (3.7-4).

$$P_{NL} = \frac{1}{1 + B_g^2 M^2} \qquad (3.7\text{-}4)$$

B_g in Equation (3.7-5) is the geometric buckling, which can be used to estimate the core radius. Using a cylindrical core shape, the neurotically maximized case occurs where height equals diameter. The geometric buckling for a cylinder is:

$$B_g^2 = \left(\frac{2.405}{r}\right)^2 + \left(\frac{\pi}{h}\right)^2 \tag{3.7-6}$$

where r is the radius and h is the height. Rearranging equation (3.7-3) and substituting into equation (3.7-6), the buckling term can be found in terms of the multiplication factors.

$$B_g^2 = \left(\frac{k_\infty}{k_{eff}} - 1\right)\frac{1}{M^2} \tag{3.7-7}$$

Now, the radius can be solved for in terms of the migration area and the multiplication factors

$$r = 2.8725\sqrt{\frac{M^2}{\left(\frac{k_\infty}{k_{eff}} - 1\right)}} \tag{3.7-8}$$

from which we can estimate the dimensions of the core by varying k-ratios to allow for optimization of reflector worth.

By using a homogenous core composition approximation, we can both estimate a core averaged density and construct a model for MCNP. The homogenous approximation is justified for fast neutrons because, as their position varies, the neutrons will see negligible effects from small changes and heterogeneities in material and density. More quantitatively, the migration length for fast neutrons is much greater than local material variations. Assuming the height and diameter are equal, the radius of the core varies as

$$r = \sqrt[3]{\frac{m}{\rho_{smear}\pi}} \tag{3.7-9}$$

where m is the mass and ρ_{smear} is the density of the homogenous core approximation. Therefore, the mass dictates the radius, which then dictates the enrichment and composition to first order approximation.

We can now put k_∞/k_{eff} in terms of mass by substituting radius, rearranging equation (3.7-9):

$$\frac{k_\infty}{k_{eff}} = 8.2512M^2\left(\frac{\rho_{smear}\pi}{m}\right)^{2/3} \tag{3.7-10}$$

so that, constrained with an upper limit on the mass, we can surmise k_∞/k_{eff}, which is of great importance for reflector design.

A small mass is necessary, so a constraint can be placed on the radius. Given

$$P = \phi V \upsilon \Sigma_f E_f = \phi \pi r^3 \upsilon \Sigma_f E_f \tag{3.7-11}$$

where P is the total thermal power, V is the volume, υ is the average net number of neutrons produced per fission, E_f is the energy released per fission, and φ is the neutron flux. Solving for the radius, Equation (3.7-10) becomes

$$r = \left(\frac{P}{\phi \pi \upsilon \Sigma_f E_f}\right)^{1/3} \tag{3.7-12}$$

Furthermore, power can be found in terms of k_∞/k_{eff} after substitution of equation (3.7-8) in equation (3.7-12)

$$P = \phi \pi \upsilon \Sigma_f E_f \left(\frac{M^2}{\frac{k_\infty}{k_{eff}} - 1}\right)^{3/2} \tag{3.7-13}$$

Given the equations above, and the small mass and volume design goal, the core radius is between 15 cm and 25 cm.

MCNP5 Simulation

Using the above range of radii estimated by diffusion theory, we encoded several trial cores into MCNP and then iterated the calculations. MCNP output provides spectrum averaged cross sections, energies per fission, fluxes and ν. Each parameter obtained from MCNP was then inputted back through the analytical calculations above, and through an iterative trial and error process – the radius converged to 18.5 cm for the initial core design. The radius later evolved to the final 24 cm dimension as lifetime burnup, accident scenarios and reflector design dictated.

The aim of the simulations was to attain the greatest Δk_{eff}, as calculated in Equation (3.7-14).

$$\Delta k_{eff} = k_{MaxControl} - k_{MinControl} \qquad (3.7\text{-}14)$$

Utilizing the linear reactivity model, enrichment can be employed to optimize k_{eff}. With the control drums rotated fully in, a sub-critical k_{eff} is necessary, while with our control drums rotated fully out, a supercritical k_{eff} is necessary. The larger Δk_{eff}, the more control is available for accident and transient scenarios. The exact values of k_{eff} for each case must then be chosen so that the reactivity insertion from a worst-case accident scenario, such as being submerged in wet sand, keeps the core subcritical. Meanwhile, it is necessary to choose an operating enrichment such that the beginning of life k_{eff} is high enough to allow for a 5-year operating time.

The results of the MCNP simulations yield a core size of 42 cm in height and 48 cm in diameter. The enrichment is 31.8 w/o ^{235}U and the Δk_{eff} at the beginning of life is 0.05189. The behavior of the system over the lifetime is addressed below in Section 3.7.5.

Core Composition

The final composition of the homogenous core after accident scenario and burnup iteration, Sections 3.8, and 3.7.5, are shown in Table 3.7-1 below.

Table 3.7-1: Core Homogenous Composition

Material	Purpose	Volume Fraction
^{7}Li	Coolant	0.072759469
^{15}N	Fuel Compound	0.353381879
^{Nat}Nb	Heatpipe	0.076032901
^{181}Ta	Poison	0.037550786
^{Nat}Re	Cladding/Structure	0.110216571
^{235}U	Fissile Fuel	0.116593812
^{238}U	Fertile Fuel	0.233464583

All parameters were carefully adjusted using a lengthy and thorough iterative MCNP simulation process, given heat removal requirements and dimensions of the heat pipes, structural volume fractions needed for tricusp support, fuel pin dimensions, poison reactivity flattening, and enrichment.

3.7.2 MSR Physics Characteristics

In addition to the physical attributes, the design group must understand the physics characteristics of the MSR. This section describes the reactor physics characteristics of the core.

Mean Neutron Generation Lifetime

L* is the mean neutron generation lifetime which is the mean time a neutron exists before undergoing a reaction [4].

$$L^* = \frac{1}{v\nu\Sigma_f} \qquad (3.7\text{-}15)$$

where v is the neutron average speed, ν is the average number of neutron emitted per fission, and Σ_f is the macroscopic fission cross-section. At beginning of life the MSR has:

$$v = 468\,keV = 9.5*10^{6}\ \tfrac{m}{s} \qquad \nu = 2.43$$
$$\Sigma_f = 0.0236\,cm^{-1}$$

Therefore,

$$L^* = 1.84\,\mu s$$

Delayed Neutrons

β_{eff} is the ratio of the number of delayed neutrons to the number of total neutrons per fission, corrected for the increased fission cross section of the lower energy delayed neutrons. Assuming fission only in U^{235} at BOL, β_{eff}=0.0064 [50]. Table 3.7-2 shows the delay groups for fast fission in U^{235} [50].

Table 3.7-2: Fast Spectrum Delay Groups [50]

Group	λ_i (s^{-1})	β_i (E-03)
1	0.0127	0.243
2	0.0317	1.36
3	0.115	1.20
4	0.311	2.60
5	1.40	0.819
6	3.87	0.166

Radiation Environment

An important consideration, when characterizing a core design in an extraterrestrial environment, is the radiation inside the core and leaving the core. In case unanticipated maintenance is required, the radiation hazard for workers in close proximity to the core needs to be characterized. Instead of characterizing radiation outside the core, this section aims to describe the radiation both inside the core and out to the edge of the reflector. Radiation beyond the edge of the reactor is dealt with by the shielding group in Chapter 6.

In Core Neutron Flux

The in-core neutron flux is of importance in not only reactor physics and burnup calculations, but also in radiation damage calculations. It is beyond scope to determine radiation damage to internal core components; rather, the design group provided a flux for further analysis.

Using MCNP, a core internal neutron flux was determined. MCNP output provides normalized flux measurements (tallies), which can then be used to calculate the neutron flux at a given power level. The method of approach will be to use the power equation

$$P = \phi V \nu \Sigma_f E_f \qquad (3.7\text{-}16)$$

The volume is readily calculated and the flux is part of the MCNP output. Using the normalized fission cross-section, also provided by MCNP, an absolute fission cross-section can be established as

$$\Sigma_f = N \frac{T_{n4}(\sigma_f)}{T_{n4}(\phi)} \tag{3.7-17}$$

so that for a given power, flux is completely determined.

Neutron Current

The neutron current leaving the reflector edge is of importance in carrying out shielding calculations and determining doses to workers. As such, the neutron current has been simulated using MCNP. Similar to the flux calculation, current is given in normalized units and must be converted. Because of unit cancellation, the current can be determined using the flux.

$$J_{reflector} = \frac{T_{n1}(J_{neutron})}{A_{reflector}} \frac{\phi_{reflector}}{T_{n4}(\phi)} \tag{3.7-18}$$

Photon Current

For the same reason as neutron current, the photon current coming out of the reflector edge will factor into the shielding and dose calculation. The photon current is pulled almost straight out of the MCNP output.

$$J_{photon} = \frac{T_{n1}(J_{photon})}{T_{n4}(\phi)} \tag{3.7-19}$$

Calculations

Carrying through the calculations, Table 3.7-3 presents the neutron flux, neutron current and photon flux.

Table 3.7-3: Core Radiation Characterization

Partially Reflected Core (poison out)	
Neutron:	
Average neutron flux in core (fi)	4.155E+12
Current at reflector edge (J)	1.100E+10
Photon:	
Core edge	8.345E+14
Reflector outer edge	5.157E+13
Fully Reflected Core (poison in)	
Neutron:	
Average neutron flux in core (fi)	4.156E+12
Current at reflector edge (J)	1.135E+10
Photon:	
Core edge	8.295E+14
Reflector outer edge	5.291E+13

For more detailed shielding and dose calculations, neutron and photon spectra were simulated by discretizing energy (binning), calculated by using the methods described above and shown in Figure 3.7-2 through Figure 3.7-5.

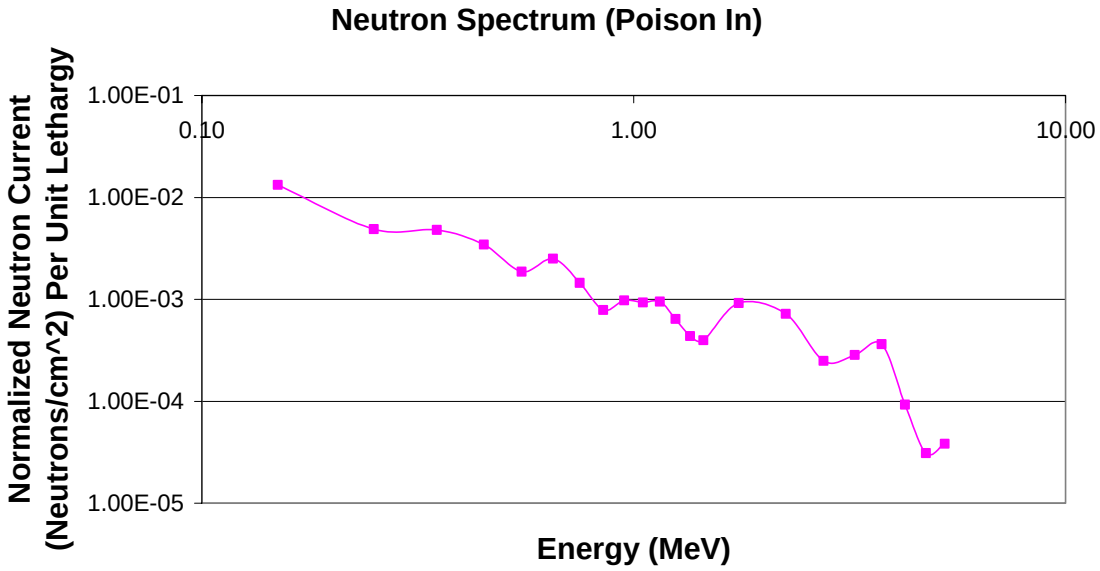

Figure 3.7-2: Neutron Spectrum at Reflector Edge with Drums Rotated In

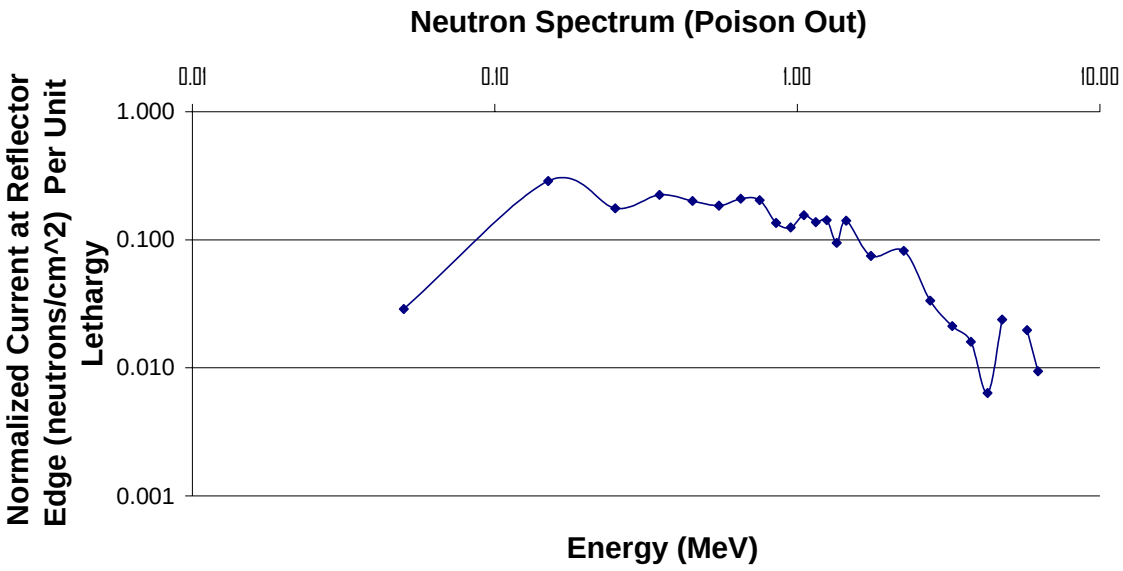

Figure 3.7-3: Neutron Spectrum at Reflector Edge with Drums Rotated Out

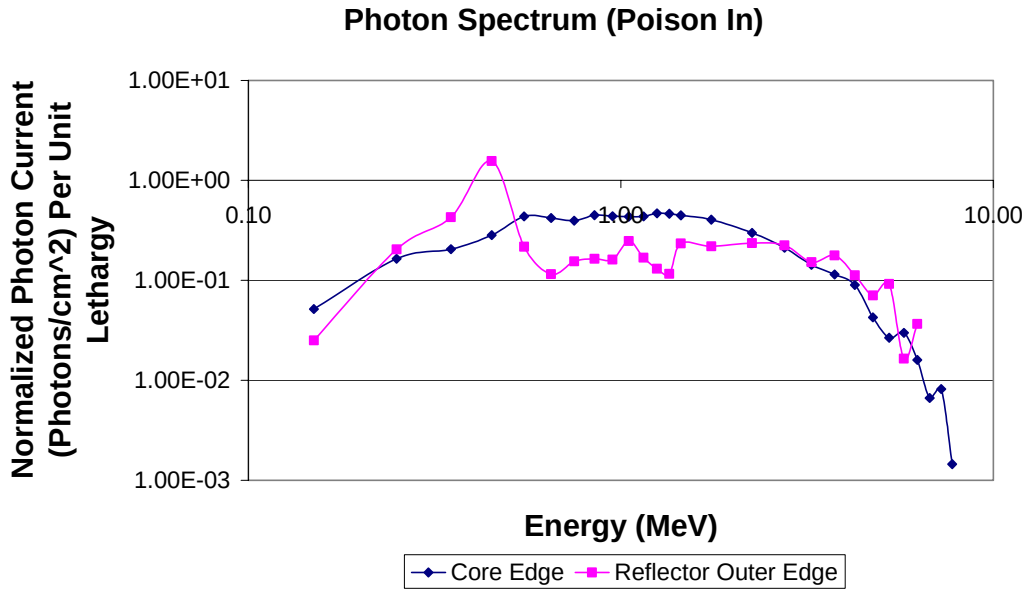

Figure 3.7-4: Photon Spectrum at Reflector Edge with Drums Rotated In

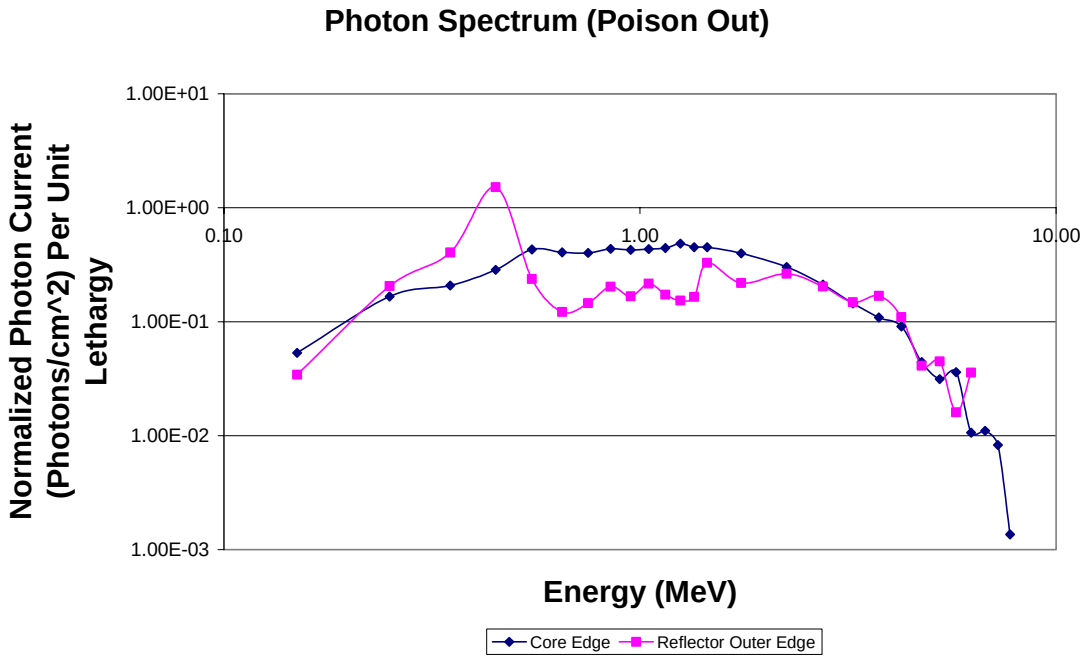

Figure 3.7-5: Photon Spectrum at Reflector Edge with Drums Rotated Out

3.7.3 Power Profile

One core physics parameter of great importance when evaluating the safety aspects of any core is the power peaking factor. When properly normalized, the peaking factor can be used as a measure of power distribution, temperature distribution and flux shape.

Calculation of Peaking Factor

By diffusion theory, the axial power peaking factor can be calculated using

$$APPF = \frac{H}{2H_{ex}} \frac{\pi}{\sin\left(\frac{\pi H}{2H_{ex}}\right)} \qquad (3.7\text{-}20)$$

where H is the height of the core and H_{ex} is the extrapolated height of the core accounting for reflector. For the MSR, using the diffusion model approximation, the height and extrapolated height are

$$H = 42\,cm$$
$$H_{ex} = 58.7\ cm$$

Therefore,

$$APPF = 1.25$$

The radial power peaking factor can be calculated by:

$$RPPF == \frac{\frac{\nu_1 R}{R_{ex}}}{2J_1\left(\frac{\nu_1 R}{R_{ex}}\right)} \tag{3.7-21}$$

where R is the radius of the core, R_{ex} is the extrapolated radius of the core accounting for reflector, and ν_1 is the first zero of Bessel J_0. For the MSR, the diffusion model approximation gives

$$R = 24\,cm$$
$$R_{ex} = 29.4\,cm$$
$$\nu_1 = 2.405$$

Therefore,

$$RPPF = 1.35$$

The radial power peaking factor can also be calculated using MCNP by determining the ratio of positional to core-averaged numbers. The peaking factor, F(r), can be calculated as

$$F(r) = \frac{\phi(r)}{\langle \phi(r) \rangle_{core}} \tag{3.7-22}$$

And since $\phi \propto$ power $\propto$ linear heat flux (q'), we have

$$F(r) = \frac{\phi(r)}{\langle \phi(r) \rangle_{core}} = \frac{P(r)}{\langle P(r) \rangle_{core}} = \frac{q'(r)}{\langle q'(r) \rangle_{core}} \tag{3.7-23}$$

Knowledge of the linear heat flux enables calculation of a temperature distribution.

Simulation of Peaking Factor

While analytic calculations are expected to give a good approximation of the power shape, numerical simulation provides more accurate results given enough histories are run for statistical uncertainties to fall within reason. In order to obtain peaking factors numerically, the core model was input into MCNP5 and simulations were conducted. Peaking factor data was obtained by creating concentric cylindrical cells, 1 cm apart,

throughout the core and measuring (tallying) the flux. A side view of the reactor, with tally cylinders in the core, is shown in Figure 3.7-6 schematically for reference.

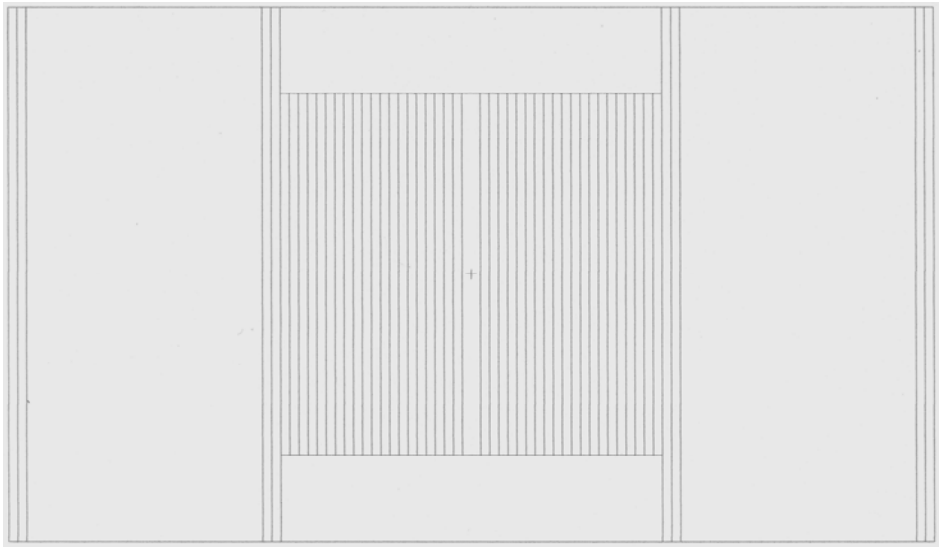

Figure 3.7-6: Reactor Schematic from MCNP5 Onput Showing Tally Cylinders for Peaking Factor Calculation

The MCNP5 output was then used to obtain the core-averaged, normalized flux, $\langle \phi \rangle_{core}$ and $\phi(r)$ for 1 cm radial steps. Using this simple formula, the radial power peaking is shown below in Figure 3.7-7 and Figure 3.7-8 for two scenarios: the control drums fully rotated in (where the poison is closest to the core) and fully rotated out.

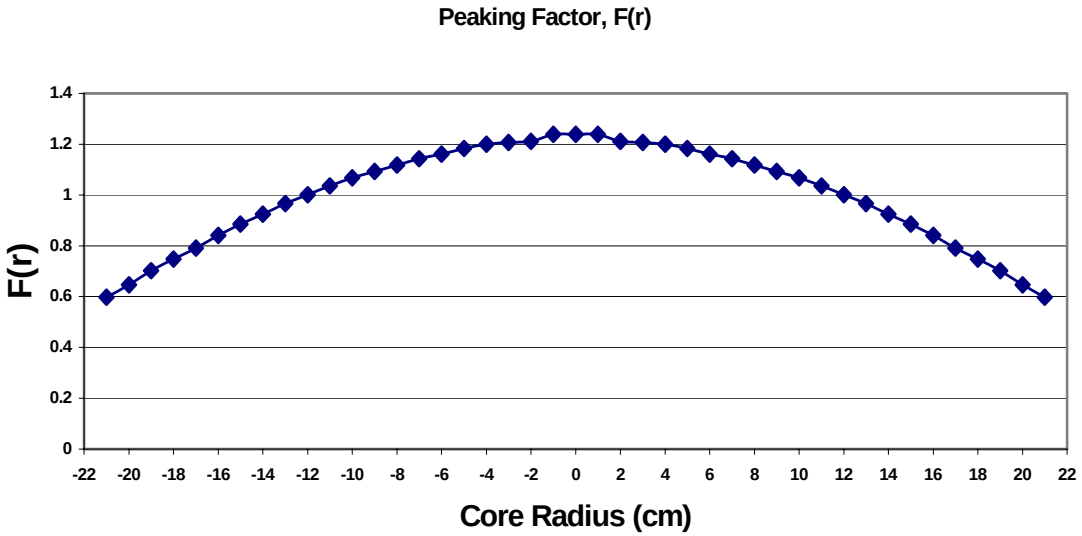

Figure 3.7-7: Radial Peaking Factor with Drums Rotated Fully In

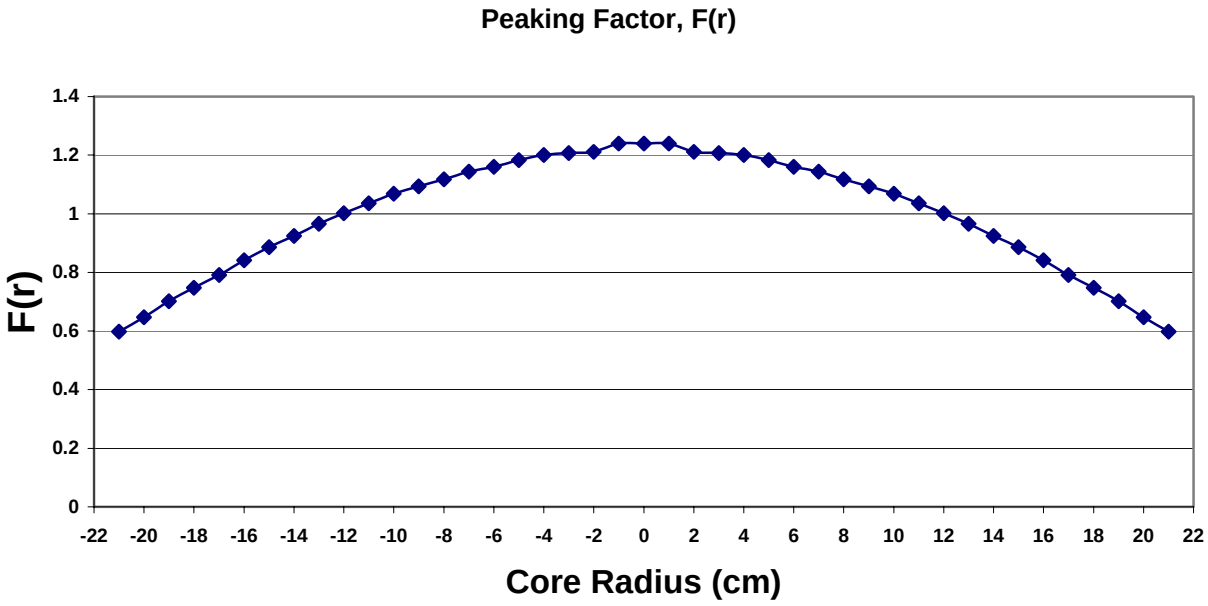

Figure 3.7-8: Radial Peaking Factor with Drums Fully Rotated Out

The maximum radial peaking factor at the center of the core with reflectors rotated in is $RPPF_{Drums\ In} = 1.31$ and the maximum power peaking factor with the reflectors rotated out is $RPPF_{Drums\ Out} = 1.24$. The maximum peaking factors are very close to the theoretical numbers calculated using diffusion theory. Both of these numbers fall well within acceptable and common peaking factor ranges for terrestrial reactors.

3.7.4 Thermal Behavior

As established in Section 3.3.4, heat pipes transfer heat from the fuel pins to the power conversion system isothermally. However, transferring heat to the heat pipes does is not isothermal. It is important to calculate the temperature rise across the fuel pin and tricusp to determine if the materials are safely below the melting point under normal operation. A safe temperature margin is at least 200 K between operating temperature and the melting point.

The design group used the thermal resistance circuit analogy to determine the temperature rise across the tricusp and fuel pin. This method approximates the temperature drop across multiple materials by adding the resistances of each material. Figure 3.7-9 depicts a radial view of the transition from the centerline of a fuel pin to heat pipe and the resistance circuit.

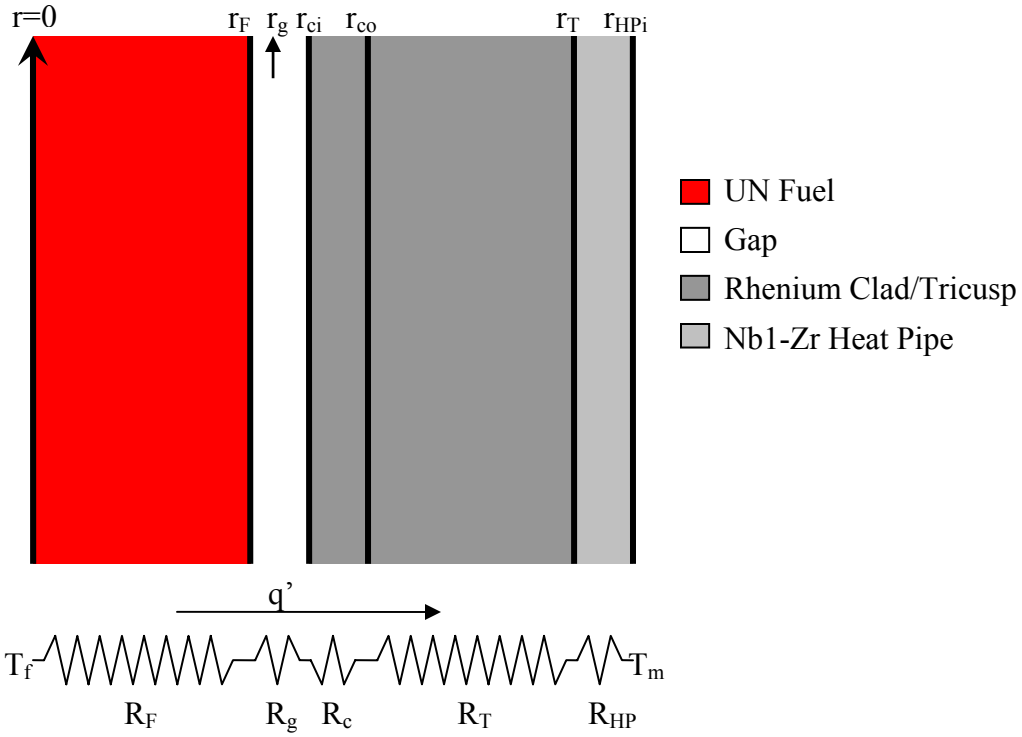

Figure 3.7-9: Thermal Resistance Circuit between Center of Pin to Center of Heat Pipe

Equations (3.7-24) through (3.7-28) are the thermal resistances of the fuel, gap, cladding, tricusp, and heat pipe. These expressions were derived from references [43] and [44].

$$R_F = \frac{1}{4\pi k_F} \tag{3.7-24}$$

where k_F is the thermal conductivity of UN.

$$R_g = \frac{1}{2\pi r_g h_g} \tag{3.7-25}$$

where r_g is the mean radius of the gap and h_g is the convection heat transfer coefficient of the gap. The value for h_g was obtained from reference [43].

$$R_c = \frac{1}{2\pi k_c} \ln\left(\frac{r_{co}}{r_{ci}}\right) \tag{3.7-26}$$

where k_c is the thermal conductivity of the cladding, r_{ci} is the inner radius of the cladding, and r_{co} is the outer radius of the cladding.

$$R_T = \frac{1}{2\pi k_T} \ln\left(\frac{r_T}{r_{co}}\right) \tag{3.7-27}$$

where k_T is the thermal conductivity of the tricusp material and r_T is the outer radius of the tricusp.

$$R_{HP} = \frac{1}{2\pi k_{HP}} \ln\left(\frac{r_{HP}}{r_T}\right) \tag{3.7-28}$$

where k_{HP} is the thermal conductivity of the heat pipe material and r_{HP} is the radius to the inside of the heat pipe.

The maximum centerline temperature of the hottest fuel pin is

$$T_{f_{\max}} = T_m + q'_{\max}\left[R_F + R_g + R_c + R_T + R_{HP}\right] \tag{3.7-29}$$

where

$$q'_{\max} = APPF \cdot RPPF \cdot \left(\frac{\dot{Q}}{NL}\right) \tag{3.7-30}$$

N is the total number of fuel pins, L is the active fuel length in each pin, $\dot{Q}$ is the thermal power, and T_m is the temperature of the moderator [43]. The maximum heat flux, which corresponds to the pin with the highest axial and radial power peaking factors, was calculated because the hottest pin will be the closest to its melting point.

Using the dimensions determined from MCNP simulation in Section 3.7.1, and the core characteristics determined in Section 3.7.2, the core temperatures can be determined. Table 3.7-4 summarizes the values used in the analysis. Applying these values, the maximum centerline fuel temperature was determined to be 1889 K.

Table 3.7-4: Thermal Resistance Parameters

Parameter	Value
N	387 pins
L	42 cm/pin
Q	1.2 MW
RPPF	1.35
APPF	1.25
q'	103.82 W/cm
T_m	1800 K
k_F	0.3 W/cmK
h_g	0.6 W/cm^{2}K
k_c	0.711 W/cmK
k_T	0.711 W/cmK
k_{HP}	0.523 W/cmK
r_F	0.85 cm
r_g	0.875 cm
r_{ci}	0.9 cm
r_{co}	1.0 cm
r_T	1.5 cm
r_{HP}	1.7 cm

Due to time constraints, the thickness of the tricusp material was not determined. The thickness was assumed to be 0.5 cm. To understand how the tricusp thickness would affect the centerline temperature, a sensitivity study was conducted. Figure 3.7-10 displays the results of this study.

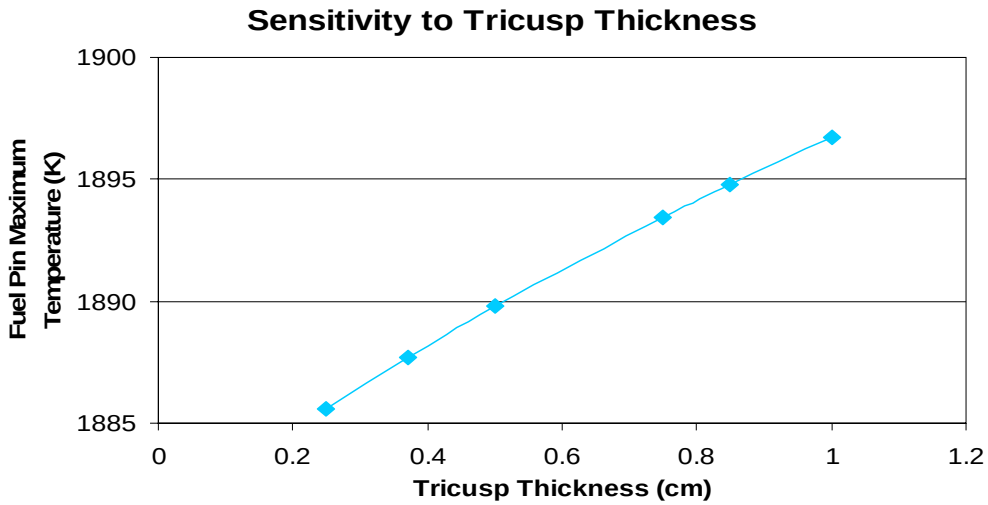

Figure 3.7-10: Fuel Pin Centerline Maximum Temperature for Varying Tricusp Thicknesses

To maintain a flat temperature profile, it is best to keep the tricusp thickness to a minimum. However, even up to a thickness of 1 cm, the centerline maximum temperature is 3000 K according to Figure 3.7-10.

3.7.5 Behavior over Lifetime

The entire design of the Mars reactor is inadequate if it cannot survive five-year burnup at full power. As such, it is imperative that the core is designed so that it is completely controllable, including all reactivity feedbacks, over a period of 5 years. As a major component of stringent design parameters, operation for 5 years requires that the reactor stay subcritical with the drums rotated inward and supercritical with the drums rotated outward, while leaving enough reactivity buffer to handle all feedback mechanisms throughout operation.

MCNP Burnup Simulation

To characterize varying operating conditions over the core lifetime, the reactor model was encoded for MCNP. Input decks were created in yearlong time steps. Each deck reflected the varying material composition of the core. The scope of this analysis was restricted to including depletion of ^{235}U and ^{238}U as well as buildup of ^{239}Pu and ^{135}Xe. Fission burnup of ^{239}Pu was also considered, which restricted buildup to some extent. An approximation for ^{181}Ta poison burnup and fission fragment creation was also input. Extreme care was taken to ensure that atomic mass was conserved in these calculations.

Calculation of Burnup for MCNP Input

To provide material cards for MCNP input decks, individual isotopic burnup and creation was calculated. The burnup of any isotope can be calculated with

$$N(t) = N_0 e^{-\phi\sigma t} \tag{3.7-31}$$

Using the flux calculated from simulations in Section 3.7.1 and the cross sections provided by MCNP, the number of atoms at any time is completely determined. For plutonium buildup calculations, a simple method was used,

$$N_{buildup}(t) = (1 - N_{burnup}(t) e^{-\phi\sigma_f t}) \tag{3.7-32}$$

where appropriate cross sections are inserted. For example, this was used for ^{238}U and for ^{235}U and ^{239}Pu. The production of ^{135}Xe was approximated by simply multiplying the number of fissions occurring throughout each time step by the fission yield of ^{135}Xe, which was taken as 0.06.

Table 3.7-5 in the *Results* section below shows the results of these calculations. The numbers displayed in this table were multiplied by isotopic weight fractions to create the MCNP deck.

End of Life Characteristics

When the reactor reaches its target lifetime of 5 effective full power years (EFPY), it must be able to shut down. That is, with the drums rotated fully in, the core must remain subcritical. Coupling this constraint with the already calculated drums out-drums in from Section 3.6, the long and tedious process of trial and error based simulation was undertaken. Some direction was provided by using the linear reactivity model as a first approximation, allowing simulation of only BOL and EOL points while varying enrichment. Steps of 0.1 enrichment were considered accurate enough for the process. The result of these simulations is shown in the last column of Table 3.7-5, in the *Results* section below. It is important to note here that, because of breeding, if the reactor is not shutdown after just over five years, then there will not be enough worth in the control drums to bring the reactor subcritical again – this is discussed more below.

Breeding

While consciously planned within the framework of the fast reactor and high ^{238}U content, it was not expected, a priori, that the reactor would have a breeding ratio of greater than one. One of the design parameters set forth was to have a flat reactivity vs. burnup curve; however, it became apparent once the simulations were run that the reactor would breed over the entire operational lifetime of the core. The ability to adjust this characteristic was well within the reach without major core overhaul; however, it was decided to allow the core to breed. Instead of planning for enough BOL, drums-out reactivity to allow for a decline into discharge burnup, core enrichment was simply adjusted to allow for a lower BOL, drums-in reactivity such that after 5 years, the reactor

would still be subcritical. To verify that this would occur, the MCNP deck was configured for a drums-in, EOL simulation.

Results

The results of the calculations and simulations are shown below in Table 3.7-5, Figure 3.7-11, and Figure 3.7-12.

Table 3.7-5: Isotopic Time Variance In Weight Percent of Core Materials with Burnup at Full Power

Time	^{235}U (enrichment)	^{238}U (enrichment)	^{239}Pu (buildup)	^{135}Xe (buildup)	Fission Fragments + Poison	k_{eff} (drums out)
BOL	0.3380	0.6620	0.0000	0.0000	0.0338	1.0274
1 year	0.3378	0.6616	0.0005	4.18E-6	0.0338	1.0295
2 years	0.3376	0.6613	0.0011	8.35E-6	0.0339	1.0334
3 years	0.3373	0.6609	0.0016	1.252E-5	0.0339	1.0365
4 years	0.33713	0.6606	0.0021	1.669E-5	0.0340	1.0411
5 years	0.3369	0.6602	0.0027	2.086E-5	0.0341	1.0446

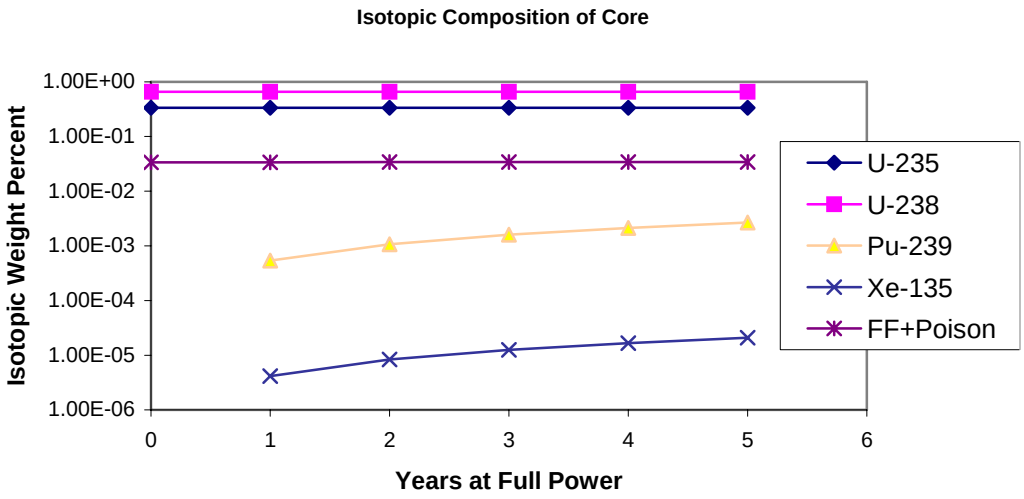

Figure 3.7-11: Isotopic Composition of Core Operating at Full Power

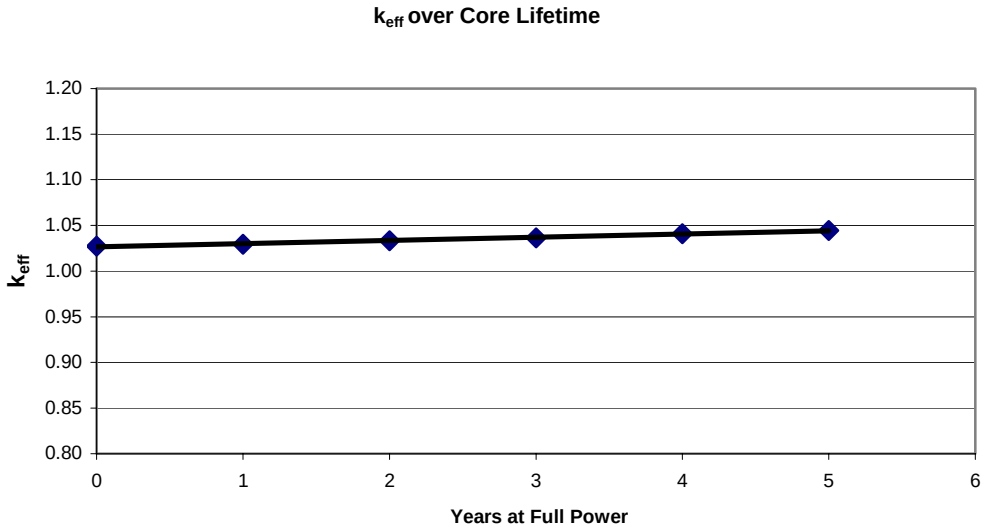

Figure 3.7-12: Change In k_{eff} Over the Lifetime of the Reactor at Full Power

The reactor will operate within the ability of the rotating drums to control reactivity over 5 years operating at full power. It should, however, be noted that that the reactor is not designed to operate for much more than 1 year after planned shutdown as the drums-in k_{eff} will rise over 1. Utilizing the high ^{238}U content and fast spectrum, the reactor has a breeding ratio over 1, constantly inserting controllable reactivity throughout its operating life.

3.7.6 Discussion

There is no doubt the UN fuel can survive five years at full power. Calculations have shown the fuel can provide power much beyond this expected period due to breeding. The design group selected the core materials to withstand the high-temperature high-radiation environment.

3.8 Launch Accident Analysis

3.8.1 Motivation

Throughout the history of the nuclear industry, safety has served as the basis for several design decisions. In 1992, the Nuclear Safety Policy Working Group concluded in its Recommended Programmatic Space Reactor Safety Policy Statement that

> "ensuring safety is a paramount objective of the space nuclear reactor program… all program activities shall be conducted in a

> manner to achieve this objective. The fundamental program safety philosophy shall be to reduce risk to levels as low as reasonably achievable. In conjunction with this philosophy, stringent design and operational safety requirements shall be established and met for all program activities to ensure the protection of individuals and the environment. These requirements shall be based on applicable regulations, standards and research."[55]

Therefore, to satisfy this requirement, a design specific safety analysis was completed to demonstrate an acceptable balance between the safety of the system and the operational attributes of the reactor. For the purposes of this study, safety, safety risk and safeguards/security were defined as follows. Safety is the protection of human health, planetary biospheres and assets from the effects of radiological and toxic materials. This is intimately related to system reliability and lifetime considerations. Safety Risk is a measure of the expected consequences of an accident or event sequence. This is a product of the probability and consequence of occurrence. Safeguards and Security protect against the theft, diversion, loss or sabotage of Special Nuclear Material (SNM) [6].

The general safety criteria used in this analysis, which Dieckamp developed, are as follows:

1.) Safety and Ease of Handling – The reactor system will be designed so that personnel can handle, install and repair the system before launch with safety.
2.) Prevention of Accidental Criticality - The reactor system will be designed to prevent criticality of the reactor under any condition except controlled operation.
3.) Inherent Shutdown – The reactor system will have inherent shutdown characteristics (i.e. a negative temperature coefficient and full utilization of any fundamental energy release limiting mechanism).
4.) Extraterrestrial Startup – Reactor system full power operation need not begin until after a suitably safe landing on either the Lunar or Martian surface has occurred. Thus there is no radioactivity hazard with pre-launch accident or pre-orbit abort.
5.) Extraterrestrial Shutdown – After the mission has been completed, the reactor is designed to be shutdown by a redundant combination of on board and command actuated devices.
6.) Since safety concerns permeate every step of the mission from "factory to flight" the main aspects are organized according to operational sequence.

3.8.2 Accident Scenarios

Accident scenarios considered here are those that could happen between the assembly of the MSR to the possible reentry of the MSR. The design group divided this period into four periods: transportation and assembly, launch pad testing, launch to orbit, and reentry. Each period is described and evaluated below.

Transportation and Assembly Period

During the transportation and assembly of the surface reactor's nuclear components into the launch system, the possibility of accidental criticality and an uncontrolled power excursion must be prevented. The core can be shipped to the launch pad in pieces surrounded with poisoned packaging to mitigate the possibility of a criticality event. By coupling these physical transportation requirements with carefully planned procedures and trained personnel, the potential of accidental criticality and personnel injury during the transportation and assembly period is significantly reduced.

Launch Pad Testing Period

The reactor unit is always subcritical during all launch pad checkout operations and is never operated at full power on nuclear heat prior to landing in the chosen extraterrestrial environment. Accidental criticality from extraneous neutron reflecting media is prevented by the integration of neutron poison materials in and around the core. Any sort of manual assembly which introduces moderating material, water, around the reactor, will not have the potential to cause accidental criticality. While motion of the control drum mechanisms can cause inadvertent criticality, an additional mechanism locking the control drums into place will be included in the design. This locking mechanism is not to be unlocked until the reactor has safety landed on the extraterrestrial environment.

It is important to point out that the radioactive inventory is a function of the operating history. Therefore, in the worst-case major chemical accident accompanied by a subsequent power excursion, previous analyses have indicated that only minor hazards, such as surface contamination, to the general public immediately outside of the normal launch complex exclusion radius are credible. Here, a major chemical accident was defined as complete release and/or explosion of rocket fuel or any other chemicals

utilized in the pre-launch process. The deposition of radioactivity within the exclusion radius may require temporary evacuation of personnel but after a short decay time and decontamination procedures, the launch pad can be quickly restored to usefulness [56].

Launch to Orbit Period

The wide variety of non-explosive delivery vehicle abort options including; return to launch site, east coast abort landing site, transoceanic abort landing, abort once around, and abort to orbit [57], present no significant concern since the delivery vehicle would simply touch back down on another landing strip with the reactor assembly intact. The primary concern at this stage of the mission is the chemical explosion of the launch vehicle and subsequent reactor power excursion of the system. Because of the geographic location of the U.S. launching sites, the missile path passes over land only during the early stages of launch. For this stage, previous research has indicated only minor hazards outside of the normal exclusion area. After liftoff, the dispersal and dilution factors for the altitudes associated with the missile path over land further decrease the already minor hazard. Given an explosion, the dose due to complete dispersion of 500 kg of low-enriched uranium is very low. The bottom line is that the potential hazard to the general populace from a contamination standpoint is negligible over the complete range of possible abort conditions.

Reentry Period

The previous mission periods considered allowed for the minimization of hazards through site selection, emergency procedures, etc. However, for the reentry period, the payload could reenter the earth's atmosphere at any arbitrary location and hence present a hazard to the general populace. Previous work in the SNAP development program has produced fuel element designs that can burnup and disperse at high altitude. This research went on to state that the potential effects of reentry heating, disassembly and partial burnup coupled with core deformation upon earth impact virtually eliminates any nuclear consequences from reentry on land [56]. Calculations completed in this analysis confirm that the core is in its most reactive state when launched (i.e. length of core/diameter of core = 1) so that any deformation upon ground impact would decrease the core reactivity.

A final nuclear criticality analysis was completed assuming that the reactor reentered the earth's atmosphere without burning up and crash-landed into the ocean. In order to ascertain the worst possible configuration neutronically, several different test scenarios were analyzed utilizing MCNP5. Table 3.8-1 summarizes the possible accident scenarios.

Table 3.8-1: keff for various accident analyses

k_{eff}	Reflectors Stowed	Reflectors Detached
Water	0.97081±0.00092	0.95343±0.00109
Wet Sand	0.97387±0.00095	0.96458±0.00099

3.8.3 Discussion

The "Reflectors Stowed" scenario was defined as the reactor splashing down with all of its reflector pieces intact and in-place with the poison control drums rotated fully in. The "Reflectors Detached" scenario was defined as the complete removal of all reflector materials so that the only remaining piece was the bare core itself with a 1 cm thick wrapping of Hafnium around the perimeter. The "Water" scenario was defined as the total immersion of the undeformed reactor core assembly (reflected or not) in water with all heat pipes ruptured and completely filled with water. The "Wet Sand" scenario utilized the same assumptions as the water scenario except that the water was replaced with wet sand.

As shown in Table 1, the wet sand coupled with stowed reflectors was the worst-case accident scenario for this reactor assembly since it had the highest value for the BOL K_{eff} of 0.97387±0.00095. Fortunately, from a practicality standpoint, the probability of rupturing all of the heat pipes without deforming the core is nearly zero. Therefore, this safety analysis proves that in any conceivable sort of reentry/splashdown accident scenario, this reactor assembly will remain subcritical.

The radiological concerns associated with this reactor configuration do not present any significant hazards. The pre-launch and launch period hazards can be mitigated through operational procedures and appropriate equipment and facilities. Burnup/dispersal analysis can be done to show that the system would not contribute a significant hazard if

the core's inventory were to be vaporized in the upper atmosphere. Finally, a crash-down and splash-down analysis proved that upon impact over land or water, the reactor system would remain subcritical through any kind of a worst case core deformation/separation scenario.

3.9 Summary

The core design presented in this chapter fulfills the design goals set forth in Chapter 2, such as 5 EFPY, accident safety, and controllability. In fact, the innovative design options chosen have exceeded expectations, resulting in a very robust design. The core can be launched without accident criticality concerns, will breed plutonium for 5 years on a slightly increasing reactivity curve, will operate at 1800 K with a relatively flat temperature profile, and transients will be easily controlled with rotating poison drums, which have a reactivity change of 0.049. Table 3.9-1 summarizes the key properties of the MSR.

Table 3.9-1: MSR Core Properties

Dimensions (cylinder):		**Operating Conditions:**	
Radius	24 cm	Thermal Power	1.2 MWth
Height	42 cm	Burnup	5.814 MWd/kgU
Radial Reflector Thickness	20 cm	Pellet Peak Temperature	1890 K
Control Drum Thickness	30 cm	Lithium Temperature	1800 K
Drum Poison Thickness	1.5 cm	Peaking factor (drums in)	1.31
Core Vessel Thickness	0.5 cm	Peaking factor (drums out)	1.24
Axial Reflector Height	10 cm	Flux (drums in)	4.156E+12
Materials:		Flux (drums out)	4.155E+12
Fissile Fuel	Uranium Nitride	Neutron Current (reflector OD, drums in)	1.135E+10
Cladding	Rhenium		
Structure	Rhenium	Neutron Current (reflector OD, drums out)	1.100E+10
Burnable Poison	Tantalum		
Core Vessel	Hafnium	Total Mass	2860 kg
Reflector	Zr_3Si_2	**Enrichment:**	
Reflector Poison	Tantalum Diboride	^{235}U	33.1 w/o
Coolant	Lithium	^{15}N	99.9 w/o
In-Core (tricusp array):		^{7}Li	99.9 w/o
Number of Heatpipes	129	All Others	Natural
Heatpipe Radius	1 cm	**Neutronics:**	
Lithium Radius	0.8 cm	k_{eff} (drums in, BOL)	0.976
Number of Fuel Pins	387	k_{eff} (drums out, BOL)	1.027
UN Radius	0.85 cm	k_{eff} (drums in, EOL)	0.989
Gap Outer Radius	0.9 cm	k_{eff} (drums out, EOL)	1.045
Cladding Outer Radius	1.0 cm	k_{eff} (wet sand)	0.976

3.10 Future Work

After completion of the analyses presented here, the design group determined other analyses could be conducted to better characterize the core. First, the poison content in the fuel should be optimized. Second, the cladding thickness and tricusp material thickness should be optimized to create a flatter temperature profile. A flat temperature profile is vital to provide a large margin between the operating temperature and the melting points of the materials.

Next, the radiation effects of hard neutrons and impurities on the performance of lithium coolant should be investigated. Lithium undergoes the following reactions when bombarded by neutrons:

$$^{7}Li + n \rightarrow {}^{3}T + n + {}^{4}He$$
$$^{6}Li + n \rightarrow {}^{3}T + {}^{4}He$$

The effects of these reactions on the heat pipe cooling properties must be determined. In addition, radiation effects on control electronics and in-core sensors should be evaluated and an appropriate set of sensors and control electronics chosen.

Recent investigation of UN revealed it decomposes into solid uranium, liquid uranium and nitrogen gas. Pure UN is stable up to about 2400 K. Nitride fuel with Pu, however, lowers the decomposition temperature to about 2000 K [19]. The decomposition limit is much lower than the melting point and therefore UC may be better suited for the MSR.

The reactivity coefficients also should be determined to better understand the power and temperature transients. After determining the reactivity coefficients, a power transient analysis and single drum failure accident analysis should be conducted.

To improve the safety characteristics of the system, additional launch accident protection systems should be studied. Specifically, a core ejection system might be an attractive option. Such a system could expel the core from the launch vehicle in case of an accident and allow it to parachute safely back to Earth. Such systems already exist on human rated launch vehicles and it should be possible to adapt this technology for the MSR.

4 Power Conversion System

4.1 Introduction

The purpose of the power conversion system is to convert thermal energy from the core into usable electricity and then to transfer that power to equipment on the Lunar or Martian surface. Specifically, the design criteria required that the system accept 1.2 MW of thermal power from the core, convert it to at least 100 kW of electric power and then transfer the excess energy, which the system was unable to convert, to the radiator. Once production of the electricity was complete, that power must be transformed to an appropriate voltage and current for transmission to surface instillations.

To accomplish these tasks, the power conversion system consists of three subsystems. The power conversion unit (PCU) is responsible for the production of electricity. The radiator couple is responsible for removing unconverted energy. Finally, the conversion and transmission system has the job of transforming and transmitting electric power. What follows is a discussion of the options, design and analysis of these three subsystems.

4.2 Power Conversion Unit Options

This section outlines possible PCU options for the MSR, including a brief system description and the pros and cons of each option.

4.2.1 Turbomachinery

Turbomachinery refers to the use of turbines and other dynamic devices to produce power. The greatest advantage of turbomachinery cycles is their capacity to run at thermal efficiencies as high as 50%. In space applications, however, it is important to point out that high thermal efficiency is not a critical design concern. In order to launch a system into space it must be light and compact, high efficiency must therefore give way to low specific mass. That is, an optimal system has the highest possible power generated per unit mass, not necessarily a high thermal efficiency. Thermal efficiency increases as

the temperature drop over the PCU increases. Unfortunately, as the outlet temperature from the PCU decreases, the mass of the radiator system increases. Even so, it is still appropriate to discuss three turbomachinery cycles: Brayton, Stirling and Rankine cycles.

Brayton Cycle

The Brayton cycle uses a single-phase gaseous coolant to convert thermal energy to electricity. In this cycle, energy enters at a constant pressure with a rise in temperature, as shown in Figure 4.2-1.

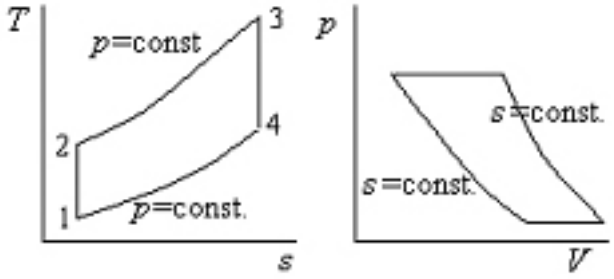

Figure 4.2-1: T-S Diagrams for Brayton Cycle [58]

The Brayton cycle can operate in either open or closed mode. In open mode, a working fluid is taken in from the environment (i.e. CO_2 in the Martian atmosphere), circulated once through the reactor, used to power turbines and then ejected from the system. In a closed Brayton cycle, a working fluid is recycled through the system continuously by recompressing it. The only moving parts in a Brayton cycle are the shaft, the turbine and the compressor as shown in Figure 4.2-2.

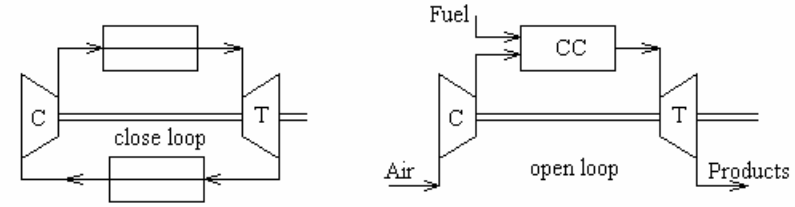

Figure 4.2-2: Closed and Open Brayton Cycles [58]

Many factors determine the efficiency of a Brayton cycle. First, in order for a Brayton cycle to produce more power than it consumes, the turbine and the compressor must have very high efficiencies – over 80%. Work is also lost in compressing the working fluid, reducing the overall efficiency. The Brayton efficiency depends mainly on the inlet and

outlet temperatures – higher inlet temperatures and lower outlet temperatures allow for more effective energy conversion [58]. The following equation, (4.2-1), for Carnot efficiency assumes 100% efficient turbines and compressors:

$$\eta_e = \frac{W_{net}}{Q_{out}} = 1 - \frac{T_{out}}{T_{in}} \qquad (4.2\text{-}1)$$

where η_e is the efficiency, W_{net} is the work out, Q_{out} is the total energy used in the cycle and T_{in} & T_{out} are the inlet and outlet temperatures, respectively. Typical efficiencies for Brayton cycles routinely approach 70% of Carnot efficiency.

The advantages to a Brayton system are most notably the large experience base that exists. In addition, the ability to use inert gaseous coolants such as helium makes this cycle attractive from a materials standpoint, minimizing corrosion concerns. Brayton cycles can also be built very compactly – one multi-megawatt system designed using dual Brayton cycles occupied the space of a cylinder 1.8 m in diameter and 1.2 m high [59]. This cycle can also accommodate high inlet temperatures, leading to higher efficiencies, or higher outlet temperatures for the same efficiency.

There are, however, disadvantages to a Brayton system in the context of space reactor design. The most notable disadvantage is the large mass required. While Brayton systems can be very light and compact, a heat exchanger is necessary to remove heat from the primary core coolant, because the system uses a gas and therefore must be physically isolated from the primary coolant, assumed to be a liquid metal. This will result in a decreased efficiency due to thermal losses and a massive heat exchanger. Thermal conductivity is approximately 30 times greater in metals than in most gases, so a large surface area is required for an effective heat exchanger from liquid metal to gas. Another disadvantage, as with any turbomachinery, is the need for fast-moving parts. For the turbine to produce sufficient electricity, it would need to spin at about 40,000 rpm. These very high speeds introduce mechanical stresses to turbine parts, increasing the possibility for turbine failure. Such a failure is difficult to fix, as it requires shutting down the reactor for maintenance. Finally, in order to achieve even modest efficiencies, the Brayton cycle demands an inlet temperature between 1000-1300 K, further stressing moving materials.

This combination of rapidly moving parts and high temperatures presents significant engineering challenges.

One Brayton cycle that seems promising in the context of a Lunar or Martian reactor is the supercritical-CO_2 cycle. Using CO_2 instead of the more common helium allows for much lower inlet temperatures (~830 K for CO_2 compared to 1170 K for He) at the tradeoff of a much higher pressure of ~10-30 MPa. Such a high pressure in a near-vacuum atmosphere presents a challenge to structural materials once again. The main advantages of this system are its efficiency and its size – cycles with inlet temperatures of 830 K have shown efficiencies of up to 50% and, as an example, a 300 MW_e turbine was designed with a diameter of only one meter. This could potentially decrease in size much more to accommodate our 100 kW_e system [60]. The system will likely not scale linearly, but it seems feasible to design a Brayton PCU with dimensions on the order of one meter for a 100 kW_e system.

The other possible working fluid would be a mixture of helium and xenon. While xenon is expensive, using a He-Xe mixture with an equivalent molecular weight to the supercritical CO_2 system, would provide a more inert working fluid with a higher thermal storage capacity.

Table 4.2-1: Estimated System Parameters for Brayton Cycle for 100kW_e System

Inlet Temperature	830K-1170K
Outlet Temperature	300K-500K
Operating Efficiency	>30%
Working Fluid	CO_2 or He-Xe
Pressure	10-30MPa
Mass	~2MT + heat exchanger + transmission cable

Stirling Cycle

The Stirling cycle also uses a single-phase gaseous fluid to convert thermal energy to electricity. The four steps in the Stirling cycle, as shown in Figure 4.2-3, are isothermal compression, constant volume compression by energy input, isothermal energy rejection through the turbine and finally constant volume heat rejection to a regenerator or radiator.

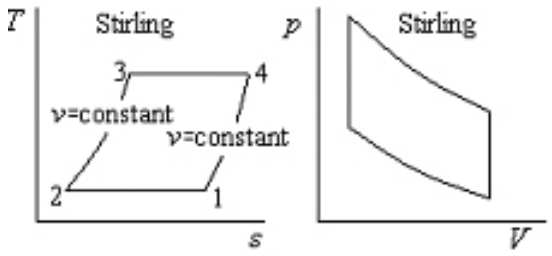

Figure 4.2-3: T-S and P-V Diagrams for Stirling Cycle [58]

The main advantage of the Stirling cycle is that it can achieve nearly Carnot efficiency even at relatively low temperatures. Systems have been demonstrated in the range of 1-2 kW_e, with efficiencies of up to 50% [58]. However, systems in the 1 kW_e range also have been prone to leaking at pressures as low as 4 MPa. Finally, a Stirling cycle requires two heat exchangers: one to get energy from the primary core coolant and one to remove energy to the radiator. These components each add mass to the system.

Recently, NASA has devoted much effort to developing Stirling systems for space applications. As part of their 25 kW_e Advanced Stirling Conversion Systems Program (ASCS) several systems have emerged. Their operating specifications are very similar and are documented in Table 4.2-1 below.

Table 4.2-2: System Parameters for a 25kW_e Stirling Engine

Inlet Temperature	980K
Outlet Temperature	330K
Operating Efficiency	>20%
Working Fluid	Helium Gas
Pressure	10-18 MPa (but hermetically sealed)
Mass	0.8MT [61] + 2 heat exchangers + transmission cable

Using four of these 25 kW_e Stirling engines produces the requisite 100 kW_e while providing a mechanism against single point system failures via redundancy. The mass of each of the conversion units in the ASCS program was about 800 kg. Four such units would be 3200 kg, which is not prohibitively large, but is significant. The low output temperature, however, is a problem from a radiation perspective. It would be necessary to

raise the inlet and outlet temperatures to achieve a reasonable radiator size. Using such unproven, high-temperature systems would require materials and reliability analyses.

Rankine Cycle

The Rankine cycle employs a phase change to aid in extracting energy from a system. This cycle takes a liquid or gaseous working fluid, heats it to the boiling point, and adds energy to turn it into a vapor. At this point there is an option to superheat the fluid, as is often done in the case of steam – superheating at a fixed temperature can be employed by reducing the pressure, and often results in a slightly higher efficiency. After heating, the fluid rejects heat isentropically. Finally, the fluid cools by means of a secondary coolant or radiator. Figure 4.2-4 illustrates this process.

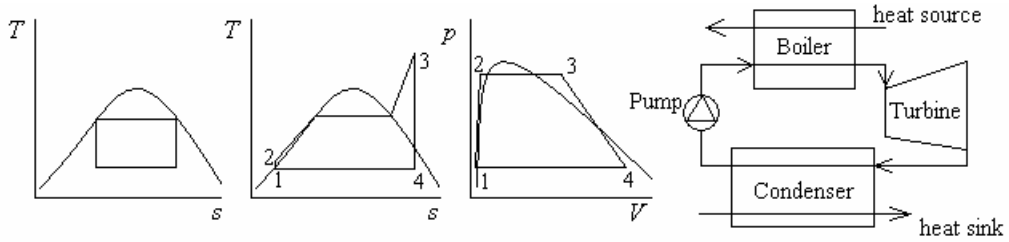

Figure 4.2-4: Diagram Showing Carnot T-S, Rankine T-S and P-V, and Cycle [58]

The work involved in condensing the working fluid is very small. Also, because heat is added and rejected at nearly constant temperature (due to the phase change), efficiencies approaching Carnot efficiency are possible.

The most viable working fluid for this cycle is NaK. There are many advantages associated with this fluid, including its non-reactivity with structural metals, low vapor pressure at high temperatures, high thermal conductivity and low turbine speeds due to its high density [63].

A disadvantage of the system is the difficulty of condensing a liquid coolant in the low gravity environment of the Moon and Mars. Normally gravity separates the phases, but the reduced gravities present a challenge. While mercury Rankine cycles have been developed for space applications, these systems require a phase separation unit which adds mass and complexity to the system. This separation is especially a problem in light

of the fact the coolant must remain gaseous in the turbine, as high-speed liquid droplets damage turbine blades.

Table 4.2-3: Estimate System Parameters for NaK Rankine Cycle for a 100kW$_e$ system

Inlet Temperature	1000K-1200K
Outlet Temperature	700K-900K
Operating Efficiency	15-25%
Working Fluid	NaK
Pressure	3atm
Mass	1MT + heat exchangers + transmission cable

4.2.2 Solid State Power Conversion

One of the major design goals of the MSR is high reliability and therefore no required maintenance. Given the violence of launch, the high operating temperature of the core and the five-year lifetime, picking a PCU system that excludes moving parts is quite advantageous. Following are a few solid state PCU options that meet this criteria.

Thermophotovoltaic Cells

Thermophotovoltaic (TPV) cells work on the same principle as traditional solar cells. Photons impinge on a semiconductor device, promoting some of the electrons to a conduction band, thereby driving an electric current. Power drawn from the TPV drives a load across the photovoltaic device. TPVs have lower bandgap energy than solar cells in the converting semiconductor, so they can operate at the temperatures of hot, radiating bodies, rather than at the energy of visible light photons [64]. Figure 4.2-5 shows a diagram of the workings of a TPV cell.

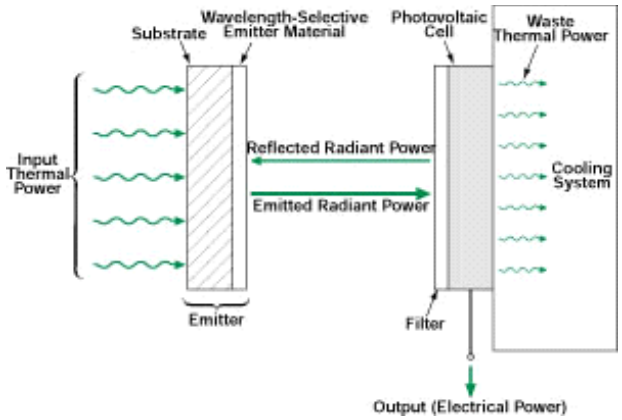

Figure 4.2-5: Operation of a Thermophotovoltaic Cell [73]

Everyday solar cells must be very large to produce a reasonable amount of power. This is because of the relatively low energy flux of the light from the sun. Positioned only a small distance from the heat source, TPVs experience a much higher energy flux than solar cells and so can be much smaller.

TPVs work best at high temperatures, as this creates higher energy photons. This ensures that the device does not require a small bandgap to operate efficiently [64]. Because of the specific bandgap energy of the semiconductor device, the TPV cells are not able to use the radiation of the entire blackbody spectrum. Photons with energies lower than the bandgap energy are not able to promote an electron to the conduction band, and photons with energies higher than the bandgap energy give the electron extra kinetic energy, which heats the TPV cell. Thus, the TPV cell is inefficient for photons with energies not equal to its bandgap energy.

The specific photon energy needed for high cell efficiencies does not match well with the broad blackbody spectrum produced by radiating bodies. One way to combat this inefficiency is to use a narrow band optical filter in front of the TPV cell [65]. The filter transmits photons with energy equal to the bandgap energy and reflects all other photons back to the blackbody. This raises the efficiency of the conversion device, since the energy from these other photons returns to blackbody rather than simply being lost as radiation out from the TPV.

The efficiency of the TPV system also increases by using a selective emitter, such as ytterbium [65]. Ytterbium is a member of a class of rare earth metals, which instead of emitting a normal blackbody spectrum, emits spectra that resembles line radiation spectra. This allows the relatively narrow emitted energy spectrum to match the bandgap of the TPV cell. Using an ytterbium emitter at 2000 K and a silicon TPV cell, researchers have been able to build a system with a total efficiency of just over 10% [65]. Evidence of higher efficiencies have not been presented, but higher efficiencies of up to 40% of the Carnot efficiency are not out of the range of theoretical possibility [65],[67]. To achieve such efficiencies would require substantial developmental work.

Table 4.2-4 shows a description of an ideal GaSb cell. At 1500 K, there is an ideal efficiency of 2.13 W/cm^2 [65]. For scaling the reactor to 200 kW$_e$, the design requires 10^5 cm^2 of TPV material. This could be satisfied by a modestly sized cylinder two meters in height and diameter.

Table 4.2-4: System Parameters for TPVs

Operating Temperature	1500-2000K
Efficiency	10-20%
Power Conversion Density	2-2.5W/cm^2
Approximate Dimensions	2 meters x 2 meters
Approximate Weight	100s of kilograms

The fact that TPVs are solid state brings a number of advantages to the system. It ensures the system is lightweight and therefore small in mass. The TPV also acts as its own radiator as it rejects frequencies not in its range. However, the semi-conductor must be cooled to several hundred degrees, posing a significant engineering challenge. Finally, the materials used to manufacture TPVs are inert and cheap due to recent advances in solar cell technology.

Thermoelectric Conversion

Thermoelectric conversion uses a solid slab of semiconductor material to convert thermal energy directly to electricity. Energy flows from the core through a thermoelectric converter into a heat sink. The temperature difference produced across the converter's

semiconductor produces a voltage difference across the two ends [69]. Figure 4.2-6 shows a diagram of a typical thermoelectric cell configuration.

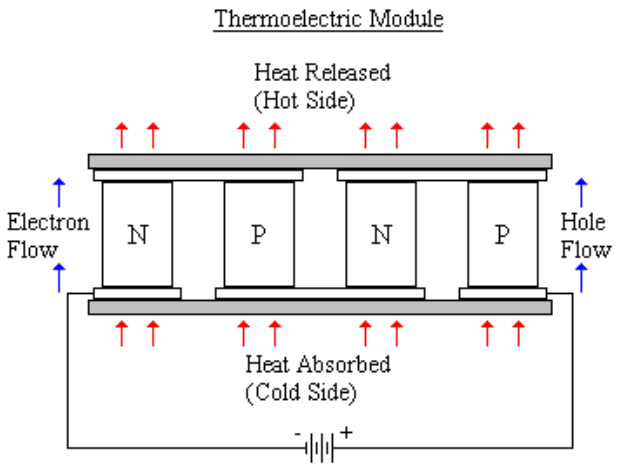

Figure 4.2-6: Thermoelectric Cell Configuration [75]

Commonly used materials in space systems are various alloys of germanium and silicon (GeSi), lead-telluride (PbTe), and lead-silicon-telluride (PbSnTe). The PbTe systems are limited to a low temperature (~800 K) by sublimation and have a theoretical conversion efficiency of 15% of the Carnot efficiency. GeSi systems have a lower conversion efficiency of 10-15% of Carnot [69].

Most thermoelectric conversion studies involve very low power systems. The systems used in space previously have been about 2 kW_e [69]. Because of the low efficiency and low operating temperature, a large radiator is required, adding to the size of the system.

The total system size is manageable for low power levels, but for high power levels, the size and mass of the system are substantial. Assuming the system mass scales linearly with power level, the total mass of a 100 kW_e system is approximately 30 MT. Table 4.2-5 summarizes these specifications.

Table 4.2-5: System Parameters for Thermoelectric Devices [69]

Operating Temperature	~1000K
Efficiency	5-10%
Power Conversion Density	Low
Approximate Dimensions	Prohibitively Massive
Approximate Weight	10s of tons

Again, using a solid-state device, such as thermoelectric, ensures reliability and has the advantage of previous space experience. However, these devices require a low operating temperature, have an inherently low efficiency and can be quite massive.

Thermionic Power Conversion

Thermionic conversion uses energy from the core to boil electrons off a hot filament in a small vacuum device. The electrons flow to a cold electrode, where they are collected and provide current to a load [69].

There are several options for the vacuum device. A thermionic using a vacuum diode, where a hard vacuum separates the anode and the cathode, requires an anode/cathode separation of several thousandths of a millimeter. On the other hand, if a cesium diode is used, where the vacuum gap contains a small number of positive cesium ions, the spacing requirement is less stringent and the system operates at a higher efficiency [69].

Using a cesium diode, these systems can operate at emitter temperatures of 1500-3000 K, power densities of 5-15 W/cm^2 and efficiencies of 6-18% [69]. Higher temperatures are required to achieve the highest power densities, since at lower temperatures thermal radiation dominates over the electron boiling mechanism. Higher temperatures also lead to the highest system efficiencies [69].

In addition to the choice of diode, an appropriate choice of material for the thermionic electrode will increase the robustness of the system as it can protect against the degenerative effects of high neutron flux expected from the MSR core. The only material constraint on a thermionics cathode is that it requires a relatively low electron work

function to allow current to flow. In principle, any metal will suffice. Table 4.2-6 provides a summary of a model 100 kW_e thermionic system.

Table 4.2-6: System Parameters for Thermionic Devices

Operating Temperature	~1500-3000K
Efficiency	6-18%
Power Conversion Density	5-15W/cm^2
Approximate Dimensions	10,000 cm^2 of cathode surface area
Approximate Weight	Low (100s of kilograms)

These systems exhibit very high reliability and are well characterized. Because they can be made of metal instead of semiconductors, they can better resist damage from high neutron flux, making them especially robust for a fast reactor. Finally, the thermionic converters are small in both size and mass. They do however require high operating temperatures.

Magnetohydrodynamic Power Conversion

Magnetohydrodynamic (MHD) power generation is a method of power generation based on passing plasma (high temperature ionized gas) perpendicularly through a magnetic field [71]. In accordance with Faraday's law of induction, this process generates a current perpendicular to both the gas flow and magnetic field. Figure 4.2-7 below illustrates this concept. The biggest advantage in using MHD technology in space is that it operates at high temperatures, 2000 – 3000 K, and at high efficiencies, 70% [76].

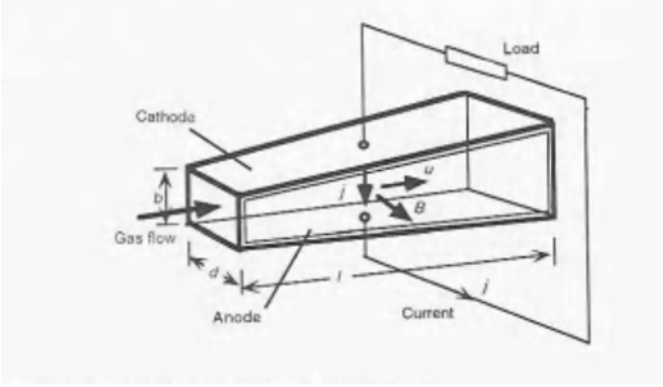

Figure 4.2-7: Schematic of Magnetohydrodynamic Power Generation Concept [72]

For this technology to operate properly, a super-cooled magnet must be employed and a high-energy plasma must be maintained. In addition, a 2000 K gradient is needed in a small, confined space. This technology is currently under development for space applications; however, it is still at the stage of development where a majority of the research is unpublished, proprietary information. Thus, in addition to the extreme complexity of the system, the level of development of this technology and access to information about it limits MHD viability as a PCU option for this project.

4.2.3 Electrochemical Cells

Electrochemical cells use chemical potentials to convert thermal energy to potential energy, then into electricity. Theoretically, this can be done with a high efficiency, and does not require as high a temperature as the systems described above.

Electrolytic Cells

Electrolytic cells are non-spontaneous. They require an ionic bond to be broken, the ions to drift to the appropriate terminal (cation to the cathode, anion to the anode), thus creating a current. Figure 2.3-2 clearly illustrates this process. NaCl is boiled to form liquid sodium and chlorine gas. The sodium ions migrate toward the cathode, where they reduce to sodium metal. Similarly, chloride ions migrate to the anode and oxidize to form chlorine gas. This type of cell produces sodium and chlorine which can be recombine and reused. We have ruled out electrolytic cells for this project as they have a low power density and because they are a completely unproven technology on the scale needed here.

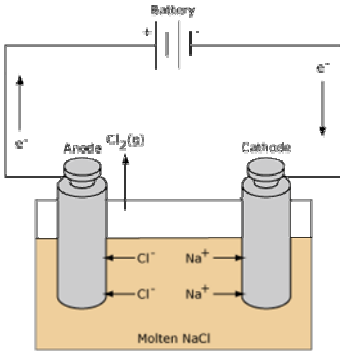

Figure 4.2-8: Electrolytic Cell [77]

4.3 Power Conversion Unit Decision

With the above PCU options in hand, the design team selected an appropriate system using the formal decision methodology as described in Section 2.3. First, each option passed through the litmus test to eliminate obviously unsuitable candidates, and then the remaining options underwent further scrutiny using the extent-to-which test. Presented below are the details of this analysis.

4.3.1 Litmus Test

Through the litmus test, the design team eliminated the following four (of eight) power conversion options: Rankine, TPVs, electrochemical cells and MHDs. The Rankine cycle failed the safety test. The working fluids for the Rankine cycle are unfavorable from a launch accident perspective: NaK may react violently upon splashdown and mercury is highly toxic. In addition, there is high risk associated with the possible leakage of gaseous NaK. Further problems with this system include working fluid activation and difficulties of phase separation in the low gravity environments of the Moon and Mars.

Due to the large temperature gradient required for TPVs to function, the design team determined that, due to materials concerns, they could not be expected to operate for five EFPY in a reliable manner. Furthermore, this technology has very low efficiency and requires much more development to work at lower band gap energies.

Electrochemical cells failed because they do not meet the $100kW_e$ criterion. They have too low power densities and voltages.

Finally, the design team rejected the magnetohydrodynamic power conversion system because it also failed the 5 EFPY litmus test. The system is too complex and unproven to function reliably. Another, specific, concern regarding MHD is maintaining a superconducting magnet in the Lunar or Martian environment.

4.3.2 Extent-to-Which Test

Having ruled out half of the power conversion options, we can now apply the extent-to-which test on the remaining four: Stirling, Brayton, thermoelectrics and thermionics. Table 4.3-1 below illustrates the extent-to-which test:

Table 4.3-1: Power Conversion Unit Decision Methodology

		Option			
		Brayton	Stirling	Thermoelectrics	Thermionics
Criterion	***Small Mass and Size (Cost) - 1.35***				
	Actual PCU	3	2	1	4
	Outlet Temperature	2	2	3	4
	Peripheral Systems (i.e. Heat Exchangers)	3	3	3	3
	Launchable/Accident Safe - 1.13				
	Robust to forces of launch	3	3	3	4
	Fits in rocket	4	4	4	4
	Controllable - 1.14	3	3	4	4
	High Reliability and Limited Maintenance - 1.00				
	Moving Parts	1	2	4	4
	Radiation Resistant	3	3	1	4
	Single Point Failure	1	2	3	3
	Proven System	3	3	3	3
	Inlet Temperature	3	3	3	1
	Performance Index	**33.1**	**33.75**	**35.88**	**43.41**

Small Mass and Size

In order to be able to rank the four systems based on mass and size, the design team designated three subcategories affecting size and mass of the system: actual PCU size, size of peripheral systems and outlet temperature.

For actual PCU size, thermionics is the best and thermoelectric is the worst. A 25 kW_e Stirling engine, operating at 25% thermal efficiency, weighs roughly 800 kg. A 100 kW_e Stirling PCU system would be four 25 kW_e engines operating in parallel, weighing 3200 kg. Thermionics weigh hundreds of kilograms, and a Brayton system would fall somewhere in between these two systems. Thermoelectrics, because of their low power density would be significantly heavier than even the turbomachinery designs.

Each of the PCU options have accompanying accessories required to operate. Both Brayton and Stirling require two heat exchangers: one on the reactor side and one on the

radiator side. The thermionic system requires a cesium reservoir (of negligible mass), DC-to-AC conversion unit and a possible heat exchanger for the radiator. Thermoelectrics require a similar system to thermionics for DC-to-AC conversion and transmission. To a first approximation, the peripheral systems for all four options seem to be equally massive.

The outlet temperature is part of the mass metric because it dictates the radiator size. For thermionics and thermoelectrics, inlet temperatures must be on the order of 1800 K, giving an outlet temperature of roughly 950 K at 10% efficiency. The highest temperature at which Stirling systems currently function is about 1000 K [61]; however, we assumed that with development, this temperature could be raised to 1200 K. With this optimistic inlet temperature, the outlet temperature is 950 K for operation at 25% efficiency. Brayton cycles are less efficient than Stirling engines and so a slightly worse outlet temperature is expected. When taking into account appropriate inlet temperatures, all three options have an outlet temperature of roughly 950 K, and are equal in this category.

Launchable / Accident Safe

Assuming a helium working fluid for Brayton and Stirling cycles, none of the four systems had toxic components that could release into the environment in the case of a launch accident. Therefore, the only two criteria of launchable/accident safe that required consideration were: robustness to launch vibrations and stresses and ability to fit inside the launch vehicle. The robustness to forces of launch is directly proportional to the number and precision of moving parts in the system. This ranks Brayton behind Stirling. Thermionics and thermoelectrics are solid-state technologies, and are less sensitive to the violent vibrations and large forces associated with launch. This is not to say that static systems are insensitive to launch forces; they may potentially short out if launch forces are so violent such that the contacts come together. This may be mitigated, however, by using ceramic spacers. Also, these systems have a history of space flight as they have been widely used in satellite power systems.

The multiple Stirling engine option takes an estimated 5% of the available volume of the assumed launch vehicle. Thermionics and thermoelectrics take almost no volume and

Brayton lies somewhere in between. Even though the systems have different volumes, they were all small compared to the available volume so all were equally weighted.

Controllable

All four systems rely upon simple methods of control. Brayton and Stirling systems need to regulate pressure, and Brayton needs to control turbine speed as well. Because cesium undergoes transmutation to barium when bombarded with neutrons, it is necessary to have a cesium reservoir and control system for proper operation of thermionics. Finally, thermoelectrics are completely passive devices.

High Reliability and Limited Maintenance

In order to compare the reliability of the four systems, five criteria exist, determined according to possible weaknesses in each system. Mechanical strains were the primary concern in the reliability question, and so four of the five reliability criteria address this issue: number of moving parts, radiation resistance, effects of a single point failure, and inlet temperature. Finally, technology readiness was also included as a measure of reliability because there is a much larger risk associated with untested technologies.

Brayton engines have more moving parts than Stirling engines, and thermionics and thermoelectrics have essentially none; therefore, these last two are inherently more resistant to mechanical breakdown.

Thermionics and thermoelectrics are the least radiation resistant as thermionics undergo cesium transmutation and thermoelectrics employ semiconductors. Brayton turbine blades and Stirling metal flexors can become embrittled by radiation. However, in Stirling engines, using gas bearings can enhance the radiation resistance of the system significantly.

Single point failures occur when the failure of one part of the system causes the entire system to fail. The solid state systems are equally susceptible to single point failures in the peripheral systems (i.e. heat exchangers), but in the actual PCU system, they are essentially unsusceptible to single point failures. The wiring scheme of these systems is such that if one cell shorts, then the system only looses a small fraction of its power

conversion capabilities. Stirling also has a bit of flexibility when it comes to single point failures. There are four Stirling engines, and if one fails then 25% of total power conversion capabilities are lost. The Brayton option consists of one turbine, so a failure in this system would result in total loss of conversion capabilities.

By NASA standards, using proven technology is important to reduce both risk and cost. In regards to space applications, Stirling engines have undergone substantial testing, and industry has adequately demonstrated 25 kW_e engines [61][62]. Thermionics have also undergone much development in the context of space application. The Russian Topaz II and the American SNAP-10A (flown in Earth orbit) used thermionics as their PCU [79]. In addition, the DOE currently has a program underway to develop and test a 40 kW_e thermionic conversion unit for space applications. Brayton cycles have also been tested for space application, and as a terrestrial technology it is the most well known of the four options. In absence of a readily available Technology Readiness Level designation for the four systems, they received equal rankings for the extent-to-which test.

Finally, the last measure of reliability was inlet temperature. Higher temperature leads to more mechanical stress on the system – both in the PCU and, perhaps more importantly, in the actual reactor core. Thermionic and thermoelectric cells require a much higher hot-side temperature than the turbomachinery systems can stand (1800 K versus 1200 K). Therefore, they are worse than both Brayton and Stirling in terms of inlet temperature needs as relevant to reliability.

4.3.3 Thermionics as the Power Conversion Unit

The overall score of the extent-to-which test led to selection of thermionics as the PCU for the MSR, with thermoelectrics coming in second. Overall, thermionics were smaller and more launchable/accident safe than the other systems. Thermionics, however, ranked low in reliability, specifically ranking lowest in radiation resistance and inlet temperature requirements. It is now appropriate to address these reliability concerns to justify the thermionics selection.

In terms of radiation resistance, as said before, cesium undergoes transmutation to barium during neutron bombardment. Placing light neutron shielding between the core and the

thermionic cells, in addition to having a cesium reservoir to replace the transmuted cesium, alleviates this problem. Section 4.4.2 provides further discussion of radiation effects on thermionics.

The high postulated inlet temperature of 1800 K presents, in general, certain difficulties, however, the chosen thermionic design, discussed in section 4.4.2, specifically allows for operation at these temperatures. Over five years at 1800 K, ceramic spacers resolve possible issues of creep in the thermionic cells [80]. From the core perspective, 1800 K is not unreasonable as these types of systems have been designed and tested for five or more years – specifically, the Topaz II had an operating temperature reaching 1900 K [137].

An important concern facing thermionics that is not well captured in the extent-to-which test is power transmission. Solid state PCUs output direct current. DC-to-AC conversion is generally inefficient, and DC transmission losses over long distances can be large. Section 4.5 addresses the problem of power transmission in more detail.

4.4 Design and Analysis of Thermionic PCU System

With thermionic emitters now selected as the most feasible PCU technology, we shall discuss the details of that technology and then the design of the system. We begin with a brief description of the workings of thermionics and then proceed to delineate design parameters, the implications of these parameters and other specifics of the design.

4.4.1 Introduction to Thermionic Technology

Thermionic converters convert thermal energy directly to electrical energy. The thermionic device is a diode in which a vacuum or a very low-pressure cesium gas separates the two electrodes. Heat applied to the cathode of the device causes electrons to boil off the surface of the cathode. The anode collects these electrons. The cathode and anode connect electrically across a load such that the electron boiling mechanism acts as a current source, and is therefore the mechanism for the heat-to-electricity conversion [84]. Figure 4.4-1 shows a basic schematic of this system.

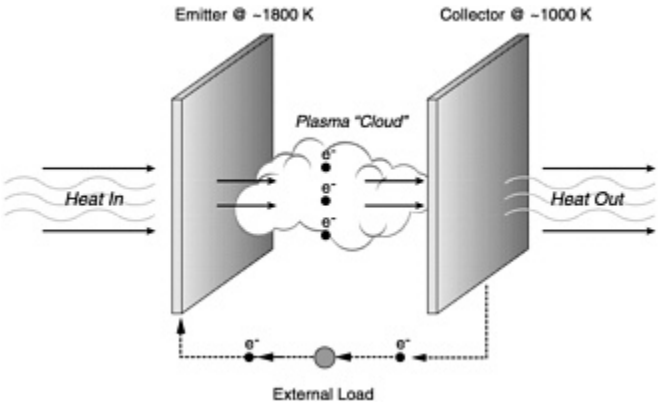

Figure 4.4-1: Schematic of a Thermionic Device [83]

The thermal energy in the system is the only energy available to eject an electron from the emitter surface. Thus, temperatures in thermionic converters must be high enough to eject an electron from the surface of the emitter. Inefficiencies in thermionic systems arise because of the constant thermal energy loss mechanisms of thermal radiation between the diodes and heat losses through the supporting structure and electrical leads connected to the system. It is therefore necessary that the work function of the thermionic emitter be sufficiently low that cooling of the thermionic cathode through electron boiling occurs at a rate comparable to the other thermal dissipation mechanisms. In order to have a thermionic converter with conversion efficiency above a few percent, the work function of the cathode must be on the order of a few eV.

Vacuum diode thermionics are the simplest diode design. In these systems, a vacuum separates the two electrodes of the thermionic cell. Vacuum diodes work well for very low power levels, but since they provide only approximately 1-2 W/cm^2 of power, they do not provide the power density necessary for the MSR [84]. The difficulties in producing higher power vacuum diode thermionics come about because of space charge within the thermionic converter. Electrons flowing across the gap between the thermionic diodes produce a net negative charge within the gap, repelling other electrons emitted by the cathode. Because of this phenomenon, the diodes must lie extremely close together and the current density must be low in order to limit the number of electrons in the gap. These devices require relatively low temperatures (1000-1200 K) when compared to cesium thermionics.

Both power density and efficiency increases significantly upon introduction of cesium vapor into the gap between the diodes [84]. The vapor deposits in a monolayer on the cathode surface where the cesium ions are heated, forming a low-density cesium plasma in the inter-electrode gap [81]. The positive cesium ions cancel out the space charge caused by the electrons flowing across the thermionic. This allows cesium diode thermionic converters to have a larger gap and to be able to sustain higher current densities. These devices require emitter temperatures between 1500-2200 K to operate effectively.

The cesium deposited on the cathode surface also has the effect of dramatically lowering the work function of that surface [81]. A tungsten emitter, for example, normally has a work function of about 4eV, but this value can drop to 1.8eV when coating the surface with a monolayer of cesium. This allows cesium diode converters to operate at a much higher efficiency than vacuum diode converters; studies have shown up to 25% efficiency for cesium diode converters compared to 2-6% efficiency for vacuum diode converters [84].

Thermionics require a high cathode temperature to be able to operate efficiently [84]. When applying thermionic technology to nuclear reactor power conversion, the high temperature demands that the thermionics be physically close to the reactor core in order to minimize temperature drop between the core and the emitter, and to maximize efficiency [81]. Thus, thermionics in previous designs have typically been located inside the core itself, or directly outside of the core. Figure 4.4-2 shows examples of power densities for different designs.

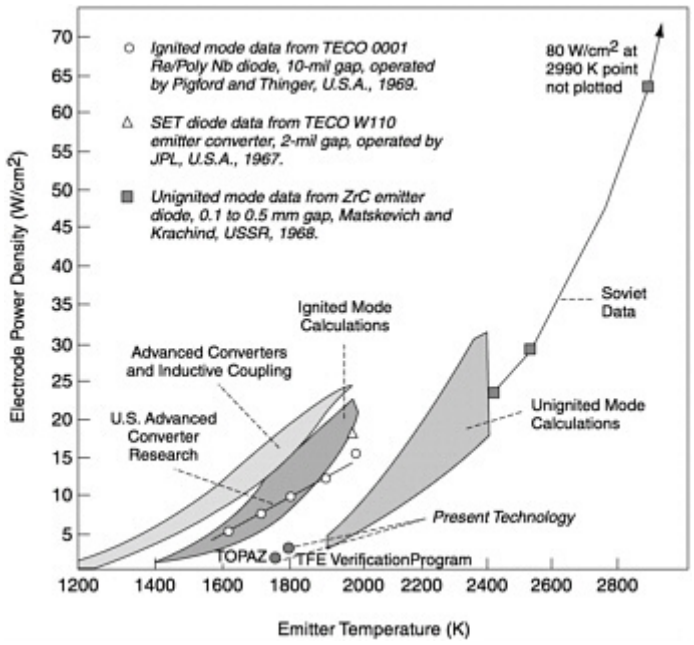

Figure 4.4-2: Examples of Calculated Power Densities for Thermionic Systems [86]

Thermionics bring several benefits to the design of the PCU. As said before, they are solid-state devices, so there is no opportunity for failure of moving parts. A relatively small surface area of the thermionic devices is necessary to convert the power from the core, so the mass of the thermionics themselves is quite low [81]. They have efficiencies up to 25% [81], and they have a high operating temperature. These characteristics lower the required radiator mass for the conversion system.

Thermionics also have several drawbacks that bare some consideration in the design of the system. They require sub-millimeter separation of the electrodes in order to operate efficiently [84]. This leads to the possibility of electrical shorts in the system which would render the thermionic useless. Careful attention is necessary when choosing the electrode materials, electrode spacing and cesium pressure to assure that the system will operate above design threshold efficiency, here selected to be 10% to balance core and radiator requirements. These issues are discussed further in this section.

4.4.2 System Description and Specifications

The thermionic power conversion system met the design criteria outlined in Chapter 2. The thermionic cathodes run at a temperature of 1800 K, and the anodes at a temperature of 950 K to increase efficiency of the system while still minimizing radiator size. The

system uses an out-of-core thermionic design in order to simplify core design and minimize radiation damage to the thermionic system. Heat pipes transport heat from the reactor to the thermionics. Each core heat pipe has its own thermionic emitter. In order to minimize the temperature drop between the core and the thermionic conversion system, the surface of the heat pipes is in direct contact with the thermionic cathode as shown in Figure 4.4-3.

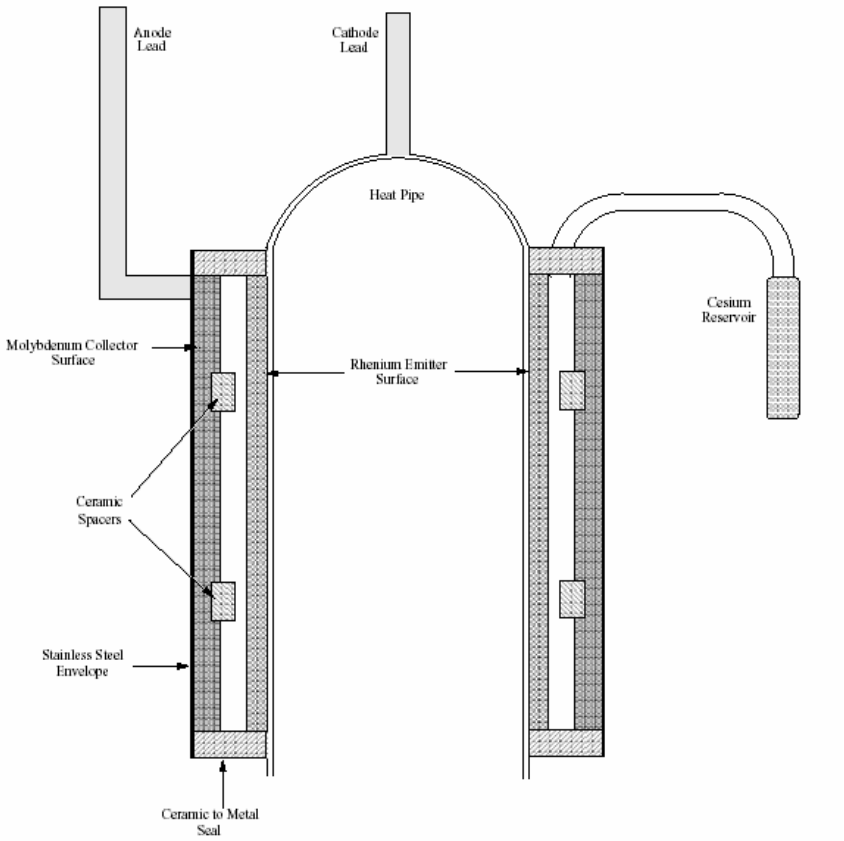

Figure 4.4-3: Schematic of Thermionic Emitter Deposited on a Core Heat Pipe

The thermionic anode forms a cylinder surrounding the heat pipe/thermionic cathode. The anode must be machined to the correct dimensions such that, after the thermal expansion of the materials, the correct inter-electrode spacing will exist in the thermionic device. The inter-electrode spacing is on the order of 0.13 mm post-expansion; however, determining the exact spacing of the thermionic system is best determined experimentally and is left to future research.

In addition to expansion of the anode, the heat pipe cathode design placed requirements on the power density of the conversion system. The system has to have a power density high enough that the heat pipes from the core would have sufficient surface area to convert the 100 kW_e demanded from the system. This goal specified a target power density of 10 W/cm^2 [82]. We turn now to the individual components of the device.

Diode Type

Because of the high power density requirement and high operating temperature of the reactor, a cesium diode design was appropriate. A cesium reservoir is located near the thermionic devices to provide cesium vapor to the gap between the electrodes. The pressure of cesium between the electrodes is a function of the reservoir temperature, and this temperature can easily be maintained with a heating coil and a small microcontroller [81]. The optimum cesium pressure can, again, most easily be determined experimentally with a prototype thermionic converter manufactured with the materials and dimensions described here.

In addition to the electrical benefits of a cesium diode device, Table 4.4-1 shows a comparison of vacuum and cesium diodes. Note that cesium diode thermionics offer many advantages over vacuum diode thermionics. Cesium diode thermionics operate at a higher temperature, meaning that the output to the radiator is also at a higher temperature and system mass is lower. The inter-electrode spacing is greater, which decreases the possibility of developing electrical shorts from creep. The power density is greater, allowing a smaller power conversion unit to be constructed. Furthermore, the efficiency of the system is superior.

Table 4.4-1: Typical Thermionic Converter Performances [69]

	Vacuum Diode	***Cesium Diode***
Emitter Temperature (K)	810-1310	1700-2200
Collector Temperature (K)	644-866	866-1033
Inter-electrode spacing (μm)	7.8 to 13	52 to 130
Power Density (watts/cm^2)	1 to 2	5 to 15
Efficiency (%)	2 to 6	6 to 18

As mentioned in Section 4.4.1, one disadvantage of using a cesium diode is the transmutation of cesium to barium by high-energy neutrons. This is not considered excessively detrimental for two reasons. First, each thermionic device will have a cesium reservoir that continually replenishes the cesium plasma in the diode. Shielding on these reservoirs prevents transmutation of the cesium inside. Second, the work function of barium, which higher than that for cesium, is also quite low – studies have shown that transmutation of all the cesium to barium in a cesium diode will only increase the work function by 0.8V [85].

Emitter Material

In order to increase thermionic emission from the emitter diodes, the emitter must have as low a work function as possible, with the additional requirement that the emitter be able to withstand the high temperature produced by the core. Refractory metals are able to withstand the 1800 K temperatures without melting, and their work functions are reasonably low. Electro-etched rhenium met these requirements as it had the potential for the highest power density of the refractory metal emitter materials at 1800 K [81]. With the cesium coating then, the work function approaches 1.81eV, the work function of pure cesium [81].

Rhenium is notably difficult to machine, but in the thermionic design presented, the rhenium does not need to have a great deal of structural integrity. Rhenium deposition on the outside of the heat pipe to form the emitting surface allows the heat pipe to provide structural stability to the rhenium emitter.

Emitter Temperature

In general, higher emitter temperatures produce better thermionic performance; power density and conversion efficiency dramatically increases with increased temperature in the range from 1600-2000 K [81]. This range arises from the electrical characteristics of thermionic conversion systems. As temperature increases, the increased rate of electron boiling more than compensates for the increased losses through radiation and conduction

caused by the increased operating temperature [83]. Figure 4.4-4 is an example graph of electron current vs. temperature.

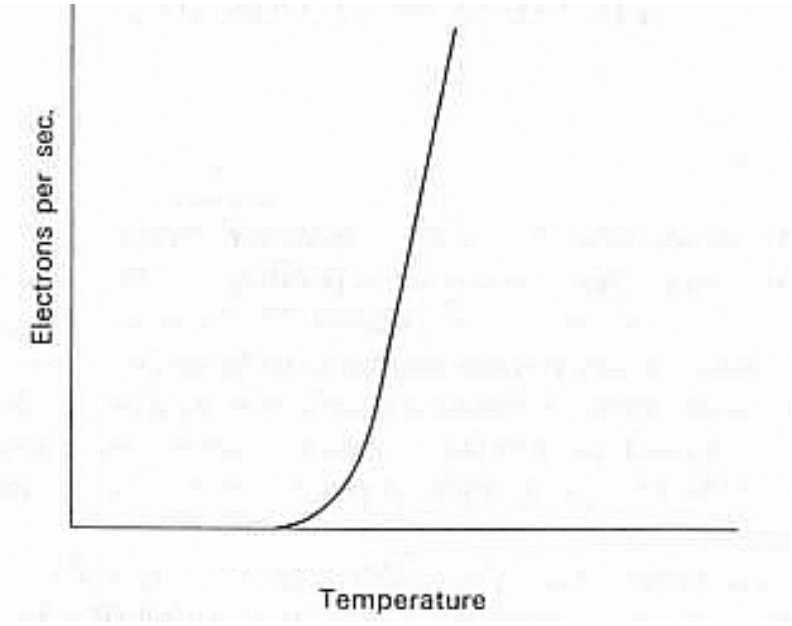

Figure 4.4-4: Example Curve of Electron Current vs. Emitter Temperature [86]

For our applications, the emitter temperature arose from the need to balance thermionic efficiency with materials constraints in the core. A maximum core operating temperature of 2000 K immerged during the design process, so after a 10% safety margin, the team agreed on an emitter temperature of 1800 K.

Collector Material

The work function of the collector material gives an approximate determination of the output voltage of the thermionic converter [81]. In reality, the output voltage will depend on several complex interactions with the cesium plasma between the diodes and on the output current density of the thermionic device. For an emitter temperature of 1800 K, the investigators chose the work functions of the emitter and the collector to be separated by about 1eV [81]. The same requirements of resistance to high temperature apply to the collector. There is an additional requirement that the material be structurally sound, since the collector material will be required to form a separate structure on the outside of the thermionic device. The high operating temperature and low work function requirements

steer the decision again towards refractory metals. Molybdenum met these needs as well as the needs for structural integrity and machinability.

Collector Temperature

The collector temperature has an effect on the electrical characteristics of the system since increased temperature lowers the collector work function, and, therefore, the thermionic output voltage, as shown in the equation below [82]. At high temperatures, electrons can boil off the collector as well as the emitter, creating a back current. To minimize this back current, the collector needs to have a high work function. The work function (φ_E) of a surface is given by Equation (4.4-1)

$$\phi_E = kT_E \ln \frac{120 T_E^{\ 2}}{J} \qquad (4.4\text{-}1)$$

where k is Boltzmann's constant, T_E is the temperature of the surface, and J is the current leaving the surface [81]. We see that lowering the collector surface temperature is advantageous, for this increases the work function of the collector. This in turn lowers the electron emissivity of the surface, increasing the emitter to collector current and therefore the efficiency of the device. While lower collector temperatures are preferable from the thermionics standpoint, the radiator mass grows substantially as the collector temperature decreases, and thus a trade off occurs.

The ideal collector temperature is extremely difficult to calculate from first principles, and, in general, can only be accurately determined by experimentally measuring the electrical characteristics of a thermionic system for a range of collector temperatures. For a system similar to this one, with an emitter temperature of 1800 K, an ideal collector temperature of 950 K was optimal [82]. This temperature is not prohibitively low from a radiator mass perspective, and so the investigators chose 950 K as the collector temperature with the understanding that optimization of this temperature is future work.

Electrode Spacing

The electrode spacing of the thermionic device affects the electrical characteristics of the device as well as the efficiency. Again, experimentation most accurately determines the

effects of the electrode spacing, and performing an optimization of the electrode spacing in the manufacturing phase of thermionic development would not pose difficulties. Figure 4.4-5 is an example curve of electrode spacing vs. output voltage for a similar system. The optimum electrode spacing was 0.13 millimeters [81].

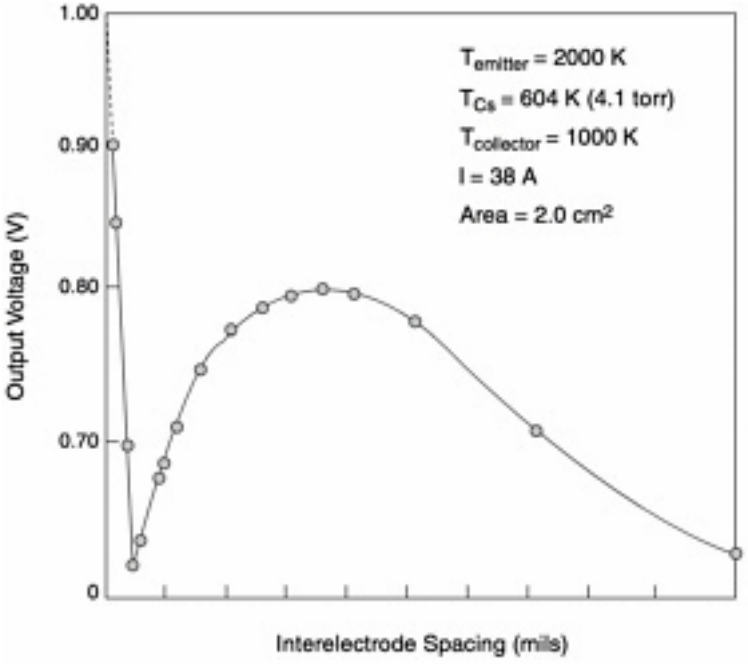

Figure 4.4-5: Output Voltage vs. Inter-electrode Spacing of a Thermionic Device [86]

Estimate of Cesium Reservoir Size

The cesium vapor has a pressure of no higher than 1.3 kPa with a temperature of no lower than 650 K. The volume of the vapor space of the system is approximately 96 cm^3, which is the approximate material volume of 127 hollow cylinders with a 1.5 cm radius, 16 cm length and 5 mm wall thickness corresponding to the 127 core heat pipes.

Using the Ideal Gas Law, PV=nRT, $1.21*10^{21}$ atoms of cesium are required in the system. This translates to $2*10^{-3}$ moles of cesium. Cesium has a weight of 132.9 g/mol and a density of 1.873 g/cm^3. Therefore, the system requires 0.14 cm^3 of cesium in order to operate. There is some additional cesium in the tubing connecting the cesium reservoir to the thermionic units. A reservoir with a volume of 10 cm^3 (approximately 19 grams of cesium) would contain more than enough cesium for the entire power conversion unit.

Cesium to Barium Conversion Rate

Cesium-133, the only stable isotope of Cesium, undergoes the following reaction in the presence of a neutron flux:

$$Cs^{133}(n,\gamma) \rightarrow Cs^{134} \rightarrow Ba^{134} + \beta \qquad (4.4\text{-}2)$$

A significant fraction of barium impurity in the thermionic system would lower the efficiency of the system since barium's work function is larger than that of cesium.

The neutron current coming out of the top of the core is about $4*10^{12}$ neutrons/cm^2 with an average energy of 500 keV. At this energy, the cross-section of Cs^{133} for the (n, γ) reaction is 0.111 barns. The maximum cesium pressure will be 1.3 kPa, and the minimum temperature will be 650 K. Using an ideal gas model for the cesium vapor, the number of particles per cubic centimeter is determined:

$$n = \frac{PV}{kT} = 1.49*10^{17}\ \frac{particles}{cm^3} \qquad (4.4\text{-}3)$$

The reaction rate based on the cross section, the neutron current, and the number of target nuclei is:

$$Rate_{reaction} = J*\Sigma = 6.6*10^{4}\ \frac{1}{cm^3 * \sec} \qquad (4.4\text{-}4)$$

Over the entire operating lifetime of the reactor, 5 years, $1.1*10^{13}$ particles of barium would result per cubic centimeter of thermionic gap. Since there will be $1.49*10^{17}$ particles of cesium in the gap, the barium will account for a maximum impurity of 0.01% in the cesium system. This level is negligible.

4.4.3 Expected Performance Characteristics

In calculating the expected performance characteristics, conservative estimates were used to ensure reliable functioning of the devices. The investigators are aware of recent developments in efficiency as well as manufacturing techniques, but still decided to use well-proven technologies, data and figures in these calculations. Any improvements in

stated assumptions only serve to increase the electrical output of the system without noticeably affecting operation.

Efficiency

Figure 4.4-6 shows examples of thermionic efficiencies. It shows that 1800 K is close to the minimum input temperature required for a system efficiency of greater than 10%. Performance improves dramatically for small increases in input temperature in the range from 1600-2200 K. Thus, small increases in the output core temperature can translate into greatly improved power conversion. Our system expected an efficiency of about 10%, which the figure supports. More detailed efficiency calculations based on first principles appear in Appendix A. These calculations purport a much higher efficiency, but do not capture certain physical abnormalities that serve to lower efficiency. As such, Figure 4.4-6, was the best estimate of efficiency available.

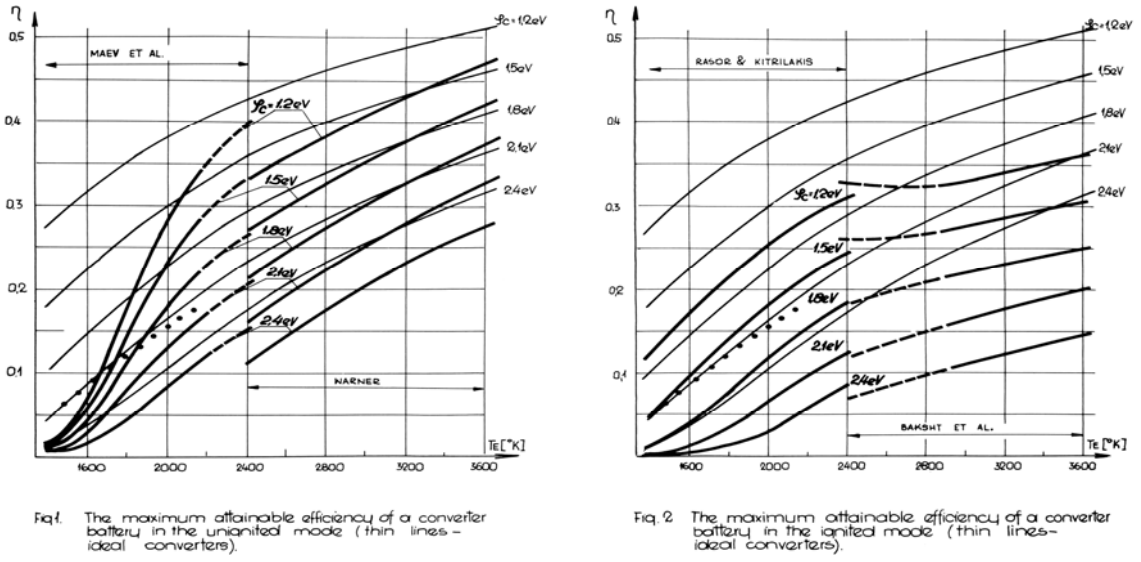

Fig.1. The maximum attainable efficiency of a converter battery in the unignited mode (thin lines – ideal converters).

Fig. 2 The maximum attainable efficiency of a converter battery in the ignited mode (thin lines – ideal converters).

Figure 4.4-6: Maximum Efficiencies for Thermionics at Various Temperatures [83]

Mass and Area

The thermionics require 10,000 cm^2 of surface area in order to operate at a power density of 10 W/cm^2 and produce 100 kWe. Since there will be 127 heat pipes, each heat pipe will have 80 cm^2 of thermionic surface area. The total mass per thermionic device is

approximately 2.4 kilograms, yielding a total system mass of 240 kg. Detailed mass calculations appear in Appendix B.

4.4.4 Failure Modes and Redundancy

Thermionic devices rely on the electrical isolation of the two diodes to be able to convert thermal energy to electrical energy. In the event of an electrical short in the thermionic, the device will no longer be able to perform that conversion. While a single short will fail the effected unit, it will not lead to a failure of surrounding thermionics, and thus not significantly influence power generation or energy removal from the core due to the large design margins of the device. Each thermionic emitter runs at about half capacity, so if one shorts, the six surrounding it can surely fill in. If a short were to happen, the mechanisms of thermal radiation and conduction to the collector surface would still be operational, so the thermionic device would still be capable of removing 85-90% of the thermal power that it removes when fully operational. Furthermore, inserting ceramic spacers between the thermionic diodes would reduce the possibility of a short in the thermionic system. The spacers should have axially milled slots to permit the free passage of cesium gas within the diode as shown in Figure 4.4-7.

Figure 4.4-7: View of Holes in Ceramic Spacers for Cesium Passage

The spacers will help maintain the inter-electrode gap in the event of material bowing at high temperatures [81].

In addition to the possibility of an electrical short, a loss of vacuum in the diode may render a thermionic device inoperable. On the Moon, a failure in the vacuum seal would lead to complete evacuation of the cesium, causing the electrical efficiency of the unit to drop significantly. On Mars, the space between the diodes would fill with CO_2 from the Martian atmosphere, rendering the system inoperable. In both cases, the system continues to act as a heat sink for the core heat pipe and would lot lead to loss of cooling in the core. Both, however, would lead to a reduction in electrical power production. It should be noted that all of these accident scenarios are low probability events.

4.4.5 Scalability

The number of thermionic PCU units scales approximately linearly with the power needed. As the length of the thermionic on the core heat pipe is increased, its ability to generate electricity increases almost one for one. The core design calls for 127 heat pipes of radius 1 centimeter, and so a 16 cm segment will need thermionic coverage in order to generate 100 kWe. If future missions require additional electric power, the current design could easily accomplish this by making the core bigger and adding more thermionic devices on the new heat pipes.

4.4.6 Discussion

The system described in this section exceeds the design requirements of the MSR. Its most significant advantage is its robustness. The system has no moving parts, eliminating the possibility of mechanical failure and significantly reducing any maintenance requirements. Since each core heat pipe has its own thermionic emitter, failure of one heat pipe lowers the total power output by less than 1 kWe. Then the heat pipes surrounding the failed one pick up the extra heat and deliver it to their thermionic devices. Since both the heat pipes and the thermionics are operating with ample design margins, little to no loss of power will be experienced even should multiple non-adjacent heat pipes fail. In addition, should a thermionic device fail or drop in efficiency during operation, almost no change in thermal power delivered to the radiator occurs. This implies that even if large parts of the PCU fail for an unknown reason, heat removal from the core will continue safely and reliably. This system has no single point failure modes, and failure modes that do exist do not influence core-cooling functions.

4.4.7 Summary

The thermionic conversion system will consist of electro-etched rhenium cathodes attached, outside of the core, to the heat pipes. Table 4.4-2 summarizes the key parameters.

Table 4.4-2: Key Parameters for Thermionic System

Emitter Temperature	1800K
Collector Temperature	950K
Operating Voltage	50V
Electrode Spacing	0.13 mm
Power Density	>10W/cm^2
Output Current	2kA
Surface Area	10,000cm^2
Efficiency	>10%
Mass	240kg

4.5 Radiator Couple

While the thermionic emitters can convert 10% of the heat produced in the reactor into electricity, the rest of the thermal energy must be removed from the PCU and dissipated into the radiator. This heat is mainly due to radiative losses in the PCU. Therefore, even if the PCU is not operating, coolant must continue to flow and cool the PCU to dissipate the heat produced by the reactor.

4.5.1 Options

The investigators recognized two possible methods to transfer energy from the PCU to the radiator, one using a working-fluid heat exchanger and the other using heat pipes. A working-fluid heat exchanger includes any of a number of geometries designed to maximize the flow of thermal energy from one fluid to the other. These include plated-fin exchangers, spiral designs, printed circuit designs and many more. Each has its own advantages and disadvantages – for example printed circuit heat exchangers can be very compact, but often have high mass. The main disadvantage to all of these designs is that at some point the working fluid must be pumped out of the heat exchanger, introducing another location for single-point failure. Should this heat exchanger fail, cooling to the

PCU will cease, overheating it and eventually leading to overheating of the core. Therefore a more robust and modular design is required for this system.

Any of these designs would require a form of interface to the radiator, which uses embedded heat pipes to distribute heat across the surface of the radiator. So the investigators were naturally led to the concept of using these radiator heat pipes and coupling them directly to the thermionic emitters, adding an annular section inside which each thermionic would have a direct thermal connection.

4.5.2 Annular Heat Pipes – Concept

Heat pipes remain nearly isothermal if properly designed. Pressurizing the heat pipes so that the working fluid boils at the temperature we wish to radiate at, ensures that all the heat transfer results from liquid undergoing a phase change, vastly increasing its efficiency.

Each heat pipe contains an annular section in which the heat pipe fits around a thermionic emitter as shown in Figure 4.5-1. Above the height of the thermionic emitter, the heat pipe gradually decreases in radius until it is that of the radiator heat pipes.

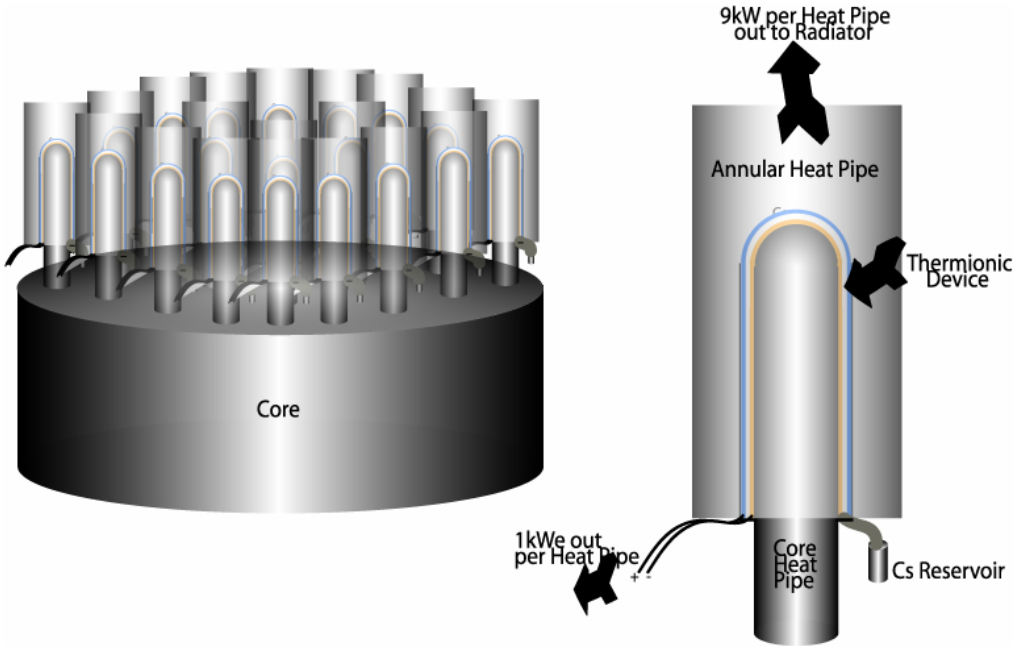

Figure 4.5-1: Annular Heat Pipe Sketch

4.5.3 Heat Pipe Design

Each annular heat pipe is designed to match the specifications of a core heat pipe as closely as possible. In this case, each heat pipe must only transport 9 kW of thermal energy, since 1 kW of energy is converted into electricity by each thermionic device. Designing the heat pipe to transport 10 kW introduces a design margin to account for inefficiencies introduced when the heat pipes are bent to the radiator.

The collector wall of each thermionic emitter will be in direct thermal contact with the inside wall of each annular heat pipe. Potassium is used as the working fluid, as its boiling point is very close to the temperature to which we wish to cool the thermionics. A 20 layer, 400 mesh titanium wick will be used to keep the liquid potassium in contact with the wall of the heat pipe. The annular heat pipes will have a 2 cm outer radius on this annular section, with a wall made of a niobium-zirconium alloy. The heat pipes will be slightly evacuated in order to reduce the boiling point of the potassium to 950 K.

The heat pipe is annular as long as it fits over the thermionic emitter, giving an evaporator region of 40 cm. The condenser region consists of the entire length of the radiator, with an adiabatic region in between. This includes a section with 180º bend before entering the bulk material of the radiator, as depicted and described further in Section 5.4.

The wick structure will lie along the entire inner wall, so that capillary action will bring the liquid potassium down from the outside section of the inner wall to the inside one, where the potassium will boil. The outer walls of the heat pipe will be thermally insulated so as not to impede liquid flow to the thermionics due to boiling on the wall.

4.5.4 Thermal Analysis

Using the equations outlined in the Core Heat Pipe Section 3.3.4, it can be shown that once again the capillary limit is the limiting factor. Assuming the parameters in Table 4.5-1, the capillary limit was found to be 13.758 kW per heat pipe.

Table 4.5-1: Parameters for Annular Heat Pipe Radiator Couple

Heat of vaporization	1938 kJ/kg
Liquid Density (kg/m^3)	675.4 kg/m^3
Vapor Density (kg/m^3)	4.86 g/m^3
Liquid Viscosity	0.12
Liquid Surface Tension (N/m)	0.0672 N/m
Annular Outer Radius (m)	0.02
Annular Inner Radius (m)	0.014
Length	~7m
K x10^{-10}	0.302

Similar studies have shown similar parameters [88]. Because each heat pipe must only transfer 9 kW this gives a sufficient design margin. For example, should the heat pipe at the hot spot fail, the potassium heat pipes around the failed lithium heat pipe will each have to transfer 7/6 of their normal load, or 13.125 kW per heat pipe. This gives us a design margin of 4.6% in a worst-case analysis, which leaves little room for transients. However, this also assumes that only the nearest neighbors of the failed heat pipe remove the excess heat, which is itself a conservative assumption.

4.5.5 Coupling to Radiator

The annular heat pipes will gradually change radius until they match those installed in the radiator. This ensures fast and reliable thermal coupling between the PCU and the radiator, with no room for single-point failure – this redundancy can clearly be seen in Figure 4.5-2 below. This is quite an improvement when compared to traditional heat exchangers, which employ a single working-fluid loop.

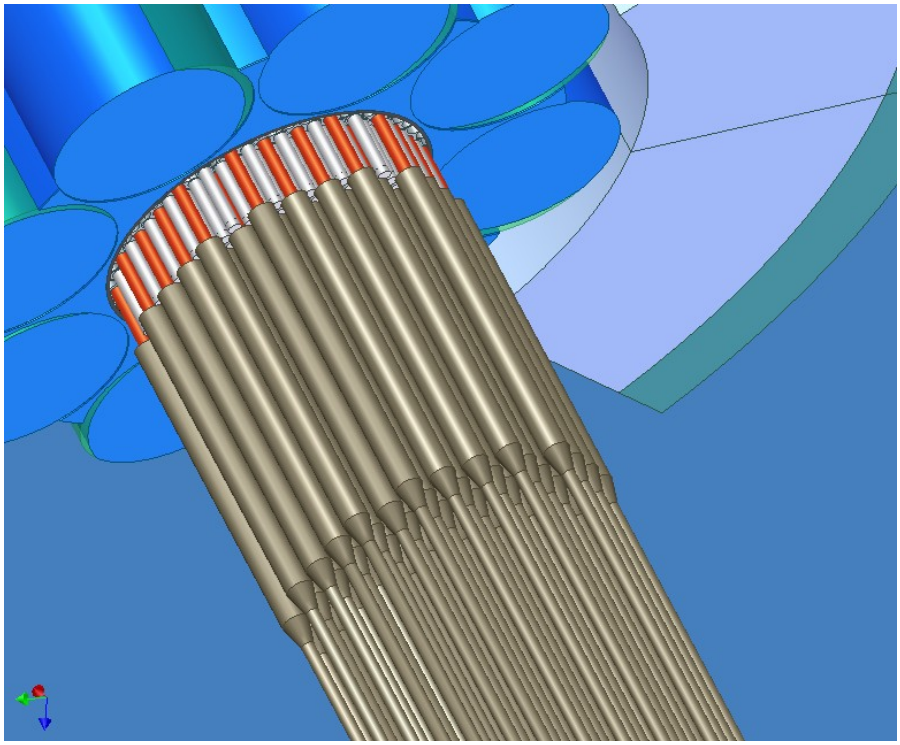

Figure 4.5-2: Power Conversion Unit and Heat Exchanger Units

4.5.6 Discussion

The system described above employed one heat exchanging heat pipe per core heat pipe. This ensures that should one or multiple heat pipes fail, cooling of the PCU and core still occurs, and the PCU still generates nearly full power. The system is robust, dependable, includes ample design margins, and technologies involved have been well developed. The only aspect about the heat exchanger system that is not well developed is the annular section of the radiator heat pipes. However, capillary action still pulls liquid potassium to the evaporator region, and boiling still takes place. Therefore, the annular section should not noticeably affect heat pipe operation.

4.6 DC-to-AC Power Conversion & Transmission System

After conversion of the reactor's thermal energy into electricity, this power is ready for transmission to structures and equipment on the Lunar or Martian surface. It is not possible to know exactly how far these items will be from the reactor as we expect limits to the capabilities of precision landing technology. We therefore assumed that power

transmission capabilities of up to a kilometer would be appropriate. In addition to transmission, the system requires power transformation as electricity produced by the thermionics is at 50 VDC with 2 kA, a form which is not practical to transmit. In order to transmit, first, the DC must be converted to AC to reduce power attenuation. Second, the power must then be transformed to a higher voltage to limit current-carrying losses. The following sections describe the system selected to achieve this objective.

4.6.1 DC-to-AC Conversion Options

There were several possible types of systems available to convert DC to AC. The first system considered uses a motor-alternator configuration where a DC motor turns a shaft that couples to another motor run in reverse. This combination would generate AC electricity. This system is very massive and relatively inefficient, and so was not appropriate for the MSR.

The second system considered was an inverter. An inverter is a semiconductor-based device that has large efficiency improvements over a motor-alternator, since there is far less dissipation in an efficient semiconductor device than in the coils of a motor. While the optimal way to proceed would have been to design such a device from scratch, time constraints necessitated selecting an existing inverter. The investigators completed a survey of available commercial inverters and found several attractive options.

4.6.2 DC-to-AC System Selection & Analysis

The investigators decided to use Behlman Electronics' 5 kVA system, which consists of two 2.5 kVA systems mounted together in a rack. These systems can each accept 100 A at 50 VDC and output electricity at 120 VAC with 90% efficiency [87]. An example picture is shown in Figure 4.6-1.

Figure 4.6-1 – Behlman DC-AC Inverter

Twenty-five of these systems are used in the MSR design, attaching five thermionic emitters to each 5 kVA unit. This ensures that, should a transient occur and the thermionics deliver more power than normal, the DC-to-AC system will not fail. This also includes a 25% design margin in this component of the system as the DC-to-AC systems do not run at full capacity.

Thick wires exit each thermionic emitter at the top of the emitter in the core's inverted configuration. These wires then exit the reactor area in a large bus and enter the 5 kVA DC-to-AC converters, which are located behind shielding to reduce damage to the electronics. The system is placed as close to the reactor as possible to reduce DC losses, but behind enough shielding in order to ensure reliable operation of the devices.

4.6.3 Transformers

In order to reduce transmission losses, a transformer with a turn ratio of 83.5:1 is employed to provide a transmission voltage of 10 kV. This will step up the voltage over the transmission lines so that very little total current (~10A) is flowing. Each 5 kVA system had its own transformer to eliminate the possibility for single-point failure.

The weight for an individual transformer carrying 120 VAC at 60 Hz with 48 A of current is estimated at about 20 kg, putting the total transformer weight at 0.5 MT. Weights were estimated using 10 m of 10 AWG wire, whose current carrying capacity is 55 A (well over our load of 48 A) [88].

4.6.4 Transmission Cable

In choosing the transmission cable, a low resistance was desired to minimize dissipative losses. A thin wire is also desired in order to keep the mass of the cable down. The investigators chose a 22 AWG copper wire to transmit electricity to equipment and structures on the surface. It was assumed that up to one kilometer of cable might be required. This wire gives a resistance of 52.94 ohms over the entire transmission line [88]. This gives a voltage drop of 52.94 V across the transmission cable, giving a total voltage loss of 0.53%. The weight of one cable is calculated at 21 kg per kilometer; bringing the total weight of 25 cables to 525 kg/km. Twenty-five separate cables are used in the design.

4.6.5 Discussion

The investigators chose to include transformers and multiple smaller cables for the purpose of decreasing transmission losses and increasing reliability. While the voltage drop across the multiple cables is slightly larger then the corresponding drop for one large cable, when compared to the transmission voltage of 10 kV, it is negligible. This small loss is compensated for by the large reduction in the probability of single point failures. It is noted, that because of this configuration, equipment and structures on the surface will likely require step down transformers. For a structure using the standard 120 VAC, this configuration will deliver 25 separate 120 VAC lines running at 48A without the need to further divide the voltage. Table 4.6-1 gives a mass break down of this system.

Table 4.6-1: Mass Breakdown for Power Conversion and Transmission System

Component	Mass (kg)
DC-AC inverters	360
Transformers	500
1km Transmission Cable	525
Total	1,385

4.7 Summary

The power conversion system outlined in this report provides no single location that induces failure of any system, let alone the entire reactor. In fact, the largest power drop should any one component fail is 4%. The core still cools effectively, and nearly full power is still delivered to the habitat.

Should an inverter, a transformer or a transmission cable fail, the power level and cooling rate drops by 4%. Should a core heat pipe or an annular heat pipe fail, the power level drops by less than 1%. Finally, should one section of a thermionic diode fail the power level drops by about 0.1%, assuming 10 sections in each diode.

This system is modular enough for easy assembly, is fairly resistant to neutron and gamma radiation, and is robust enough to withstand transients and hot-spot failures at the same time. In terms of safety analysis, the only releases that can occur are release of lithium or potassium from core and radiator heat pipes, and release of cesium from the

thermionics. However, the amount of these materials used in this design is very small. In addition, should these metals be exposed to the ambient temperature, they will solidify.

The total mass breakdown of the power conversion system is as follows:

Table 4.7-1: MSR Power Conversion System Mass

Component	Mass
Core heat pipes	Included in Core analysis (Section 3.3.4)
Thermionic emitters	240kg
Inverter/transmission	1,385kg
Annular heat pipes	Included in Radiator heat pipe mass (Section 5.4)
Total mass of PCS	1,825kg

4.8 Future Work

While the power conversion system is well designed to meet and exceed all specifications, there are a few optimizations and analyses that remain to be done.

The thermionic emitters work quite well in this system. They can certainly work better, in terms of efficiency and maximum heat flux. Research in thermionic emitters is not as extensive as one would hope. Actual efficiency curves and calculations are difficult to determine, and few fully developed systems are documented. Qualitative effects of varying system parameters are developed, but there are no standard formulas or calculations to determine the optimum parameters for a given system, such as diode spacing, cesium vapor pressure, or collector temperature. Furthermore, much of the optimization work in determining exact specifications are best done experimentally.

The power conversion/transmission system leaves much room for optimization. First, the decision to transmit electricity using AC instead of DC was made because there is little information available on DC transmission on the relatively low power scale the MSR is operating on. Further investigation may prove DC transmission to be the preferable option. Second, the investigators decided to use existing systems, while designing an inverter/amplifier tailored to our specific system may prove to be slightly more efficient and less massive. In addition, studies must be done on the possible damage to the electronics due to radiation even behind the shielding. While the transformer basics are

outlined in the description, exact parameters such as wiring scheme, core size and material choices, and total number of turns are yet to be decided.

The transmission cable decision underwent much iteration, but a few parameters still need to be selected. These include the type and thickness of the insulator (since we are transmitting 10,000 volts), the exact wiring configuration out of the transformers, and the metal to use. For example, while aluminum is a far lighter metal than copper, it is also more resistive, so studies must be performed that address the tradeoffs between wire material, gauge and resistivity. In addition, there may be a more optimum transmission voltage, but increasing the transmission voltage also increases the weight of the transformer.

Finally, the issue of scalability must be addressed. Assuming the core power doubles to 2.4 MWth, more thermionics would be placed over the heat pipes, and double the number of transformers and inverters would be used. Otherwise, the PCU will remain the same. The only analysis that remains to be done in order to scale up to a 200 kWe system is how to improve the heat pipes between the PCU and the radiator to handle the elevated heat flux.

5 Radiator

5.1 Introduction

The purpose of the radiator is to dissipate the waste heat from the MSR. Specifically, the radiator group was charged with the task of disposing 900 kW_{th} to the Lunar/Martian environment while maintaining a PCU collector temperature of 950 K. Furthermore, integration of the radiator with the other systems was critical in the creation of an overall tenable design for the MSR. To this end, the radiator group worked closely with the power conversion group, which in turn collaborated with the core group, to ensure that the three systems interfaced appropriately, and to verify that the choices made by the radiator team met the entire design team's requirements. This chapter lays out the options, design, analysis and system integration of the MSR radiator.

5.1.1 Modes of Heat Rejection

There are three thermal transfer processes that can be used for heat rejection: conduction, convection and radiation. To dissipate the waste heat from the MSR, heat radiation was the most viable option. On the Moon and Mars, the only mode of conduction-as-heat-rejection is to dispose of the heat to the Lunar/Martian surface. Unfortunately, both the Lunar and Martian surfaces are thermally insulating and do not provide a good medium for heat rejection. Underneath the soil top layer, the ground is cooler and more conducting, thus allowing for the possibility of borehole cooling. This type of cooling, however, is unattractive because instillation requirements are extensive. Likewise, convection is not viable because unfavorable environmental conditions – both the Moon and Mars have no appreciable atmosphere to make convection a feasible option. Thus, the design team was left with radiation as the chosen mode of heat rejection.

5.1.2 Design Requirements

From the overall MSR design goals in Chapter 2, the radiator group created a set of more specific requirements. These requirements pertain to how the radiator interacts with the other systems and the environment. From the systems side, consider how the radiator fits

into the sequence of events from launch to surface operation; first, it must fit into the launch vehicle along with the other reactor components. This means that not only must there be sufficient contiguous volume, but also the weight of the radiator, when added to the weight of the rest of the reactor, must not exceed the available launch capacity. This requirement necessitates give and take between the various system groups to arrive at the optimal parameters. Second, the radiator must be able to withstand the large g-forces and vibrations associated with launch and landing without damaging itself or neighboring components. Third, the radiator must be in a configuration where it operates correctly after landing. Whether or not there is unpacking required after the lander positions the reactor, the radiator must be able to mate with the other systems and operate when the startup command is given. This dictates consideration of the linkages between the radiator and the other components and its role in the reactor startup procedure.

Using the same sequence of events, the design team generated the environmental requirements. It is likely the radiator will contact the Earth's atmosphere when it is first constructed and packaged into the rocket. The design must ensure that the high atmospheric pressure (compared to its destinations) does not damage any components, and chemicals present in the air do not corrode or contaminated its surfaces. Next, during the rocket's transit from Earth to either the Moon or Mars, the radiator will experience a low-gravity environment and be subject to direct radiation from the sun. Once the radiator lands on the surface, the design must take into consideration the effects of gravity, temperatures in the range of 100-400 K and material reactivity with the atmosphere and soil. In addition, since the radiator will begin to operate, it is important to assess how operation interacts with the planetary environment.

The environment is a critical factor in our design since the peculiarities of the Martian and Lunar surface conditions control the effectiveness of a radiator. The design group brought the major environmental factors into consideration by taking into account the physical conditions on the Lunar and Martian surfaces, including meteorological conditions, temperature swings and chemical composition of the atmosphere and soil. See Appendix IV – Extraterrestrial Environments for a detailed discussion of the Martian and Lunar environments. In particular, the design team evaluated the important chemical

interactions that could occur on exposed surfaces. Since it is beyond the scope of this project to determine the landing sites for the reactor, in general the group used average planetary conditions when doing these analyses.

5.2 Radiator Options

Before beginning major design work, the radiator group researched past heat rejection systems in order to take advantage of the experience already gained in this field. Previous work on space power has given these concepts serious consideration; they represent a valuable compilation of technical solutions to the many challenges of practical radiator design. These concepts include designs for both interplanetary and surface operations, and the design team considered both because of the sparse atmospheric conditions on the Moon and Mars. This section explains and tabulates the important points of function, materials and operating parameters for each of the seven heat rejection concepts the group investigated. The radiator group used this information to determine the optimum starting concepts for the Martian and Lunar surface radiators, from which our MSR design ultimately evolved.

5.2.1 Helium-Fed Radiator

A recent reactor system envisioned by NASA was a high-temperature fusion powered spacecraft that utilized partial power conversion; some of the energy created by the reactor generates electricity while the rest powers the propulsion system or radiates into space as waste heat. The heat rejection system uses gaseous helium pumped through two separate but parallel loops to transport heat from the reactor to large panel radiators [92].

The center of the power generation system is a 7900 MW_{th} fusion reactor. Of this energy, 6685 MW_{th} powers the craft's magnetic propulsion system or is lost to space. About 100 MW_{th} of the remaining 1215 MW_{th} powers the craft's Brayton cycle power conversion system and generates 29 MW_e. The 100 MW of thermal energy is carried from the reactor by a high-pressure helium loop to a turbine, and then to a low-temperature radiator measuring 10,000 m^2. The helium temperature is 1700 K at the core outlet and

1000 K after the turbine. The coolant experiences a 500 K temperature drop across the radiator, and flows through a compressor in-line with the turbine before returning to the reactor.

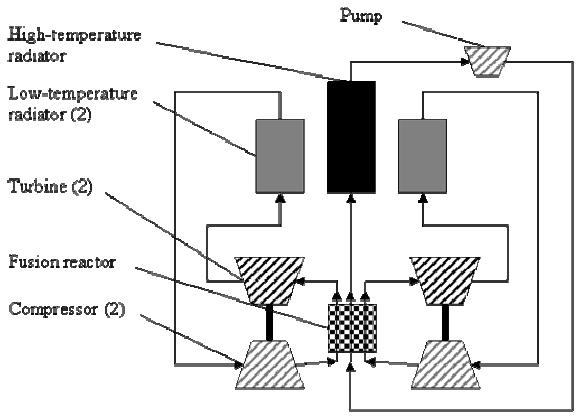

Figure 5.2-1: Schematic of helium coolant flow in the high-temperature fusion space reactor system

A separate low-pressure Helium flow carries the other 1115 MW_{th} directly to a 4070 m^2 high-temperature radiator at 1700 K. This coolant loop experiences a 700 K drop across the radiator and flows back into the fusion core via a motor-driven compressor pump. See Figure 5.2-1 for the layout of the reactor systems.

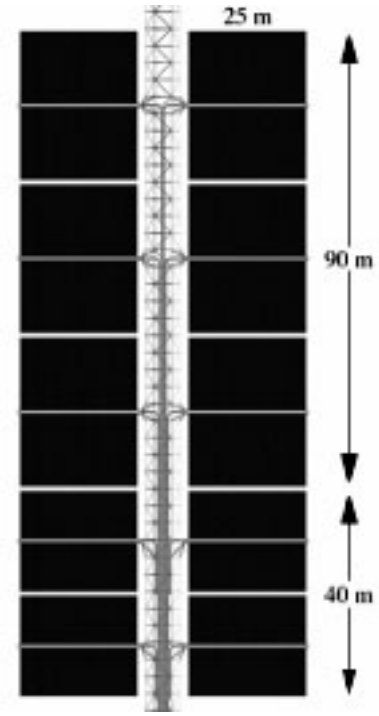

Figure 5.2-2: The layout of the helium-fed radiator panels. The helium flows through pipes in the central truss, and then out and back across the ends of the panels of heat pipes (shown in black) [92]

Table 5.2-1: Properties of the Helium-based heat rejection system

Radiated Power		1186 MW_{th}
Radiator Inlet Temperature	**high-temperature radiator**	1700 K
	low-temperature radiator	1000 K
Radiator Area	**high-temperature radiator**	4070 m^2
	low-temperature radiator	10000 m^2
Primary Coolant		Gaseous Helium
Heat Pipes		Carbon-Carbon composite with Lithium or Sodium-Potassium fluid
Structure		Carbon-Carbon composites, refractory metals, high-temperature ceramics
Linearly Scaled Radiator Mass for Rejecting 900 kW_{th}		1 MT

The low-temperature radiator is composed of Carbon-Carbon heat pipes with sodium-potassium eutectic coolant. The helium flows over the evaporator section of the heat pipes, and the condensing end of the heat pipes attach to high-emissivity fins for radiating the energy into space. The piping and supports for the radiator system are made of

refractory metal alloys such as aluminum and zirconium oxides and ceramics like SiC and Si_3N_4. The high-temperature radiator uses a similar design, except that the heat pipe working fluid is lithium, and most of the radiator's superstructure is composed of Carbon-Carbon composites. In both radiators, zones separate the heat pipes in order to maximize temperature and thus efficiency. Table 5.2-1 is a summary of the properties of the helium-fed radiator.

This design has several very good attributes, namely that it operates at high temperatures and radiates a very large amount of power. Because the working fluid is a light gas the radiator panels are much less massive than liquid metal systems. The drawbacks of this system are the weight and complexity of its auxiliary components (compressor/pump, high-pressure piping) and the lack of inherent redundancy (although the radiator area does include a safety factor of 1.2). The primary source of cooling is through the forced-flow high-temperature loop, which requires a high output electric powered pump. The dependency on electrical power and the mechanical complications of a motorized high-rpm component present reliability issues when considered for use in a remote 5-year life reactor system. In addition, the helium coolant will be at high pressure, which only increases the problems of leaks and introduces a single-point failure mode for the system.

It would not be difficult to scale down this system to 900 kW_{th}, with the helium circulating through a heat exchanger to recover heat from the PCU, although the auxiliary components (pump and heat exchanger) would dominate the mass. The helium would flow through a smaller version of the low-temperature radiator with the same heat pipe construction. An electric pump would then force the gas back into the heat exchanger to repeat the cycle. The pressures and flow rates in this system would need to be kept high to provide adequate cooling.

5.2.2 SNAP-2

The Systems for Nuclear Auxiliary Power (SNAP) projects resulted in the development of multiple fission reactor and radioisotope thermal generator designs for space use [108]. The goal of the SNAP-2 program was development of a nuclear auxiliary power unit

capable of generating 3 kW_e for one year with a total weight less than 340 kg [95]. See the layout of the reactor, power conversion unit and radiator systems in Figure 5.2-3.

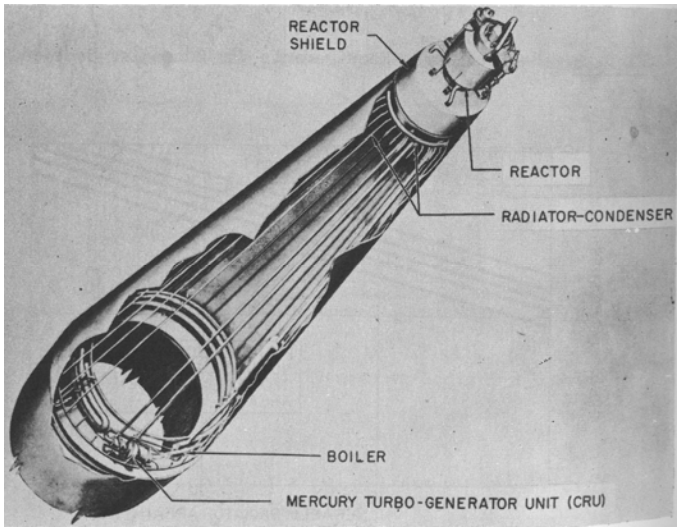

Figure 5.2-3: Layout of the SNAP-2 reactor system with cut-away of the radiator-condenser. The long axial tubes carry gaseous mercury as it condenses into a liquid, dumping heat into the surrounding radiator shell [108]

The SNAP-2 reactor utilizes a sodium-potassium eutectic (NaK) coolant to heat a secondary Mercury loop that is the working fluid for a Rankine power conversion cycle. The reactor produces 50 kW_{th} that the PCU utilizes to generate electricity. After passing through the turbine at 894 K, the radiator cools and condenses the gaseous Mercury at 589 K. An integral subcooler in series with the radiator then reduces the liquid Mercury temperature to 489 K before it returns to the Hg-NaK heat exchanger. The radiator is a hollow cone-shaped surface with the reactor shield truncating the tip, and the PCU located at the base. The radiator is 2.87 m long with a diameter of 0.76 m at the tip of the cone and 1.52 m at the base, giving an effective radiator area of 10.2 m^2.

Table 5.2-2: Properties of the SNAP-2 radiator-condenser

Radiated Power	47 kW_{th}
Radiator Inlet Temperature (condenser and subcooler)	600 K
Radiator Area	10.2 m^2
Radiator Mass	51.7 kg
Radiator Coolant	Hg
Structure	Steel pipes with an Aluminum shell
Linearly Scaled Radiator Mass for Rejecting 900 kW_{th}	1.5 MT

The radiator-condenser is made of steel tubes arrayed beneath an Aluminum shell 0.5 mm in thickness. The inside of the tubes are an eccentric shape, with the inner diameter offset, so that additional steel is located at the steel-aluminum interface for protection against micro-meteor penetration. The tubes have an inner diameter of 6.9 mm and an outer diameter of 9.3 mm. The dry weight of the radiator (tubes and shell) is 51.7 kg. Table 5.2-2 contains a summary of the radiator's properties.

The SNAP-2 radiator design is interesting because it takes advantage of the condensing fluid to maintain a constant temperature over most of the radiating surface, similar to a heat pipe. The radiator is also a very low weight given the amount of power radiated, with a power-to-mass ratio of 0.139 kW/kg. The two drawbacks of the system are the need to provide pumping for the coolant and single-point failure characteristics. Mercury is the working fluid for the Rankine power conversion unit as well as the radiator coolant, and therefore the two systems share the mass penalty for pumping a dense fluid; however, it comes at the mass benefit of not having a secondary heat exchanger. In a system where the coolant is not part of the PCU cycle, a heat exchanger introduces significant complexity. In addition, a failure in any one of the radiator pipes will cause a rapid depressurization of the system and loss of cooling for the reactor. In order to reduce this possibility the design requires additional armor. Also, Mercury is toxic, and in the case of a launch accident, or leak of mercury on the Martian surface, it poses a hazard both to human health and the local environment.

This concept might provide an acceptable size for this project, assuming the size and mass scale linearly with power level. Scaled up to a rejection power of 900 kW_{th}, this system would require a pump to circulate the coolant through a heat exchanger and out to the radiator. The major drawback is the greater pressure drop across the radiator, since radiator area will scale upwards with the power.

5.2.3 SNAP-10A

The SNAP-10A is the only fission reactor launched and operated in space by the United States. Placed into orbit on April 3, 1965, the SNAP-10A operated for 43 days before shutting down due to an electrical malfunction in the orbital booster [95]. The SNAP-10A design called for continuous operation for at least one year, operation without moving parts (although initial startup uses rotating control drums), consistent operation independent of its position with respect to the Sun or Earth, the ability to withstand the forces of launch and spaceflight, and presentation of a minimal hazard during launch and orbit [108]. Figure 5.2-4 is a drawing of the SNAP-10A launch system.

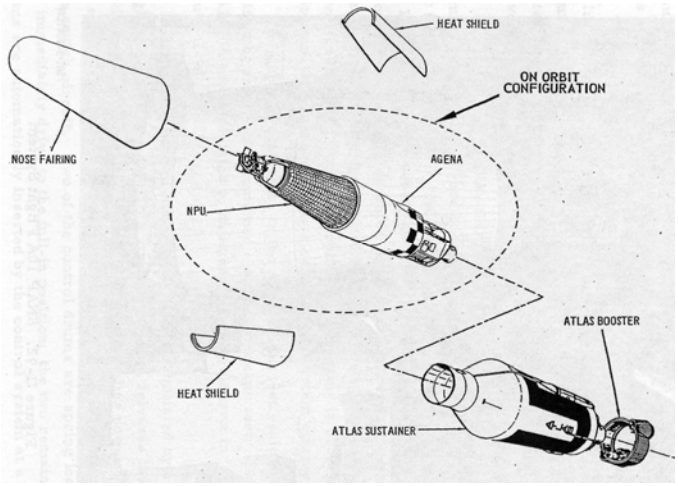

Figure 5.2-4: The SNAP-10A launch vehicle in an exploded view, with the reactor and radiator assembly denoted as the NPU. The radiator is composed of the 40 parallel aluminum strips that run axially from the tip of the cone. The Agena is the orbital booster that maneuvered the reactor into final position after its separation from the Atlas launch vehicle [95]

The SNAP-10A reactor produced 43 kW_{th} with a core similar to the SNAP-2 design. Liquid metal circulated through the core and into 40 tubes running axially below the reactor vessel. Thermoelectric generators mounted against these tubes absorbed the

thermal energy by conduction. The radiator plates then attached directly to the outside end of the thermoelectric converters and emitted the excess heat into space. Figure 5.2-5 depicts the layout of the radiator and power conversion system.

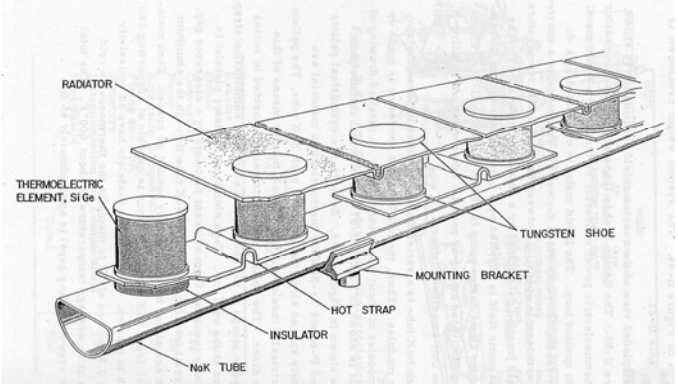

Figure 5.2-5: A schematic view of a SNAP-10A coolant tube with the thermoelectric pills and radiator strips [95]

The NaK coolant for the SNAP-10A circulated through the coolant tubes with the aid of an electromagnetic pump. The NaK left the reactor with a temperature of 833 K and reentered at 761 K. Thermocouples attached between the tubes and the radiator supplied the pump's electrical power. Seventy-two germanium-silicon thermoelectric generator pills were spaced along each coolant tube and held in place with tungsten shoes. The wiring separates the generators on each tube into three electrical modules, each with 24 generators; each module had an electrical output between four and five watts. The total power output from the thermoelectric system was about 500 W_e. Welded to the outside end of the thermoelectric pellets are the radiator panels. The panels are made of thin aluminum strips with an emissivity of approximately 0.9. Small gaps placed between the strips maintain their electrical isolation, and they keep the cold end of the thermoelectric pills at approximately 611 K. Table 5.2-3 is a summary of the SNAP-10A radiator properties.

Table 5.2-3: Properties of the SNAP-10A radiator

Radiated Power	42.5 kW_{th}
Radiator Temperature	611 K
Radiator Area	6 m^2
Radiator Mass	340 kg
Radiator Structure	Aluminum strips welded to cold end of thermoelectric pellets
Linearly Scaled Radiator Mass for Rejecting 900 kW_{th}	7 MT

The SNAP-10A design is significantly lower power than our goal; however, it is instructive overall because it is the only completely flight-proven fission reactor system available. The system's main weakness is the continuous NaK loop, which presents many opportunities for a single-point failure because it covers the entire radiator area. One advantage of this design is that the radiator does not require unfolding or setup once on the surface, removing the need for moving components or flexibility.

A version of this design rejecting 900 kW_{th} is similar to the SNAP-2 but without the need to condense the coolant; the use of an electromagnetic pump rather than a compressor or fan further simplifies the operation. The downside is that this design would be too heavy at this power level – around 7 MT. Because the SNAP-10A was actually constructed and operated in space, this mass prediction is more believable than the much lower estimate (1.5 MT) given by the SNAP-2 designers.

5.2.4 Liquid Droplet Radiator

A Liquid Droplet Radiator (LDR) creates a flowing mist of fine droplets between an emitter and the collector in space [91]. The idea is the very large surface area of the mist (the sum of the surface area of each droplet) will promote radiative energy loss to space while the actual mass of the mist is significantly less than a solid plate radiator and working fluid. To minimize thermal radiation re-absorption, the generator maintains the mist at approximately a millimeter in thickness. Although not tested in space or with a

high-power application, there have been extensive studies of the LDR since the 1950's [97].

The LDR system consists of five main components: the liquid reservoir, pumps, heat exchanger, droplet generator and droplet collector. The radiator functions by first drawing heat through the heat exchanger into the working fluid, either a silicon-based oil or a liquid metal. It is necessary to use these types of fluids because their low vapor pressures will minimize losses during droplet transmission; however, these fluids are also undesirable for use in most thermodynamic cycles and therefore an intermediate heat exchanger between the PCU and the radiator loop is generally necessary. Next, pipes carry the fluid to the droplet generator, which creates the droplets and forms them into a thin, rectangular, directed mist. This mist travels through space over a distance up to several hundred meters. The collector is located directly across from the droplet generator. It absorbs the droplets and returns the liquid to the closed piping system where pumps return the cooled fluid to the heat exchanger. See Figure 5.2-6 for a schematic layout of the LDR, and Table 5.2-4 for a summary of the radiator's properties.

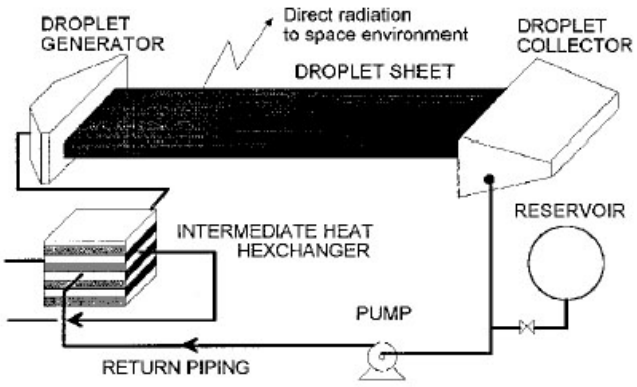

Figure 5.2-6: Schematic of the liquid droplet radiator with a connection to a secondary loop through a heat exchanger [91]

The most common liquid metal coolant for this design is NaK, although for lower power applications the silicon oils FC75 and DC705 are preferred. The high-temperature coolant contacts almost half of the components in the system, meaning they will need to be made of either refractory metals or high-temperature composites like Carbon-Carbon. Metals such as aluminum make up the lower temperature components.

Table 5.2-4: Properties of the liquid droplet radiator

Radiated Power (optimum range)	5-50 kW_{th}
Radiator Inlet Temperature (optimum)	400 K or less
Radiator Area	On the order of 100 m^2 per generator, one is needed two reject 50 kW
Primary Coolant	NaK or silicon-based oil
Mechanical Components	Regulating valves, electrical pumps, and droplet generator
Structure	Carbon-Carbon composites, refractory metals, Aluminum

The major benefit of this design is the ability to create radiator area out of empty space; thereby realizing significant mass savings compared to the tube/panel type radiators. Given sufficient efficiency in the droplet generator and integrity of the overall structure, it is possible to create an extremely long radiator length in zero gravity. The presence of low gravity on Mars and the Moon presents a problem then, because the droplet stream will face serious deformation after a few meters. Certainly, on Mars, where the atmosphere and wind are not negligible, utilizing an open heat rejection system is of questionable feasibility from both an operations viewpoint and an environment protection viewpoint. Although the radiator coolant is not from the primary system, it still could release activation products into the environment because it is still in close proximity to the reactor. In fact, even during normal operation in space there are significant evaporative losses in the system, requiring a large reservoir of coolant for online replenishing. The mechanical and electrical complexity and needs of the system are also a negative factor when you consider the operation of pumps, valves, and the droplet generator for five years. Finally, while this design is scalable from the size examined in the literature, it is only mass-competitive with heat pipe systems in the 400 K or less operating range due to evaporative losses. The ideal system would have an inlet-side temperature of 320 K at the heat exchanger with a total system radiated power of up to 50 kW_{th}.

5.2.5 Liquid Sheet Radiator

A Liquid Sheet Radiator (LSR) radiator is very similar to the LDR system except that a very thin layer of liquid replaces the mist of radiating droplets [97]. An LSR works by exposing a planar liquid sheet of sub-millimeter thickness to space; a film fluid emerges at a set speed from the injection slot of the generator, creating a liquid sheet in space. A collector recovers the fluid and re-circulates it by means of a system of pipes and pumps. The liquid then enters an intermediate heat exchanger in order to take up the waste heat from the power cycle fluid [91]. See Figure 5.2-7 for a schematic of the LSR.

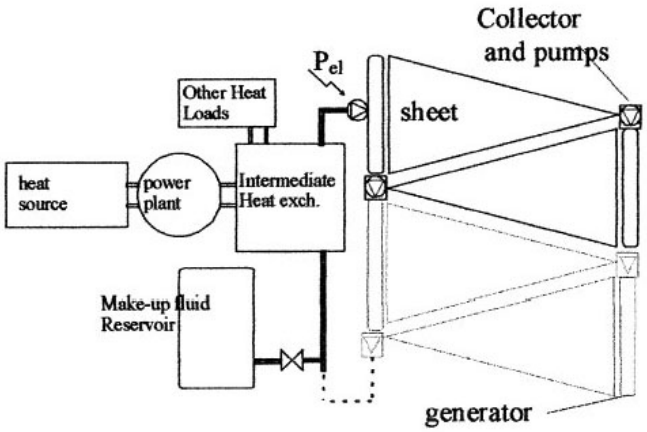

Figure 5.2-7: Schematic of the liquid sheet radiator showing multiple radiating segments in series [97]

The main components of the LSR are the sheet generator, collector, intermediate heat exchanger and circulation pump. The generator vessel must be large enough to blunt any pressure oscillations and the sheet generation precise enough to ensure uniform fluid velocity over the entire length of the injection slot.

The characteristic element of an LSR is the fluid sheet. Since the fluid used in the radiator has to operate in an extremely low-pressure environment, it must possess a very low vapor pressure in order to minimize evaporative losses. The liquid metals, such as NaK, generally present better features than silicone fluids. Liquid metals have higher thermal conductivities and lower viscosities (by up to an order of magnitude). In addition, due to the fluid dynamics governing sheet formation, there is a limited distance over which the sheet may deployed. The sheet starts as a plane but converges into a cone of

fluid after about ten meters if it starts with an initial (optimum) width of approximately one meter. See Table 5.2-5 for a summary of the properties of the LSR radiator.

Table 5.2-5: Properties of the Liquid Sheet Radiator

Radiated Power (optimum range)	5-50 kW_{th}
Radiator inlet temperature (optimum)	400 K or less
Radiator area	10 m^2 per generator, at least ten required to reject 50 kW
Primary Coolant	NaK or silicon-based oil
Mechanical Components	Regulating valves, electrical pumps, and sheet generator
Structure	Carbon-Carbon composites, refractory metals, Aluminum

This is another radiator concept that is innovative in many aspects of its design. However, the LSR's main component, the liquid sheet, makes the system very complicated since it requires a pump and generator. Like the LDR this system also has an ideal operating temperature around 400 K corresponding to a radiated power of around 50 kW. At higher temperatures, the coolant evaporation rate increases, and therefore the LSR would require a very large volume of make-up fluid. An added complication is the limited length of the sheet. To increase the power radiated without going to unacceptably high temperatures, it is necessary to put multiple generator/collector pairs in series or parallel, greatly increasing the size and mass of the system. Finally, the sheet configuration is less efficient at radiating than the liquid droplet mist, and therefore the sheet system would be much more massive than a comparable LDR device.

5.2.6 SAFE-400

The Safe Affordable Fission Engine (SAFE) bridges the gap between low-power radioisotope systems and the high-power fission systems envisioned for future spaceflight. The SAFE-400 reactor provides an output of 400 kW_{th} for up to 10 years. The reactor deposits energy into gas flow via two independent heat pipe-to-gas heat exchangers; this gas then feeds two independent Brayton power cycles producing

100 kW_e total power [90][100][102]. See Figure 5.2-8 for a schematic layout of the SAFE-400 power conversion system.

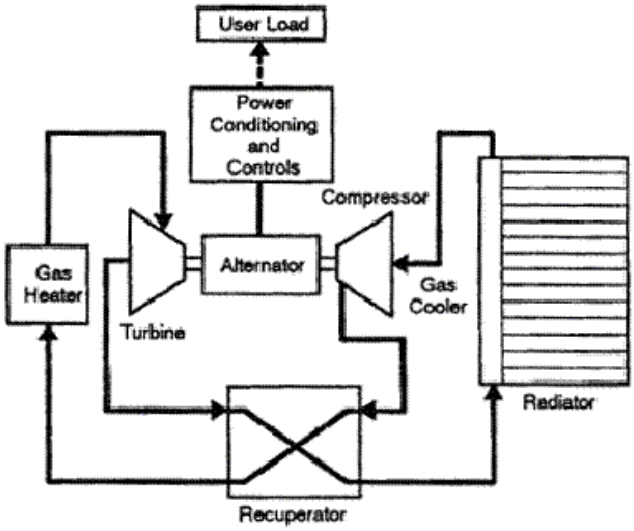

Figure 5.2-8: Schematic of the SAFE-400 power conversion system [90]

Each heat pipe-to-gas heat exchanger is composed of an array of the condensing end of the core heat pipes, which transfer their thermal energy to the gas. The working fluid for the heat pipes is sodium, and the pipe's shell is made of a Carbon-Carbon composite with a Niobium-1%-Zirconium liner. The heat exchanger inlet and outlet temperatures are 900 K and 1150 K, respectively, and the working fluid is Helium-28%-Xenon.

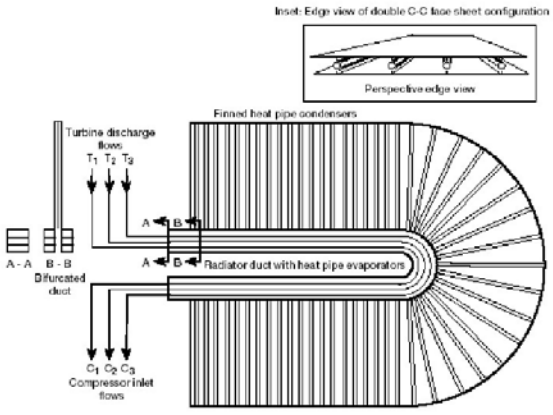

Figure 5.2-9: Schematic of the SAFE-400 radiator [90]

The SAFE-400's radiator uses heat pipes as well. The working fluid for these heat pipes is sodium-iodine (NaI), and the pipes are made of a Carbon-Carbon composite with inner

liners made of Nb-1%-Zr. The radiator panels are a Carbon-Carbon composite sandwich design, with plates mounted on either side of the heat pipes. The specific mass of this radiator is only 1.6 kg/m^2, operating with a power generation cycle outlet temperature of 510 K; the design calls for a total radiator area of 150 m^2. See Figure 5.2-9 for a schematic of the radiator, and Table 5.2-6 for a summary of its properties.

Table 5.2-6: Properties of the SAFE-400 radiator

Radiated Power	400 kW_{th}
Radiator Inlet Temperature	510 K
Radiator Area	150 m^2
Primary Coolant	He-Xe
Heat Pipes	Carbon-Carbon composite with Nb-1%-Zr liner with NaI fluid
Structure	Carbon-Carbon composite sandwich design with plates on either side of the heat pipes
Linearly Scaled Radiator Mass for Rejecting 900 kW_{th}	3 MT

The power dissipated is in the range of our design requirements, and the projected size of the radiator area is reasonable. Redundant heat pipes passively cool the reactor, which is an added safety advantage; therefore, the reactor does not require a hermitically sealed vessel or any components that are required by a pumped loop system. The biggest plus for this concept is the overall simplicity of operation [105][109].

5.2.7 SP-100

The SP-100 is a liquid metal cooled reactor rated to produce 550 kW_e. The design calls for 7 years of operation with a survival probability of 0.99. This design concept considered the reactor as the central power source for a lunar research settlement, utilizing either a Brayton or Stirling power conversion cycle [104].

For the Brayton system, liquid metal coolant flows from the core and through a liquid-to-gas heat exchanger, which passes the thermal energy to the gas. This gas flows directly into a recuperated Brayton power conversion system to produce electricity. Four panel radiators unfold perpendicular to the surface from the reactor assembly to reject the waste

heat to space as thermal radiation. For the Stirling system, the difference is the primary heat exchanger becomes liquid-to-liquid, and then the secondary liquid coolant heats the Stirling engines.

For the Brayton system, lithium is the coolant used in the core, and is pumped to the first heat exchanger that transfers heat to the power cycle working fluid, Helium-Xenon. The He-Xe gas passes through four independent Brayton engines to produce electricity. A gas-to-liquid cooler then transfers the waste heat to a second liquid metal loop. This rejection loop contains sodium-potassium eutectic that flows to the radiator, which consists of a series of heat pipes. See Figure 5.2-10 for an overview of the Brayton power conversion system.

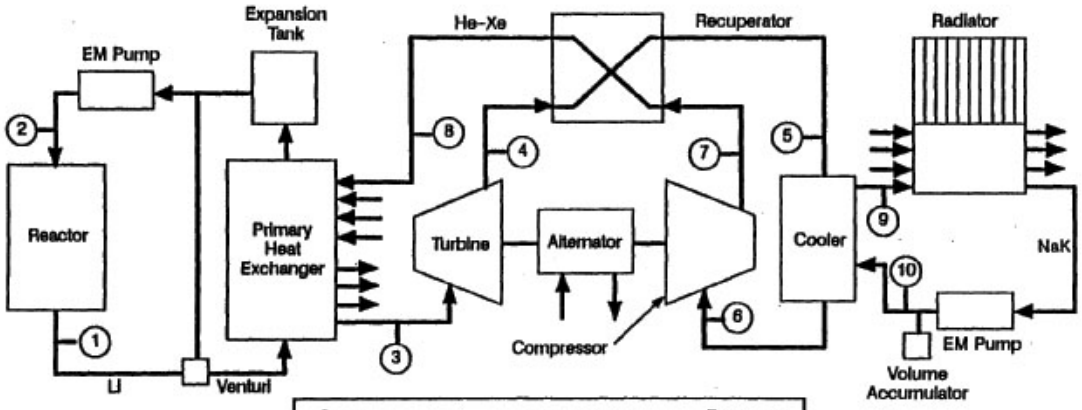

State Point	Fluid	Temperature (K)	Pressure (kPa)
1	Li	1355	--
2	Li	1276	--
3	He-Xe	1300	1,280
4	He-Xe	1041	690
5	He-Xe	640	680
6	He-Xe	406	675
7	He-Xe	556	1,340
8	He-Xe	957	1,330
9	NaK	631	--
10	NaK	397	--

Figure 5.2-10: Schematic of the SP-100 Brayton power conversion system option for a lunar base [104]

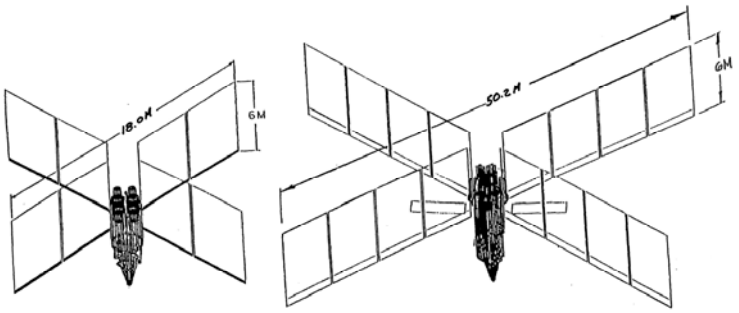

Figure 5.2-11: Layout of the radiator panels for an SP-100 based lunar reactor, the Stirling option on left, Brayton on the right. The coolant flows through pipes at the base of each arm, and the heat pipes are oriented in vertical panels [104]

The reactor produces 2.4 MW_{th}, and at the reactor outlet is liquid lithium at a temperature of 1355 K. This flows through the first heat exchanger where it transfers its heat to the new working fluid, He-Xe, at a temperature of 1300 K. The He-Xe fluid passes through the Brayton turbine and recuperator, reaching the cooler at a temperature of 640 K. The Brayton engine produces 582 kW_e. The He-Xe then passes through the cooler, yielding NaK with an output temperature of 631 K. The NaK enters the radiator system at 631K flowing into four manifolds, one through each of the radiator arms. The thermal energy from the NaK heats the evaporating end of heat pipes in twelve radiating panels; there is 2.3 MW_{th} of total heat rejection at an average temperature of 471 K. The NaK exits the radiator with a temperature of 397 K, and an electromagnetic pump then sends it back to the cooler for reheating.

The radiator is composed of 12 panels arranged in four radial arrays; each array is a radiator section of 233 Carbon-Carbon heat pipes. Of the total heat pipe inventory, 922 use H_2O and 10 use Mercury as the working fluid. The radiator panels fold in for launch, and then extend outward for operation once the reactor is in place on the lunar surface; this movement requires a drive system and flexible connections for the NaK piping. The heat pipes are vertically oriented to emit radiation from both sides, weigh about 4460 kg altogether, and are 565 m^2 in total area. The radiator assembly, including the panel support structure, weighs 4960 kg. See Figure 5.2-11 for a schematic layout of the Brayton core and radiator system, and Table 5.2-7 for a summary of the radiator parameters.

Table 5.2-7: Design parameters for the SP-100 based lunar radiator utilizing Brayton cycle power conversion

Radiated Power	1.8 MW_{th}
Radiator Inlet Temperature	631 K
Radiator Average Temperature	471 K
Radiator Area	565 m^2
Radiator Mass	4960 kg
Radiator Coolant	NaK
Heat Pipes	932 Carbon-Carbon composite heat pipes (922 with H_2O fluid and 10 with Hg fluid)
Structure	12 Carbon-Carbon heat pipe panels oriented vertically in four arrays from the reactor assembly. Coolant flows through a baffle heating evaporator end of heat pipes.
Linearly Scaled Radiator Mass for Rejecting 900 kW_{th}	2.4 MT

The Stirling system is similar to the Brayton, but there are important differences in some areas; see Figure 5.2-12 for a schematic of the Sterling power conversion system. First, the reactor operates with a lower power, only 1.89 MW_{th}. The primary heat exchanger takes lithium from the core at 1355 K and transfers the heat to a second lithium loop, outputting liquid lithium at 1304 K. This loop passes the heat to the four independent Stirling engines, which produce 596 kW_e. The NaK coolant loop exits the Stirling engine at 625 K and enters the radiator manifolds. The Stirling's radiator uses only 415 heat pipes, giving an overall area of 185 m^2 to radiate 1.29 MW_{th}. On each arm there are about 73 H_2O and 30 Hg fluid heat pipes with Carbon-Carbon composite shells. These heat pipes are also vertically oriented and radiate at an average temperature of 576 K with a total mass of 1675 kg; the radiator assembly, including support structure, weighs 2025 kg. See Figure 10 for a schematic layout of the Sterling core and radiator systems, and Table 5.2-8 for a summary of the parameters of the radiator.

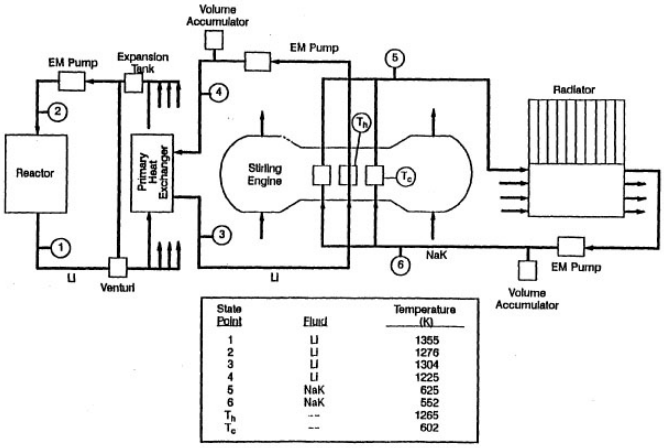

Figure 5.2-12: Schematic of the SP-100 Stirling power conversion system option for a lunar base [104]

Table 5.2-8: Design parameters for the SP-100 based lunar radiator utilizing Stirling engine power conversion

Radiated Power	1.29 MW_{th}
Radiator Inlet Temperature	631 K
Radiator Average Temperature	576 K
Radiator Area	185 m^2
Radiator Mass	2025 kg
Radiator Coolant	NaK
Heat Pipes	415 Carbon-Carbon composite heat pipes (294 with H_2O fluid and 121 with Hg fluid)
Structure	12 Carbon-Carbon heat pipe panels oriented vertically in four arrays from the reactor assembly. Coolant flows through a baffle heating evaporator end of heat pipes.
Theoretical Radiator Mass for Rejecting 900 kW_{th}	1.4 MT

The overall design for this reactor is useful given the objectives of this project. The power levels and temperatures are in useful ranges so the materials choices should be similar. This model has an expected life of 7 years, and with only 11 of the 12 panels operating the radiator will still function normally. The vertical orientation of the radiator panels is an interesting design choice; it allows for heat rejection from both sides of the panels, but increases the amount of solar energy absorbed by the radiators. The double-sided design also means the panels will receive radiation from direct heating and reflection off planetary surfaces.

5.3 Concept Choice

After researching seven major past radiator concepts, the radiator group applied the appropriate decision methodology to all of the concepts. See Chapter 2 for details about the development of the design team's decision methodology. The concept with the highest overall ranking, the SP-100, was determined to be the optimum starting point from which the radiator group evolved the MSR design. The SAFE-400 concept also ranked close to the SP-100 and very highly compared to the others; these two concepts use similar components and design methods. The radiator group's conceptual design therefore utilizes the thin Carbon-Carbon panel radiators with embedded Carbon-Carbon heat pipes found in both concepts. The heat pipes transport the waste energy beneath the panels, which conduct the heat away, and then radiate it into space.

5.3.1 Litmus Test

The seven radiator concepts under consideration were first evaluated using five litmus test criteria: safety, 100 kW_e, 5 EFPY, works on the Moon and Mars, and obeys environmental regulations for the appropriate extraterrestrial environments. If a concept fails to satisfy one or more of these criteria then it will not be subject to further analysis or consideration for use in this project.

After an evaluation of the seven concepts, only two failed to satisfy all of these criteria: the liquid droplet radiator (LDR) and the liquid sheet radiator (LSR). These are similar designs that suffer from the same basic deficiencies. In order to meet the requirements for 100 kW_e for 5 years, both the area and mass of these systems become prohibitive. The theoretical liquid droplet radiator, considered the more efficient but physically more difficult of the two designs, has a rating of around 170 W_{th}/kg, equating to a mass of over 5 MT for the MSR system. In addition, this mass estimate only takes into consideration the active components; it does not account for the fluid reservoir, which LDR needs to make up for evaporative losses from the droplets. Therefore the mass might as much as double when considering an operating temperature of around 1000 K [91][97].

Another critical issue for the liquid droplet and liquid sheet designs are their ability to operate on the Moon and Mars. While they are ideal for work in space, but the presence of even small amounts of gravity and atmospheric gasses, particles, and wind would make their operation much less efficient, less predictable and less reliable. Contamination of the system by foreign substances and accelerated loss of the liquid stream during the radiation segment are major problems. Coupled with this are the environmental considerations, as the LDR and LSR are operating in what is essentially an open system. In even the most efficient design, significant coolant losses are expected, and therefore this coolant (either a silicon-based oil or liquid metal) will be contaminating the local atmosphere and soil.

Because of the difficulties in meeting the criteria of radiating 900 kW_{th}, functioning for 5 years, working on the Moon and Mars and satisfying environmental regulations, the radiator group will not consider the liquid droplet and liquid sheet radiators any further. While they are promising designs for the future, they require significantly more research and testing in order to sufficiently quantify their physical properties and allow development of models to predict accurately their performance and operational limitations on the surface of the Moon and Mars.

5.3.2 Extent-to-Which Test

The radiator group ranked the five remaining radiator concepts based on eleven extent-to-which criteria divided between four main categories: small mass and size, controllability, launchability, and reliability/low-maintenance. See Table 5.3-1 below for a listing of the criteria and the concept rankings.

The radiator group ranked the concepts one through five, with five denoting that the design fulfills the criterion better than the other four concepts. A lower score indicates that the concept does not fulfill the criterion as well as another concept, not that it necessarily fails to fulfill the criterion at all. This is important, since this means that a concept could receive the lowest score in a category but still meet and exceed our design requirements in that category.

Table 5.3-1: Radiator Decision Matrix

	SP-100	SAFE-400	SNAP-2	SNAP-10A	Helium fed
Small Mass and Size - 1.35					
Radiator mass is small	4	3	2	1	5
Peripheral systems mass are small	4	4	3	5	1
Radiating area is small	3	1	2	4	5
Controllable - 1.14					
Minimal setup	4	4	2	1	5
Minimal operational control	5	5	2	3	1
Launchable/Accident Safe - 1.13					
Not mechanically fragile	4	4	3	5	1
Not chemically hazardous	4	4	1	2	5
High Reliability and Limited Maintenance - 1.00					
Few single point failures	5	5	1	1	1
Few moving parts	5	5	3	4	1
Limited maintenance	5	5	1	1	1
Proven technology	4	4	2	5	1
Total (of 62.95 possible)	*53.15*	*49.1*	*25.53*	*36.97*	*32.47*

Small Mass and Size

Under the small mass and size category, the radiator mass was evaluated based on the mass per kilowatt of power radiated. Similarly, the group based the comparison of radiator areas on area per kilowatt of power radiated. This method of ranking allows a fair comparison of all the concepts even though the power levels and output temperatures specified in our previous analyses were not all equivalent, assuming they scale linearly. This linear scaling is reasonable because the system temperatures are the same, and therefore the calculation only changes rate of energy generation. Power and area are in one-to-one correlation in the radiative heat transfer equation and thus scale with each other when the other variables (such as temperature) are constant. The group recognizes that there are properties that vary based on temperature and materials choices, and that we can adjust some temperatures and materials while staying within the same overall design concept.

Peripheral systems mass and size refers to items besides the radiating surface and its supports. It relates directly to whether any other devices such as pumps, reservoirs or heat

exchangers are required, and how massive such items are when compared to components for the other conceptual systems.

Controllability

The group defined the two items under the controllability category by the guiding principal that radiator deployment and control should be as simple as possible. The need to thaw coolant, mechanically extend the panels and regulate pressures and flows are all examples of the types of controllability issues used to evaluate the various concepts. Setup refers to actions that would need to taken by controllers or performed automatically after launch but before reactor operation. Operational control refers to any manipulation that would need to occur, again either by operators or automatically, in the course of normal system operation over the five-year life.

Launchable/Accident Safe

The group placed fragility and potential chemical hazard under launchability because the launch subjects the radiator to tremendous physical stress, and a launch failure should not present an excessive hazard to the environment. One of the main parts of the pre-flight testing of a component that will be launched into space is vibration testing. With this in mind, the weakest points of any design are likely to be moving and mechanical connections such as rotating parts, joints, seals, bolts and welds. The chemical hazard comes into play in the event there is a rupture of a part of the radiator assembly during takeoff, flight or initial orbit. In such an event, toxic or reactive chemicals should not enter the atmosphere or disperse in large quantities. All these concepts pass the safety and environment litmus tests because they will not cause a large environmental impact. However, it is still important to differentiate on a relative scale the impact of, say sodium versus helium release. A helium leak would quickly deplete the system's helium inventory, but helium is inert. A punctured heat pipe would release a small volume of sodium, but it will react with water and produce hydrogen gas, which will burn in an oxygen environment. Liquid mercury, in contrast, will not react violently with the environment but is a toxic hazard to humans and wildlife [95][108].

High Reliability/Limited Maintenance

The reliability and maintenance criteria cover operation of the radiator system once it is in place on the planetary surface. Single point failures present a major problem for reliability because it alerts us that any breach or puncture in one component would render the entire system useless. The next criterion under reliability is moving parts, since they will wear and are a principle malfunction and failure risk. While any need for maintenance during any phase of the mission is undesirable and the group's design seeks to avoid it, if there is a need to perform maintenance and is possible, it is important to asses how readily it could be accomplished. The maintenance criterion takes into account the modularity and accessibility of the components in the radiator system and answers the question: how easy are most maintenance tasks? This covers replacement of major components (and depends on how many auxiliary components exist) as well as patching and other in-place repairs to the entire system. Finally, proven technology is a plus for our design because it gives us an idea of the reliability and of the experience engineers have with the technologies involved in each concept. The highest rankings here suggest the components have well-characterized behavior and have been flight-tested and operated in an extraterrestrial environment.

5.3.3 Choice Analysis

The SP-100 lunar radiator concept received the highest overall ranking in the ETW test evaluation, followed closely by the SAFE-400. It ranked highest among the concepts in mass and size, controllability and maintenance, and second in launchability. The heat pipes, which are central to its design, are also its biggest benefit: they are a proven technology that provides redundancy and passive operation. Even if a heat pipe is punctured or otherwise malfunctions, it does not impede the function of its neighbors. So long as there is sufficient leeway in operating parameters, neighboring heat pipes will be able to dissipate the excess heat imparted by a pipe failure. They are passive because they do not require any active control and do not dynamically interface with other systems. Only the dimensions and temperature differences at the ends of the heat pipes dictate the fluid flow; there are no valves, regulators or moving parts. Because the heat pipes do not rely on any auxiliary components, and the failure of a few heat pipes will not fail the system, this concept is also inherently low-maintenance [104].

The SP-100 concept received its lowest ranks in radiator size and chemical hazard. The power radiated per unit area was not as high as other concepts such as the helium-fed or SNAP-10A; however, it was not significantly worse when considering the radiating temperature. At high temperatures, the radiative efficiency increases considerably, which is one of the reasons the helium-fed system had such good characteristics. Increasing the average radiating temperature is much easier in a heat pipe system because they are isothermal over a large part of their length, and thus increasing their temperature in order to radiate efficiently in the 900 kW_{th} range will greatly improve the power per unit area.

A chemical hazard is generally inherent when using heat pipes, and is a result of the liquid metal working fluid. While not present in very large amounts, in the event of a failure during launch, leading to the rupture of heat pipes in the terrestrial environment, there is the possibility of fire or toxic contamination over a small area. This is a shortcoming of all the heat pipe systems evaluated, and therefore the group ranked them lower than the helium system since helium is an inert gas. However, heat pipe systems are significantly better than a system that pumps a large volume of liquid metal through a loop configuration [108].

The SAFE-400 also received high rankings and in the end measured up well to the SP-100 design, and much better than the next best concept. Indeed, the SAFE-400 is similar in form to the SP-100 since both used a working fluid to transfer waste energy to an array of heat pipes. Therefore, the designs received similar marks regarding mass, safety, control and reliability. The area per unit of power radiated of the SAFE-400 design is slightly greater than the SP-100 mainly because of its lower operating temperature [100][105].

5.3.4 Decision

The SP-100 radiator concept passed all five of the litmus test criteria and received the highest overall ranking on the ETW criteria covering the various critical elements concerning our design project. The categories where it received its lowest rankings reflect items to note about this concept, but not significant problems or obstacles to obtaining a launchable design. Therefore, when making our final design choices and parameter

selections the radiator group will use the SP-100 design as the primary reference concept. For the purposes of this project it embodies the best of the past space-based radiator work relevant to the MSR system and thus provides an excellent starting point for our own design. Since the SAFE-400 is a similar design and ranked very highly compared to the other concepts under consideration, we will also use it as a foundation from which to choose our other radiator components. This does not mean that the design team will use the specifications of these two designs exclusive of other ideas or without innovation. By starting with a preexisting concept the radiator design team is able create an evolutionary design that gives due consideration to the extensive previous work done by experts in this field.

Both the SP-100 and SAFE-400 utilize a finned heat pipe array to dissipate energy to space, and the MSR's radiator design will also use this fundamental concept. The fins of each heat pipe connect to create a single continuous panel, and the panels will have a sandwiched design, meaning that the heat pipes are located beneath or between the panels and must conduct all their heat to a surrounding sheath that is a part of the fin. Both the outer shell of the heat pipes and the fins will be a Carbon-Carbon composite, chosen for its low density, excellent strength, high thermal conductivity and high emissivity. The fin composite needs a high thermal conductivity and emissivity so that heat spreads out evenly from the heat pipes and radiates efficiently into space. Figure 5.3-1 below shows a schematic of this radiator panel concept.

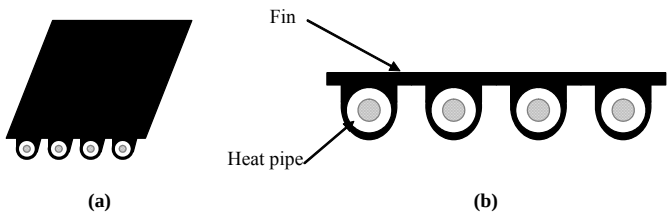

Figure 5.3-1: Conceptual radiator design, with a section of the radiator panel assembly (a) and a cross section view (b)

Other aspects of the SP-100 and SAFE-400 designs, such as the orientation of the panels, supports, working fluids and heat exchanger construction are more system-specific. The

next section discusses the selection of these characteristics for the MSR, along with improvements to the original design, and provides the final design of the MSR radiator.

5.4 Radiator Design

Based on the MSR project's goals, operational constraints and the radiator technologies discussed in the previous sections, the radiator group designed a thermal radiator. The basic concept is a heat-pipe based radiator similar to the SP-100 and SAFE-400 designs discussed in Section 5.2. This section discusses the design considerations and explains the choices that the group made. It also details the final design, a finned heat pipe radiator, and reviews the physical parameters.

5.4.1 Constraints

As an integral part of the MSR system, the radiator has several requirements that it must fulfill. The goals of the project dictate some of these constraints, and the design choices of other groups influence others. The most obvious interaction is between the radiator and the power conversion system. The 127 core heat pipes exit vertically from the bottom of the reactor vessel and enter thermionic sleeves, which are just over 1 cm in diameter and 60 cm in length. The radiator system will require a heat exchanger to interface with these sleeves and transport the energy to the heat pipes, while minimizing temperature drop in order to maximize efficiency.

Because the thermionic conversion system is only 10% efficient in generation and there will be additional losses in transmission, in order to transmit 100 kW_e the reactor produces 1.25 MW_{th}. Consequently, the radiator has to be able to dispose of 900 kW_{th} of excess heat. The radiator must provide this heat removal from the outside of the thermionic sleeves, and ensure they maintain their design temperature of 950 K, in order to ensure proper power output.

The ultimate energy removal mechanism is radiation, and therefore the rate of heat dissipation is:

$$\dot{Q} = \sigma \varepsilon A \left(T_s^4 - T_\infty^4 \right) \qquad (5.4\text{-}1)$$

Where $\dot{Q}$ is the power radiated, σ is the Stefan-Boltzmann constant and T_∞ is the apparent temperature of the environment [101]. The properties of the surface are the emissivity, ε, the radiator area A, and the temperature of the surface T_s. It is apparent from Equation (5.4-1) that temperature is the controlling factor in the efficiency of the radiator. Since the power level is set, in order to minimize the size of the radiator it is important to use a high-emissivity material for the fins, and to keep the fins at as high a temperature as possible.

The radiator must also be able to operate at full power for five years. Because the heat pipes are a sealed loop and operate passively, their performance should not degrade over this time. The radiator has no other mechanical or electrical systems that operate after its initial startup. This passive operation also maintains the systems safety – a break in a heat pipe would release only very a small amount of fluid and vapor to the environment, and does not compromise the safety of other systems. The thermal radiation emitted by the panels is non-ionizing radiation in the infrared and visible spectrum, so there is no danger of radiation damage. Furthermore, the panels direct the energy away from the other MSR components and the surface to prevent overheating.

Because the project objectives call for the use of the same MSR design for the Moon and Mars, the radiator must be versatile enough to handle the attributes of both environments. See Appendix IV for a discussion of the geophysical and meteorological properties of the Moon and Mars. On the Moon, there is no atmosphere, which allows the apparent temperature of the sky to be near 0 K, while it is around 300 K on Mars. However, the Moon is much closer to the Sun than Mars, so the incident solar energy is double, on average the solar flux is 1360 and 590 W/m^2, respectively.

Finally, the radiator must accommodate the MSR launch mass limitation of 10 MT. Based on the expected masses of the other MSR components, the radiator group decided on an upper bound of 2 MT. In addition, as discussed above, the size of the launch vehicle payload area is a 5 m tall cylinder, with a diameter of 5 m. The reactor module, as well as the shielding and thermionic converters, occupies a cylinder 1.19 m in radius at

about 1 m tall. These dimensions give a large amount of room around and above the rest of the components to situate the radiator panels.

5.4.2 Design

The design team separated the MSR radiator design into several sections. First is the structure of the PCU interface, panels and physical supports. Next are the operational components concerned with control, monitoring and dust removal. Finally this section will discuss the major chemical reaction of concern, oxidation.

PCU Interface

In conjunction with the PCU group, the radiator group decided on annular heat pipes as the most effective method of transferring heat from the thermionic sleeves to the radiator. See Section 4.5 for a description of the PCU to radiator heat exchanger. After the 60 cm annular length, the heat pipe contracts down to a normal heat pipe, 2 cm in diameter with the same wall thickness. This diameter allows the central vapor channel to retain approximately the same cross-sectional flow area between the two segments.

The major differences in design between the core and radiator heat pipes are the shell material and working fluid. The Carbon-Carbon shell has a high melting point (3650 K) typical of ceramics, with a thermal conductivity (66 W/m K) comparable to a metal. This combination avoids the danger of softening or deformation without introducing a large thermal resistance [94].

The design group chose potassium as the heat pipe working fluid for its excellent thermal properties and low density compared to other liquid metals. Among the fluids the group investigated, potassium's melting point, 1032 K at STP, is the closest to the radiator input temperature of 950 K. By decreasing the ambient pressure inside the heat pipe to 39.8 kPa, roughly one-third atmospheric pressure on Earth, the boiling point reduces to 940 K.

Radiator Panel

After the annular section, the heat pipes make a 90º bend with a 0.5 m radius of curvature. The pipes are arranged so that they emerge equally spaced around the circumference of the core and extend outwards horizontally to a maximum radius of 2.4 m from the centerline. The pipes make another bend before reaching the horizontal limit and angle back towards the reactor at 52º from the ground. After exiting the bend, a Carbon-Carbon fin encases each heat pipe; these fins connect between all of the pipes to form a conical sheet. To improve conduction between the pipes and the fins, the design has the heat pipes inset 3 mm into grooves on the front side of the sheet, and a 5 mm thick sleeve encases each pipe and is contiguous with the panel. The conical radiator surface alone is 2.34 m in height and 4.58 m wide at the base. The heat pipes and paneling end at distance of 46 cm from the centerline of the craft, giving a total surface area of 41.5 m^2. Figure 5.4-1 below shows a cross section of the panel design, and Figure 5.4-2 is a cross section of the entire assembly.

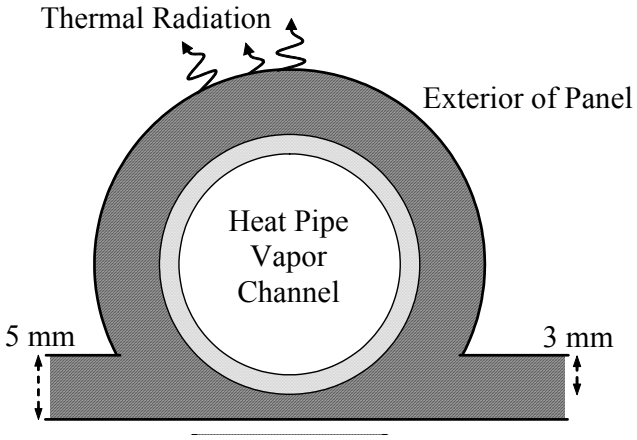

Figure 5.4-1: Cross section of MSR radiator panel

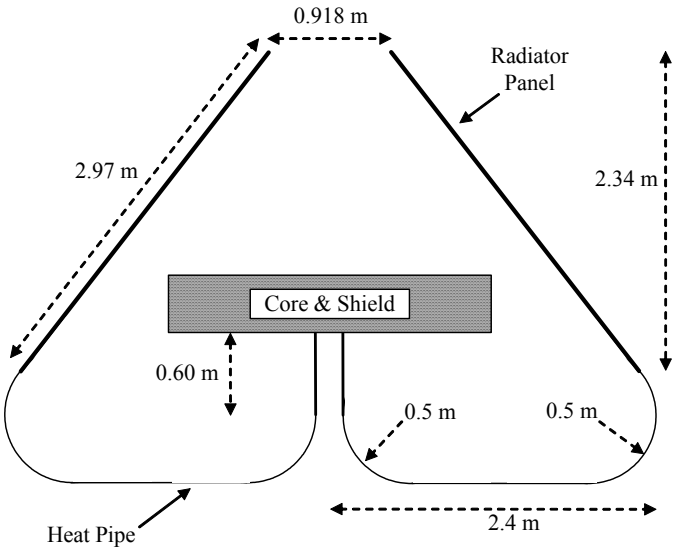

Figure 5.4-2: Diagram of MSR radiator with two heat pipes shown and the internal support structure omitted

The radiator assembly has a total height of 3.34 m and a diameter of 4.8 m yielding an average heat pipe length of 6 m. The conical shape with pipes on the outside maximizes radiator area as well as angle from the ground. As the angle of the radiator panels becomes steeper, the amount of incident solar radiation decreases, because there is diminishing contribution due to reflection from the planetary surface. The outside surface of the radiator panel is polished to achieve an emissivity near 0.9, while the inside surface is roughened or coated to minimize the emissivity. Lowering the inside emissivity reduces the amount of thermal radiation directed back at the other reactor components. The radiator group modeled the radiator as a grey body and therefore its emissivity is equal to its radiative absorptivity, which is the fraction of incident radiation a material absorbs versus the amount it reflects. Reducing this factor on the inside surface limits absorption of thermal radiation emanating directly from the core. The total mass of the panel is 360 kg, while the heat pipes, with potassium fluid, are about 155 kg.

Supports

The finned heat pipe concept offers excellent thermal transfer characteristics, but in order to maximize the temperature across the fin surface it is important to make the fin as thin as possible. Likewise, to decrease the thermal resistance between the heat pipe fluid and the fin, the group designed the heat pipe's shell to be as thin as possible. This necessitates

the inclusion of a separate structure to support the weight of the radiator and secure it to the rest of the MSR assembly.

A titanium frame spans the inside surface of the conical surface to provide support to the panel and the heat pipes. The choice of titanium alloy would maximize strength in the high temperature range, but in general, titanium's melting point is well above 1800 K. This frame mounts at a central point above the reactor to prevent interference with shield movement. Eight beams, each 2 cm in diameter, start from a central hub at an angle of 6.54º, and intersect the panels at their midpoint 1.5 m from the reactor centerline. Each of these main supports connects to a titanium spreader bar, which attaches to three rectangular titanium strips running along the inside surface of the conical panel. These strips form three equally spaced rings, and support the weight of both the panel and the heat pipes. The spreader bars are 1.25 m long and 1 cm in diameter, while the strips have a height of 4 cm and a thickness of 5 mm. Figure 5.4-3 below shows a cross section of the radiator support frame and the location of the support rings. The total mass of the support structure is 50 kg.

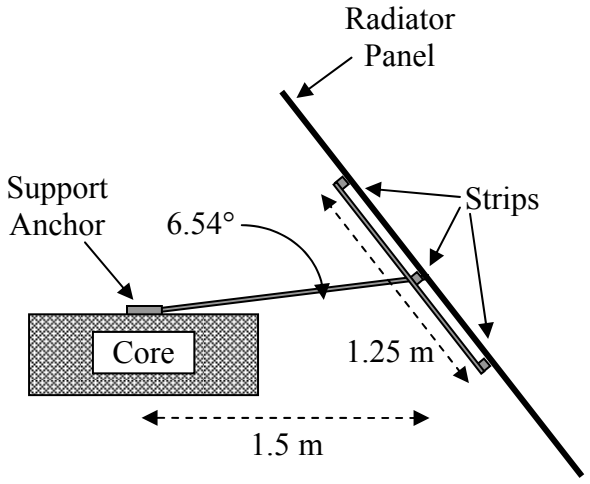

Figure 5.4-3: Cross-section of MSR radiator's titanium support structure with one of eight radial beams shown

The titanium frame distributes the mass of the radiator to the same structural assembly supporting the reactor, which in turn connects to the landing vehicle. Because of the low weight of the panels, the geometry of the radiator cone will not raise the MSR's center of

mass appreciably. Therefore, this design assumes the lander will already have sufficient stability to prevent the MSR assembly from swaying or tipping.

Operation

One of the major advantages of using heat pipes is their passive operation. Each pipe is independent of the others and is a completely sealed loop without pumps, valves or junctions. This simplifies their design and improves reliability. The SP-100 design does incorporate mechanical operation, however. Because of the large size of its heat pipe radiators, the panels are stored folded against the reactor until it is in place on the surface. Such a range of motion would require motors and joints to allow the panels to unfold, heating to thaw the working fluid in the heat pipes, and a supplementary electrical system to provide the needed power before activation of the reactor.

This design requires no folding or unfolding system, which greatly simplifies construction and eliminates the need for any mechanical controls. However, the liquid metal working fluid will be solid before reactor startup and therefore requires thawing. The reactor could accomplish thawing by slowly increasing core power and allowing conduction through the heat pipes to melt the fluid. However, in the event this process is too slow or unreliable, it may be desirable to have a system to heat the pipes directly and independently of core power. The thawing system consists of wire heating elements wrapped around the lower exposed pipe runs. Activated on command just before reactor startup, a battery runs a small current through the wires, warming the solid potassium and accelerating the thawing process once the core becomes hot. Thermocouples attached to exterior of the heat pipes and panels at various locations will provide temperature data to ensure the thawing is proceeding as expected. In addition, these probes will provide important data on the long-term operational characteristics of the radiator system.

Once thawed, as long as the appropriate thermal conditions exist at the two ends, heat will be absorbed in the evaporator section and transported naturally to the condenser region. Like with the SP-100, however, the initial startup may require activation of the un-packaging sequence and operation of heaters. This might require an uplink to human controllers, but an onboard computer should be able to perform the same tasks. To

monitor this operation the design should include diagnostic instrumentation installed at different points in the radiator. Monitoring may also be required for verification or study of the operational performance of the radiator. The design team would need to integrate such a system into the radiator without interfering with its operation, and transmit the data back to a central processor on the MSR lander.

Dust Removal

A fine layer of dust covers the surface of both the Moon and Mars. This dust could be stirred up into the atmosphere by activity (such as landing and unpacking) and by the wind on Mars. Because the radiator will have a large surface area exposed to the atmosphere, it is likely that this dust will settle out on its panels. Dust buildup tends to degrade the radiator's performance by decreasing the fin's effective emissivity, however this effect varies based on materials and temperature. A dust removal system will mitigate this problem by either removing the dust from the surface or preventing its accumulation [98][93].

Several studies have shown that Carbon-Carbon exhibits a minimal emissivity penalty due to dust buildup of micrometer thicknesses [99][93]. This thickness of buildup is very difficult to prevent, although on Mars the wind will likely prevent large amounts of accumulation on the inclined panels by blowing it off. However, models have predicted more significant dust buildup on the Moon, especially due to multiple launches and landings over a five-year multi-mission period. Every time a spacecraft lands or takes off from the surface, rocket thrust will blow soil around and the resulting dust could drift towards the radiator. This dust buildup tends to improve emissivity initially, but after five years, the performance may drop by five percent. The best strategy for preventing this degradation is to limit the amount of activity near the reactor, especially those that might stir up large amounts of soil. In addition, the radiator must have sufficient surface area to withstand the expected 5% loss of emissivity over operating lifetime. See Figure 5.4-4 for the required radiator area based on effective panel emissivity.

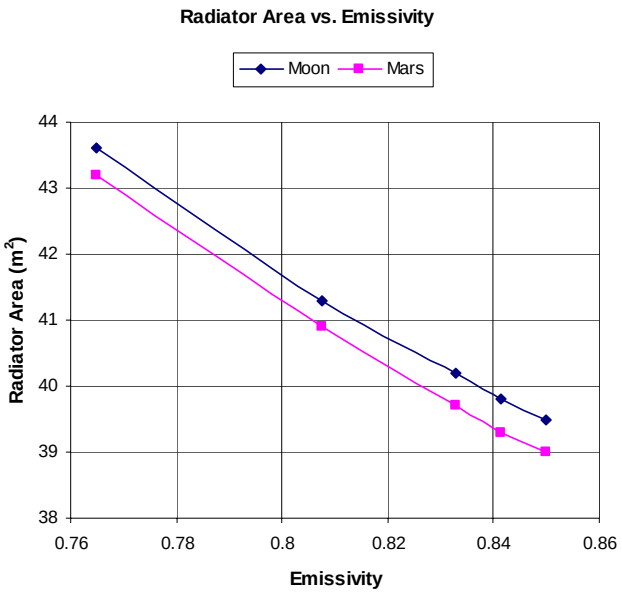

Figure 5.4-4: Required radiating surface area as a function of surface emissivity for conditions on the Moon and Mars

Oxidation

The main drawback to the use of Carbon-Carbon composites is the potential for oxidation at temperatures above 600 K. Chemical oxidation occurs when oxygen diffuses into the composite matrix and combines with the carbon atoms, forming CO and CO_2 gasses. Although oxygen is present as oxides in the soil of the Moon and Mars and in the Martian atmosphere, the lack of atomic oxygen will reduce the oxidation rate considerably. To forestall any further degradation of the radiator's surfaces or the heat pipes, the design team decided to treat all exposed Carbon-Carbon surfaces with a silicon carbide coating. This coating will react with oxygen and create an inert layer SiO_2. Both SiC and SiO_2 have thermal conductivities similar to Carbon-Carbon, and the presence of the coating should not decrease the emissivity of the panels appreciably [106]. Oxidation of the titanium supports should not be an issue, since, if a layer of oxide forms on the outside, this will prevent further oxidation, and the thermal performance of the supports is not important.

Reliability

The design group ensures reliable operation through a variety of approaches: redundancy, protection, artificial safety margins and system versatility. When properly designed, the heat pipes offer a high degree of redundancy. If a pipe fails, the neighboring units immediately compensate by absorbing the additional thermal load. This flexibility also allows the system to survive sudden temperature and power variations. It is important that design includes safety margins in other components as well, anticipating a reasonable fluctuation in the predicted operating conditions. To as large a degree as possible, the radiator should be able to perform as needed even if other systems do not operate as expected. Finally, the construction of the radiator should protect its components from damage due to physical stress, corrosion and high temperatures. The group did not analyze micrometeorite impacts because they are very rare occurrences even on the Moon, which does not have an atmosphere to shield its surface [107].

5.4.3 Summary of Parameters

The MSR radiator rejects power at 22 kW/m^2 with a specific mass of 14 kg/m^2. Table 5.4-1 gives a summary of the MSR radiator's design parameters.

Table 5.4-1: Summary of the MSR radiator design

Radiated Power		900 kW
Radiator Inlet Temperature		950 K
Radiator Average Temperature		940 K
Radiator Area		41.5 m^2
Mass	**Panel**	360 kg
	Heat Pipes	155 kg
	Supports	50 kg
Heat Pipes		127 Carbon-Carbon composite heat pipes with potassium working fluid and Nb-1%-Zr wick, 2cm diameter, 6m avg. length
Radiator Surface		Conical Carbon-Carbon panel overlaying heat pipes, 5mm thick at 52 degree incline
Corrosion Resistance		SiC coating on Carbon-Carbon surfaces
Support Structure		8 titanium beams radiating from top of reactor and connected to 3 circular strips running along the inside surface of the panel

The mass of the heat pipes and panels is 515kg, while the titanium support frame is 50kg. The entire system occupies a space 4.8 m in diameter and 3.34 m tall. Because it does not require any unpacking once on the surface, these dimensions are the same at launch and during operation. In addition, the same system will work on the Moon and on Mars.

For the same core and PCU configuration, the power the radiator is able to reject scales approximately linearly with the area if temperatures are constant. For scalability, in order to increase the maximum power, the design team would need to increase the number of heat pipes and area of the radiator such that the power rejected by each pipe, and its radiative area, remains constant.

Finally, the radiator panels and heat pipes are not load bearing, so the weight of the entire system rests on a titanium frame. The radiator connects to the other MSR systems at two points: at the bottom of the core where the heat pipes fit over the thermionic sleeves and the top of the reactor at the titanium support anchor.

5.5 Design Analysis

The radiator group used an iterative process to arrive at the final design. The team members identified constraints, created a model, evaluated system performance and then made changes as needed. While the previous section presents the results of the analyses, this section delineates the types of evaluation and calculation that the radiator group conducted in order to achieve these results. These analyses addressed three primary areas of concern: size, mass and radiator performance. This section will discuss those analyses and the computational methods employed. In addition, there will be a review of how the system would respond to different accident scenarios.

5.5.1 Size and Mass Analysis

Calculation of the heat flow through the radiator system is critical for determining the efficiency of the design. The radiator group used a number of different approaches to solve this problem, and the initial approximations were gradually refined as the group decided on more specifics of the design. The overall thermal performance hinges on a number of factors: the temperature of the hot junction with the PCU, the amount of power that the radiator must dissipate, the efficiency with which the piping conducts heat from the PCU to the radiator, and the effective heat sink (cold side) temperature.

The radiator group calculated the size and mass of the radiator using two different approximations: one represents the entire radiator as an isothermal surface, and the other considers the condensing and sensible heat loss sections separately. For each of these models, the group conducted a separate analysis for the Moon and Mars in order to determine the variance and find the maximum size requirements. The major differences between these two locations are the solar radiation flux and the apparent temperature of the sky. The model assumed the radiator on the Moon experienced the maximum solar flux of 1360 W/m^2 and had a sky temperature of 0 K. Meanwhile the Martian surface receives 590 W/m^2 due to solar flux, but has an apparent sky temperature of 300 K.

Isothermal Approximation

Using an isothermal approximation the design team was able to obtain a basic estimate for the size of the radiator. Using the radiative power equation given in (5.4-1) and

assuming ideal radiating conditions, the only parameters that the design must specify are the radiator temperature and the emissivity. Emissivity is a material property that measures the efficiency of the radiator relative to an ideal model (blackbody); careful surface preparation can modify the emissivity of many solids. The design team decided to use a base emissivity of 0.85 since this should not be difficult to achieve during manufacturing of most of the materials under consideration. Based on the dust buildup considerations detailed in the previous section, the actual emissivity used in the all the design team's calculations took into account a 5% emissivity loss so that the area provides adequate design margin over operating lifetime. See Figure 5.5-1 below for a plot of the required radiator area versus temperature for the isothermal model. According to this model, the required radiator area is 24.9 m^2.

The major limitation of this model is the assumption that the radiating area is isothermal. While it is true that a large section of the condensing region of a heat pipe is isothermal, there are also temperature drops due to sensible heat loss on either side of the phase transition.

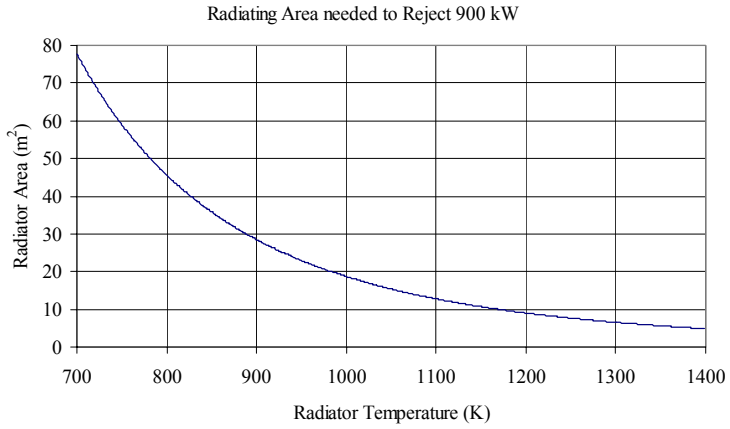

Figure 5.5-1: Isothermal estimation of the area of the radiator based on temperature

Once the area was calculated using this method, it is very straightforward to find the mass of the system. The volume of the panel is simply the area multiplied by the thickness, which is 5 mm. In order to find the total mass of the heat pipes the team then calculated the contributions from the shell, the wick fibers and the fluid (assuming that it fills the remaining volume and is 50% vapor). See Figure 5.5-2 for a comparison of the volume

and mass fractions of the heat pipe constituents. These calculations will provide an over-estimate of the mass of these components, however since the total mass is small it should be reasonably conservative. Table 5.5-1 gives the results of this analysis.

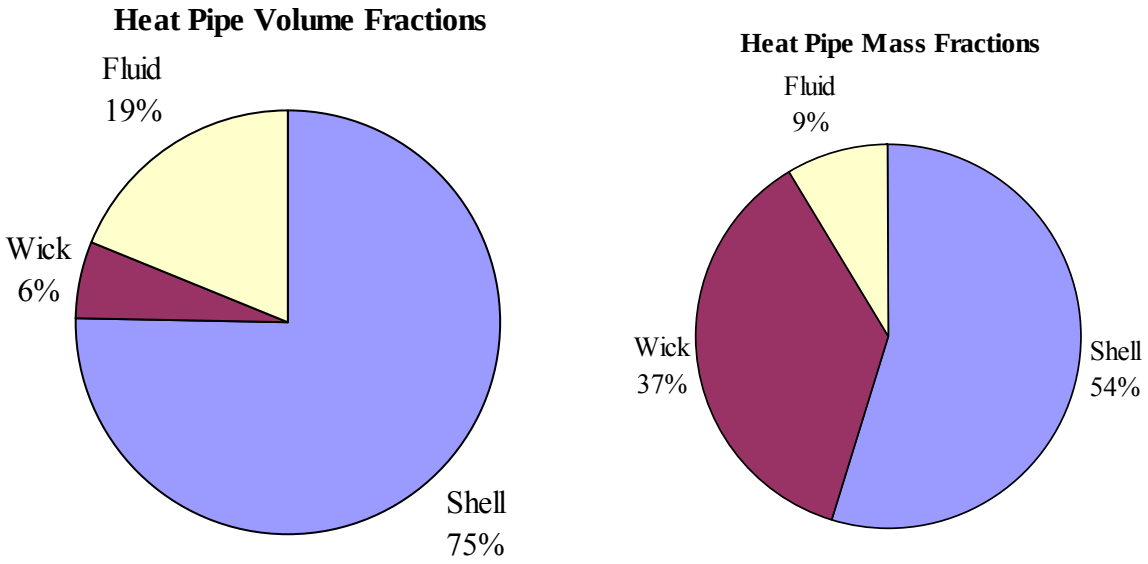

Figure 5.5-2: Volume and mass fractions of the heat pipe constituents

Linear Condenser Model

After reviewing the isothermal analysis, an alternative method was employed to obtain a more precise estimate of the radiator area. This calculation takes into account some of the thermodynamic effects of fluid condensation as well as the temperature drop across the radiator.

The energy loss from the heat pipe working fluid goes through three stages in the radiator panels: sensible heat loss as the fluid temperature drops to its boiling point, latent heat loss as it condenses from a gas to a liquid and sensible loss as the temperature begins to drop again after the phase change is complete [101]. The design group is only concerned with the first two stages because the third occurs during the fluid's return through the wick. The sensible energy transfer in the working fluid is

$$\dot{Q} = \dot{m} c \Delta T \qquad (5.5\text{-}1)$$

Here $\dot{m}$ is the mass flow rate of the fluid, c is the specific heat, and ΔT is the change in temperature. The amount of energy released during the condensation process, which occurs at a constant temperature, is

$$Q = mh_v \qquad (5.5\text{-}2)$$

The latent heat of vaporization, h_v, relates the energy per unit mass required to convert between liquid and gaseous phases of a substance. This is very important because most of the energy the heat pipes transport is stored in this phase change, not in the working fluid's temperature change. This fact allowed the design team to estimate the average mass flow rate through the condenser by using Equation (5.5-2) and including the small power losses in the first region. Next, because the condensing sections of the heat pipes are isothermal, the area calculation is straightforward. Equation (5.4-1) describes the power dissipation in the condenser, the area being the only unknown.

All that remains is the calculation of the smaller sensible heat loss section. See Figure 5.5-3 for a depiction of the radiator zones. The difference between the temperature of the vapor as it leaves the annular evaporator and the boiling point of the fluid determines the length of this section. The temperature of the fluid is a function of the amount of energy that the radiator has dissipated; however, as discussed above, the rate of dissipation decreases with temperature. Solving this differential equation yields temperature as a function of position. See Figure 5.5-4 for a graph of the results of this temperature analysis. In order to obtain the length of the first section, the position at which the temperature drops to the fluid boiling point must be determined.

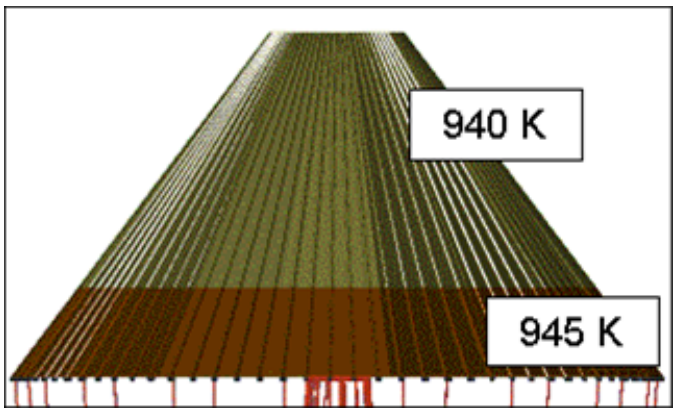

Figure 5.5-3: Major temperature zones on radiator surface with average temperature shown. The red zone is the approximate sensible heat loss region, while the green region is the isothermal condensing region

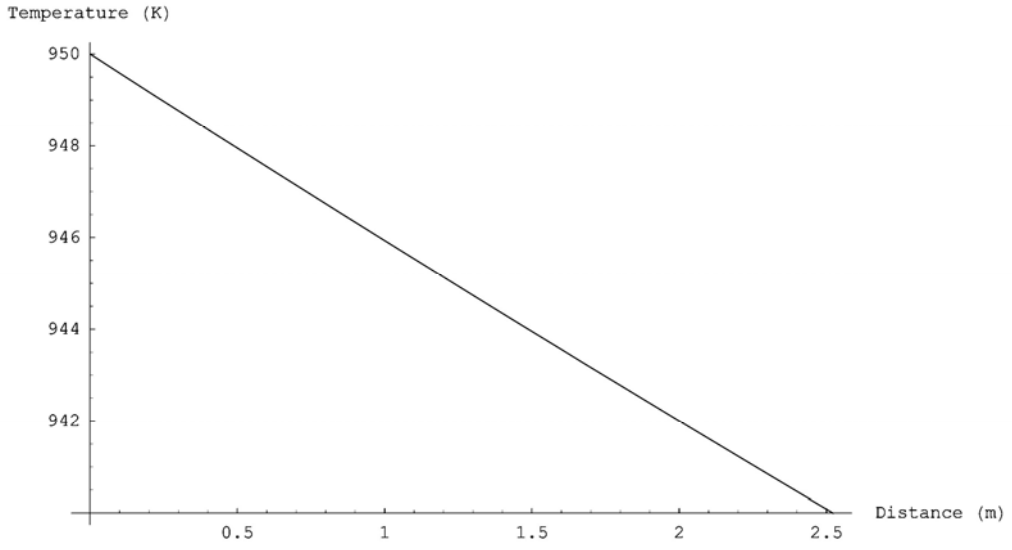

Figure 5.5-4: Calculated temperature drop in the sensible heat loss section of the radiator. The rate of heat loss is nearly constant over this length

The total area of the radiator is therefore the condenser length plus the length of region needed to decrease the temperature of the vapor to its boiling point. Once the team found the area, it calculated the mass by the same method used for the isothermal model above. Table 5.5-1 gives a comparison of the results of these two models for the Moon. For both models, the radiator on the Moon was slightly larger than the one needed for Mars (but within one percent).

Table 5.5-1: Comparison of models used in radiator performance analysis

Model	Isothermal	Condenser
Input Temperature	950 K	950 K
Output Temperature	940 K	940 K
Radiator Area	24.9m^2	41.5m^2
Radiator Mass	336 kg	515 kg

Support Structure

The calculation of the titanium frame mass only takes into account the radial beams, spreader bars, and three circular strips. The anchor itself will be an integral part of the MSR's main structural backbone and therefore is not included in this analysis.

5.5.2 Design Comparison

The MSR radiator has a number of attributes that make it superior to past designs. The entire system is simpler and more reliable than even the two concepts used as a design basis, the SP-100 and SAFE-400. It requires no electrical or mechanical components, such as pumps or valves, during operation. The configuration of the radiator is the same during launch, transit and operation, so there is no need for unpacking or moving parts.

The high rejection temperature allows the radiator to achieve a high specific power of 22 kW/m^2 compared to 2.7 and 7.0 kW/m^2 for the SAFE-400 and SNAP-100 systems, respectively. Its specific mass, 14 kg/m^2, also compares favorably with these systems.

5.5.3 Accident analysis

Because this radiator design is both simple and highly redundant, major failures are unlikely. However, there are transients that could cause the system to malfunction by either disabling components or exceeding the operating parameters.

In the event of a sudden increase in temperature at the PCU interface, the system would initially respond by removing the heat at a faster rate. The radiator is able to operate in a temperature range defined by the heat pipe working fluid and geometry. The lower limit is the boiling point of the potassium in our evacuated pipes, 940 K. Below this temperature the vapor flow driving the heat pipe completely liquefies and heat can be

removed only very slowly by natural convection in the pipes. There is not as clear-cut of a definition for the upper limit. Because the radiator heat pipes are a very similar construction to the core heat pipes, but with a greater length, a similar heat flux limitation applies. See Section 3.3.4 for a discussion of heat pipe operation. Around 1200 K the high vapor pressure and heat fluxes in the evaporator region will begin to limit the recirculation of liquid in the heat pipe. In addition, high temperatures will cause film boiling along the inner wall of the heat pipe, creating a high thermal resistance.

At the other extreme, a decrease in temperature at the PCU interface (to below the potassium boiling point) would greatly reduce heat removal capability. However, this situation, akin to the conditions at reactor startup, is not likely to have negative consequences. As the loss of cooling causes temperatures to climb back above 940 K, vaporization will begin again, restoring normal cooling. There may be issues of fatigue if this thermal cycling continues for long periods. Very low temperatures (below 350 K) might allow the potassium to begin re-solidifying in parts of the radiator, but this would be a very long process due to the extremely small thermal radiation rate at such temperatures.

If there is a failure of the initial potassium thawing system, the operators can still start the reactor. As long as the temperature increase is gradual, the heat pipes should be able to thaw completely (reach 337 K) well before the PCU interface reaches the operating temperature of 950 K. Even before boiling begins, natural convection will circulate the hot potassium from the annular section out to the panels.

Another accident scenario is damage to the radiator heat pipes causing one or more to fail. If there is a breach that exposes the heat pipe's interior, the working fluid will escape and the pipe will loose the ability to transport heat. This would lead to the insulation of the condenser end of one of the core heat pipes, causing it to fail to remove heat from the core. Conduction across the core would then redistribute the power to neighboring core heat pipes, and eventually to the neighboring radiator heat pipes. The limiting factor for the radiator is the maximum power that each heat pipe can transfer. As the core group

calculated in Section 3.3.5, the physical limitation is around 27 kW per heat pipe, whereas normally each heat pipe transports about 7 kW.

5.6 Summary

The MSR radiator is a finned heat pipe design. The fins combine to form a conical panel around the reactor, and rejects the excess thermal energy into space. Operating with a hot side temperature of 950 K, the radiator utilizes an area of 41.5 m^2 to reject 900 kW_{th}. The entire radiator system, including supports, heat pipes and panel, has a mass of 565 kg.

The major benefit of this design is redundancy; there are 127 independent heat pipes, and the system has enough flexibility to compensate for several heat pipe failures. A five-year lifetime is quite reasonable considering the high reliability of the heat pipes, and because the system does not rely on any mechanical or electrical components. The radiator is safe since it is a sealed system, and it contains only small amounts of chemically reactive substances, namely the heat pipe's potassium working fluid.

5.7 Future Work

The constraints of time and the limited scope of this project dictated that the radiator group could not explore all areas of the design. There is opportunity for additional analyses and broader considerations in follow-up evaluations. In addition, future work in this area can benefit from the lessons learned in this report and take advantage of expanded understanding and radiator technology.

5.7.1 Extensions

There are many areas of this design that merit supplementary analysis – these cover all aspects of the project, from thermal analysis to specifics of the landing site. First, future investigators should perform more a precise analysis of the operation of the radiator's heat pipes. While the numerical correlations used in this report give the necessary information, use of a detailed computer model would allow much greater certainty in operational parameters.

The heat pipe performance analysis would then be a part of a larger reevaluation of the thermal transfer characteristics of the radiator. Researchers can expand the relatively simple thermal models used in this report to include more analysis of the temperature profiles and greater exploration of secondary radiation heating and losses. Future work should explore the heat conduction from the heat pipes to the radiator panels, since this represents a point of increased thermal resistance. This design team did not consider the lateral temperature distribution on the radiator surface, which varies as a function of both the distance from other heat pipes, distance from edges and height from the base of the radiating surface. In addition, because there is a distribution of temperatures in the core, there will be a distribution of hot side temperatures for the radiator. This means that neighboring heat pipes will not have the same temperature profiles and therefore there is increased lateral heat flow.

Another aspect of the thermal design, which requires a much more involved series of calculations, is the precise thermal loading on the radiator due to radiation from the core. The design group decided that because the radiator components are very thin, low-Z materials, gamma-ray heating would be minimal, but this would still be an interesting effect that is non-uniform over the volume of the radiator. In addition, because this is a low-Z material, neutron interactions with the radiator material might lead to deleterious effects.

Another factor not thoroughly explored by this project was the possibility of mechanical or electromagnetic dust removal or shielding. From the research conducted by the radiator group, it is not clear how effective such systems would be, or whether the emissivity penalty due to dust is significant enough to offset the added mass and complexity of a removal system.

Aside from the other avenues for thermal analysis, additional mechanical stress analyses would also benefit the design. The current radiator design assumes that the heat pipes are not load bearing structures, and therefore a titanium frame distributes the weight of the panels and the pipes and secures them to the core. Future work can simulate this design,

and calculate what stresses the heat pipes can reasonably withstand (taking into account launch and landing phenomena) to determine how extensive and rigid this frame support needs to be.

One major item, which was well beyond the scope of this project but may have a major impact on the design, is the choice of landing sites on the Moon and Mars. As on Earth, meteorological conditions and environmental composition vary depending on location. If the design team knows the exact location and therefore can obtain the local conditions, this removes a great deal of uncertainty in the design constraints and may allow greater freedom in orientation and structure. As a part of this, it might be worthwhile to conduct more analysis on convective heat transfer on Mars. Because of the very low atmospheric pressure, this project did not consider convection as a mode of heat rejection. However, there might be enough of an effect to provide detectable heating or cooling of some surfaces.

5.7.2 Transient Analysis

For the majority of the work in this project, the radiator group made calculations assuming that the radiator system was operating in a steady-state condition. While this assumption will be true most of the time, there are also a number of transient effects. The radiator design team did not analyze these effects rigorously because of the large amount of modeling and computational work required. Given more time, supplementary research will be able to take advantage of thermal analysis programs and perform these simulations.

The primary transient is reactor startup (and thus radiator startup). While the current design does consider this sequence, it would aid future research to obtain a model for the thermal performance of the radiator as it transitions from cold zero power to hot full power. This would verify that the radiator would provide sufficient cooling before the rise in temperature is sufficient to fully activate the heat pipes, and ensure that no unexpected temperature feedback mechanisms exist.

A second transient is solar heating, which has a regular variation on both the Moon and Mars, although the exact amount depends highly on location. While the radiator design team expected that this would be a minor transient, it is one of the few ways that the environment will regularly effect the operation of the reactor. By better quantifying this effect, future research can assure that the design is able to accommodate it fully.

Finally, while nothing in the MSR system gives the design team a reason to anticipate reactor power transients, modeling how these transients effect radiator operation is an important part of validating the overall reliability of the system. Both over- and under-power transients would modify how the heat pipes operate and thus affect their heat-removal capability. Analysis in this area can determine important factors such as the rate at which different system configurations respond to transients and precisely what the radiator operating limitations are as a function of time, power and temperature.

6 Shielding

6.1 Introduction

There are several types of shielding for space systems, however in this context, shielding is needed primarily to protect against biologically damaging ionizing radiation resulting from fission and fission product decay emitted by the core. The objective of this group was to design a system that will reduce the nominal radiation dose received by crew and radiation-sensitive instrumentation to as low as reasonably achievable (ALARA). This chapter establishes dose limits to the crew and describes various methods of shielding the MSR to reduce the nominal radiation dose to these limits.

It is important to note here that constraints of a particular mission or campaign dictate the shielding design. An optimal shield is dependent upon the local topography, soil composition, distance from habitat, and exploration region of the crew. Instead of tailoring a design for a particular mission type, the team will chose the most robust and flexible shielding system.

6.2 Dose Limit

While the question of how much radiation is too much is contentious, the occupational guidelines of the United States Department of Energy offer a suitable limit. These rules stipulate that a radiation worker cannot receive greater than 5 rem in a year (or an average dose rate of 0.57 mrem/hr) [112]. This value very nearly approaches the estimated 0.6 mrem/hr for naturally occurring radiation on the Lunar and Martian surfaces due to galactic cosmic radiation (GCR) [113]. For astronauts, however, the acceptable dose increases as NASA stipulates a maximum occupational dose of 50 rem/yr (5.9 mrem/hr). Thus, if the core radiation output is reduced to a compromise magnitude of 2.0 mrem/hr, the same system that protects crew from natural ionizing radiation can easily be adapted to protect them from the remaining core radiation, as radiation attenuation is exponential with shielding thickness.

Dose rates due to radiation from the reactor are a function of distance from the reactor; therefore, it is meaningless to declare a limit on dosage without specifying a distance at which the astronauts will receive this dose. As stated above, the goal of the shield is to protect the crew regardless of mission type. However, it is unfeasible to shield to a dose rate of 2.0 mrem/hr at distances very close to the core because the shielding system will become prohibitively large. To appropriately integrate with the rest of the MSR, we have imposed a mass constraint of 2 MT on the shielding system. Thus, exclusion zones are required.

6.3 Radiation Interactions

In order to lay the groundwork for choosing appropriate shielding materials we will first examine the interaction of various types of radiation with matter. Charged particles are easily attenuated, or absorbed, and are thus inconsequential in this shielding analysis. Gamma rays, on the other hand, are the most challenging to attenuate, as photons penetrate matter more effectively than particulate radiation at a given energy. Neutrons, while slightly easier to shield than gammas, make up the most potentially damaging radiation component due to a high and varying linear energy transfer and possible neutron activation of nuclei.

Materials comprised of high Z elements provide the high electron density and nuclear charge crucial to effective gamma attenuation. Gamma rays interact primarily via interaction with orbital electrons in the form of photoelectric absorption, Compton scattering and electron-positron pair production. By offering more loci for photon-electron interactions, high Z materials generally attenuate gammas most effectively.

The most effective neutron shields are those which have a low atomic mass. Materials composed of low Z elements slow neutrons primarily via elastic scattering. Collisions of neutrons with nuclei similar in mass transfer more energy per scatter than collisions with heavy nuclei, and so require fewer scattering events for the same average energy loss. Thus, hydrogenous materials, such as concrete and water, are often the neutron shielding of choice for terrestrial reactors.

Since neutrons and gamma rays make up the primary sources of biologically hazardous radiation from a reactor, a shielding system must consist of both low and high Z materials. In addition, because neutron attenuation produces secondary photons through inelastic scattering events, it is suggested that the gamma-shielding layer be the outermost layer of any two-component design in order to stop this secondary gamma radiation.

6.4 Natural Shielding

The first decision the design team had to make, after determining the dose limit, was whether it is best to construct a shield on Earth and launch it with the system, or take the approach of *in situ* resource utilization – piling Lunar/Martian soil on the reactor as a shield. In this section, we will examine the possibility of natural shielding. This method could substantially reduce the weight of the MSR, however it will limit available shielding materials to the surface soil composition and require bringing machines capable of digging and transporting metric tons of Lunar or Martian rock.

The limiting factor for deploying any shielding technology is launch mass, because therein lies the problem of cost: estimated launch costs are several thousand dollars per kilogram [118]. To launch a shield massive enough to sufficiently attenuate ionizing radiation from the reactor core, the price tag will be large. In light of the mass-prohibitive nature of heavy and bulky shielding systems, the use of "natural" shielding becomes attractive. A remaining possibility is the use of a "mixed" system of artificial shielding to stop most of the radiation and surrounding it with a natural barrier for bringing the dose down to our specified limit of 2.0 mrem/hr.

6.4.1 Natural Shielding on the Moon

By utilizing material already existing on the moon's surface, the weight requirement will fall substantially. Given its barren landscape, interspersed with mountains and valleys, and a surface comprising a powdery soil, the moon offers little for a makeshift shield other than the bare ground itself. With basalt rock of an average density of 3.4 g/cc [119],

a shield of arbitrary thickness can, in principle, be constructed without the need for launching any extra weight other than the tools used for digging or blasting into the surface.

Lunar rock composition includes many oxides, mostly silicon based, but also oxides of refractory elements including calcium, aluminum and titanium, all of which are difficult for working and digging (see Appendix IV for a detailed description of Lunar soil composition) [119]. Approximating the moon's surface to be SiO_2 at a density of 3.4 g/cc, a natural shield of this material will exhibit a macroscopic removal cross section for gamma rays of 0.152 cm^{-1} for gammas of energy 2 MeV or higher. Thus, a thickness of half a meter can reduce the intensity of the flux from the reactor by 99.9% [120]. To construct a hemispheric shield of Lunar surface material large enough to cover a radius of 10 m would require moving 1,000 MT of Lunar soil.

One method of covering the core is to employ a rover with a bulldozer attachment. This method will not result in the full mass savings expected from using a natural shield because the bulldozer would have to be launched as part of the MSR package. The advantage of this system, however, is that the crew may have other uses for the bulldozer (i.e. shielding the habitat).

Another method for generating the raw dirt is to detonate some form of an explosive on the surface, construct the base inside the resulting hole and then replace the displaced dirt on top of the reactor. While a possibility for the Mars base, this technique will be more difficult to implement on the Moon. The Moon's small surface gravity, 1.62 m/s^2 [122], will limit the amount of dirt available for refilling over the base. The detonation of an explosive on the surface will spread material over a much wider range than a similar explosion on Earth. With a Lunar escape velocity of 2.38 km/s, there is no guarantee that any of the dirt will return to the moon's surface. This dispersion will leave the base with a hole but a limited amount of dirt with which to refill it. It may even bear a resemblance to many common Lunar surface features, namely craters, of which there is clearly no short supply. Instead, a more feasible solution may be to use the topology of the moon as a shield. Mountains, craters and cliffs present numerous potential locations for placement

of the reactor such that a geographical landmark obstructs the emitted radiation. For example, the reactor can rest at the bottom of a crater with the human habitat behind the crater edge, with tens of meters of Lunar surface material between radiation-sensitive equipment (including people) and the reactor. Issues with this solution include lack of precision landing and lack of flexibility in mission architecture.

6.4.2 Natural Shielding on Mars

The most abundant Martian surface material, ferrous oxide, has a slightly higher density but somewhat lower mass attenuation coefficient than silicon oxide, resulting in comparable gamma attenuation. The option of blasting a hole in the Lunar surface was eliminated for reasons delineated above. With twice the gravity and limited surface features including few craters on most parts of the Martian surface, the detonation of an explosive on Mars remains a reasonable option for creating a natural reactor shield.

Although it is a feasible option, the design team has rejected natural shielding because it is dependent on other mission parameters like having a bulldozer and picking a landing location with soil soft enough to dig in. In order for our reactor to be as robust as possible, the chosen shield must be independent of landing site and extra equipment. To construct a natural shield would require moving 32 MT of regolith before starting the reactor; thus, an alternative power source would be required. Also, in light of suggested geometries discussed in Section 6.8.2, placing regolith in these locations would require alterations to the rest of the system, such as specifying a new geometry for the radiator and power conversion systems.

6.5 Neutron Shielding Material

6.5.1 Choice Summary

Given that we ruled out natural shielding as a design choice, the design team is limited to the option of creating a shield from materials available on Earth and launching it with the rest of the reactor. The following section outlines the project team's shield design choice for protection from fission-borne neutrons. After carefully examining several options, the shielding team chose boron carbide (B_4C) to serve as the primary neutron shield. This

selection is optimal not only because of the superior attenuating characteristics of boron, but also because boron carbide is a strong structural material, is relatively low in mass and has a high melting point. Boron carbide being the third hardest material in existence, the manufacturing of this material is potentially difficult.

6.5.2 Dose Rates without Shielding

Operating at 1.2 MW_{th}, the bare MSR core (including reflector) emits a neutron current J_0 of 3.23×10^{11} neutrons/cm^2-sec ranging in energy from slightly epithermal neutrons ~100 keV to very fast neutrons upwards of 10 MeV. Thermal neutrons do not exist in the core due to specifications of the reactor (see Section 3.7). Any sporadic thermal neutrons that are in the core are unlikely to penetrate far past the reflector, thus the primary focus of neutron shielding materials is slowing of fast neutrons and subsequent absorption at thermal energies.

Core design studies delivered a neutron output spectrum divided into thirty-two energy groups. The design team approximated the output current as the output spectrum equally distributed over a reflector surface area of 11.7×10^3 cm^2. Estimates of the dose rate relied on modeling the energy-absorbing material by the ICRU-44 convention of a four-component tissue model [123]. This model approximates tissue as a homogeneous mixture of nitrogen, carbon, hydrogen and oxygen in appropriate mass fractions.

$$R_{fn} = \frac{J_n E_n \Sigma_s f}{\rho} \qquad (6.5\text{-}1)$$

The dose rate R_{fn} for each energy group results from Equation (6.5-1), where J_n is the current, E_n is the group energy and Σ_s/ρ is the macroscopic scattering cross section of tissue. Quality factors Q are included because neutrons of high energies exhibit up to Q=10 [116]. (In some cases, Q rises as high as 11, but we chose 10 because over 75 percent of the neutrons have $Q < 10$). Additionally, at high energies, the neutron scattering imparts a vast majority of the dose. Absorption cross-sections for fast neutrons in human tissue are very small and largely dependent on the concentration of ^{14}N in the tissue. This is because the major contributor to dose is from the reaction shown in Equation (6.5-2).

$$^{14}N + {}^{1}n \rightarrow {}^{14}C + {}^{1}p \qquad (6.5\text{-}2)$$

Summing the dose component of each group at the reflector boundary results in a dose equivalent of $2.4*10^{7}$ mrem/hr just outside the unshielded core. At distances much greater than the radius of the reactor core (>> 54 cm), this dose decays as the inverse square of the distance from the center of the reactor. This fact is significant because, with only moderate shielding, the dose will decay to safe levels after several meters. As is illustrated in Figure 6.5-1, the unshielded dose falls to 2.0 mrem/hr at a distance of about 25 m from the edge of the reflector, and to the equivalent of Lunar surface galactic ray background (0.6 mrem/hr) after about 44 m. These doses may seem relatively low, however it is still advantageous to use shielding to keep the neutron dose as low as reasonably achievable.

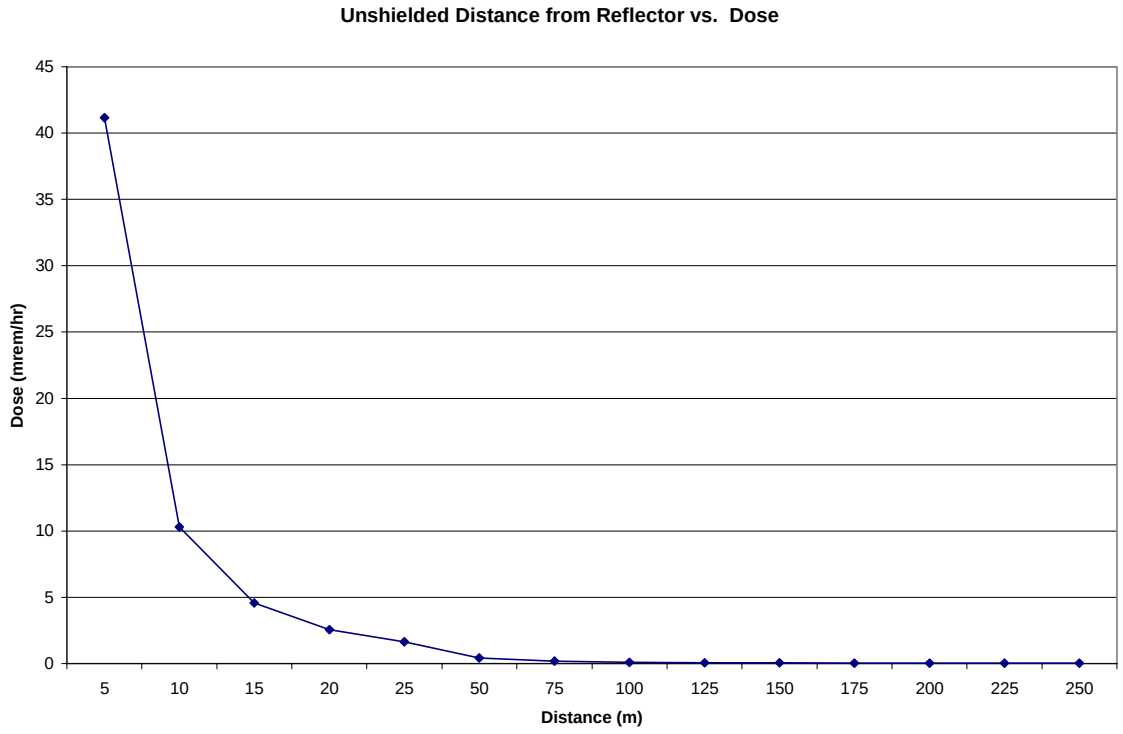

Figure 6.5-1: Neutron Dose Equivalent without Shielding

6.5.3 Material Selection

Neutron attenuation through media occurs via elastic scattering, inelastic scattering and absorption interactions with nuclei. In general, as the mass of the target nuclei approaches the mass of a neutron, neutron energy loss per collision increases. Thus, lower Z

materials attenuate neutrons more effectively than higher Z elements since atoms of those materials have a mass closer to that of a neutron. Additionally, low Z elements are desirable because these elements have a high number density of nuclei for a given mass. They provide more sites for neutron interactions and thus higher macroscopic cross sections.

In addition to the mass of the target nuclei, the neutron cross section also plays a role in judging the effectiveness of attenuation. The energy dependent neutron cross section is the interaction probability per unit atom density and distance in cm^2. There are three cross sections of importance to fast neutron attenuation, which correspond to two different types of neutron absorption. The first type of absorption is fast neutron absorption, and for this rate to be calculated, the absorption cross section at high energy is required. The second mode of absorption is thermal neutron absorption, where the neutron has to slow (to energy kT, where k is Boltzmann's constant and T is temperature of attenuating medium) before it is absorbed. Neutron scatter and thermal neutron absorption cross sections are necessary to determine thermal absorption rates. Consequently, when considering materials for a neutron shield, one must look at materials that are not only light, but also have high cross sections for the chosen mode of absorption. Table 6.5-1 below lists the described cross sections for possible neutron shielding material.

Table 6.5-1: Macroscopic Neutron Cross Sections [117]

Material	**Nuclide density (nuclei/cm^3)**	**Fast (2MeV) capture cross section (cm^{-1})**	**Fast (2MeV) scatter cross section (cm^{-1})**	**Thermal absorption cross section (cm^{-1})**	**Fraction attenuated after 10cm**
Water	3.346×10^{22}	8.36×10^{-7}	0.1673	0.1111	~52%
Lithium-6	5.33×10^{22}	5.33×10^{-7}	0.1066	2.052×10^{-3}	~54%
Lithium-7	4.594×10^{22}	1.97×10^{-7}	0.0597	3.216×10^{-3}	~41%
Boron-10	1.391×10^{23}	1.11×10^{-5}	0.01391	6.955×10^{-2}	~84%
Cadmium-114	4.565×10^{22}	5.21×10^{-5}	0.002	2.803×10^{-4}	~49%

Obvious choices for neutron shielding lie at the top of the periodic table where masses are lowest. It is easy to reject all transition metals; the density is far too high and the masses too great. One would need a large amount of this heavy material to attenuate the neutrons and a large amount of this material would be impractical due to weigh

restrictions of the landing module. It is easy to reject elemental gases due to low atomic density; otherwise, hydrogen would have been the best material for attenuation. A very low-density material will do little to attenuate neutrons unless the gas is pressurized or kept a low enough temperature where the gas becomes liquid. These however are unfeasible options because they are prone to single point failures and the extra equipment needed to sustain these systems would negate any mass savings gained from their superior attenuation properties.

After removing heavy elements and gases from consideration, we turned to other light elements on the periodic table, examining their cross sections, melting temperature, and stability. The first neutron moderating material considered was water. Water is widely used in land based thermal reactors, however is not practical for compact fast reactors due to the disadvantage of reflecting thermal neutrons back into the fast core. Furthermore, water would not work well on the extreme Lunar and Martian environments; the water would need to be kept pressurized to keep from evaporating at the temperature just outside the reactor (1500-1800 K).

The next group of materials considered was lithium-based materials. Lithium (Z=3) has a low mass density making it very lightweight. Lithium also has a high neutron scattering cross section at fast energies (~1 barn at 10 MeV). However, elemental lithium is an alkali metal and extremely reactive, therefore one must look at lithium compounds for shielding. Furthermore, elemental lithium melts at 453 K [124], again far too low for reactor shielding application. The salt lithium hydride (LiH) is an obvious choice, however, much like elemental lithium, the melting point is still too low at 953 K [125]. This problem was recurrent with most lithium compounds examined; the only lithium compounds with high melting points had undesirable masses or cross sections, thus ruling out lithium for MSR shielding. See Table 6.5-2 below for a complete list of lithium compounds reviewed and reasons for their rejection.

Table 6.5-2: Rejection of Lithium Compounds for Neutron Shielding.

Material	Reason for Rejection
Elemental Li	Highly reactive, low melting point ~550K
LiH	Low melting point ~950K
$LiAlH_4$	Heavy and high cross section

The final group of materials considered was boron-based compounds. Elemental boron has a very high thermal and fast cross section, a melting temperature of 2348 K [124] and a high resistance to thermal expansion. Elemental boron however is a brittle material and would not make a good stand-alone shield. However, boron-based compounds are very attractive for the above reasons, and are widely used in fast reactors around the world.

The first boron-based compound examined was borane (BH_3). Unfortunately, borane is an extremely reactive substance widely used in organic chemistry [126]. The next compound examined was boral (B_4CAl). Boral is widely used for terrestrial fast reactor shielding. Boral has a high scatter and absorption cross-section because it is approximately 40% boron by weight. Boral also has a melting point of 2349 K, which is much higher than lithium based compounds. The downside to boral is that the aluminum matrix gives excess weight without much neutron or gamma moderation ability.

The next compounds considered were borated graphite and boron carbide (B_4C). The design team removed borated graphite from consideration because it is essentially a graphite matrix with 4% boron [127]. Although borated graphite is very strong, chemically inert and has a high melting point, the fact that it does not have a large amount of boron mitigates its neutron moderating ability. Boron carbide (B_4C) has all the neutron attenuation benefits of a boron rich material (78.5% by weight) [128] and does not contain large fractions of non-moderating material. Boron carbide is also the third hardest material known to exist and extremely stable and chemically inert in the harshest conditions. The melting point of boron carbide is 2718 K [128].

In order to evaluate effectiveness of each of the boron shielding candidates, the shielding group compared the moderation power of the maximum thickness (given a 1MT weight limit) of shielding of each material. The definition of the maximum thickness of each material is the maximum thickness of a cylindrical shell surrounding and flush with the

radial reactor core reflector. By solving Equation (6.5-3) for a mass of one metric ton, the maximum shield thickness results. Even if the ultimate geometry of the material does not conform to this model, the resulting choice of shield will be maximally flexible because the cylindrical model represents the heaviest possible configuration of the shield.

$$\text{Mass} = \text{height} \times \rho \times [\pi(\text{thickness} + \text{radius})^2 - \pi(\text{radius})^2] \qquad (6.5\text{-}3)$$

The calculation of attenuation of neutron current utilizes an exponential function shown in Equation (6.5–4) using the macroscopic removal cross section for each energy group from the Kaeri chart of nuclides online database [129].

Table 6.5-3 below outlines the thickness of the materials that would result in a mass of 1 metric ton and the attenuation power of shields of that thickness. The unshielded dose is included for reference.

Table 6.5-3: Neutron Attenuation of Materials at Neutron Shield Weight of 1 MT

Material	Maximum thickness (cm)	Dose Rate at shielding edge (mrem/hr)	Dose rate at 10 m (mrem/hr)
Unshielded	N/A	2.40×10^7	10.29
Boral (B_4CAl)	20.3	1.24×10^5	0.1242
Borated Graphite (BC)	22.7	4.28×10^4	0.0427
Boron Carbide (B_4C)	21.1	3.57×10^4	0.0357

At distances greater than ten times the radius of the reactor (at about 2.5 meters), the core can be approximated as a point source, and neutron dose decays as a factor of $(r_0/r)^2$, see equation (6.5-4) below.

$$J = \frac{r_0}{r} J_0 e^{-\Sigma_r x} \qquad (6.5\text{-}4)$$

Because of its greater boron content, boron carbide outperforms both boral and borated graphite for a cylindrical geometry and thus became the neutron shielding material for the MSR. While the dose rates given in Table 6.5-3 appear rather high at the shielding edge, the rates drop off significantly as one moves away from the reactor. In the case of a boron carbide shield, the dose at a distance of 2.5 meters falls to 0.38 mrem/hr, well below the galactic background dose of 0.6 mrem/hr.

6.5.4 Boron Carbide Performance and Burn-Up Modeling

When a boron atom absorbs a neutron, it transmutes to lithium, thus decreasing the overall attenuation ability of the shield – this is burn-up. In this section, the design team will do a detailed analysis of boron carbide performance as a neutron shield, including an examination of the aforementioned burn-up effect.

Calculation Approximations

In the neutron dose calculations presented here, the dose from scattered neutrons was not taken into consideration because their effects on dosage were assumed to be small. Although the resulting current of thermal neutrons (<1 eV) produced will be sizable, $2.62*10^{11}$ neutrons/cm^2-sec (81% of total current after passing through shield), this current can largely be neglected since the thermal capture cross section is 3840 barns. The boron carbide shield will absorb virtually all of these neutrons so they will not penetrate the outer surface. This assumes the neutrons lose energy by scattering but take a straight path (40 cm) through the shield. This is unlikely since the neutrons scatter off of boron and carbon at a variety of angles meaning the path a neutron takes through the shield will likely be considerable more than 40 cm. Furthermore, many of the neutrons will be scattered down to the planet's surface or up into space where they will pose no threat. Thermal neutrons that do make it through the boron carbide shield will likely be absorbed by the tungsten gamma shield (see Section 6.6), which has a thermal capture cross section of 25.27 barns. All these factors make it reasonable to ignore the thermal neutron current in dosage analysis.

Throughout the rest of this section, dose calculations result from combinations between the $(r_0/r)^2$ dose dependence at large distances ($r > 10r_0$), when the core can be approximated as a point source, and the r_0/r dose dependence at small distances ($r < 2r_0$) when the core can be approximated as an infinite cylinder. For intermediate distances, the dose decays as a continuous linear combination of $(r_0/r)^2$ and r_0/r. See Section 0 for complete discussion of dose modeling. Figure 6.5-2 illustrates dose rate as a function of distance for a 21.1 cm thick boron carbide shield. As is visible in the graph, dose rate decreases exponentially with increasing shield thickness, thus optimizing geometry is crucial in obtaining an effective shielding system.

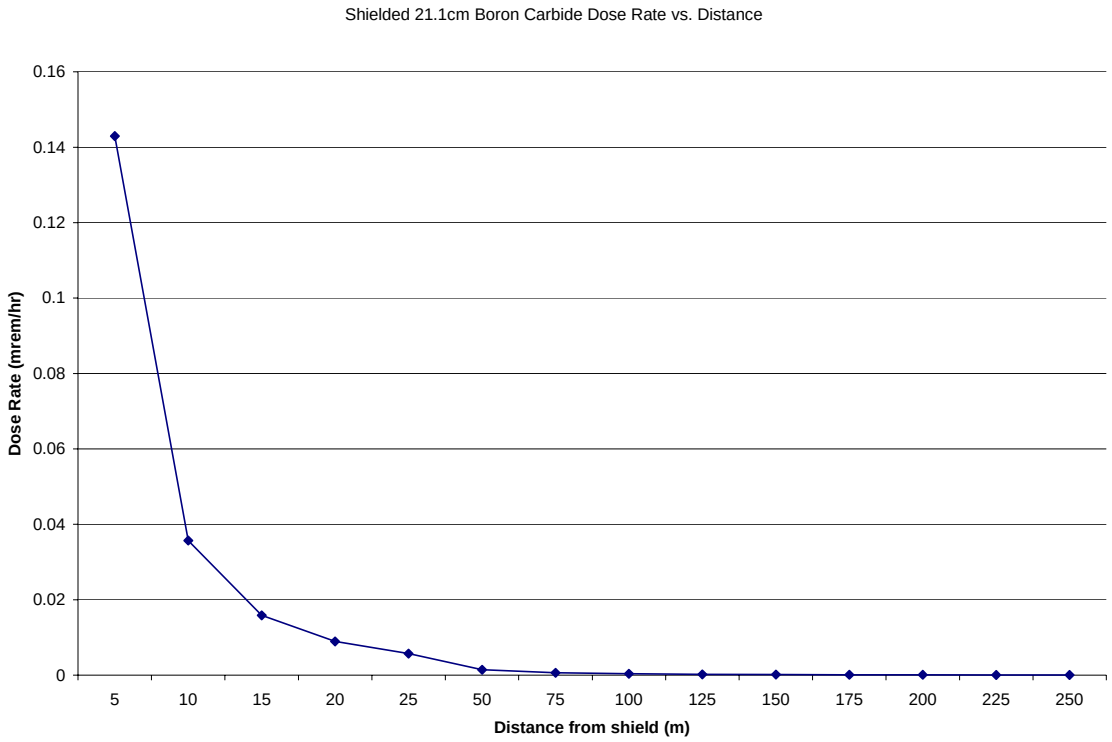

Figure 6.5-2: Neutron Dose Rate with Distance for Boron Carbide

Boron Carbide Manufacturing

Boron carbide is superior to all of its competitors in terms of melting point, neutron attenuation ability, strength and effective density. However, there are several known issues associated with this material, one of them being manufacture.

Various boric acid reactions synthesize boron carbide in the form a fine black powder. It is then necessary to sinter the material into a sizable solid structure. Sintering will involve the addition of additives such as epoxy resins in order to hold a coherent structure. The additives will consist of less than 2% of the shield by mass. Land based reactors do not use large B_4C shields as the sintering process is expensive, costing over $100 per pound of powder. Price aside, it is possible to sinter B_4C to a density of 97% of theoretical density. For calculation purposes, the effective density of 2.45 g/cm^3 was used in place of the theoretical B_4C density of 2.52 g/cm^3 [130].

Boron Burn-up Analysis

The other issue with B_4C is the burn-up rate of boron. Boron-10 undergoes the transformation given in equation (6.5-5).

$$^{10}B + {}^{1}n \rightarrow {}^{7}Li + {}^{4}He \qquad (6.5\text{-}5)$$

This reaction occurs greater than 99% of the time when a neutron is absorbed at energies less than 1eV [129]. Equation (6.5-6) characterizes the burn-up rate of boron in the shield.

$$n(t) = n(0)e^{-\sigma_a \Phi_0 t} \qquad (6.5\text{-}6)$$

where n(t) is the number of remaining atoms of boron, n(0) is the initial number, σ_a is the energy dependent neutron absorption cross section and Φ is the neutron flux. After 5 years of reactor operation at full power, the percentage of boron left will be approximately 82.2%, yielding a total burn-up of 17.8% over 5 years. This rate should not significantly affect the dose to the habitat over time as seen in Figure 6.5-3 below. This figure conservatively ignores the effect of absorption due to lithium produced after boron neutron capture. Actual fluxes will be much lower as this model overestimates the dose in the aged boron-depleted shield. The burn-up of boron also produces helium that can lead to swelling in the shield. However, this will not be an issue because the shield is only constrained on two sides and still has four degrees of freedom to swell.

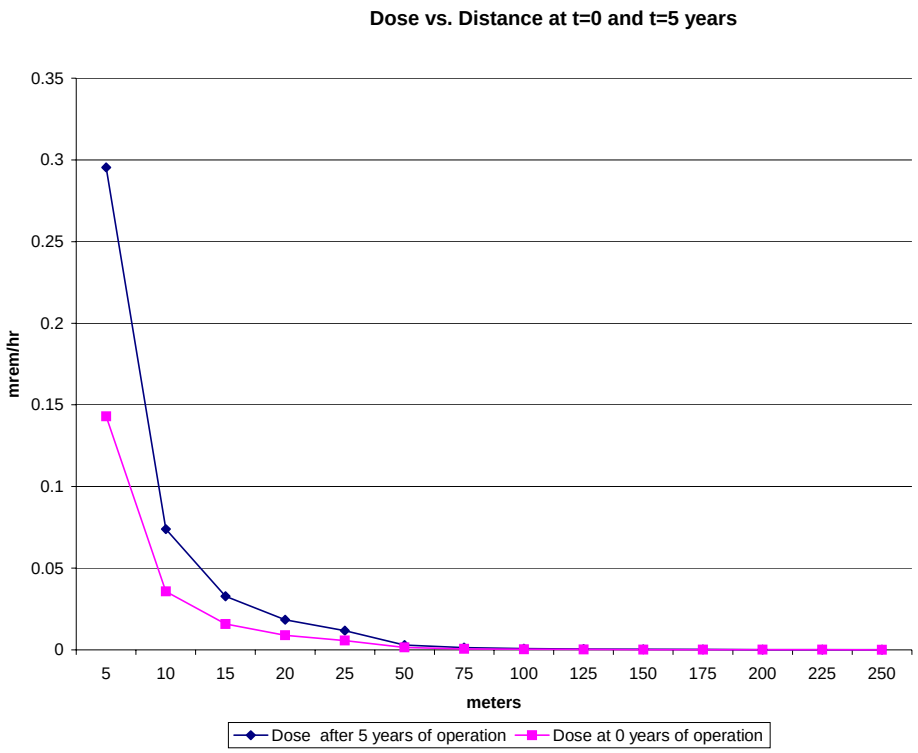

Figure 6.5-3: Neutron Dose Rate with Distance After 5 Years of Operation

Based on the data presented in Figure 6.5-3, the dose rate due to neutrons emanating from the shield approximately doubles after 5 years of operation. This is a significant increase in dose as time increases; however, it is not a large enough increase to affect the shielding design or compromise mission parameters. The dose remains under the set does limit. This, however, is a worst-case scenario; the doses in the above figure do not take into account the significant additional stopping power of lithium produced after neutron capture in boron.

6.6 Gamma Shielding Material

6.6.1 Choice Summary

The following section outlines the design team's selection for fission-borne gamma ray shielding. The shielding team chose a tungsten cylindrical shell to serve as the gamma shield. Tungsten's primary advantages include high Z, high density (70% greater than that of lead), and high melting point (3700 K).

As outlined in the mission statement in Section 6.2, the shielding design aims to reduce crew radiation dose to 2 mrem/hr as a compromise between NASA's existing occupational dose limit for astronauts at 5.9 mrem/hr (50 rem/yr) and the terrestrial radiation worker dose of 0.6 mrem/hr. In the models below, the shielding team considered these limits in light of both extremes in choosing an appropriate shielding material.

In addition, landing vehicle mass constrains the shield mass to about two metric tons. Two metric tons of any material is insufficient for a complete gamma shield around the core, given the core design.

Core design analyses with MCNP code determined the gamma output current at the reflector boundary. The reflector design comprises a series of rotating drums of poisoning material. To be conservative, to determine the ideal shielding material, the design team modeled shielding for a fully reflected core because this configuration is the state in which the core maximally radiates gamma rays.

6.6.2 Gamma Dose Rates without Shielding

At a thermal power of 1.2 MW, a bare core with no shielding radiates an outward photon flux, Φ_0, of 5.3×10^{13} photons/cm^2-sec ranging in energy from soft gammas ~10 keV to high-energy photons upwards of 9 MeV. Photons below these energies do appear in the core; however, low-energy photons are subject to substantial attenuation by fuel elements since core materials have high atomic numbers.

Core design studies delivered a gamma output spectrum divided into thirty-two energy groups. The design team approximated the output flux as the output spectrum equally distributed over a reflector surface area of 11.7×10^3 cm^2. Estimates of dose rate relied on modeling the energy-absorbing material with the ICRU-44 convention of a four-component tissue model [123]. Below is the function used to calculate the dose rate:

$$\dot{D}(E) = \Phi(E) * E \frac{\mu(E)}{\rho} \qquad (6.6\text{-}1)$$

In the above equation, D is the dose rate for each energy group, Φ is the flux , E is the group energy and μ(E)/ρ is the mass energy absorption coefficient of tissue. Quality factor, Q, is neglected because photons of all energies exhibit Q=1. Tissue energy absorption cross sections vary more or less linearly with energy over the relevant range. Summing the dose component of each group at the reflector boundary results in a dose equivalent of 7.8×10^6 mrem/hr. At distances much greater than the radius of the reactor core (>>54 cm), this dose decays as the inverse square of the distance from the center of the reactor. As is visible in Figure 6.6-1, without shielding the dose does not fall to 2.0 mrem/hr until a distance of about a kilometer, and to 0.6 mrem/hr only after 1.8 km.

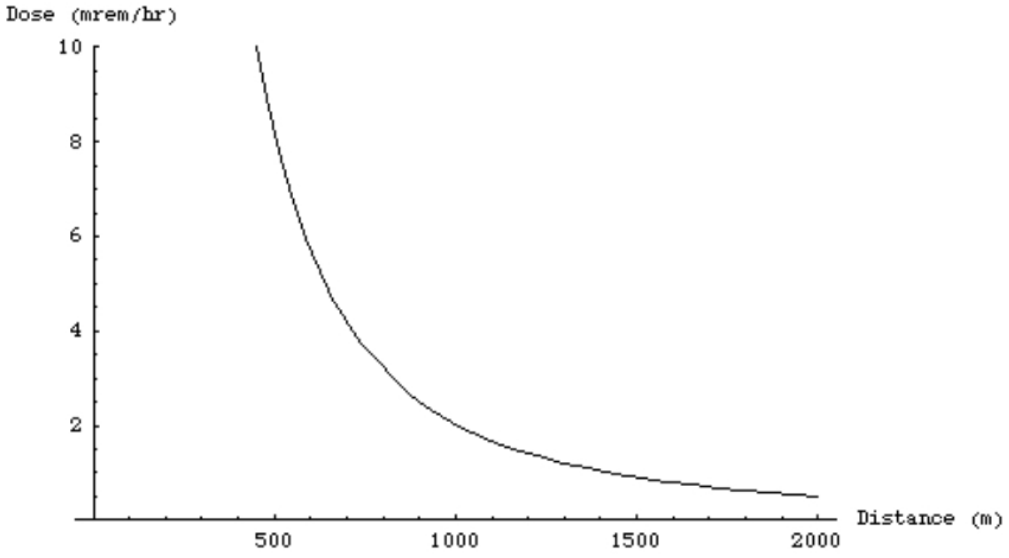

Figure 6.6-1: Dose Equivalent Rate for a Core without Shielding

As demonstrated above, the chosen reactor core design requires gamma shielding since power transmission to a distance of several kilometers may not be desirable.

6.6.3 Material Selection

Photon attenuation through media occurs through electromagnetic interactions with nuclei and electrons. Thus, higher Z materials attenuate photons more effectively than lower Z elements since atoms of those materials have more charged particles.

Obvious choices for gamma shielding lie at the bottom of the periodic table where mass density is highest. It is reasonable to reject materials with atomic number higher than that

of bismuth (Z=83) for reasons of either nuclear instability or unacceptably high reactivity. For example, polonium is naturally radioactive and so is less effective as a radiation shield than materials of similar atomic number. The same is true of radon; an additional issue with radon is that it is a gas and would have to stay under pressure to achieve densities high enough for useful shielding.

Similar considerations leave bismuth (Z=83) and lead (Z=82) as the highest Z elements with suitable material properties. However, both these elements melt at temperatures much less than the operating temperature of the reactor, 1800 K. Bismuth melts at 544 K and lead melts at 600 K. If the shield falls in contact with the reactor or near the reactor such that thermal radiation heats it, these materials will melt. If used, these materials will have to remain in containers that can tolerate these temperatures. The containers will also have to tolerate the expansion of the metals during phase changes. On melting, the volume of lead expands about 5.7 % and bismuth expands about 2.7 % [132]. Vacuum-filled voids must exist in the containers to accommodate the melting of lead or bismuth if they are to be part of the gamma shield. The expansion will also lower the density of the shield. Though the shield will appear thicker with the expansion, this process will not occur uniaxially, requiring additional compensation in initial shield thickness.

A container must also be comprised of highly attenuating, high Z materials with high melting points. These may include the several refractory metals in the same group as lead and bismuth on the periodic table (Z=72 through Z=77). Rhenium (Z=75), osmium (Z=76) and iridium (Z=77) exhibit the highest densities but they are very difficult to manufacture in the very large quantities needed. While it may be reasonable to construct fuel cladding from rhenium, obtaining enough rhenium for a shield within a reasonable cost is unfeasible. Similarly, both osmium and iridium are not easy to fabricate in high volumes: osmium because it forms very toxic airborne oxides and iridium because it is not abundant on Earth [133]. However, iridium does exist in much higher concentrations on extraterrestrial bodies. If an option for asteroid mining becomes available, iridium would become the most attractive choice for a gamma shield material or shield container. The most dense and most attenuating refractory metal that remains is tungsten (Z=74). As shown later (see Table 6.6-1), producing a lead or bismuth shield with a tungsten

container allowing for lead melting and thermal expansion would not be a viable option because tungsten is already more highly attenuating for gamma rays than lead or bismuth.

To determine the shielding effectiveness of each of the remaining material candidates (lead, bismuth and tungsten), the shielding group compared the attenuation power of the maximum thickness (for a given weight limit) of shielding of each material. The definition of the maximum thickness of each material is the maximum thickness of a cylindrical shell surrounding and flush with the reactor core. By solving Equation (6.5-3) for a mass of three metric tons, the maximum shield thickness results. Even if the ultimate geometry of the material does not conform to this model, the resulting choice of shield will be maximally flexible as this model exhibits the highest weight penalty for a thicker shield.

The calculation of attenuation of gamma flux utilizes an exponential function (identical in form to Equation (6.5-4)), using attenuation cross sections for each energy group from NIST's XCOM online database [120]. Table 6.6-1 outlines the thickness of the modeled materials and their attenuation power. At the output of the shield, photon current is lower due to an additional multiplicative factor of r_0/r because the same flux spreads out over a wider area proportional to the radius. At even further distances, this factor changes to $(r_0/r)^2$, since at large distances, the core appears to be a point source. Section 0 further explains the consequences of dose change with changes in distance. The dose rate results from Equation (6.5-1) with Φ from Equation (6.6-2). This dose rate estimation neglects buildup factors, as this quantity becomes less important with distance.

$$\Phi = \Phi_0 * \frac{r_0}{r} e^{-[(\mu/\rho)*\rho*thickness]} \qquad (6.6\text{-}2)$$

Because of its greater density, tungsten outperforms both lead and bismuth for a given mass and geometry in spite of its lower mass attenuation coefficients. While the dose rates given in Table 6.6-1 appear rather high, simple revisions of geometry can further reduce these rates. For example, only half the reactor surface or less needs shielding because the habitat will only be on one side of the reactor. A reduction in size of a half will permit roughly twice the prior thickness. In the case of a tungsten shield with a new

thickness of 19.7 cm, the dose rate at 90 cm from the shield will fall to 0.36 mrem/hr, well below the goal of 2.0 mrem/hr. The details of the exact geometry of the gamma shield will be discussed in Section 6.7 on shielding design.

Table 6.6-1: Gamma Attenuation of Single Materials at Gamma Shield Weight of 3 MT

Material	Maximum thickness (cm)	Dose rate at 90 cm (mrem/hr)
Lead (Pb)	17.1	594.66
Bismuth (Bi)	19.4	599.88
Tungsten (W)	10.6	480.00

6.6.4 Tungsten Performance Modeling

Shield thickness, and thus weight, will vary depending on numerous mission parameters including required proximity of crew to the reactor, limitations of Lunar or Martian surface area excluded to entry by humans and other similar issues related to mission goals. Thus, characterizing the shield performance at a range of thicknesses and distances is vital to the continued flexibility of the current models.

Throughout the rest of this section, dose calculations with distance result from compromises between the $(r_0/r)^2$ dose dependence at large distances when the core can be approximated as a point source and the r/r_0 dose dependence at small distances when the core can be approximated as an infinite cylinder. The representation of intermediate values is a hybrid of the two systems such that at all distances the dependence factor is a continuous function. This function f(r) appears in Figure 6.6-2; this function is continuous but not differentiable at points where the dependence mode changes.

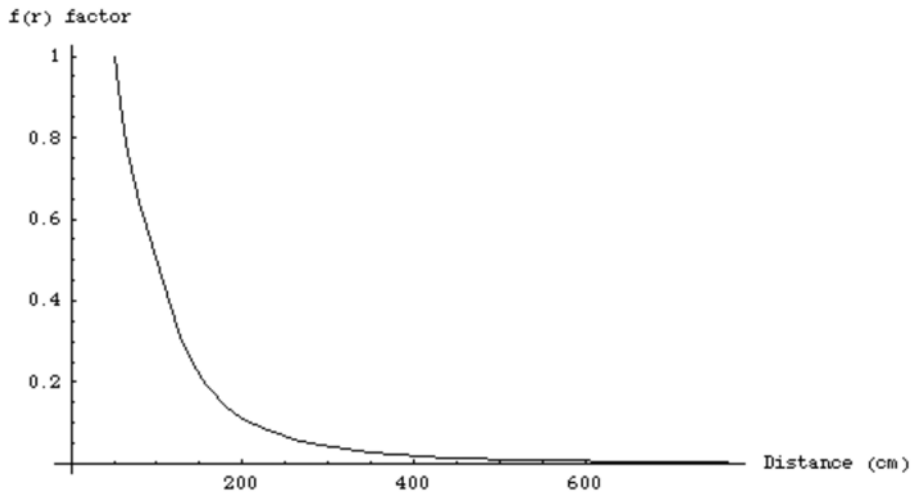

Figure 6.6-2: Distance dependence f(r) with distance

Figure 6.6-3 illustrates dose rate as a function of distance and shield thickness for a tungsten shield. As is visible in the graph, dose rate decreases exponentially with increasing shield thickness, thus optimizing geometry is crucial in obtaining an effective shielding system.

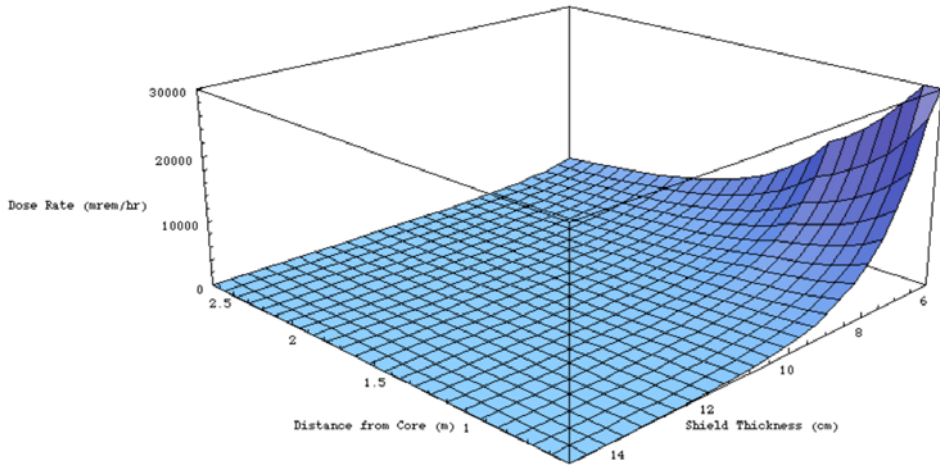

Figure 6.6-3: Dose Rate with Distance and Shielding Thickness for Tungsten

In the case where dose rate is too high even with the existing shield, the implementation of an exclusion zone becomes necessary. In this region, the dose rate is too high for crew to occupy for extended periods without risking the deleterious effects of high, though not acute, radiation exposure. Figure 6.6-4 displays a plot of which areas are noteworthy for radiation dose for a tungsten shield of various thicknesses at given distances and Figure 6.6-5 is a graph of dose versus distance for 12 cm thick tungsten shield.

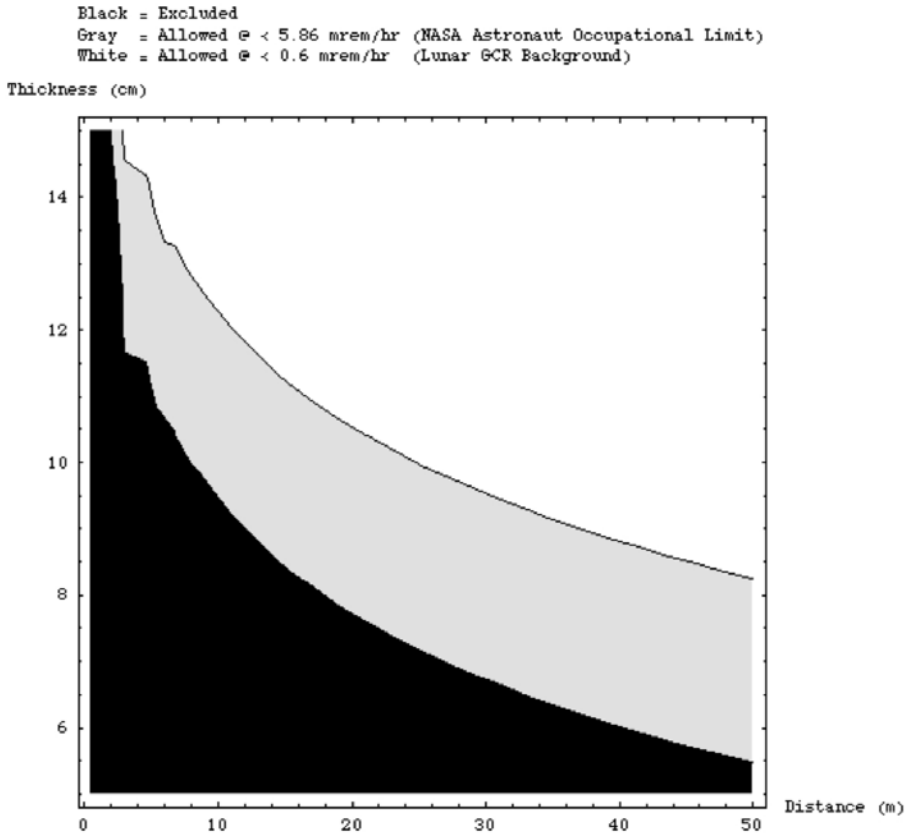

Figure 6.6-4: Excluded and Allowed Zones for Tungsten Shield

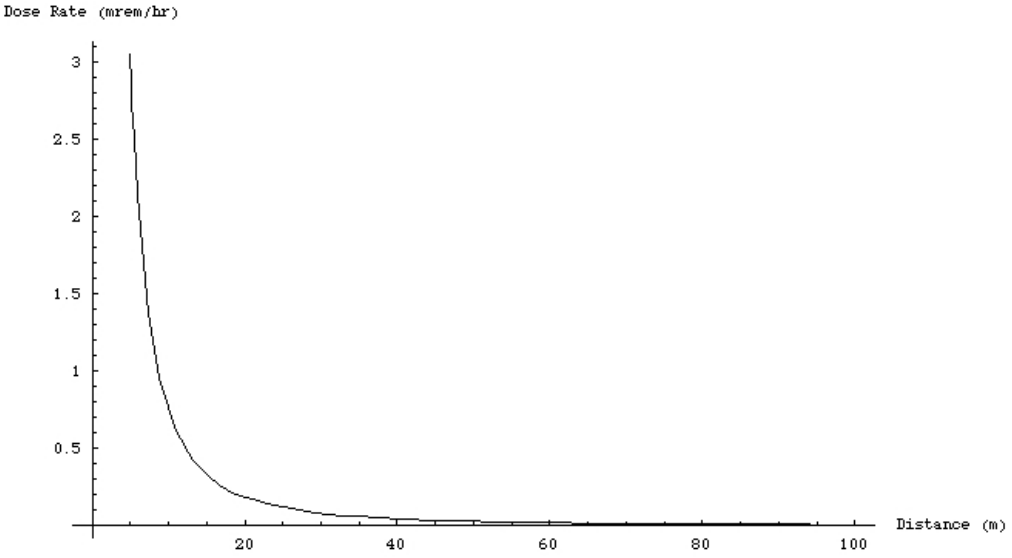

Figure 6.6-5: Dose rate with Distance for 12 cm Thick Tungsten Shield

Oxidation of Tungsten

At the reactor operating temperature, tungsten will oxidize in the presence of carbon dioxide. Thus, a metal silicide coating will also be necessary to protect the outer tungsten shield from corrosion in the Martian environment.

6.7 Shielding Design

6.7.1 Summary

Now that we have chosen proper shielding materials, it is possible to design the final configuration of the neutron and gamma shields to minimize mass while still meeting the maximum dose limit of 2 mrem/hr. The ideal geometry is to have the neutron shield of cylindrical geometry encompassing the entire core. However, given the mass constraints of roughly 2 MT, a shadow shield will be employed to shield an 80º arc around the core.

The shield system consists of two separate but identical pieces, each covering the full height of the reactor with an excess of 2 cm above and below to ensure protection from axially emitted radiation . Each piece covers a forty degree arc of the radial reflector surface. Depending on mission requirements, each piece can move around the reactor via a mechanical system. Thus, instead of having a stationary shield just shielding the habitat, the shielding can rotate to protect radiation-sensitive equipment and crew who may need to explore or enter otherwise unshielded regions.

Each of the forty degree segments of the shield is comprised of two layers: a 40 cm thick cylindrical shell of boron carbide (B_4C) falling flush against the reflector, and a 12 cm thick cylindrical shell of metallic tungsten (W) placed immediately outside the boron carbide layer. This arrangement will bring total radiation dose due to core radiation below the magnitude of background radiation on the moon (0.6 mrem/hr) at a distance just under fifteen meters from the core. The total shield weight for both pieces is 1.97 metric tons. Given that the chosen shield is a shadow shield, which only wraps part way around the reactor, it is important that the habitat fall within the region protected by the shield. Crew must avoid entering areas near the reactor on the unshielded side to avoid high radiation exposure.

6.7.2 Geometry

Shielding Thickness

The design team selected a boron carbide thickness of 40 cm and a tungsten shield thickness of 12 cm. This required optimizing total dose over varying thicknesses of the two shielding components. Boron carbide is much less dense than tungsten. The boron carbide layer's thickness was only limited by the excess weight of tungsten created by pushing the tungsten layer out to a greater radius due to the thickness of the inner B_4C layer. Through compromising the shielding thickness with the shielding dose output, the design team calculated the above thicknesses as the optimal shield for the constrained weight.

Decreasing the thickness of the neutron shield will greatly decrease the gamma shield mass by decreasing the circumference. Under appropriate mission parameters, this arrangement may be preferable because the dose rate from neutrons at any significant distance from the reactor is very small.

Layers

As mentioned, rather that using one material to shield both neutrons and gammas, the design team chose to layer two materials together to create a shield. The inner boron carbide layer serves to reduce radiation dose due to neutrons emitted during fission events in the reactor. The purpose of the outer tungsten layer is to attenuate photons produced in the core as well as the secondary radiation from neutron attenuation. See Figure 6.7-1 below for an illustration of the shielding design.

In absorbing and scattering the neutrons, the collision events in the boron carbide layer will result in the emission of secondary radiation, particularly ionizing photons. Several mechanisms for the generation of secondary radiation exist. When a nucleus absorbs a neutron, it may end up in an excited state. The nucleus relaxes through the emission of high-energy gamma photons. In addition, particularly at high energies, inelastic scattering of neutrons from nuclei will result in recoil photons.

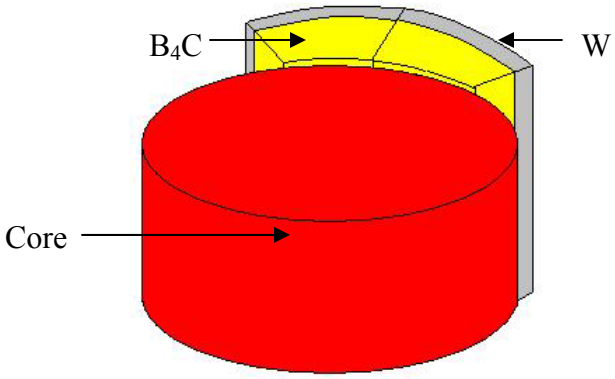

Figure 6.7-1: Overhead Schematic of Shielding Implementation

The secondary photon flux will not exceed the core-produced gamma radiation flux, however, so the tungsten layer designed to absorb the core gamma radiation will be more than sufficient shielding for these secondary photons. Thus, the gamma shield must lie outside the neutron shield, notwithstanding further complications in design (see alternate design in Section 6.8).

Other particles can be produced as a result of neutron capture events such as (n,p) and (n,α) reactions in the shield. These heavy charged particles deposit their energy within a very short range, so these species will not escape the neutron shield in any significant number; the only type of secondary radiation in need of mitigation are gamma rays [114].

It is true that by placing the denser tungsten shield outside the thick neutron shield, the mass of tungsten will increase for any given protected range and gamma attenuation. However, it is a necessary penalty to bear because of the secondary gamma radiation produced in the neutron shield. Placing the tungsten shield inside the boron carbide layer would leave this radiation un-attenuated.

Shielding Extent

This shield design, as outlined above, does not cover the entire core, owing to landing module mass constraints. Consequently, the unprotected side will be freely releasing radiation into the environment in the exposed direction as illustrated in Figure 6.6-1[1].

[1]For human shielding purposes, the shadow shield is more than adequate to protect the crew even at moderately close proximity to the core. However, the Planetary Protection Policy recommended to NASA by the Committee on Space Research (COSPAR) might not allow for only partial shielding of the reactor

Given material constraints for radiation attenuation and weight constraints for extraterrestrial landing capabilities (2 MT for the shielding system), no shielding system can surround the entire reactor. A system with the given thicknesses surrounding the core would have a mass of 8.47 metric tons, which, when added to the mass of other system components, would exceed the assumed landing capability limit of 10 MT.

Given that we cannot shield the entire core, an alternate geometry is necessary. This alternate geometry is in the form of a shadow shield – only shielding the part of the core facing the crew (the habitat). In order to determine how large this arc should be, one must have a good sense of approximately where and how big the habitat is. Available precision landing technology can land units to within a kilometer of a chosen target. In the worst-case scenario, the mission planners would attempt to land the reactor directly by the habitat. Thus, we shall assume the MSR will land within one kilometer of the habitat, and has an equal probability of landing at any given point within this range. With that assumption, using Cartesian coordinates with the habitat at the origin, Equation (6.7-1) gives the probability of landing the reactor at a given point.

$$P(x,y) = 1/(\pi \times (1\text{ km})^2) \text{ for } x^2 + y^2 < (1\text{ km})^2 \qquad (6.7\text{-}1)$$

Rewriting this equation, the probability of landing at a given distance r from the habitat is given by Equation (6.7-2).

$$P(r) = 2 \times r/(1\text{ km})^2 \qquad (6.7\text{-}2)$$

Thus, on average, the reactor would land at a distance of 666.7 meters from the habitat. To be conservative, we will suppose the reactor lands at one-fourth this distance, or 166.7 meters from the habitat. Assuming the longest edge of the habitat will be no more than 30 meters in length, the shield must protect a zone, again being conservative, ten times this length for astronauts to travel near the habitat without worrying about the radiation exposure from the MSR. This means that the shielded arc must be large enough to shield

---

due high radiation exposure to possible life on Mars. On the unshielded side of the reactor, there is roughly a 1.5-2km radius semi-circle in which the dose is above (sometimes significantly above) the background radiation of Mars. If this is unacceptable, then it is possible to add more shielding to shield the entire core, but this comes at a large mass penalty.

300 m at 167 m away. As is visible in Figure 6.7-2, to accomplish this, the shield needs to extend over an angle of eighty degrees around the core.

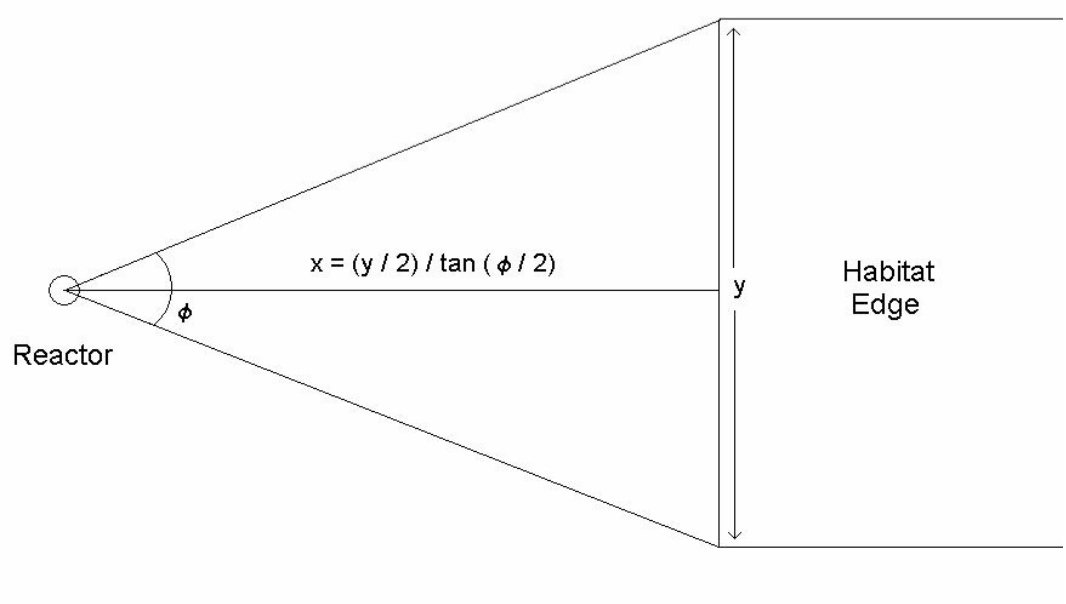

Figure 6.7-2: Chart of Reactor and Habitat Edge

Even with a thirty-meter wide habitat, the reactor could still land to within as close as sixteen meters and still have sufficient shielding to protect crew and instrumentation. However, regions immediately outside and in front of the habitat would have doses high enough that crew should avoid prolonged exposure. Still, under the above assumptions, the probability of landing the reactor within 16 meters is just over one in four thousand.

To be sure radiation scattered off the axial reflectors does not reach crew, the shield will extend 2 cm above and below the vertical bounds of the core. With a 40 cm boron carbide layer and a 12 cm tungsten layer shielding an eighty degree arc, the mass of this shield is 1.97 metric tons, well within the bounds of available extraterrestrial landing technology even when coupled with the mass from the rest of the MSR system.

Shield Mobilization

One caveat of using a directional-based shielding system is that the reactor may land with the shield facing the opposite direction of the habitat. In such a case, some mechanism must exist to realign the shield with the habitat so it can protect the crew and radiation-sensitive equipment.

Additionally, there are many potential missions where shielding a triangular segment of space near the reactor will be insufficient to accomplish mission objectives. Crew may need to explore regions of the Lunar or Martian surface away from the habitat, and these may lie in regions that are unprotected in the initial alignment of the shield. To address this issue, the shield is comprised of two identical pieces, each covering forty degrees of the reactor surface. These pieces can move around the reactor allowing mission planners to choose in which direction the shield will protect.

The precise nature of the mobilization and choice of a system with sufficient reliability will depend on mission parameters and remain as future work for mission planners according to their objectives. The initial movement to align the shield with the habitat needs only function once at the beginning of the mission. Afterwards, the shield can stay in one place. If the shield needs adjustment throughout the mission, the development and confirmation of a robust system will be necessary, as each segment will weigh at least 860 kg.

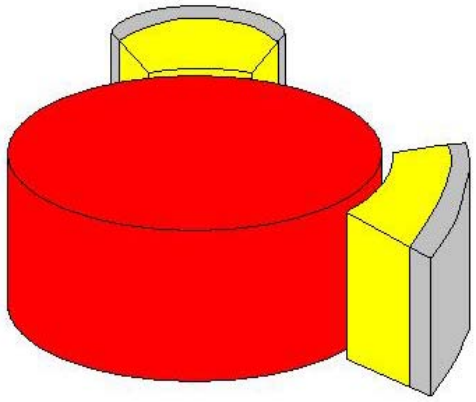

Figure 6.7-3: Shielding Mobility Demonstration

6.7.3 Discussion

The design described above satisfies all prescribed criteria. The neutron shield brings neutron dose down to a magnitude where it is negligible relative to gamma dose. This is ideal because it allows us to neglect complicated issues such as neutron activation and

neutron buildup factors in estimating dose, as both those factors will be significantly smaller than gamma dose.

The gamma dose several meters beyond the shield is at an innocuous level – at 10 meters, the dose is less than 0.5 mrem/hr. On the shielded side, humans can approach the core safely, for limited periods. This limitation can be easily overcome with the use of the mobile shielding units, which can accommodate virtually any mission parameters. Figure 6.7-4 below shows the suggested zoning method that can be accommodated with this shielding design. There are three zones: an allowed, a limited and an excluded. In the allowed zone, the dose rate never exceeds 2 mrem/hr and can be occupied indefinitely by crew. The limited zone exhibits a higher dose rate and time occupied there cannot exceed anywhere from several days on the outer part to several hours on the inner part. For the excluded zone, acute radiation effects are not seen, but if a person were to spend one hour on the border of the excluded zone and spend the rest of the year at the border of the allowed zone, that person would accumulate the ICRP annual dose limit. Thus, dose for crew in the excluded zone must be monitored and calculated closely to ensure that crew do not exceed the recommended ICRP radiation dose limit.

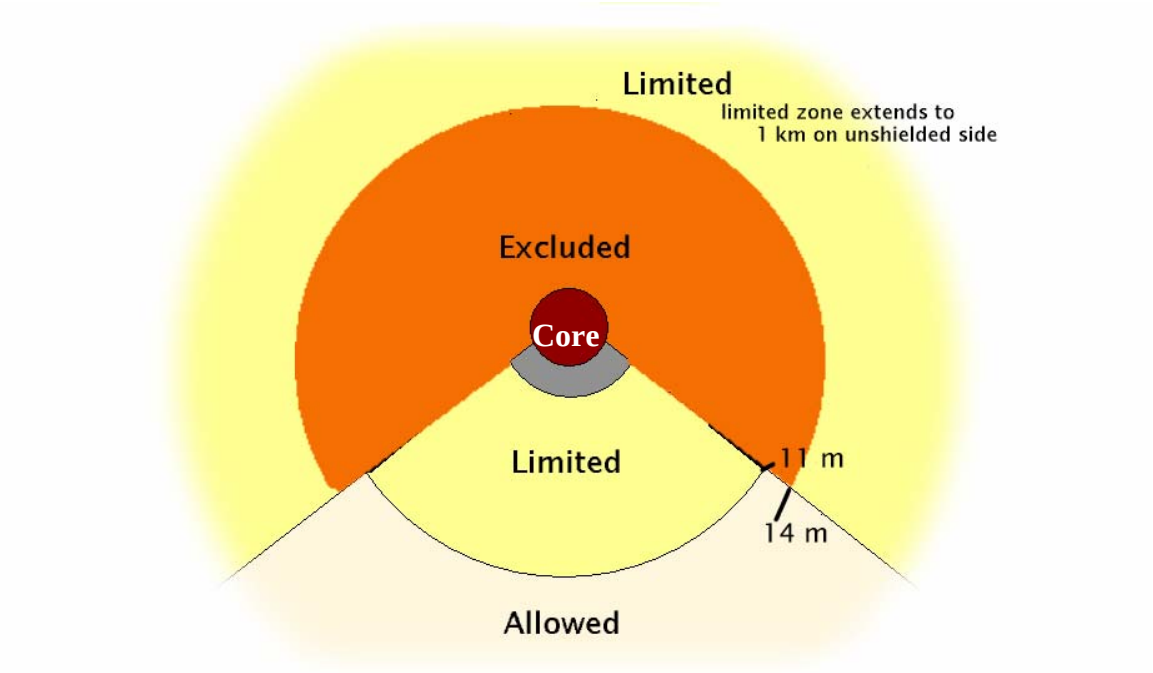

Figure 6.7-4: Suggested Dosimetry Zoning Near Core

To give a better idea of what the figure above means, here are some key dose limits as distance. On the shielded side, the dose is 400 mrem/hr at the shield boundary, 2.0 mrem/hr at 11 m from the core and 0.6 mrem/hr at 20 m from the core. On the unshielded side, the dose is 32 rem/hr at 14 m from the core, 2.0 mrem/hr at 1008 m from the core, and 0.6 mrem/hr at 1841 m from the core.

In addition, since this design does not depend upon exact surface composition, and the materials involved are not particularly reactive, this shielding system works equally well on the Moon and Mars. Also, this system is scalable with power. Furthermore, the redundancy of a two segment shield improves the robustness of this design.

6.8 Alternate Designs

6.8.1 Three Layer Shield

One alternate design that could potentially be superior to the above design involves a three-layer shield, two tungsten layers, one thick (inside) and one thin (outside) sandwiching a boron carbide layer 40 cm thick (see Figure 6.8-1). In the main design described above, the primary reason for keeping the gamma-attenuating tungsten layer on the outside was so that it could shield secondary photons emitted during neutron interactions in the boron carbide layer. This resulted in making the gamma shield much heavier than required to shield the gammas from the core because there is extra mass associated with the extra circumference added by having to wrap the tungsten around the thick neutron shell as well. However, as the secondary photon flux is much smaller than the core flux, only a thin layer of tungsten would actually be necessary to shield the secondary flux.

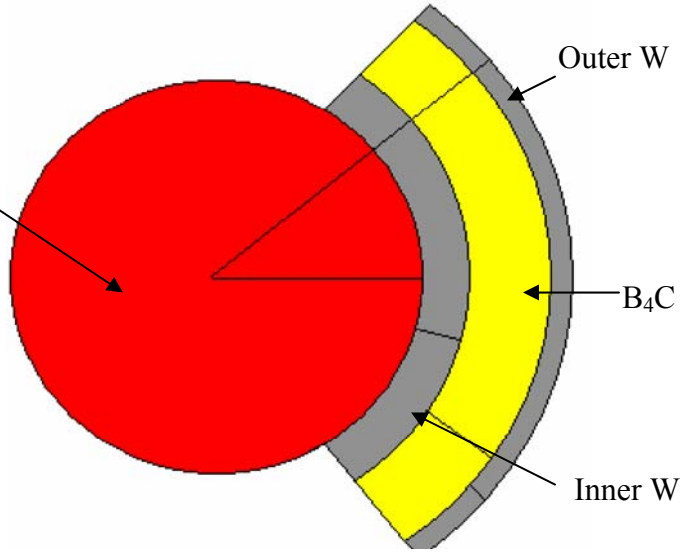

Figure 6.8-1: Three-Layer Shield Schematic

By keeping a thin layer of tungsten outside the boron carbide layer to stop the secondary radiation, and a thicker layer inside the boron carbide layer to stop the primary gamma radiation, the shield would stop the same radiation while significantly reducing its mass. The inside layer would have a 12 cm thickness but exhibit a mass of only 1.085 MT as opposed to the tungsten mass of 1.46 MT in the original design. The boron carbide layer would weigh slightly more at 306 kg for the three-layer design, instead of 259 kg as in the original design. Even so, as long as the thin tungsten layer does not need to be more than 2.47 cm thick, a three-layer design would be more effective per unit mass than the above two-layer design.

Because the analysis of secondary radiation in the neutron shield is rather complex and beyond the scope of this design, the design team still recommends the two-layer design and leaves the analysis of a three-layer shield as future work. Furthermore, the two-layer design fits within the mass constraints of the current objective and thus there is no present need to complicate the design and sacrifice its current simplicity.

6.8.2 Shielding with Lunar Surface Materials

The proposed system requires launching about 2 metric tons of shielding to the Moon or to Mars. If launching this amount of mass is deemed an unfeasible option, shielding material can be found in the extraterrestrial environments.

Previous volcanic activity covered the moon with igneous rock of density 3.3 g/cc. As the bulk density (the soil per unit volume) of the moon is 3.4 g/cc, research indicates the Moon must be almost entirely composed of this rock, [119][134] which is predominantly alkaline and metal oxides, of which SiO_2 is the most abundant [135]. An outline of the most common materials on the Lunar surface appears in Appendix IV.

Gamma ray attenuation coefficients of this oxide mixture are calculated and removal cross sections are used to determine the effectiveness of Moon rock in absorbing radiation. The thickness of the shield necessary to maintain the 2.0 mrem/hr limit from gamma rays alone is plotted in Figure 6.8-2 as a function of distance from the center of the reactor. At a 10 m radius from the reactor, about 1 m of surface material shielding is required to reduce dose to the 2.0 mrem/hr limit.

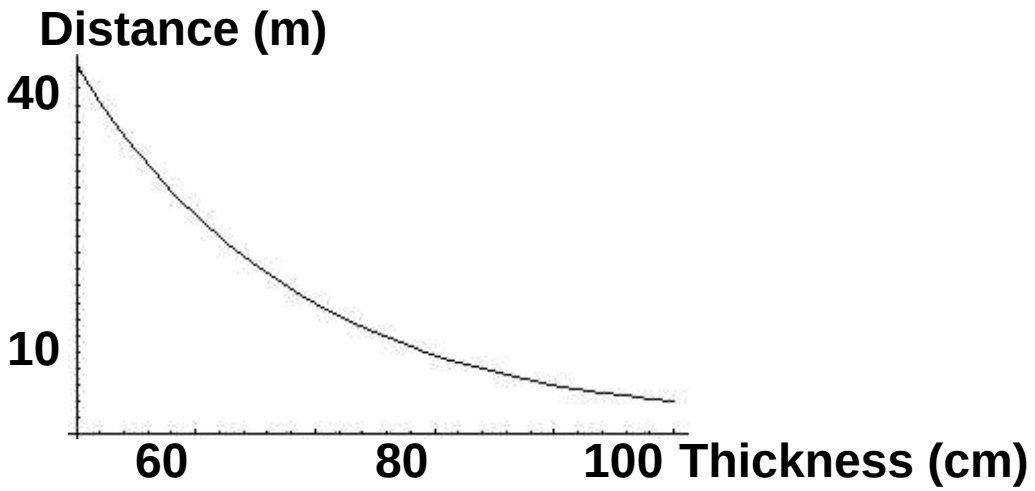

Figure 6.8-2: Distance from Reactor to Maintain 2 mrem/hr Dose as a Function of Shield Thickness

The shield would be a hollow cylinder with an outer radius of 2.1 m, an inner radius of 1.1 m, and a height of 1 m surrounding the core; the shield volume is 9.425 m^3 (see Figure 6.8-3). A shield of this size requires transporting nearly 32 metric tons of rock to build walls around the reactor, a non-trivial endeavor. Dirt and rock excavation and transportation equipment will be needed.

The surface of the moon is marked with craters of varying sizes, which can be taken advantage of for shielding. To shield moon explorers, while maximizing the area for which exploration is safe from high radiation exposure, the reactor can be placed in a crater (see Figure 6.8-4 (left)) or any geological feature that drops down below surface level (see Figure 6.8-4 (right)). As the reactor is 42 cm in height, the minimum depth of the crater or cavity should be 49 cm to surround all parts of the lateral surface of the core. A foundation would be constructed into the surface upon which the reactor could be set up in the rock shield, and the radiation would then be confined to the chasm and beneath the moon's surface.

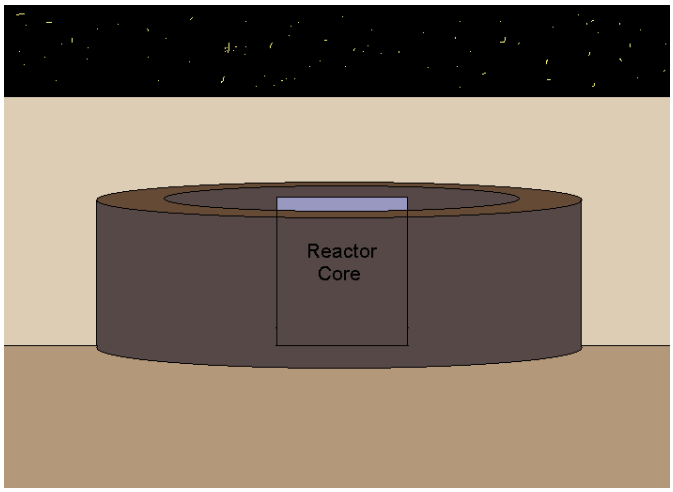

Figure 6.8-3: Core Surround by Surface Material Shields (side view)

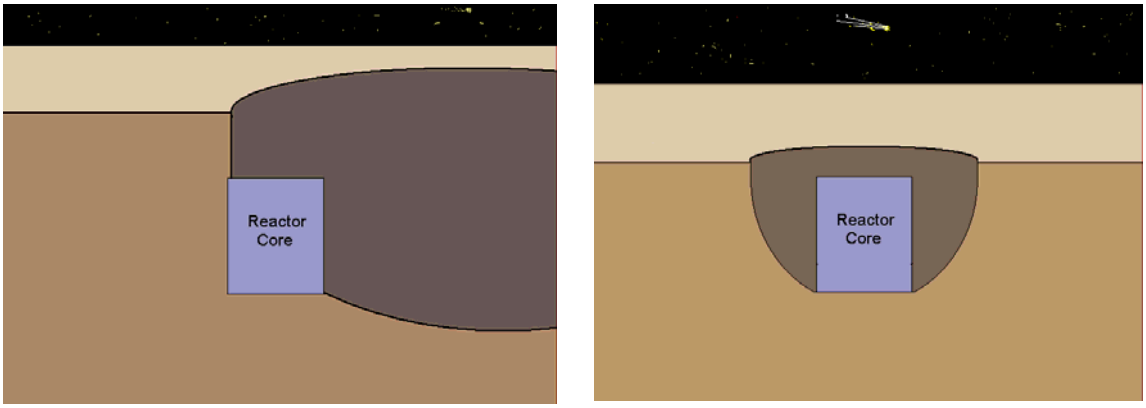

Figure 6.8-4: Reactor Built into Side of Crater (left), Reactor Below Surface (right)

6.8.3 Shielding with Martian Surface Materials

Mars has a crust with an oxide composition similar to that of the Moon according to soil analysis data (See Appendix IV) [136]. Radiation attenuation is nearly identical (attenuation data in Appendix IV), and the rock shield thickness of 1 m keeps the dose below the 2.0 mrem/hr limit. As such, *in situ* shielding options are the same for the Moon and Mars. Mars is not dotted with craters as abundantly as the Moon, but concave geological features can be sought out, craters can be dug, or, if complications arise in situating the reactor below ground level, a rock shield can be constructed.

6.9 Summary

Table 6.9-1: MSR Shielding Properties

	Gamma Shield	Neutron Shield
Number of units	2	2
Material	W	B_4C
Height	55 cm	55 cm
Coverage	40º of arc	40º of arc
Thickness	12 cm	21 cm
Weight	1,460 kg	259 kg
Thermal tolerance	< 3790 K	< 2718 K

6.10 Future Work

As is inherent with all scientific research and calculations, there is always a degree of uncertainty. The research and calculations done on the shield were no exception. As a result, it was necessary to be very conservative when doing many of the calculations. Worst-case scenarios were always assumed when calculating dose or current emanating from the reactor. These conservative estimates and calculations allowed for maximum safety but also led to a more massive system than needed.

When calculating dose for neutron interactions with tissue, a quality factor is assigned to account for the extra damage a fast neutron can do by additionally slowing down in tissue rather than being absorbed quickly. The quality factor is determined by the energy of the neutron and the type of tissue the neutron interacts with. To err on the side of caution, a quality factor of 10 was assigned to all of the 32 energy groups of neutrons. Most of the

neutrons were relatively fast (>0.1 MeV) but may not have warranted a quality factor of 10. This led to over estimation of the dose and a thicker neutron shield than necessary.

The next example of where dose calculations were conservative was when dealing with attenuation in non-idealized material. Essentially, the neutron dose calculations did not account for additional neutron attenuation when passing through the tungsten shield and likewise the gamma dose calculations did not account for gamma attenuation through the boron carbide shield. Refining the dose models to account for these two effects is recommended and could reduce shielding mass.

Besides dose estimates, boron burn-up calculations over the lifetime of the reactor were also conservative. When calculating the dosage increase due to boron burn-up, the lithium-7 production that would take the place of boron-10 was not taken into account. Lithium-7 also has a reasonably high cross section at fast and thermal energies. The dosage increase due to boron burn-up will likely decrease when lithium production is taken into account.

All of these conservative estimates and calculation strategies were done purposefully to account for a worst-case scenario when dealing with radiation. If the shield can effectively protect the inhabitants of a Lunar or Martian colony from the highest dose imaginable, then it can effectively protect from more realistic scenarios. This methodology, of worst case analysis, leaves open the possibility for additional future optimization of the shield.

7 Conclusion

There are many reasons which prompted the Untied States government to make exploration of Mars a priority. One of these reasons, as put forth by President Bush in a speech declaring the country's "new vision for space exploration", was that "the fascination generated by further exploration will inspire our young people to study math, and science, and engineering and create a new generation of innovators and pioneers." As students in the Nuclear Engineering Department at MIT, we are the start of this new generation of innovators inspired by the possibility of human exploration of new frontiers. It is for this reason we chose to pursue the design of the Martian Surface Reactor as our design project, and it is this design which we delight in presenting.

7.1 Design Summary

In attempt to take a holistic approach at design and optimization of this 100 kW_e Martian/Lunar surface reactor system, the team created a formal decision methodology and maintained a continuous, informal dialogue between system groups throughout the process. After much integration, iteration and optimization of design between the four major system groups (core, power conversion, radiator and shielding groups), a final MSR design was obtained as depicted in Figure 7.1-1 below.

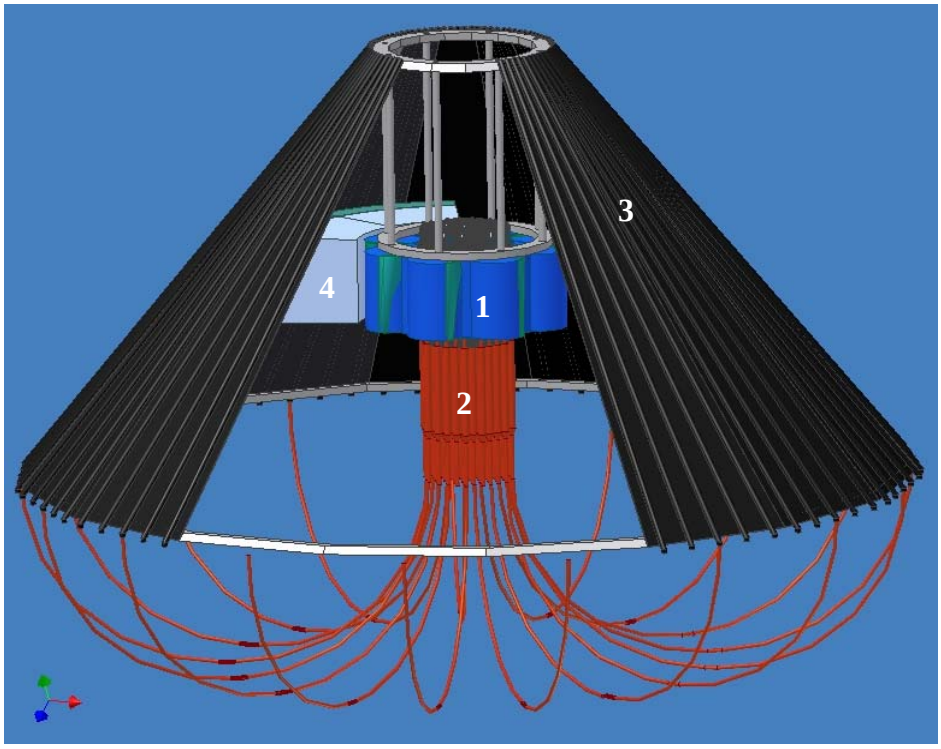

Figure 7.1-1: MSR Concept Drawing

The core is labeled "1" in the figure above, and a cross section of the core can be seen in Figure 7.1-2 below. The core produces 1.2 MW_{th} and operates in a fast spectrum, with an average neutron energy just over 0.5 MeV. The spectrum was chosen to minimize system mass and allow for uniform reactivity over the entire core life via breeding. The core is cooled with Li heat pipes, and operates at a temperature of approximately 1800 K. These heat pipes extend out of the core and couple to the power conversion system. With this selection of cooling system, we used a pin-type fuel geometry in a tri-cusp configuration. The reactor fuel is uranium nitride ($33.1^{w}/_{o}$ enriched), chosen for its excellent thermal conductivity and high melting point. The cladding and structural material in the core is rhenium, and a hafnium vessel surrounds this configuration. Surrounding the core are the reflector and control components. The reflector is Zr_3Si_2, chosen for its high albedo, and good thermal and chemical properties. Control is achieved by rotating drums, using a TaB_2 shutter material. Under a wide range of postulated accident scenarios, this core remains sub-critical and poses minimal environmental hazards.

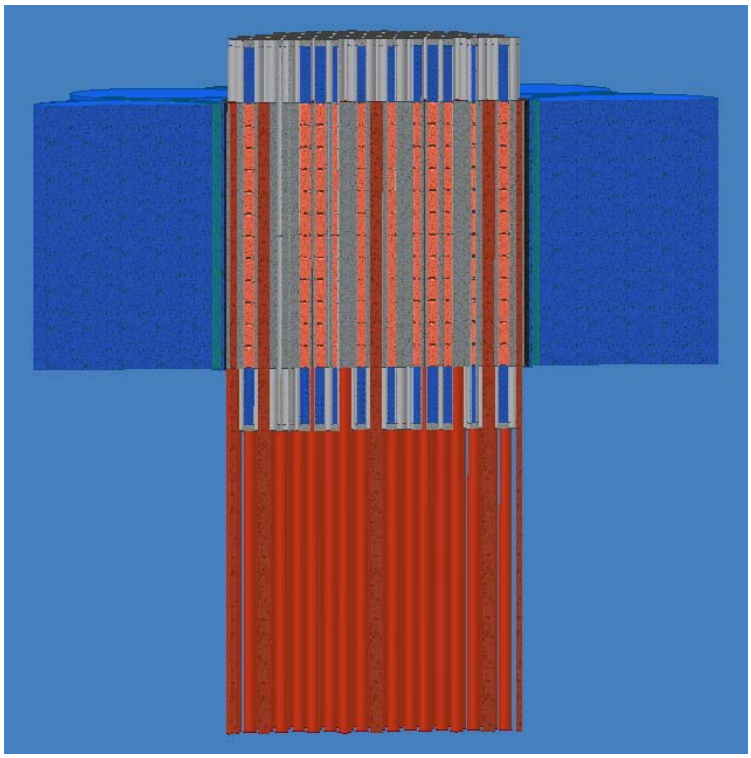

Figure 7.1-2: MSR Core Cross Section

The power conversion system, labeled "2" in Figure 7.1-1, consists of three parts: a power conversion unit, a power transmission system and a heat exchanger. The power conversion unit consists of cesium thermionic units wrapped around each of the 127 heat pipes extending from the core. The thermionic emitter is rhenium at 1800 K, and the collector is molybdenum, kept at 950 K. These thermionic units operate at about 10% efficiency, producing 125 kW_e DC and transmitting 100 kW_e AC. The power transmission system includes 25 separate DC-to-AC converters, transformers to step up the transmission voltage, and 25 km of 22 gauge copper wire for actual electricity transmission. The remaining 900 kW_{th} of waste heat then gets transmitted to the potassium heat pipes of the radiator via an annular heat pipe heat exchanger that fits over the thermionic systems. In conjunction with the radiator, the heat exchanger is also responsible for maintaining the 950 K thermionic collector temperature. This power conversion system was designed with much redundancy and high safety margins; the highest percent power loss due to a single point failure is 4%.

From the power conversion system, the waste heat flows to the radiator for dissipation. The radiator, labeled "3" in Figure 7.1-1 above, is a series of heat pipes with carbon-carbon fins attached. For each core heat pipe there is one radiator heat pipe that removes heat from the core via the heat exchanger described above. The series of heat pipe/fin combinations form a conical shell around the reactor, radiating only from the outer surface of the radiator. Given that the potassium-filled heat pipes transfer heat nearly isothermally, there is only a 10 degree temperature drop between the heat exchanger and the entire radiator surface, making the radiating temperature about 940 K. Like the power conversion system, in the radiator there is much redundancy and high safety margins; the highest cooling loss due to a single point failure is less than 1%.

Finally, the forth system of the MSR is the shielding, marked "4" in Figure 7.1-1 above. The final shielding system is a bi-layer shadow shield that blocks an 80 degree arc of the core. The inner layer of the shield is a boron carbide neutron shield; the outer layer is a tungsten shield that blocks both primary gamma radiation from the core and secondary gamma radiation from neutron scattering. The tungsten shield is coated with SiC to prevent oxidation in the Martian atmosphere. At a distance of 11 meters from the reactor, on the shielded side, the radiation dose falls to a safe dose of 2 mrem/hr; on the unshielded side, an exclusion zone extends to 14 m from the core. The shield is broken up into two 40 degree arcs which are movable to shield crew no matter which direction they are with respect to the core. The shielding system weighs roughly 2 MT. Natural shielding designs were considered, and using the surface topography, such as landing the reactor behind a mountain or in a crater, was determined to be feasible if precision landing capabilities become an option.

When combine together, the four systems comprise the MSR, as seen in Figure 7.1-1. The radiator basically defines the system dimensions: it is roughly a cone with a base that is 4.8 m in diameter and less than 3m tall. Also, not depicted in the figure, the core and radiator would have a support structure, as the heat pipes were not intended to be load bearing structures. The total mass of the reactor is 6.5 MT, and Table 7.1-1 below gives a detailed breakdown of mass. Thus, the MSR fits well within the assumed launch vehicle limits of 98 m^3 and 10 MT.

Table 7.1-1: MSR Component Mass

Reactor Component	Mass (kg)
Core (w/ Heat Pipes)	1080
Core Reflector (w/ Drums)	1780
Power Conversion Unit	240
Power Transmission (1 km)	860
Radiator (w/ Heat Exchanger)	565
Shielding	1975
Total	**6500 kg**

7.2 Design Variations

While the design presented above is the final iteration of the MSR design process, the flexibility of this design is one of its biggest strengths. The MSR is a scalable system that can be used either on an extraterrestrial surface or in space. The system is extremely modular, with a module containing a tri-cusp, a core heat pipe, a thermionic unit and an annular heat pipe which extends to the radiator. To increase or decrease electrical power, within the bounds of core neutronics, it is only necessary to add or remove modules. As none of the systems require gravity or atmosphere to operate, the system can function in space with greatly simplified (and lighter) shielding and power transmission components. Furthermore, depending on the specific application of the reactor, there are several modes of mass reduction that can be employed without significantly altering the design.

Mass Reduction

There are two important modes of mass reduction: elimination of shielding or elimination of radiator. If the mission requirement allows for the reactor to simply be placed a kilometer away from the habitat and crew exploration region, then a net 1.5 MT of mass could be saved by removing the shielding and adding an extra kilometer of transmission lines. This would bring the total system mass to 5 MT, or 50 g/W_e.

If the one of the functions of the MSR was to provide power for an *in-situ* resource utilization (ISRU) plant, then it would be economical to use this plant as a thermal heat sink. A majority of the power consumed by ISRU plants goes toward converting

electricity to thermal energy, which is used to heat various elements of the Lunar/Martian environment in order to extract valuable resources like oxygen, water and methane. The reactor produces 900 kW of thermal energy that gets dissipated as waste heat, but could be used to facilitate the necessary chemical reactions in the ISRU. In addition to gaining a significant amount of usable power, using an ISRU plant as a heat sink would allow us to get rid of the radiator by extending the heat pipes straight to the plant, saving roughly 0.5 MT of mass.

7.3 Future Work

In addition to the future work laid out at the end of each chapter, there are three areas that, if pursued, will greatly improve this MSR design: spectrum optimization, improved materials analysis/selection and more detailed radiation attenuation modeling. As a group of twelve undergraduates and one graduate student, the design team approached this project with a considerable amount of enthusiasm but with essentially no previous nuclear power system design experience. In order to identify a starting point for the design process the team made a few assumptions that over simplified parts of the design. This over-simplification, however, did not come to light until near the end of the semester. While none of these assumptions invalidate the MSR concept, as a result, some of the system components bear some further consideration.

In the design of the core, one of first decisions made was the selection of a fast spectrum. This selection was completely appropriate, but the extent to which this spectrum is fast was not fully considered. All core materials were selected to minimize moderation and fuel configurations were chosen to harden the spectrum. When the design was complete it was found that the average neutron energy in the core was 468 keV. Having such a fast spectrum led to a large reflector and control assembly and an increasing reactivity over life from over-breeding. By moderating the spectrum slightly, we would have been able

to significantly reduce the mass and dimensions of the core (and thus, the shielding size) and flatten the reactivity profile, thereby extending the system life.

In addition to the spectrum, core materials deserve more intensive future consideration. While presenting this design, the major critique of the MSR was the ability of Re to withstand radiation effects at 1800 K. While sufficient attention was not given to radiation embrittlement effects and time at temperature fatigue, the design team made the best choice possible at the time given the lack of materials data available. While there is not much literature available on the performance characteristics of rhenium, there are other materials in existence that would be sufficient for our system. For example, it is possible that alloying the core rhenium with other materials, such as molybdenum, might improve material stability and possibly simplify manufacturing. Possible rhenium issues do not invalidate the MSR design as there have been proven reactor systems operating at temperatures well above 1800 K for five years built and tested, namely the Russian TOPAZ II reactor. It would not be unreasonable, therefore to substitute the rhenium in our design for the molybdenum alloy used in the TOPAZ II [137].

The shielding system would benefit primarily from more detailed modeling efforts. The shielding system was designed neglecting the effects of scattered neutrons and abstracting the contributions of secondary gamma rays. With a more detailed radiation attenuation model, the lighter, three layer shield concept presented at the end of the shielding chapter could have been further developed.

For the power conversion system it was initially assumed that an in-core thermionic system would overly complicate the core geometry and analysis, so this option was eliminated. Further work and research on the system has indicated that an in-core thermionic system is perfectly feasible and could possibly raise the efficiency of the PCU. While in-core thermionics have their drawbacks, this option is worth further consideration.

7.4 Project Summary

Given this design was a student group project, what we lacked in technical expertise we made up for in enthusiasm, research and innovation. The Martian Surface Reactor system is light weight, highly redundant, safe, scalable and robust. However, the lack of experience has led us to make a few (fixable) sub-optimal choices, which were identified and delegated to future work. With more optimization done in these areas, the MSR design becomes a very good preliminary design concept for an extraterrestrial nuclear surface power station. Having learned a tremendous amount about nuclear systems design, as a class we are proud of the level of effort and dedication that was poured into the MSR design. In this modern era of exploration new technologies will continue to emerge, some with our help, and we will continue to be inspired by the infinite possibilities that lay ahead.

8 References

[1] T.L. Saaty. *The Analytic Hierarchy Process: Planning, Priority Setting, Resource Allocation and Management of Energy's Environmental Remediation Program*, National Academy Press, Washington DC, 1994.

[2] Lamarsh, John R., *Introduction to Nuclear Reactor Theory.* Addison-Wesley Publishing Company, Inc., 1966.

[3] Beynon, T.D., "Fast Reactor Physics". Reports on Progress in Physics, Volume 37, November 1974.

[4] Knief, Ronald A., *Nuclear Engineering: Theory and Technology of Commercial Nuclear Power.* Hemisphere Publishing Corporation, 1992

[5] Murry, Raymond L., *Nuclear Energy: An Introduction to the Concepts, Systems, and Applications of Nuclear Processes.* Butterworth – Heinemann, 2001.

[6] Poston, D. et al. (2003) *Notes from Space Reactor 101 Conference*. Arcadia, CA.

[7] Eastman, G., Yale and Ernst D.M. *Heat Transfer Technology*. Kirk-Othmer: Encyclopedia of Chemical Technology. Volume 12. John Wiley and Sons, Inc. 1980.

[8] Dunn, P. D., & Reay, D. A. (1994) *Heat Pipes, 4th Ed*. New York, NY: Pergamon

[9] About Planetary Protection: Requirements. (Online), 11/18/04. Planetary Protection. http://planetaryprotection.nasa.gov/pp/about/reqments.htm

[10] Ivnovskii, M. N., Sorokin, V. P. & Yagodkin, I. V. (1982) *The Physical Principles of Heat Pipes*, Oxford, England: Clarendon Press

[11] Nucletron Products, 12/8/2001. Heat Pipes (Online). Retrieved 11/1/2004. http://www.nucletron.de/nuvte/heat pipe.htm

[12] Busse, C. A. (1973) "Theory of Ultimate Heat Transfer Limit of Cylindrical Heat Pipes." *Heat and Mass Transfer*, Vol 16, pp. 169-186.

[13] El-Genk, Mohamed S. & Tournier, Jean-Michel. (2/4/2004) Reactor Lithium Heat Pipes for HP-STMCs Space Reactor Power System. AIP Conference Proceeding, Vol 699, p. 781

[14] Garner, Scott D. Thermacore, Inc. Heat Pipes for Electronics Cooling Applications (Online). Retrieved 11/7/2004. http://www.electronics-cooling.com/Resources/EC_Articles/SEP96/sep96_02.htm

[15] Pointwise JEF-2.2 Library, Nuclear Data Evaluation Lab, Korea Atomic Energy Research Institute, available on the Internet at: http://atom.kaeri.re.kr/cgi-bin/endfplot.pl (accessed September, 2004).

[16] BARC collaboration, *India's advanced research on $^{232}Th/^{233}U$ fast breeder reactors*, available on the Internet at: www.barc.ernet.in/ (accessed September 2004).

[17] Kulcinski, Gerald, *Nuclear Fuel Design for SP-100*. The Fusion Technology Institute at the University of Wisconsin-Madison.

[18] Yarsky, Peter, *Neutronic Evaluation of GFR Breed and Burn Fuels*, MIT Nuclear Engineering Department, MIT-GFR-005, May 2003.

[19] Yarsky, Pete. Private Communication. 22 November 2004.

[20] Cochran, Robert and Tsoulfanidis, Nicholas, *The Nuclear Fuel Cycle: Analysis and Management*, American Nuclear Society, 1990 pg 80.

[21] Wallenius, J, N15 *Requirement for Second Stratum ADS Nitride Fuels*, Stockholm Center for Physics, available on the internet at: http://nucleartimes.jrc.nl/Doc/Janne_N15_Paper.pdf (accessed September 2004).

[22] MCNP Library, ENDF/B data set, Nuclear Data Evaluation Lab, Korea Atomic Energy Research Institute, available on the internet at: http://atom.kaeri.re.kr/cgi-bin/endfplot.pl (accessed September, 2004).

[23] Etherington, Harold (1958). *Nuclear Engineering Handbook.* New York: McGraw-Hill.

[24] Berte, Marc. Private Communication, 20 October 2004.

[25] MatWeb, *Material Property Data*, available on the Internet at: http://www.matweb.com/search/SpecificMaterial.asp?bassnum=NL3040 (accessed October, 2004)

[26] International Nuclear Safety Center, *Zircaloy Thermal Conductivity: Preliminary Recommendation*, available on the Internet at: http://www.insc.anl.gov/matprop/zircaloy/zirck.pdf (accessed October, 2004)

[27] Tonoike, Kotaro, *Reactivity Measurement Effect of Neutron Interaction between Two Slab Cores*, Japan Atomic Energy Research Institute, January, 2003, available on the Internet at: http://wwwsoc.nii.ac.jp/aesj/publication/JNST2003/No.4/40_238-245.pdf (accessed October, 2004)

[28] Special Metals, available on the Internet at: http://www.specialmetals.com/documents/Incoloy%20alloy%20MA956.pdf (accessed October, 2004)

[29] Bloom, E.E. Journal of Nuclear Materials, 258-263 (1998) page 13

[30] Zinkle, S.J. *Overview of Radiation Effects in Refractory Metals*, APEX Study Meeting PPPL, May 12-14, 1999, available on the Internet at: http://www.fusion.ucla.edu/apex/meeting7/zinkle1.pdf (accessed September, 2004).

[31] Refractory Metals Association, *What are Refractory Metals?*, available on the Internet at: http://www.mpif.org/design/refractory.pdf (accessed September, 2004).

[32] Shields, John A, et al. *Molybdenum and Tantalum offer Competitive Edge in Hostile Environments*, available in the Internet at: http://www.industrialheating.com/CDA/ArticleInformation/features/BNP__Features__Item/0,2832,18422,00.html (accessed October, 2004).

[33] Webster's Online Dictionary, available on the Internet at: http://www.websters-online-dictionary.org/definition/english/Re/Re.html (accessed October, 2004)

[34] Rembar Corporation, *Rhenium Technical Data*, available on te internet at: http://www.rembar.com/Rhenium.htm (accessed October, 2004)

[35] Kurishita, Hiroaki, *Development of Tungsten Materials for PFC*, 2002 Japan-US Workshop on High Heat Flux, "Components and Plasma Surfaces Interactions in Next Fusion Devices", December 9-12, 2002, Nagoya University, Japan page 2.

[36] Babak, A.V. and Uskov, E.I., *On the Problem of High-Temperature Embrittlement of Tungsten*, in Problemy Prochnosti, May 1983 no.5 page 65-69.

[37] Stevens, Joseph, R. *Thermal Aging Effects in Refractory Metal Alloys*, NASA Lewis Research Center, Space and Nuclear Power Systems, Orbit Book company, Inc. 1986 page 291-304.

[38] Honeywell Corporation, *Process for Manufacturing Rhenium Rocket Nozzles or Articles*, available on the Internet at: http://honeywell.t2h.yet2.com/ (accessed October, 2004).

[39] Kubel, Ed, *Advances in Powder Metallurgy Rhenium*, 2001 International Conference on Powder Metallurgy & Particulate Materials, available on the Internet at: http://www.industrialheating.com/CDA/ArticleInformation/features/BNP__Features__Item/0,2832,62965,00.html (accessed October, 2004).

[40] Andrew, J.F. and Latimer, T.A. Report LA-6037-MS (1975)

[41] Blank, H. "Nonoxide Ceramic Fuels," in *Materials Science and Technology, Vol. 10 A*, ed. B.R.T. Frost, VCH (1994)

[42] Matzke, Hj. *Science of Advanced LMFBR Fuels.* North-Holland, (1986)

[43] Todreas, Neil and Kazimi, Mujid. *Nuclear Systems I: Thermal Hydraulic Fundamentals Volume 1.* Hemisphere Publishing Corporation: Massachusetts Institute of Technology, 1990.

[44] Çengel, Yunus and Turner, Robert. *Fundamentals of Thermal-Fluid Sciences.* McGraw-Hill: University of Nevada, Reno, 2001.

[45] Yu, K. (2003) *Neutronic Evaluation of GCFR Core Diluents and Reflectors.* Unpublished master's thesis, MIT, Cambridge, MA.

[46] *Handbook of Chemistry and Physics 84th Edition.* (2003) CRC Press.

[47] MCNP and ENDF Cross Section Data, (Online). October 2004. KAERI. http://atom.kaeri.re.kr/endfplot.shtml

[48] Poston, D.I. (2002). Nuclear Design of SAFE-400 Space Fission Reactor. *Nuclear News*, *Vol. 45 – Number 13*, pg. 28-36.

[49] Poston, D.I. (2002). Nuclear Design of HOMER-15 Mars Surface Fission Reactor. *Nuclear News, Vol.45 – Number 13*, pg. 36-43.

[50] Ott, K.O. and Neuhold, R.J. (1985). *Introductory Nuclear Reactor Dynamics*.

[51] *Handbook of Chemistry and Physics 84th Edition.* (2003) Chemical Rubber Publishing Company, Cleveland, OH.

[52] MSDS Resource Library, (Online). September 2004, Reade Advanced Materials. http://www.reade.com/Products/Product_Index.html

[53] WebElements Periodic Table: Professional Edition. (Online). September 2004. http://www.webelements.com/webelements/-compounds/text/U/N1U125658439.html

[54] Fisher Scientific, (Online). September 2004, Material Safety Data Sheet. https://fscimage.fishersci.com/msds/25883.htm

[55] Nuclear Safety Policy Working Group. (1992) *Recommended Programmatic Space Reactor Safety Policy Statement*.

[56] Dieckamp, H. (1967) *Space Nuclear Power Systems*. Canoga Park, CA. Atomics International.

[57] John F. Kennedy NASA Space Center. (2001) *Space Shuttle Transoceanic Abort Landing (TAL) Sites.* KSC Release FS-2001-05-012-KSC. Kennedy Space Center, FL.

[58] William, R.A., et al. (1967). *Nuclear, Thermal and Electric Rocket Propulsion -- Fundamentals, Systems and Applications*, AGARD/NATO First and Second Lecture Series, 12-21 November 1962 and 28 September - 2 October 1964. New York, NY: Gordon and Breach.

[59] Mason, Lee. (2003). A Power Conversion Concept for the Jupiter Icy Moons Orbiter, First International Energy Conversion Engineering Conference, August 17–21, 2003.

[60] Dostal, Vaclav. (2004*). A Supercritical CO_2 Cycle for Next Generation Nuclear Reactors*. Massachusetts Institute of Technology, Cambridge, MA.

[61] Shaltens, R.K., & Schreiber, J.G. (1989). Comparison of Conceptual Designs for 25kWe Advanced Stirling Conversion Systems for Dish Electric Applications. In Energy Conversion Engineering Conference, 1989. IECEC-89. Proceedings of the 24th Intersociety, 5, 2305-2315.

[62] Shaltens, R.K., & Schreiber, J.G. (1990). Preliminary Designs for 25kWe Advanced Stirling Conversion Systems for Dish Electric Applications. In Energy Conversion Engineering Conference, 1990. IECEC-90. Proceedings of the 25th Intersociety, 6, 310-316.

[63] El-Wakil, M. M. *Nuclear Energy Conversion*. Intext Educational Publishers.

[64] 22.33 project report (2003). Massachusetts Institute of Technology, Cambridge, MA.

[65] J. Luther et al. (n.d.) Efficiency and power density potential of thermophotovoltaic energy conversion systems using low bandgap photovoltaic cells (Online), retrieved 11/2/04. Proceedings of the 10th Workshop on Quantum Solar Energy Conversion, http://www.esqsec.unibe.ch/%5Cpub%5Cpub_22.htm

[66] K. Shukla et al. (n.d.) Thermophotovoltaic Energy Conversion Development Program (Online), retrieved 11/2/2004. http://gltrs.grc.nasa.gov/cgi-bin/GLTRS/browse.pl?1998/CR-1998-208512.html

[67] B. Bitnar et al. (2002). Simulation and Demonstration Model of a High Efficiency Thermophotovoltaic System (Online), retrieved 11/2/2004. Proceedings of the 14th Workshop on Quantum Solar Energy Conversion. http://people.web.psi.ch/palfinger/pubs/2002-quantsol14-bitnar.pdf

[68] R. Mahorter et al. (2004). Thermophotovoltaic system testing (Online). Semiconductor Science and Technology, October 22. http://www.iop.org/EJ/article/0268-1242/18/5/314/s30514.html

[69] Dieckamp, H.M. (1967). *Nuclear Space Power Systems, Atomics International*.

[70] General Atomics. (n.d.). Space Power (Online), retrieved 11/2/2004. http://www.ga.com/atg/sp/pcs.html

[71] Rosa, R. (1987). *Magnetohydrodynamic Energy Conversion*. New York, NY: Hemisphere Publishing Corporation.

[72] Messerle, H. (1995). *Magnetohydrodynamic Electrical Power Generation*. New York, NY: John Wiley & Sons.

[73] Crowley, Christopher J. & Elkouh, Nabil A. (2003). Plasma-Sprayed Selective Emitters for Thermophotovoltaics (Online), retrieved 11/22/2004. http://www.nasatech.com/Briefs/Sept00/LEW16809.html

[74] Glenn Research Center. (1993). 30-Percent Efficient, Tandem Solar Cells for Line-Focus Photovoltaic Array (Online), retrieved 11/22/2004. http://sbir.gsfc.nasa.gov/SBIR/successes/ss/3-067text.html

[75] No author given. (n.d.). Thermoelectric Modules (Online), retrieved 11/22/2004. http://www.geocities.com/ResearchTriangle/Facility/9209/components/thermoelectric_modules.html

[76] Litchford, Ron J. (2001). Prospects for Nuclear Electric Propulsion using Closed-Cycle Magnetohydrodynamic Energy Conversion. *American Institute of Aeronautics and Astronautics*, 39, 1-16.

[77] Bender, Hal. (1999). Voltaic Cells (Online), retrieved 10/2/2004. http://dl.clackamas.cc.or.us/ch105-09/voltaic.htm

[78] Helmenstine, Anne Marie. (2004). Electrochemical Cells (Online), retrieved 10/2/2004. http://chemistry.about.com/library/weekly/aa082003a.htm

[79] Helmenstine, Anne Marie. (2004). Advanced Concepts Database (Online), retrieved 10/24/04. Power Database. http://sei2.sei.aero/ACDB/RWDdetails.asp?ID=40

[80] Gipson, Lillian. (1995). Aeronautics and Space Report of the President (Online), retrieved 10/24/04. Space Flight and Space Technology. http://www.hq.nasa.gov/office/pao/History/presrep95/energy.htm

[81] Hatsopoulos, H.N., & Gyftopoulos, E.P. (1973). *Thermionic energy conversion volume I: processes and devices*. Cambridge, MA: MIT Press.

[82] Hatsopoulos, H.N., & Gyftopoulos, E.P. (1979). *Thermionic energy conversion volume II: theory, technology, and application*. Cambridge, MA: MIT Press.

[83] Urbaniec, K. (1972). The maximum efficiency of thermionic converters. *Proceedings of the 3rd International Conference on Thermionic Electrical Power Conversion*, pp. 1233-1243.

[84] Dieckamp, H.M. (1967). *Nuclear Space Power Systems*.

[85] Davis, Paul R. and Magera, Gerald G. (1993). Interaction of cesium and barium on partially oxygen covered Nb(110). *Journal of Vacuum Science & Technology A: Vacuum, Surfaces, and Films*, 4, 2336-2341.

[86] National Research Council. (2001). *Thermionics Quo Vadis?* Washington D.C.: National Academy Press.

[87] Behlman Electronics. (2004). Custom Systems (Online), Retrieved 11/5/2004. http://www.behlman.com

[88] Powerstream. (2003). Wire Gauge and Current Limits (Online), Retrieved 11/16/2004. http://www.powerstream.com/Wire_Size.htm

[89] El-Genk, Mohammed S. and Tournier, Jean-Michel. (2004) Performance Analysis of Potassium Heat Pipes Radiator for HP-STMCs Space Reactor Power System. *American Institute of Physics Conference Proceedings, 699(1)*, pp. 793-805.

[90] AE 483/583 Space Mission Design. (2003). "CORSAIR: Comet Rendezvous, Sample Acquisition Isolation and Return." University of Michigan, College of Engineering.

[91] Agazzani, A., Fossa, M., Massardo, A.F., Tagliafico, L.A. (2004) "Solar Space Power System Optimization with Ultralight Radiator," Journal of Propulsion and Power, 13.

[92] Albert J. Juhasz, A.J., Sawicki, A.T. (2003) "High Temperature Fusion Reactor Cooling Using Brayton Cycle Based Partial Energy Conversion," NASA Technical Memorandum TM-2003-212721. National Aeronautics and Space Administration.

[93] Cynthia M. Katzan, C.M. and Edwards, J.L. (1991). "Lunar Dust Transport and Potential Interactions with Power System Components," NASA Contractor Report CR-4404. National Aeronautics and Space Administration, Lewis Research Center, Cleveland, Ohio.

[94] Davis, J.R. (2002). "Guide to Materials Selection," Engineered Materials Handbook. ASM Handbooks Online. (Online). http://products.asminternational.org/hbk

[95] Diekamp, H.M. (1967). Nuclear Space Power Systems. Atomics International, Canoga Park, California.

[96] Ewert, M.K. and Hanford, A.J. (1996). "Advanced Active Thermal Control Systems Architecture Study," *NASA Technical Memorandum TM-104822*. Lyndon B. Johnson Space Center, Crew and Thermal Systems Division.

[97] Fossa, M., Tagliafico, L.A. (2004) "Proceedings of the Institution of Mechanical Engineers Part G: Liquid Sheet Radiators for Space Power Systems," Journal of Aerospace Engineering, 213.

[98] Gaier, J.R., Perez-Davis, M.E., and Rutledge, S.K. (1990). "Aeolian Removal of Dust From Radiator Surfaces on Mars," NASA Technical Memorandum TM-103205. National Aeronautics and Space Administration, Lewis Research Center, Cleveland, Ohio.

[99] Gaier, J.R., Perez-Davis, M.E., and Rutledge, S.K. (1991). "Effects of Dust Accumulation and Removal on Radiator Surfaces on Mars," NASA

Technical Memorandum TM-103704. National Aeronautics and Space Administration, Lewis Research Center, Cleveland, Ohio.

[100] Guffee, R.M., Kapernick, R.J., Poston, D.I. (2002). "Design and Analysis of the SAFE-400 Space Fission Reactor," American Institute of Physics Conference Proceedings, 608.

[101] Incropera, F.P. and DeWitt, D.P. (2002). *Fundamentals of Heat and Mass Transport, 5th Edition*. John Wiley & Sons, Inc.

[102] Kapernick, R.J., Steeve, B.E. (2004). "Design Development Analysis in Support of a Heat Pipe-Brayton Cycle Heat Exchanger," NASA Technical Memorandum TM-2004-213170. National Aeronautics and Space Administration, Marshall Space Flight Center, Alabama.

[103] Mason, Lee S. (2003). "A Power Conversion Concepts for the Jupiter Icy Moons Orbiter," *NASA Technical Memorandum TM-2003-212596*. National Aeronautics and Space Administration, John H. Glenn Research Center at Lewis Field, Cleveland, Ohio.

[104] NASA CR-191023. (1993). "Lunar Electric Power Systems Utilizing the SP-100 Reactor Coupled to Dynamic Conversion Systems (TASK ORDER No. 12)," NASA Contractor Report CR-191023. Rockwell International, Rocketdyne Division, Canoga Park, California.

[105] Poston, David I. (2002). "Nuclear Design of the SAFE-400 Space Fission Reactor," Nuclear News, 45. American Nuclear Society, Inc., La Grange Park, Illinois.

[106] Powell, Cynthia. (2003). "Properties and Performance of Ceramic-Matrix and Carbon-Carbon Composites," ASM Handbook, 21. ASM Handbooks Online. (Online). http://products.asminternational.org/hbk

[107] Smith, R.E. and West G.S. (1982). "Space and Planetary Environment Criteria Guidelines for Use in Space Vehicle Development," *NASA Technical Memorandum TM-82478*. Vol 1. NASA Center for Aero Space Information.

[108] Snyder, Nathan W. (Ed.). (1960). Space Power Systems. Academic Press, New York.

[109] Soce, Hachem A. (2003). "Nuclear Power for Deep Space Applications." Research Science Institute.

[110] White, Frank M. (2003). *Fluid Mechanics, 5th Edition*. McGraw-Hill.

[111] Wood, Kristin. (1991). "Design of Equipment for Lunar Dust Removal," *NASA Contractor Report CR-190014*. National Aeronautics and Space Administration, Center for AeroSpace Information.

[112] U.S. Department of Energy, "Occupational Radiation Protection, Final Rule," *Code of Federal Regulations*, Title 10, Part 835, December 14, 1993.

[113] "Radiation Protection and Instrumentation" *Biomedical Results of Apollo*, Section 2, Chapter 3, NASA SP-368, NASA Life Sciences Data Archive.

[114] Turner, James E. (1995). *Atoms, Radiation, and Radiation Protection, 2nd ed.* Oak Ridge, TN: John Wiley & Sons, Inc.

[115] Knoll, Glenn F. (2000) *Radiation Detection and Measurement, 3rd ed*. Ann Arbor, MI: John Wiley & Sons, Inc.

[116] Knief, Ronald Allen. (1992) *Nuclear Engineering: Theory and Technology of Commercial Nuclear Power, 2nd ed*. Mechanicsburg, PA: Hemisphere Publishing Corporation.

[117] Nuclear Data Evaluation Laboratory, Korea Atomic Energy Research Institute.

[118] "Space Plane Set for 2003 Launch," http://science.howstuffworks.com/news-item262.htm October 3, 2000.

[119] "Surface Properties of the Moon." Lecture Notes from *Astronomy 161: The Solar System*. Department of Physics and Astronomy. University of Tennessee.

[120] "NIST XCOM: Photon Cross Sections Database," http://physics.nist.gov/PhysRefData/Xcom/Text/XCOM.html. Accessed November 7, 2004.

[121] "Luna's (Earth's Moon) Thermal Environment." (2003) Thermal Environments. *Jet Propulsion Laboratory D-8160*. National Aeronautics and Space Administration.

[122] "Moon Fact Sheet," (2004) National Space Science Data Center. Goddard Space and Flight Center. Greenbelt, MD.

[123] International Commission on Radiation Units and Measurement (1989), "Tissue Substitutes in Radiation Dosimetry and Measurement," *Report 44 of the International Commission on Radiation Units and Measurements*.

Bethesda, MD.

[124] Varga, T.K. Bello, C. (1994). *The Periodic Table of the Elements.* Concord, Ontario: Papertech Marketing Group Inc.

[125] "International Chemical Safety Cards," http://www.itcilo.it/actrav/actrav-english/telearn/osh/ic/7580678.htm, Accessed November 3, 2004.

[126] Wade, L.G. Jr. (2002). *Organic Chemistry, 5th edition.* Princeton, NJ, Prentice Hall Publishing Inc.

[127] "Nuclear Power Fundamentals," http://www.tpub.com/content/doe/h1017v2/css/h1017v2_76.htm, Accessed November 10, 2004.

[128] "Boron Carbide Properties," http://www.azom.com/details.asp?ArticleID=75, Accessed November 12, 2004.

[129] "Table of the Nuclides," http://atom.kaeri.re.kr/ Accessed October 4, 2004.

[130] "Sintering Aids in the Consolidation of Boron Carbide (B4C) by the Plasma Pressure Compaction (P2C) Method," http://www.dekker.com/servlet/product/DOI/101081AMP200028083, Accessed November 13, 2004.

[131] Hubble, J.H. & Seltzer, S.M. (1996). "Tables of X-Ray Mass Attenuation Coefficients and Mass Energy-Absorption Coefficients from 1 keV to 20 MeV for Elements Z=1 to 92 and 48 Additional Substances of Dosimetric Interest," Ionizing Radiation Division, Physics Laboratory, National Institute of Standards and Technology Gaithersburg, MD.

[132] "Density of Molten Elements and Representative Salts," http://www-d0.fnal.gov/hardware/cal/lvps_info/engineering/elementdens.pdf Accessed November 7, 2004.

[133] "Webelements.com" http://www.webelements.com, Accessed November 8, 2004.

[134] http://www.geology.iupui.edu/research/SoilsLab/procedures/bulk/Index.htm. Accessed 6 November 2004.

[135] Smales, A. A., D. Mapper, M.S.W. Webb, R. K. Webster, J.D. Wilson. *Science*, New Series, Vol 167, No. 3918, The Moon Issue (Jan. 30, 1970), 509-512.

[136] McSween, H. Y. and K. Keil, 2000, *Geochemica et Cosmochimica Acta*, 64, 2155-2166.

[137] Voss, S. S., *TOPAZ II System Description*, 4th International Conference and Exposition on Engineering, Construction, and Operations in Space. LA-RU-94-4.

Appendix I – Definition of Variables Used for Core Heat Pipe Analysis

A_w	Cross sectional area of the wick
g	Acceleration due to gravity
l_{eff}	Effective length of heat pipe
m	Mass flow rate
K	Permeability of the wick
L	Latent heat of vaporization
P	Pressure
Q_{max}	Maximum thermal energy transfer
q	Heat flux
r	Radius of heat pipe
r_e	Effective pore radius in the wick
r_v	Radius of vapor channel
z	Entrainment parameter
ΔP_{Cmax}	Maximum pressure loss due to capillary limit
ΔP_g	Gravitational pressure loss
ΔP_l	Pressure drop required to return liquid from condenser to evaporator
ΔP_v	Pressure drop in the vapor's flow through the vapor channel
ε	Wire volume fraction
σ	Surface tension
ρ	Density
μ	Viscosity
φ	Inclination of heat pipe with the horizontal

Appendix II – Calculated Efficiency for Thermionic Systems

Objective

We will develop a model for estimating the efficiency of a thermionic system based on several parameters, includingits emitter temperature, collector temperature, electrical characteristics, diode spacing, and cesium gas pressure.

Energy Conservation Analysis

The calculated efficiency for a high-pressure cesium diode thermionic system is given by

$$\eta_{cal} = \frac{(V - V_L)J}{q_{in}} \qquad \text{(AII-1)}$$

where V is the voltage at the electrodes, V_L is the voltage drop across the leads, J is the measured current density, and q_{in} is the input heat-rate density.

The term is itself the sum of several terms,

$$q_{in} = q_E + q_{k1} + q_V + q_r + q_L - \frac{q_d}{2} \qquad \text{(AII -2)}$$

where q_E is the energy flux from the current J leaving the emitter, q_{K1} is the heat conduction rate through the thermionic structure, q_V is the heat conduction rate through the vapor, q_r is the energy flux associated with thermal radiation into the inter-electrode space, and $(q_L - q_d/2)$ is the heat rate through the leads.

The term q_E is the term describing the electron cooling of the emitter, and can be expressed as

$$q_E = J\frac{\phi_E}{e} \qquad \text{(AII -3)}$$

where φ_E is given by

$$\phi_E = kT_E \ln\frac{120T^2{}_E}{J} \qquad \text{(AII -4)}$$

The heat conduction rate through the vapor can be determined by

$$q_V = \frac{\lambda_m (T_E - T_C)}{d + 1.15 * 10^{-5} [(T_E + T_C) / p_{CS}]} \qquad \text{(AII -5)}$$

where T_E and T_C are the emitter and collector temperatures in Kelvin, p_{CS} is the cesium pressure in torr, *d* is the diode spacing in centimeters, and λ_m is the thermal conductivity of the cesium vapor in watts per degree Kelvin per centimeter, evaluated at the mean vapor temperature given by

$$T_m = \frac{2}{3} \left(\frac{T_E^{3/2} - T_C^{3/2}}{T_E - T_C} \right)^2 \qquad \text{(AII -6)}$$

The interelectrode thermal radiation rate per unit area is given by

$$q_r = \varepsilon \sigma (T_E^{\,4} - T_C^{\,4}) \qquad \text{(AII -7)}$$

For refractory metal electrodes, it is reasonable to assume a value $\varepsilon = 0.2$.

Thermal conduction through the supports and through the electrical leads and the supports is difficult to calculate theoretically, but as a convservative approximation can be taken to be 30% of the other thermal loss mechanisms.

Analysis of Efficiency for Proposed Thermionic System

The calculated efficiency will be determined for a system with a rhenium emitter at 1800 K, a molybdenum collector at 950 K, a diode spacing of 0.13 mm, and a cesium pressure of 10 torr.

The electron cooling of the emitter is taken as an experimentally determined value. Extrapolating data from systems similar to the proposed system, the system can be expected to produce of electric power $q_E = 10$ W/cm^2.

For $T_E = 1800$ K and $T_C = 950$ K, the mean vapor temperature $T_M = 2045$ K . At this value, $\lambda_m \approx 8.4 * 10^{-5} W / cm \cdot K$. The interelectrode spacing, *d*, is specified in the design to be 5 mils, or 0.0127 centimeters. The cesium vapor pressure p_{CS} will ber taken to be

10 torr as a conservative estimate. These numbers produce a heat conduction rate through the cesium vapor of $q_V = 4.5$ W/cm^2.

For the given electrode temperatures and an estimated emissivity of 0.3, the thermal radiation loss is determined to be $q_r = 16.5$ W/cm^2 . The thermal losses through the leads and other structure and approximated to be 9.3 W/cm^2.

The calculated efficiency of the electrical system is therefore determined to be 24.8%. This calculation does not take into account the voltage drop across the leads of the system. This loss mechanism and other inefficiencies within the system could easily bring this number down, but the efficiency will almost certainly stay above the 10% demanded by the project's goals.

Appendix III – Thermionics Mass Calculations

The thermionics require 10,000 cm^2 of surface area in order to operate at a power density of 10 W/cm^2. Since there will be 127 heat pipes, each heat pipe will need to have roughly 100 cm^2 of thermionic surface area.

The heat pipe is a cylinder of radius 1 cm. This means that 16 cm of the heat pipe surface must be covered with thermionics. The thickness of rhenium deposited on the thermionic walls will be at most 1 millimeter. The volume of rhenium will therefore be approximately 1.6 cm^3 of rhenium per heat pipe. We will assume that the outer portion of the thermionic has an average radius of 1.5 cm. We will assume a molybdenum thickness of 5 millimeters, leading to a volume of 75.4 cm^3 of molybdenum per heat pipe. We will assume that the stainless steel outer cylinder has the same volume.

Additional mass for each thermionic device is added in the form of ceramic spacers, electrical leads, and cesium reservoir tubing. A reasonable upper bound on the mass of all of these items is 1 kg per thermionic device.

The density of rhenium is 21.02 g/cc, yielding a total rhenium mass of 33.6 grams/device. The density of molybdenum is 10.22 g/cc, yielding a total molybdenum mass of 770.59 $grams/cm^3$. The density of stainless steel will be approximately that of iron, 7.874 $grams/cm^3$, yielding a total stainless steel mass of 593.70 grams/cc.

The total mass of each device is therefore:

Material	Mass
Rhenium	33.6 grams
Molybdenum	770.59 grams
Stainless Steel	593.60 grams
Auxiliary Parts	1000 grams
Total	2397.8 grams/device

The total mass per thermionic device is approximately 2.4 kilograms, yielding a total system mass of 240 kg.

Appendix IV – Extraterrestrial Environments

The Martian and lunar environments are quite different from the Earth and from each other in many respects, such as: reduced atmospheric pressure, weaker gravitational pull, surface elemental composition, and the wide and often unpredictable temperature shifts. In order to allow for appropriate and effective design adaptations and innovations, these differences must be taken into account. This section provides a brief description and listing of some important physical properties of the Martian and lunar environments. The properties described and tabulated below will serve as a standard reference, and will be useful for determining the appropriate materials and designs for the core, power conversion unit, shielding and radiator.

The Moon

Since the actual geological and weather conditions vary across the lunar surface, accurate values can only be determined once a landing site is determined. However, until that location is known, it is instructive to consider the average values for these factors. It is also important to note that while the lunar poles are the most likely future mission sites, many of the below values were obtained from the early lunar missions that landed predominately in the equatorial regions.

In the polar region, the sun continuously occupies a low position on the horizon and surface temperatures are more moderate and less variable, generally working to our advantage. In this design, while we anticipate going to the poles, we have designed the reactor to be robust and work anywhere on the lunar surface.

Lunar Atmosphere and Gravity

The moon has almost no atmosphere. With an atmospheric pressure of ~10^{-8} Pa very little convection can occur on the lunar surface, which has direct implications for material options, radiator, and shielding systems. Yet with an atmosphere composed almost entirely of inert noble gases such as helium, neon and argon, minimal corrosion is expected. Hydrogen represents a major exception, but at a concentration of roughly 35,000 particles per cubic

centimeter, hydrogen can be disregarded as a threat to material stability. [1] Gravity on the Moon is roughly one ninth of that on the Earth. See tables 1 and 2 below for data on composition and properties of the lunar atmosphere.

Table 0-1: Composition of Lunar Atmosphere

Gas	Particles/m^3
H_2	35,000
He-4	40,000
Ne-20	40,000
Ne-22	5,000
Ar-36	2,000
Ar-40	30,000
CO_2	1,000
H_3N	1,000
CH_4	1,000

Table 0-2: Average Properties of Lunar Atmosphere

Property (surface)	Value	Units
Thermal Conductivity	Effectively zero	W/m*K
Pressure	3×10^{-10}	Pa
Density	2×10^{11}	particles/m^3
Gravity	1.62	m/s^2

Lunar Geology

Much of the moon's cratered surface is composed of igneous rock, not unlike that found near volcanoes on Earth. [2] See tables 3 and 4 below for data on composition and properties of the lunar soil.

Table 0-3: Composition of Lunar Soil

Compound	Weight Percent
SiO_2	47.3
TiO_2	1.6
Al_2O_3	17.8
FeO	10.5
MgO	9.6
CaO	11.4
Na_2O	0.7
K_2O	0.6
MnO	0.1
Cr_2O_3	0.2

Table 0-4: Properties of Lunar Soil

Property	Value	Units
Thermal Conductivity	10^{-3}	W/m*K
Albedo	0.11	

Lunar Meteorological Properties

Temperature variations on the moon are extreme when compared with the Earth. The lunar day is equivalent to 28.5 Earth days, and all parts of the lunar surface, excepting the polar regions, spend half this time in the sun. With virtually nonexistent atmospheric convection and limited surface conductivity, the side of the moon exposed to the sun heats to over 373 K. When the sun sets, however, temperatures drop below 160 K. Owing to the low surface conductivity, shadowed regions on the sunny side will also fall to the night temperature, resulting in large temperature gradients. Table 5 displays some of the lunar meteorological properties.

Table 0-5: Lunar Meteorological Properties

Property	Value	Units
Temperature	100 to 400	K
Blackbody Temperature	274.5	K
Solar Radiation	1367.6	W/m^2

Mars

The Martian environment differs greatly from the moon, since Mars has a more significant atmosphere, different elemental composition, and is farther from the sun. Again, because the actual properties that will be encountered on Mars are highly variable based on location and season, average values are given below. Values obtained from the Viking I mission are also given for comparison. Once likely landing sites are identified more specific values can be obtained.

Martian Atmosphere and Gravity

The Martian atmosphere consists of 95% carbon dioxide, with the other 5% consisting of nitrogen, argon, and trace amounts of oxygen and carbon monoxide. Unlike the inert lunar environment, the Martian atmosphere is potentially corrosive, especially to potential reactor core materials. Atmospheric pressure ranges from 600-800 Pa on Mars, considerably thinner than the Earth's by about 1/150 [3] though many orders of magnitude thicker than the Moon's. The surface gravity of Mars is about one-third of that of Earth's. See tables 6–9 below for data on composition and properties of the Martian atmosphere.

Table 0-1: Composition of Martian Atmosphere [2]

Gas	Volume Percent
CO_2	95.32
N_2	2.7
Ar	1.6
O_2	.13
CO	.08
H_2O	210 ppm
NO	100 ppm
Ne	2.5 ppm
HDO	0.85 ppm
Kr	0.3 ppm
Xe	0.08 ppm

Table 0-2: Properties of Martian Atmosphere

Property (surface)	Value	Units
Thermal Conductivity [3]	0.012	W/(m K)
Pressure [2]	600 to 800	Pa
Density [2]	0.020	kg/m^3
Gravity	3.69	m/s^2

Table 0-3: Composition of Martian Atmosphere as measured during the Viking I mission [1]

Gas	Volume Percent
CO_2	95.32
N_2	2.7
Ar	1.6
O_2	0.13
CO	0.07
H_2O	0.03
Ne	2.5 ppm
Kr	0.3 ppm
Xe	0.08 ppm

Table 0-4: Properties of Martian Atmosphere as measured during the Viking I mission [1]

Property (surface)	Value	Units
Pressure	800	Pa
Density	0.0166	kg/m^3

Martian Geology

The Martian crust and soil is rich in metal oxides such as silicon dioxide, ferrous oxide and magnesium oxide. The terrain is much less severe on Mars. Flat plains cover approximately 60% of the Martian surface, the remainder being valleys and canyons that were carved, in theory, from past rivers. Furthermore, a prominent topographic feature of the Martian landscape is a small chain of volcanoes located in the northern hemisphere. These volcanoes can reach elevations of up to 25km, with diameters in excess of 500km. [3] See tables 10–13 below for data on composition and properties of the Martian soil.

Table 0-5: Composition of Martian Soil [2]

Compound	Weight Percent
SiO_2	40
Other	20
FeO	15
Al_2O_3	10
MgO	10
Na_2O	5

Table 0-6: Properties of Martian Soil [3]

Property	Value	Units
Thermal Conductivity	2.94	W/(m K)
Thermal Diffusivity	10^{-6}	m^2/s

Table 0-7: Composition of Martian Soil as measured during the Viking I mission [1]

Compound	Weight Percent
SiO_2	44.7
Al_2O_3	5.7
Fe_2O_3	18.2
MgO	8.3
CaO	5.6
K_2O	0.3
TiO_3	0.9
SO_3	7.7
Cl	0.7

Table 0-8: Properties of Martian Soil as measured during the Viking I mission [1]

Property	Value	Units
Thermal Conductivity	8.37×10^{-3} to 8.37×10^{-2}	W/(m K)
Specific Heat	0.628 to 0.796	J/(g K)
Emissivity	0.90 to 0.98	
Thermal Inertia	2.4×10^{-3} to 1.4×10^{-2}	$S^{5/2}$ K/kg
Albedo	0.2 to 0.4	
Porosity (Bulk Density)	1000 to1800	kg/m^3
Density	3933	kg/m^3

Martian Meteorological Properties

The Martian surface temperature range spans 145-300K (night-day), expectedly lower than the Moon, with an average surface temperature of 220K. The Martian weather consists of sporadic dust storms, with sustained winds up to 50m/s and gusts up to 170m/s. Martian atmosphere is less dense so the force exerted by these winds is less than the same wind speed on Earth [3]. For instance, since the density of the Martian atmosphere is about 1% of the Earth's atmospheric density, a 100m/s wind on Mars would have the force equivalent of a 1m/s wind on the Earth. However, sustained winds still have the possibility of corroding any structural surface on Mars.

Mars has a revolution period of 687 Earth days (1.88 years), and its period of rotation is similar to that of Earth's (24 hours 37 minutes 46 seconds). Mars also lacks the protection of a magnetic field, leaving it more vulnerable to charged particles from space. Due to reduced atmosphere, meteorites are also a risk on both Mars and the moon. Tables 14 and 15 below display some of the Martian meteorological properties.

Table 0-9: Martian Meteorological Properties

Property	Value	Units
Temperature [2]	145 to 300	K
Wind Speed [2]	2 to 170	m/s
Solar Radiation [4]	Spring 146 Summer 167 Fall 62.5 Winter 83.3	W/m^2

Table 0-10: Martian Meteorological Properties as measured during the Viking I mission [1]

Property	Value	Units
Temperature	130 to 290	K
Wind Speed	0 to 50	m/s
Solar Radiation	590.0	W/m^2

References

[1] "Moon Fact Sheet," (2004) National Space Science Data Center. Goddard Space and Flight Center. Greenbelt, MD.

[2] "Surface Properties of the Moon." *Lecture Notes from Astronomy 161: The Solar System*. Department of Physics and Astronomy. University of Tennessee.

[3] "Exploring Mars," http://www.exploringmars.com Accessed September 17, 2004.

[4] Ahrens, Thomas J. (1995). *Global Earth Physics: A Handbook of Physical Constants*. American Geophysical Union.

[5] Allen, C.W. (Ed.). (2000). Astrophysical *Quantities, 4th ed*. AIP Press.

[6] Papike, J.J., Simon, S.B., and Laul, J.C. (1982). The Lunar Regolith: Chemistry, Mineralogy and Petrology. *Reviews of Geophysics and Space Physics*, 20, 761-826.

[7] Racca, Giuseppe D. (1995). Moon Surface Thermal Characteristics for Moon Orbiting Spacecraft Thermal Analysis. *Planetary and Space Science,* 43*, No.* 6, 835-842.

[8] U.S. Nautical Almanac Office. (2001). *Astronomical Almanac for the Year 2001: Data for Astronomy, Space Sciences, Geodesy, Surveying, Navigation and Other Applications*. Bernan Associates.

[9] Smith, R.E. and West G.S. "Space and Planetary Environment Criteria Guidelines for Use in Space Vehicle Development," *NASA Technical Memorandum 82478*. 1982 Revision, Vol 1. NASA Center for Aero Space Information.

[10] "Exploring Mars" http://www.exploringmars.com. September 17, 2004

[11] Corasaniti, S. and Gori, F. "Theoretical Prediction of the Thermal Conductivity and Temperature Variation Inside Mars Soil Analogues," *Planetary Space and Science*. Vol 52, Issue 1-3, Jan- March 2004. pp 91-99.

[12] Appelbaum, J. and Landis, G. "Photovoltaic Power Options for Mars," *Space Power*. Vol 10, Number 2, 1991. pp 225-237.